NASA TECHNICAL NOTE

NASA TN D-7692

NASA TN D-7692

CASE FILE COPY

FLIGHT TESTS OF VIKING PARACHUTE SYSTEM IN THREE MACH NUMBER REGIMES

I - Vehicle Description, Test Operations, and Performance

by Reginald R. Lundstrom, James L. Raper, Richard J. Bendura, and E. William Shields

Langley Research Center
Hampton, Va. 23665

NATIONAL AERONAUTICS AND SPACE ADMINISTRATION • WASHINGTON, D. C. • OCTOBER 1974

1. Report No.	2. Government Accession No.	3. Recipient's Catalog No.
NASA TN D-7692		

4. Title and Subtitle	5. Report Date
FLIGHT TESTS OF VIKING PARACHUTE SYSTEM IN THREE MACH NUMBER REGIMES I – VEHICLE DESCRIPTION, TEST OPERATIONS, AND PERFORMANCE	October 1974
	6. Performing Organization Code

7. Author(s)	8. Performing Organization Report No.
Reginald R. Lundstrom, James L. Raper, Richard J. Bendura, and E. William Shields	L-9536
	10. Work Unit No. 815-20-09-03
9. Performing Organization Name and Address	11. Contract or Grant No.
NASA Langley Research Center Hampton, Va. 23665	
	13. Type of Report and Period Covered
12. Sponsoring Agency Name and Address	Technical Note
National Aeronautics and Space Administration Washington, D.C. 20546	14. Sponsoring Agency Code

15. Supplementary Notes

E. William Shields is associated with LTV Aerospace Corporation, Hampton Technical Center, Hampton, Va.

16. Abstract

Four flight qualification tests of the Viking parachute were conducted behind a simulated full-scale Viking spacecraft at Mach number and dynamic-pressure conditions bracketing the range of entry conditions postulated for the Viking 1975 mission to Mars. For the supersonic and transonic tests the test vehicle was carried to an altitude of 36.6 km (120 000 ft) by means of a 980 000 m^3 (34 600 000 ft^3) balloon. The test vehicles were released and were propelled to test conditions with rocket engines. For the subsonic test a 117 940 m^3 (4 166 000 ft^3) balloon carried the test vehicle to an altitude of 27.5 km (90 000 ft) and the test conditions were achieved in free fall. Aeroshell separation occurred on all test vehicles at times varying from 8 seconds to 14 seconds after parachute deployment; this condition simulated Viking conditions.

This report describes the test vehicle and the methods used to insure that the desired test conditions were achieved. It also describes the balloon system design and balloon operations. The report presents the performance data received from onboard and ground-based instrumentation and also the results from a statistical trajectory estimation program which was used to give a continuous history of test-vehicle motions.

17. Key Words (Suggested by Author(s))	18. Distribution Statement
Test vehicle Decelerator test Blunt body Balloons	Unclassified – Unlimited STAR Category 31

19. Security Classif. (of this report)	20. Security Classif. (of this page)	21. No. of Pages	22. Price*
Unclassified	Unclassified	160	$5.00

*For sale by the National Technical Information Service, Springfield, Virginia 22151

FLIGHT TESTS OF VIKING PARACHUTE SYSTEM IN THREE MACH NUMBER REGIMES

I – VEHICLE DESCRIPTION, TEST OPERATIONS, AND PERFORMANCE

By Reginald R. Lundstrom, James L. Raper,
Richard J. Bendura, and E. William Shields*
Langley Research Center

SUMMARY

Four flight qualification tests of the Viking parachute were conducted during the summer of 1972 behind a simulated Viking spacecraft at Mach number and dynamic-pressure conditions bracketing the range of entry conditions postulated for the Viking 1975 mission to Mars. A full-scale simulated Viking 1975 spacecraft was carried to an altitude of 36.6 km (120 000 ft) for the supersonic and transonic tests by means of a 980 000 m^3 (34 600 000 ft^3) balloon and was propelled to the desired test conditions with onboard rocket engines. For the subsonic test a 117 940 m^3 (4 166 000 ft^3) balloon was used to attain an altitude of 27.5 km (90 000 ft) and the test vehicle achieved the desired test conditions by free fall.

The test vehicle had the same weight, size, and contour as the Viking 1975 spacecraft and contained equipment and instrumentation necessary to achieve the desired test conditions and to measure motions throughout the parachute test. Trajectory measurements were obtained from ground-based instrumentation at the White Sands Missile Range.

A simple pendulum system in view of the balloon load bar camera confirmed that the load bar motions under the balloon were very small and that the load bar was level at the time of drop. A system using aspect magnetometers in the test vehicle, and cold gas jets operated by ground command, was used successfully to point the test vehicle at the desired azimuth prior to drop from the balloon. Aeroshell separation was successfully demonstrated at transonic and subsonic speeds simulating Mars conditions. A statistical trajectory estimation program was used with data from onboard cameras to give a continuous history of test-vehicle motions.

*E. William Shields is associated with LTV Aerospace Corporation, Hampton Technical Center, Hampton, Va.

INTRODUCTION

Four qualification flight tests of the Viking decelerator system were conducted at the White Sands Missile Range (WSMR) during the summer of 1972. The test vehicle description and flight results are presented here and the decelerator results are presented in reference 1.

The Viking Project is a NASA program for soft landing two scientific payloads on Mars in 1976. The Viking lander capsule consists of a 3.51-m-diameter (11.5-ft) 70° half-angle conical entry vehicle which nominally decelerates aerodynamically to a parachute deployment environment at 7620 m (25 000 ft) above the surface of Mars. The parachute provides additional deceleration prior to the start of the lander terminal descent engines which effect an essentially zero velocity impact on the Martian surface. This intermediate parachute phase also provides for the stabilization and support of the vehicle during aeroshell separation and terminal engine warmup. Figure 1 presents a sketch of the Viking parachute and entry capsule geometrical relationships.

A controlling factor in the design of the Viking parachute test program was the requirement to demonstrate margin in the parachute system design while maintaining a minimum test program. An additional factor in the design and test program was the requirement to utilize state-of-the-art designs. The Viking parachute system consisted of a disk-gap-band parachute deployed by a mortar. Wind-tunnel tests (ref. 2) used to design the length of the suspension lines of the Viking parachute were instrumental in finalizing the trailing distance of the parachute 8.5 diameters behind the spacecraft (fig. 1), which is a much longer distance than was used for the supersonic parachutes tested previously. Low-altitude tests of the parachute were conducted to prove the parachute structural strength and mortar deployment capability at subsonic speeds. (See ref. 3.) Three high-altitude qualification tests of the parachute system – the subject of the current report and references 1 and 4 – were performed as final full-scale proof tests of the parachute system deployed behind a simulated Viking spacecraft. One of each of these tests was targeted at the subsonic, transonic, and supersonic speed regimes so that the full range of expected Mars entry conditions would be bracketed.

The qualification test series had the following specific objectives:

(a) Verify sufficient mortar ejection velocity
(b) Verify orderly parachute deployment and inflation
(c) Verify that sustained inflation will occur
(d) Verify adequate drag performance
(e) Verify structural integrity of all parachute elements
(f) Obtain data on inflation rates and vehicle oscillations which can be extrapolated to conditions resulting from Martian entry
(g) Demonstrate aeroshell separation

The inherent interaction between the forebody aerodynamic characteristics and the parachute inflation stability required that the test vehicle simulate the mass properties and the aerodynamic characteristics of the Viking system. Also, duplication of the bridle attachment of the parachute to the lander capsule was required so that the dynamic behavior of the lander capsule to the fluctuating parachute loads could be evaluated. Since the Viking spacecraft is a lifting body, it was required that the angle of attack at parachute deployment be simulated. These constraints eliminated the use of an erectable aeroshell on an all-rocket configuration such as was used previously on the NASA Sped II test. (See ref. 5.) The use of a balloon system to raise the test vehicle above the higher density section of the atmosphere has been previously employed on the Planetary Entry Parachute Program (PEPP) (ref. 6) series of parachute tests, and this technique was selected for the high-altitude qualification test of the Viking parachute. Because the Viking parachute qualification tests required greater velocities and heavier payloads, significant changes in the PEPP technique were required.

SYMBOLS

Values are presented in SI and U.S. Customary Units. Values were obtained in U.S. Customary Units.

a_X, a_Y, a_Z components of test vehicle acceleration at the center of gravity along test vehicle X-, Y-, and Z-axes, respectively, m/sec^2 (ft/sec^2)

g acceleration due to gravity

I_{XX}, I_{YY}, I_{ZZ} moments of inertia about the X-, Y-, and Z-axes, respectively, $kg\text{-}m^2$ $(slug\text{-}ft^2)$

M Mach number

P_{XY}, P_{XZ}, P_{YZ} products of inertia about the XY-, XZ-, and YZ-axes, respectively, $kg\text{-}m^2$ $(slug\text{-}ft^2)$

p,q,r components of test-vehicle angular velocity about test vehicle X-, Y-, and Z-axes, respectively, radians per second

t time from test-vehicle drop, sec

X,Y,Z test-vehicle axis system (see fig. 4(a))

x' distance measured from test vehicle theoretical apex to center of gravity, cm (in.)

y' distance measured from X-axis in the XY-plane, cm (in.)

z' distance measured from X-axis in the XZ-plane, cm (in.)

$\ddot{x},\ddot{y},\ddot{z}$ accelerations along the X-, Y-, and Z-axes, respectively

γ_p flight-path pitch angle relative to Earth's surface, deg

γ_y flight-path azimuth angle relative to true north, deg

$\overline{\Delta R},\overline{\Delta AZ},\overline{\Delta EL}$ mean deviation between radar and trajectory reconstruction values of range, m; azimuth, deg; and elevation, deg, respectively

$\overline{\Delta\psi},\overline{\Delta\theta},\overline{\Delta\phi}$ mean Euler angle deviation between trajectory reconstruction and camera data, deg

$\sigma_R,\sigma_{AZ},\sigma_{EL}$ standard deviation from mean deviation between radar and trajectory reconstruction values of range, m; azimuth, deg; and elevation, deg, respectively

ψ,θ,ϕ Euler angles (round Earth): test vehicle yaw, pitch, and roll angles, respectively, relative to an Earth-fixed axis system, deg

MISSION DESCRIPTION

Earth Flight-Test Limitations

The Mars atmospheric properties are very dissimilar from those of Earth, particularly in regard to temperature and gas constituents (CO_2 compared with N_2 and O_2). These atmospheric differences and the differences in gravity are the primary factors which prevented exact duplication of Mars conditions on Earth. The selection of the Earth test conditions was a compromise dictated by the test objectives. The primary flight parameters which influenced this selection because of their proven effect on parachute deployment were Mach number, velocity, and dynamic pressure. A match of Mach number, velocity, and dynamic pressure is impossible in the Earth's atmosphere. Figure 2 shows the difference in Earth altitude for a match of velocity or Mach number with dynamic pressure. When Mach number and dynamic pressure were selected for test condition matching Earth and Mars conditions, the velocity on Earth was approximately

60 percent higher than that on Mars. The test conditions at terminal dynamic pressure also were dissimilar on Earth since the vehicle weight on Mars is only 38 percent of that on Earth; however, the deeper Earth atmosphere did give a longer time at terminal conditions.

The higher velocity required for the Earth tests than for the corresponding Mars conditions did have a slightly different effect on the dynamics of the parachute opening and also on the aerodynamic heating. These two effects, which are slightly more severe for the Earth test, tend to be compensated for by the interplanetary cruise degradation factor. For the supersonic test the total of these three factors amounts to about 3 percent degradation in parachute cloth strength. These effects on parachute survival due to the loads were estimated and accounted for by adjusting the test-point dynamic pressure downward.

Test Point Selection

Figure 3 shows the envelope of Mars deployment conditions which includes the effects of possible variations in entry vehicle weight, entry capsule lift and drag characteristics, selected entry angle and entry angle dispersions, and atmosphere uncertainty. Three test conditions were selected to bracket the range of Mars conditions, as shown in the figure. One was at supersonic speeds and the highest dynamic pressure which would be expected to produce maximum parachute load conditions and also greatest parachute fluctuations. The second test point was selected at transonic speed and low dynamic pressure as a possible area where parachute opening problems might exist. This speed regime was particularly suspect because of the severe reduction in parachute drag efficiency indicated by the wind-tunnel tests. This transonic drag reduction had not previously been observed in wind-tunnel tests with small forebodies and thus the phenomenon was unique to large forebodies. A third test point chosen was at subsonic speeds because it would be expected to cause the longest inflation times. The test conditions for all four tests are further described in table I.

A maximum of four flight tests were allowed for final qualification of the Viking parachute system; these tests are referred to as AV-1 (supersonic), AV-2 (transonic), AV-3 (subsonic), and AV-4 as a backup. Since the composition and structure of the atmosphere of Mars is not accurately known, the test points necessarily had to cover worst case probabilities.

The test sequence chosen was supersonic, transonic, and subsonic. This sequence resulted from program requirements to (1) maintain a minimum test program, and (2) complete all tests with the same design parachute system. Since the supersonic test was considered to be the most severe in terms of conditions which could cause parachute design changes, it was conducted first. It should be noted that the same parachute system design was utilized in the four qualification tests.

All tests were to be conducted with flight-quality Viking parachute, bridle and attachments, and mortar, behind a full-scale simulated Viking configuration so that the flow field behind the body would be closely duplicated. For the supersonic flight, the objective was to conduct the test with a parachute loading of 1.15 to 1.30 times the expected maximum Mars conditions.

Between the parachute test of AV-1 and its repeat AV-4, additional data on the surface pressure and atmospheric pressure profile of Mars were obtained from Mariner 9. Studies of parachute performance during Martian entry with these new data indicated that the required parachute terminal conditions could be reached even if parachute deployment were initiated at a lower maximum dynamic pressure. The test conditions for AV-4 were changed to reflect the change in parachute deployment conditions. The envelope of conditions at Mars in figure 3 does include this more advanced atmospheric data rather than that which was thought to exist at the beginning of the test program.

Test Method

For the supersonic test point of $M = 2.17$ and $q = 519$ N/m^2 (10.84 lb/ft^2), the Earth conditions are approximately 44 200 m (145 000 ft) altitude and 701 m/sec (2300 ft/sec). It was necessary to attain these conditions with a full-scale Viking configuration which is 3.51 m (11.5 ft) in diameter and is shown in figure 4. It was also established that the dynamic-pressure variation with time for the Mars entry trajectory was more closely approximated in the Earth atmosphere test with a shallow ascending flight-path angle than with a steep outgoing or incoming trajectory. The balloon launch technique similar to that described in reference 6 was used to attain the test conditions. For the transonic and supersonic flights the balloon attained a float altitude of about 36.6 km (120 000 ft) and the test vehicle was carried under the balloon with its longitudinal axis pointed upward at a sufficient angle to insure the required ascending trajectory upon reaching the test conditions. Rocket engines incorporated in these test vehicles, as shown in figure 4, propelled them to a greater Mach number and dynamic pressure than required so that test conditions could be attained during coasting flight in order to avoid any damage to the parachute canopy or bridle from the rocket exhaust. A sketch showing a typical sequence of events for the supersonic or transonic test is presented in figure 5. At 1 second after release from the balloon, spin rockets imparted a roll rate of about 180°/sec to the test vehicle in order to equalize the effect of any thrust misalinement of the boost rockets that might exist. One second later the boost rocket motors ignited and propelled the test vehicle to a Mach number and dynamic pressure greater than the required test conditions. After rocket motor burnout, the spin rate was reduced by despin rockets to near zero for the parachute test. The parachute deployment was initiated by firing the mortar by ground command at the time to achieve the required test conditions. The aeroshell was separated from the remainder of the test

vehicle at about 48 seconds after drop from the balloon; thus, conditions that exist during the Viking mission were simulated for this event.

For the subsonic test the test vehicle, AV-3, was carried under the balloon to an altitude of 27.5 km (90 000 ft) with its longitudinal axis pointing nearly vertically down and after release it attained the desired test conditions during free fall. No boost rockets or spin rockets were used on the subsonic test vehicle.

In all cases the test conditions desired to be simulated were the conditions at parachute peak load. The only way to initiate the parachute deployment test was by ignition of the parachute mortar. The time for the parachute to extend and for the canopy to open to its peak load value was calculated and mortar ignition was effected early enough to insure that the desired dynamic pressure would occur at peak load as may be observed in figure 3.

It was necessary to take into account possible variations in test-vehicle performance in selecting a test condition for mortar ignition. Figure 3 shows an acceptable test condition box around each selected mortar ignition condition. For the supersonic and transonic tests the ranges of dynamic pressure were defined by possible variations in vehicle performance caused by dispersions in rocket engine thrust, burning time, and alinements, and by variations in atmospheric conditions. For the supersonic test the upper Mach number limit was defined by the maximum capability of the test vehicle and the lower limit was defined by a program requirement to qualify for at least conditions up to $M = 2.0$. The upper and lower limits for the transonic test Mach number were selected to insure a test in the Mach number range indicated by wind-tunnel tests to be of most concern. The upper and lower limits for the subsonic test dynamic pressure and Mach number were defined largely by variations in both test altitude and by atmospheric conditions.

Aeroshell Separation

Aeroshell separation was required to be carried out at conditions bracketing those that will occur for Viking shown in figure 3. Throughout this report, the remainder of the test vehicle after aeroshell separation is referred to as the payload. The purpose of this part of the test was (1) to insure that the separation of the aeroshell and payload would meet or exceed the specification of 15.2 m (50 ft) separation in 3 seconds; (2) to check the performance of the hardware design that will be used for the Viking mission; and (3) to verify that the separation would not cause objectionable aerodynamic disturbances to the payload or parachute.

TEST VEHICLE DESCRIPTION

The test vehicle was designed with three primary objectives in mind: (1) to create the same wake pattern in which the parachute would be immersed as the Viking, (2) to

accommodate the instrumentation needed to perform the test and acquire the desired data, (3) to be able to attain the desired test conditions of Mach number and dynamic pressure, and (4) to simulate tne angle-of-attack effects at deployment. It was required that the test vehicle withstand the environment caused by being at an altitude of 36.5 km (120 000 ft) for up to 6 hours while being carried by the balloon to the desired release point over the White Sands Missile Range.

Test Vehicle Structure

In order to be more certain of completing tests at the three selected conditions within the desired time period, a total of four test vehicles were constructed. The test vehicles were designed with as much common structure as possible. The supersonic test caused the most severe flight conditions and hence the greater probability of a failure; therefore, the spare was built as a supersonic test vehicle which could be modified to one of the other configurations. The primary structure was the rocket-motor support structure which was designed for four rocket motors which were capable of accelerating the test vehicle to a velocity of about 850 m/sec (2800 ft/sec). It was designed so that for the transonic test, two of the rocket motors could be omitted and replaced with ballast and the desired test conditions achieved. No rockets were required for the subsonic test and all rocket motors were replaced by ballast. Conversion from the supersonic configuration to the subsonic configuration was somewhat more involved, since the test vehicle was carried at a different attitude under the balloon. Figure 6 shows a sketch of the mortar support structure. A schematic showing how the rocket-motor support structure, the mortar support structure, and the aeroshell fit together is presented as figure 7. The launch support fitting for the supersonic and transonic vehicles, as shown in figures 4(a) and 6, was designed so that the test vehicle weight as it was carried under the balloon was tied directly through the aeroshell into the rocket-motor support structure. In the supersonic and transonic tests the test vehicle (figs. 4 and 8) was connected to the load-bar support structure by a single pyrotechnic-operated tension rod separator. For the subsonic vehicle, where the vehicle was carried point downward, the load-bar support structure tie-in was to the mortar support structure and release was accomplished by firing three pyrotechnic nuts. The test-vehicle support structure (figs. 4 and 8) had three legs bearing on the test vehicle at separated points which enabled the test vehicle to be rigidly connected to the load bar. The supersonic vehicle was carried under the load bar with its longitudinal axis pointed upward at 55°, and the transonic vehicle at 65° as these attitude angles produced the required test conditions. The subsonic test vehicle was carried pointing downward 4.5° off the vertical since this angle was approximately the natural aerodynamic trim angle at the time of mortar fire.

Parachute Mortar

The parachute pack was ejected from the spacecraft by means of a mortar which was capable of producing a differential velocity between test vehicle and parachute pack of about 33.6 m/sec (110 ft/sec). A sketch of this mortar with the parachute pack installed in the barrel is shown in figure 9. Further details of the mortar may be found in reference 7. The reaction load from this mortar had a possible peak value of about 58 300 N (13 000 lb) and was taken up by the mortar support structure shown in the sketch of figure 10. Parachute bridle attachments are also shown along with the method of retaining the parachute pack sabot. This entire structure simulated that of Viking so that the tests were also a proof of the mortar and parachute attachment methods in addition to being a test of the parachute itself. A particular concern was the effect of any rocket motor exhaust heating on the parachute bridles strung out along the mortar support structure on the base cover. Analyses indicated that additional thermal protection might be required for the qualification tests over that already required for the Martian entry. Consequently, a 1-cm-thick (0.4-in.) layer of insulation was attached to the outside of the thermal cover designed to protect the bridle. This additional insulation was employed in all vehicle tests even though it was only required in the supersonic tests in order to insure a standard basis of comparison for mortar performance.

Base Cover

The base cover enclosed the rear of the test vehicle and was attached to the mortar support structure. The rocket motor nozzles protruded through holes in the base cover as did the lenses of the rearward-facing cameras as shown in figure 4(a). The base cover had an elastomeric thermal ablative coating 0.55 cm (0.22 in.) thick to protect it from heating due to impingement of the rocket motor exhausts. A photograph of the base of the vehicle is presented as figure 11.

Aeroshell

The aeroshell (see fig. 4(a)) formed the required contour of the forward part of the test vehicle. This was a 140° total angle blunted cone having a nose radius of 0.876 m (34.5 in.) and had a maximum diameter of 3.505 m (11.50 ft). It was built as an integral unit and was designed to be separated from the remainder of the test vehicle. It was attached to the basic rocket-motor support structure with three pyrotechnic bolts. The bolts were each centered inside a spring and the three units imparted a separation velocity of about 0.3 m/sec (1 ft/sec) to the aeroshell. Three guide rails, each about 0.3 m (1 ft) long helped to insure that the aeroshell would be ejected straight and forward from

the remainder of the test vehicle. A photograph of the aeroshell showing the separation springs and guide rails is shown in figure 12.

Center-of-Gravity and Mass Characteristics

For all test vehicles the center of gravity was displaced 3.58 cm (1.41 in.) in the pitch direction from the vehicle longitudinal axis of aerodynamic symmetry. Both the vehicle mass and center-of-gravity location at the time of parachute deployment were the same as those of the Viking entry capsule; therefore, the trim angle of attack was simulated. The ballast arrangement to produce this weight and center-of-gravity location was positioned as shown in figure 4.

The rocket motor support structure was constructed with the composite thrust vector displaced 3.58 cm (1.41 in.) vertically from the longitudinal axis so that it passed through the test vehicle center of gravity. Similarly, the parachute mortar was displaced as shown in figure 4(a) so that the mortar reaction load passed through the test vehicle center of gravity. Moments of inertia did not exactly simulate Viking. A table showing the mass characteristics at various stages during the test is presented as table II.

Rocket Motor Alinement

Low dynamic pressure during the early part of rocket motor burning made it necessary to hold close tolerance on rocket alinements in order to avoid large changes in flight path during this period. Positioning of the lateral center of gravity was accomplished by static balancing the vehicle and adding weights until the lateral position of the center of gravity was within 0.76 mm (0.03 in.) from the required location which was displaced 3.58 cm (1.41 in.) from the axis of symmetry. Alinement of the rocket motors was accomplished by individually alining the motor support mounts with a precision tool and adding shims as required. Each motor's orientation was biased within the structure to account for any nozzle misalinement. Consequently, the resultant thrust vector was determined to be within 0.2° of the vehicle longitudinal axis and was laterally displaced less than 0.15 cm (0.06 in.) from the center of gravity.

Spin Motors

As a method of further reducing trajectory dispersion, the supersonic and transonic test vehicles had spin motors to spin them during the rocket motor burning period and largely cancel out the effect of any thrust misalinement which might remain. Despin motors were burned just before mortar firing in an effort to keep the test-vehicle spin rate below 50°/sec at parachute deployment. The spin motor packages, which may be seen attached to the base cover in figure 11, consisted of a total of six individual motors having a burn time of 1 second for spin up of the supersonic and transonic vehicles. Four

motors were used for despin. Orientation of the spin up and despin motor packages was adjustable in order to accommodate differences in vehicle roll moment of inertia and expected amount of spin to be cancelled. No spin motors were used for the free fall subsonic test. As noted in figure 11, the spin motors do change the contour of the vehicle base. Tests reported in reference 8 have shown that the wake pattern at supersonic speeds is not readily affected by the shape of the vehicle base.

Electrical System

In order to carry out the sequence of events shown in figure 5 with the greatest reliability, dual electrical systems were used. The onboard sources of power were five batteries: (1) main battery which supplied power to telemetry, command system A, and heating units; (2) transient battery which supplied power to command system B, the radar beacon, the pointing system, and the timing correlator for the cameras; (3) pyro battery A which provided power for one programer and for circuit A of all pyrotechnic devices; (4) pyro battery B which provided power for the second programer and for circuit B of all pyrotechnic devices; and (5) camera battery which provided power to all onboard cameras. A block diagram of the electrical systems may be found in appendix A of reference 9.

Pyrotechnic devices other than rocket motors used on the test vehicle were (a) load bar tension rod separator, (b) mortar initiation unit, (c) aeroshell separation nuts, and (d) cable cutters which released the two aft-facing camera lens covers. The subsonic vehicle used three pyrotechnic nuts for release from the load bar instead of the single tension rod separator used by the supersonic and transonic vehicles. In the interest of safety, the pyrotechnic units for all vehicles were continually "safed" until they were armed by ground command about 5 minutes prior to drop from the balloon. In addition, except for the subsonic vehicle, interlock circuits were constructed so that spin motor ignition had to occur before boost rocket ignition was possible and boost rocket ignition had to occur before mortar fire.

The programers were started by the same command which initiated release from the load bar. The programers were interlocked by a lanyard attached to the load bar so that if the lanyard was not pulled free, because of vehicle free fall, within the first 0.5 second the programers would stop at 0.5 second until the interlock was broken. Events and methods of initiation of these events for each of the test vehicles are presented in table III.

Instrumentation

Instrumentation systems onboard the test vehicle consisted of (a) radar beacon, (b) dual command systems, (c) camera system, and (d) telemetry. The C-band radar tracking beacon was furnished by White Sands Missile Range (WSMR) to be compatible

with their AN/FPS-16 radars. The transponder transmitted at 5860 MHz and received radar transmitted pulses at 5490 MHz. Antennas were located on the aeroshell and on the base cover and were used jointly by the C-band beacon and the telemetry system. The beacon was located inside the base cover and remained with it after aeroshell separation. Other radars skin tracked the aeroshell and also the balloon and load bar after separation of these units.

The command receiver/decoder operated on a frequency of 541 MHz and operated on a three-tone ground command. For redundancy, two command receivers were onboard the vehicle. In the subsonic test vehicle only aeroshell antennas were used; in the supersonic and transonic test vehicles both aeroshell and base cover antennas were used with a multicoupler. Eleven commands with corresponding IRIG tones were used and are presented in table IV.

The camera system consisted of a Milliken camera, running at 32 frames per second, looking forward to view aeroshell separation; a Milliken camera, running at 64 frames per second, looking rearward to view parachute inflation and stability, and a Photosonics camera, running at 450 frames per second, looking directly out the rear of the test vehicle to view parachute inflation in more detail. In addition there were two cameras attached to the balloon load bar which viewed the test vehicle as it was dropped, spin rocket firing, and boost rocket ignition. In addition to providing this qualitative information, the load bar cameras were also used to measure a history of vehicle orientation for several minutes prior to test vehicle drop from ground targets which were visible in the photographs. These load bar cameras were started by the balloon operations command system. All cameras in the test vehicle were started shortly before mortar fire by the onboard programers; however, the forward camera was covered until aeroshell separation was accomplished. Targets were painted on the inside of the aeroshell (fig. 12) to assist in determining a history of relative separation distance between the aeroshell and payload from the forward camera. A correlation timer put timing marks on the film of all onboard cameras and also on the telemetry record so that correlation between these two information sources could be made.

The test-vehicle telemetry was an 18-channel S-band FM/FM-PAM system operating on a carrier frequency of 2285.5 MHz. Sixteen channels provided basic data for the experiment and two channels commutated diagnostic information. Table V(a) lists the channels and type of measurement; and tables V(b) and V(c) list the commutated channels.

Pointing System

A pointing system was mounted on the load bar structure (see fig. 8) so that the test vehicle could be pointed at the desired azimuth prior to being dropped from the balloon

load bar. This system assured that all components of the test vehicle, even considering failure modes, would have a high probability of impacting within range boundaries.

The sensors consisted of two aspect magnetometers mounted 90° apart inside the test vehicle (fig. 4(a)) so that they sensed the components of the Earth's magnetic field parallel to the Earth's surface. The system was calibrated during ground test by rotating the vehicle and recording azimuth heading in terms of voltage output from the magnetometers. A more extensive description of this azimuth sensing system may be found in reference 10. The magnetometer outputs were telemetered and azimuth heading was computed and displayed in real time on a plot board at the control center.

A system of jets was positioned at the ends of the balloon load bar as shown in figure 8 so that they could be activated by ground commands to impart either clockwise or counterclockwise rotation to the load bar. A mockup of the flight configuration was suspended from the top of the Langley lunar landing facility and tests were performed to determine the torsional characteristics of the system. These tests showed that jets of 2.7 N (0.6 lb) located at each end of the load bar would be sufficient to turn the system or stop natural system rotation within the required time interval. The test-vehicle pointing system used dry compressed nitrogen at an initial pressure of 1450 N/cm^2 (2100 psi) supplied from a tank located in the center of the load bar. A schematic of the pointing system is presented in figure 13 and some of the actual hardware may be seen in the photograph of figure 8. A system was set up at the range so that the pointing system could be operated from the range control center by transmitting commands to produce thrust pulses of variable duration from 0.1 second to 2 seconds as the center point of the oscillation was passed. The pointing system operator could observe a display of azimuth and azimuth rate on the control center plot board and could make decisions concerning pointing commands.

Prior to the flight tests a simulator was constructed and set up to train operators in the use of the pointing system. It was found that with practice, an operator could easily point the load bar at the desired azimuth and hold it by starting at 10 minutes before drop. This pointing operation could be accomplished under the worst conceivable circumstances with half of the starting supply of 4.13 kg (9.1 lb) of usable gas remaining for reserve.

BALLOON SYSTEM DESCRIPTION AND OPERATIONS

Balloon System

The balloon system was designed and launched under the direction of the U.S. Air Force Cambridge Research Laboratories. A tandem balloon system somewhat similar to that described in reference 6 was used for these tests. For the transonic and supersonic flights, a main balloon volume of 979 800 m^3 (34 600 000 ft^3) and a launch balloon

olume of 100 780 m^3 (356 000 ft^3) was required to lift the gross mass of approximately 5000 kg (13 200 lbm) to an altitude of 36 600 m (120 000 ft). The main balloon was constructed from 315 tapered sections, 191 m (627 ft) long and the launch balloon from 70 rectangular sections, 40.3 m (132 ft) long. For the subsonic test the balloon system was required to lift a gross mass of about 2800 kg (6160 lb) to an altitude of 28 400 m (93 000 ft). A main balloon volume of 118 000 m^3 (4 166 000 ft^3) and a launch balloon volume of 44 730 m^3 (158 000 ft^3) was required. Up to 545 kg (1200 lb) of pourable lead shot ballast was carried for all flights as an aid in insuring that the required pressure altitude would be attained and the balloon ascent rate could be adequately controlled. The balloons were designed to reach the required float altitude with half the ballast remaining so that ballast would remain to be dropped if necessary to attain the required float altitude. A plot showing the sensitivity of the balloon float altitude to suspended weight for both of the balloon systems is shown in figure 14.

Balloons of this size and payload weight had been unsuccessful when flown previously; therefore, an extensive study was conducted as to the proper construction materials. Most balloons larger than about 141 560 m^3 (5 000 000 ft^3) were made of Mylar reinforced with a cross pattern of dacron yarn. The yarn pattern carries the load and the Mylar serves principally to contain the gas. Much of the expansion of the helium down into the main balloon takes place at a period when the temperature is approximately -56.5° C. An analysis was conducted by using the method of reference 11 to determine the sizes and patterns of dacron scrim that would be optimum for this assignment. An extensive test program on various test specimens was generated with much of the testing being performed at -68° C. Finally, manufacturing methods were reviewed to insure that the scrap rate would be minimal. The final material selected for the 979 800 m^3 (34 600 000 ft^3) main balloons was isotropic Mylar with the transverse threads at an angle of 60° to the longitudinal threads. Details of construction of the various balloon materials may be found in figure 15. (All units in fig. 15 are in U.S. units which were used to design the materials.)

A sketch showing the balloons fully inflated at float altitude and which shows their major components is presented in figure 16. At the top of the launch balloon were two motorized helium valves which could be opened intermittently during ascent by the balloon command system to slow down temporarily the rate of ascent, if needed, for balloon piloting. The valves were also opened automatically after the test-vehicle drop to start the descent of the balloon. The dual mild detonating fuse system was used to cut a large hole in the balloon in order to bring it down in as short a time as possible. The transfer duct was a 0.762-m-diameter (30 in.) aluminum tube used to connect the two balloons together and to serve as a holddown point for the launch balloon during launch operations. The lift from the balloon system was transferred to the top of the safety parachutes through a large load takeup ring at the bottom of the main balloon. A photograph of this load ring

is shown in figure 17. The safety parachutes served to soft land the test vehicle and balloon instrumentation in the event of a forced abort. The test vehicle and load bar could be lowered to the ground at any time on the three safety parachutes by sending a command through the balloon command system which opened the parachute release (fig. 17) located at the bottom of the main balloon. The parachutes also served to soft land the balloon load bar and instrumentation after completion of the test.

Balloon Load Bar

The load bar (fig. 8) served as a means of carrying the test vehicle, the balloon instrumentation, and the pointing system. The load bar consisted of a framework of steel channels (unistruts) 0.6 m (2 ft) wide and 6 m (20 ft) long supported by flexible cables. It was designed as a very lightweight structure to carry these various items needed for the flight. The ballast consisted of up to 545 kg (1200 lb) of lead pellets, half in each ballast hopper, capable of being released in variable amounts by ground command. Care was taken to insure that the flow rate from both hoppers was the same in order that the load bar remained level. All balloon instrumentation was dual and consisted of the command system and telemetry which transmitted data from pressure sensors and thermistors and indicated voltages and valve status. A radar transponder and radiosonde unit were also included. Cameras were carried to provide information on load bar motions and attitude at release and also to photograph test vehicle release. Several ground tests were run to insure that the load bar would survive even though the launch runs were made over rough terrain and to insure ballast emptying rate was the same from each of the two ballast hoppers.

In order to determine the load bar attitude at the time of test vehicle release for AV-1, AV-2, and AV-4, a pendulum was attached to the load bar in view of the downward-facing load bar camera. It consisted of a steel ball 1.9 cm (0.75 in.) in diameter suspended from a 76 cm (30 in.) cord. With the load bar level, photographs were taken to give a calibration point prior to launch. During flight the load bar camera was turned on 3 minutes prior to drop and the pendulum and ground targets were visible in the photographs. The time was sufficient to define any pendulum motion and load bar motion so that load bar attitude at drop could be determined. Any swinging of the pendulum itself could be accounted for as it had a period of 1.75 seconds whereas the complete load bar had a period of about 17 seconds.

Balloon Launch Operations

The White Sands Missile Range (WSMR) was selected as the test location because of its large area, extensive instrumentation, and real-time computing and data reduction facilities. The Roswell Industrial Air Center (RIAC), Roswell, New Mexico, served as

the balloon launch site because of its facilities and its favorable location 160 km (100 mi) east of WSMR. The upper air at this locale is such that during the summer months, the winds above the 30.5 km (100 000 ft) level blow very consistently from east to west whereas during the winter they blow from west to east usually with higher velocity and less favorable ground winds. The RIAC is located far enough east to insure that balloon float attitude was attained before reaching the eastern boundary of WSMR.

Prior to the start of inflation, the balloons encased in their protective sleeves were laid out on a ground cloth spread out in the middle of an aircraft runway and all the various balloon components were assembled. The direction of balloon layout along the runway was determined by the predicted ground wind direction for the time of launch. At the start of inflation, helium was valved into the launch balloon through two long ducts to give a lift equal to 110 percent of the gross weight. For the supersonic and transonic tests, this volume of helium was about 6510 m^3 (230 000 ft^3) and for the subsonic test about 3120 m^3 (110 000 ft^3). During inflation, the main balloon was left encased in its protective sleeve and the launch balloon protective sleeve was slowly peeled off as the balloon was inflated and permitted to assume a vertical position. A photograph taken during inflation is presented as figure 18. After inflation the fill ducts remain attached and are tied off to prevent escape of helium. The rate at which the launch balloon was permitted to reach a vertical attitude was controlled by a cable attached to the "horse collar," a large teflon-lined ring, and pulled away from the bottom of the launch balloon. At completion of inflation the horse collar (fig. 18) was removed and the balloon was left tied down with a mainstay cable attached to the transfer duct. The mainstay cable remained in place until just prior to launch and was the means by which the launch balloon was reeled up to launch position. To monitor gas flow into the balloon and to monitor balloon lift buildup, a vibratension instrument was used on the tensioned mainstay cable. This device served to check the volumetric gas calculations. The horse collar in figure 18 was an aid during the early stages of inflation. It was anchored to a truck which could be driven toward or away from the balloon. As the gas was valved into the top of the launch balloon, and the balloon started taking shape, the horse collar was permitted to slide down toward the transfer duct and thus served as an aid to prevent sailing of the launch balloon material during the early stages of inflation. It was made in two halves so that it was easily removed when it was no longer needed. When inflation was complete and all systems checked out, the balloon was erected above the crane by use of the winch and mainstay cable. A photograph taken during this procedure is shown in figure 19. At launch the mainstay was pyrotechnically released from the transfer duct by radio command and the crane driver moved the crane to position the load bar and its payload directly under the balloon to insure that the test vehicle did not pendulum back into the ground. With the crane in position and the balloon system lifting the entire payload, balloon release was accomplished by the crane operator. At release of the mainstay, a rip was deliber-

ately started in the protective material encasing the main balloon. The protective material was such that the rip was completed as altitude was gained and the gas expanded down into the main balloon and forced the main balloon to assume its nearly spherical shape. When the balloon was in the vertical position, just prior to release, it was about 270 m (900 ft) tall. It was necessary that the winds up to the 305 m (1000 ft) level be not over 7.7 m/sec (15 knots) in order to prevent excessive speed for the launch crane and sailing of the balloon and safety parachute materials. A photograph of the balloon just after release is shown in figure 20. A table showing the component and all-up weights for all vehicles at launch is shown in table VI.

During the climbout part of the flight, the balloon floated in varying directions as it passed through the diverse wind layers. By the time the 30.5 km (100 000 ft) altitude was reached, the steady prevailing east to west wind carried the balloon system to the White Sands Missile Range. The wind structure was carefully measured and continually monitored before each flight to insure that the ground track would be acceptable.

Launch Probability

The constraints established for a balloon launch were as follows:

(1) Winds up to the 0.305 km (1000 ft) level at RIAC less than 7.7 m/sec (15 knots).

(2) Winds in the vicinity of RIAC such that the balloon system would not be carried over heavily populated areas below 6.1 km (20 000 ft) altitude.

(3) Wind structure such that the balloon would intersect the range boundary at an acceptable latitude.

(4) Sufficient time would elapse to reach float altitude before crossing range boundary but not so long a time as to exceed telemetry battery lifetime.

A probability study of meeting these launch conditions was conducted for the May to October period using wind data available from several previous years. A plot showing the likelihood of launch conditions being achieved on any given day as a function of the time of year are presented in figure 21. Meteorological data over the period 1961 to 1967 from WSMR and Holloman AFB for an altitude range up to 36.6 km (120 000 ft) and available lower level wind data from the Roswell, New Mexico, area were used to determine the individual probabilities of meeting each of the four mentioned launch conditions. Figure 21 is a composite of these probabilities. The figure shows that there is a 25- to 30-percent probability that the weather conditions will be acceptable on any given day over the period mid-June to early September.

Because of the cost of establishing field operations in consecutive summers when wind conditions were acceptable, the decision was made to maximize the probabilities for program completion in the first summer, 1972. The earliest possible date depended upon

when the high-altitude winds began blowing predictably from due east to due west. Past history indicated that the wind reversal began as early as mid-May and was complete as late as mid-June. The ability to predict wind direction was critical because of the requirement for the balloon ground track to intersect the range. If the wind direction varied more than about $\pm 20^{\circ}$ from due east, the balloon would probably not pass over the range, the test would be aborted, and the vehicle would sustain damage.

The launch opportunity window was similarly constrained at the end of the summer because of another high-altitude wind reversal. Past history indicated that the reversal started as early as mid-August and was complete by mid-September. Consequently, for planning purposes, the two-month period from mid-June to mid-August was the time of highest launch probability.

FLIGHT TESTS

Launch Operations

Initiation of launch operations began on the day prior to the scheduled launch with a sounding rocket at launch minus 24 hours for high-altitude wind speed and direction and also air pressure and temperature. Based upon this information and predictions of lower level winds at RIAC for launch day and the succeeding day, a weather briefing was held at mid-day to decide whether a launch attempt would be made. Many launch attempts were cancelled at this time. If the results of the weather briefing were favorable, launch activities were started and another weather briefing was held at minus 9 hours (9 p.m.). At the 9 p.m. weather briefing, the results of current and previous weather predictions and observations were reviewed and a decision was made regarding whether to continue launch preparation. Several launch attempts were cancelled at this time. If still favorable to launch, the test vehicle and balloon components were moved from the hangar to the required runway area. An additional weather briefing was held at launch minus 6 hours (midnight) to confirm launch conditions prior to removal of the balloons from packing boxes and layout on the runway. A few launch attempts were cancelled at this point. After checkout of test vehicle and balloon electrical circuits and instrumentation, the balloons were ready for inflation. A confirmation weather briefing was held at this time based on continuing weather predictions and observations and another high-altitude rocket launch for wind speed and direction was made. A launch time was selected based upon the predicted time for minimum velocity low-altitude winds. A range crossing point, direction and time, was also predicted and relayed to the range to insure that the proper range optical stations were manned. No launch attempts were cancelled at this time. Balloon inflation was then started, a procedure which usually took about $1\frac{1}{2}$ hours but was slowed on occasion to provide more time for the ground level winds to decay to acceptable

levels for launch. Minimum wind velocity usually occurred near sunrise. Procedures for inflation and up through balloon launch were described in a previous section.

Pointing Operations

Figure 22(a) shows predicted impact points for a nominal supersonic flight after drop. Figure 22(b) shows impact dispersion ellipses (no wind) for the aeroshell, the parachute payload, and also for a condition when the parachute did not deploy. It may be seen that the failure mode results in a horizontal distance travel which about equals the width of the range.

WSMR requirements for a test were that the test-vehicle release would not be initiated until the balloon system was 9.1 km (30 000 ft) inside the range boundary and was pointed at an azimuth so that in the event of parachute failure no part of the test vehicle or balloon system would impact off range. Also, the accessibility of many areas on the range, such as lava beds and mountain peaks, would be very difficult for recovery purposes and were to be avoided if possible.

The pointing system operator was stationed in control center with a plot board display showing the pointing position and rate. During the float period prior to drop, the amplitude of the rotational motion was determined and also the period and center point of the oscillation. As the balloon neared the range boundary, a decision was made as to the desired pointing azimuth for drop. The thrust duration was determined from previously prepared charts which accounted for these oscillation parameters. The test-vehicle pointing was started at drop minus 10 minutes, and at drop minus 5 minutes all pyrotechnic systems onboard the test vehicles were armed. The command to drop the test vehicle from the balloon was transmitted by the test conductor after obtaining concurrence from the range safety officer.

Mortar Fire Command Program

The primary mortar fire signal originated from a ground computer when the proper flight conditions were reached. As a backup, the onboard programer had a switch closure to initiate mortar fire in the event a command system failure did occur. The time for the backup mortar fire programer signal was selected to occur at a time greater than that for the maximum expected vehicle performance anomalies.

Wind velocities and density obtained from meteorological data of the previous day (launch minus 24 hours) were stored in the ground computer and used with real-time radar data to compute true airspeed and dynamic pressure. Also stored in the computer were a time history of the dynamic pressure and rate of change of altitude which were determined from a reference trajectory. Real-time data from all radar sites being used were compared by the ground computer and a prime radar was selected on the basis of smooth-

ness of the data and nearness to the mean value of all tracking radars. This real-time radar data after being filtered and converted to rate of change of altitude and dynamic pressure were compared with the corresponding quantities of the reference trajectory and the differences multiplied by sensitivity coefficients. These sensitivity coefficients were derived from preflight trajectory studies of the effects of various performance anomalies and were varied with time in such a manner that altitude change was dominant during the early part of rocket motor burning but dynamic pressure was dominant at times near mortar fire. These modified altitude rate and dynamic-pressure differences were used to predict and continuously update the time difference from the nominal for the mortar fire time that would give the desired dynamic pressure. Dynamic pressure was selected as the controlling parameter rather than Mach number because of its direct relationship to parachute loads. Time delays, such as that encountered with the command system and time for the pyrotechnic system (mortar) to develop full power, were accounted for by firing the mortar a corresponding amount earlier. Computer predictions of time to mortar fire were started at drop and were continually updated until mortar fire occurred. A definite window was established for mortar fire in order to insure that mortar fire did not occur prior to despin. In the event that the predicted mortar fire time was outside this time window, the mortar fire time was made later so that the test dynamic pressure would be lower. If the flight data (radar) fed to the computer were so noisy that the mortar fire time never appeared inside the time window, the mortar fire time would be continually made later and the mortar would eventually be fired by the mortar fire backup switch on the programer. Such a mortar fire system automatically accounted for small variations that might occur in the trajectory and automatically provided additional margin by reducing the parachute load if the radar data were oscillatory or noisy. The only remaining dispersions in dynamic pressure of any appreciable magnitude from a smooth flight resulted from uncertainty in the meteorological data. This uncertainty shown by the test dispersion ellipses in figure 3 resulted largely from the necessity of using density and wind data measured 24 hours prior to the test and possibly 80 km (50 miles) or more away from the test location. A more complete description of this computer operation may be found in reference 9. The method was restricted to the supersonic and transonic tests. For the free-fall subsonic test, the computer issued the mortar fire signal at a fixed time after drop.

Recovery

It was necessary that the parachute be recovered so that its condition could be determined as part of the assessment of its overall performance. Recovery of the payload was necessary so that the onboard camera film could be obtained. The aeroshell was recovered to enable inspection of the separation hardware and so that various components could be used in possible future tests. Recovery of the balloon load bar was

accomplished so that hardware or instrumentation could be used in a backup role for the later tests and also so that the camera film could be removed and processed for analysis. The balloon material was located after impact and destroyed.

DATA REDUCTION AND ANALYSIS METHODS

Corrections to Basic Data

Linear acceleration data were corrected for angular velocities and accelerations because the linear accelerometers were not located at the test vehicle center of gravity. In addition, it was possible to improve the accuracy of accelerometer data by making use of an in-flight calibration point. Directly after release of the test vehicle from the balloon, the test vehicle was in a "zero g" condition and the small acceleration values read at that time were subtracted from all subsequent data. In a similar manner, the bias values were removed from the angular rate measurements by using a check point just prior to release of the test vehicle from the balloon load bar after having determined from the downward viewing camera that no angular rate existed at that time. The velocity obtained from radar data was corrected to true airspeed by using the wind values measured at that altitude by meteorological rockets and radiosonde. The velocity during the period from mortar fire through parachute-full-open conditions, where velocity changes are high, were obtained by integration of the data from longitudinal accelerometers using tie-in points from radar data. Both rocketsonde and radiosonde data were adjusted to pressure data from precision pressure gages located on the balloon load bar. This method was used rather than the standard method (adjusting high-altitude meteorological rocket pressure data to that of the radiosonde balloon) because the balloon load-bar gage data are more accurate above 30 km (100 000 ft). In addition, the load-bar gage data were obtained at times and locations much closer to the test points than the rocketsonde or radiosonde data. It was necessary to use 24-hour-old atmospheric data in the computer to determine the proper dynamic pressure to command mortar fire; however, final data reductions were made from radiosondes and rocketsondes launched immediately after the test. The focal lengths and distortion characteristics of the camera lenses used were measured prior to the test and, where significant, were accounted for in the reading of photographic data.

All measurements and data work-up were made in English units. They were converted to SI units for presentation in this report.

Vehicle Dynamics Data

Time histories of vehicle Euler angles (ψ,θ,ϕ) were obtained by using the Statistical Trajectory Estimation Program (designated STEP) discussed in detail in reference 12. The data period for the application of STEP in this report extended continuously from drop, through rocket motor burning, to the time of mortar fire.

The STEP is a method of uniquely applying statistical estimation theory to fit equations of motion to measured atmospheric trajectory data. Basic data used are radar tracking and onboard accelerometer and rate gyro measurements. The STEP integrates the accelerometer and gyro data in such a manner to produce a minimum variance solution to radar position data and solve for initial conditions of vehicle attitude, position, and velocity. STEP permits estimates of biases and scale factors on the accelerometer and gyro data. For this application, biases and scale factors were estimated to give the best correlation between Euler angles from STEP and those from an independent camera technique described in reference 13. The initial conditions of θ, ψ, and ϕ were obtained just prior to drop from readup of the downward-facing load bar camera. Inputs of slant range, azimuth, and elevation were obtained from radar data. Inputs of p, q, r, a_x, a_y, and a_z were obtained from telemetered data. The biases and scale factors applied are within the accuracy limitations of the data.

To check the validity of the STEP results and to serve as a guide for the STEP analysis, Euler angle data were also obtained for brief sections of the flight by the camera method described in reference 12. Data were obtained whenever the trajectory was such that identifiable Earth landmarks were in view of the rearward-facing cameras. Using this method requires a minimum of two landmarks, the Earth-related coordinates of the vehicle, the orientation of the camera with respect to the vehicle, and the focal length and distortion characteristics of the camera lens. For these flights, atmospheric refraction corrections were determined to be negligible and were, therefore, not included.

It is assumed that the STEP Euler angles are valid throughout the data period if the STEP produced histories of velocity, altitude, flight azimuth angle, and flight-path angle closely match radar data, and the STEP Euler angles compare favorably with camera data over the very brief period prior to mortar fire that camera data are available. Values of test-vehicle angle of attack, angle of sideslip, and total angle of attack were obtained by using the STEP results coupled with wind-velocity and direction data. A similar STEP analysis of vehicle motions and trajectory beyond mortar fire is presented in reference 3.

Accuracy

The estimated accuracies of the data from the instrumentation onboard the test vehicle, and from ground-based radar, optical, and meteorological equipment are presented in table VII. The accuracies listed are not maximum values but represent a best estimate using the known accuracy of some parameters, experience from repeated usage of some other parameters, and scatter in the data. The error values apply to the altitude region of 42 700 m (140 000 ft) unless otherwise stated. The telemetered data would normally have an accuracy value of ±5 percent of full instrument range; however, by making use of certain in-flight calibration points, as previously discussed, the accuracy

of the measured accelerations and angular rates are improved so that they are believed to be within ±2 percent of full range.

Space positions were measured by FPS-16 radar and cinetheodolite. In all cases except AV-3, several radars and cinetheodolites were used on each vehicle. Velocity data were obtained by differentiations of space position and by vectorially adding the wind velocities as measured from sounding rocket data. Also, the velocity data were verified by trajectory reconstruction.

Local atmospheric conditions were measured with meteorological balloons (radiosonde) up to approximately 33 500 m (110 000 ft). From 27 500 m (90 000 ft) to in excess of 61 000 m (200 000 ft), the atmospheric conditions were obtained from meteorological rockets (rocketsonde).

Precision pressure gages carried onboard the balloon load bar give a determination of pressure within ±0.05 mb (about 1 percent) at 36 000 m (120 000 ft). (1 bar = 10^5 N/m^2.) These precision pressure-gage data were used as reference points for the rocketsonde and had the advantage of a reading near the time and location of test-vehicle release.

RESULTS AND DISCUSSION

Balloon Launches

The four balloon launches were accomplished during the summer launch window and the altitude time histories and ground tracks are presented in figures 23 and 24, respectively. There were anomalies during the flights of AV-1 and AV-3. During the balloon launch of AV-1, the winds were rather gusty and at the time of balloon reel up, the winds had shifted direction from predictions and were at an appreciable angle to the runway. During the launch crane maneuvering, it was necessary for the crane to run off the paved runway and across a drainage depression in the terrain. The resulting shock force applied to the legs of the launch support fitting caused one of them to become unseated (ball and socket arrangement) and caused slight damage to the structure. The structural damage was of no consequence but the attitude angle of the test vehicle as it was carried under the balloon was changed to a more horizontal position with the result that the trajectory of the test vehicle, after release, was lower than nominal. The abnormally low trajectory resulted in the mortar being fired by the back-up switch on the programer before the dynamic pressure had decayed to the desired value for computer firing. The dynamic pressure was above the acceptable limit and two gores were split from vent to gap as the parachute was inflated. AV-1 did not fulfill its test objectives and the back-up vehicle was readied for a repeat of the supersonic test as AV-4.

The program could not be delayed until AV-4 was made ready for launch and the transonic AV-2 test was conducted between AV-1 and AV-4.

The final launch preparations for AV-3 were carried out during light intermittent rain. At the time of launch, a moderate rain shower was in progress but winds were very light and the launch was smooth. Climb-out of the balloon was very slow and erratic, and at an altitude of about 2400 m (8000 ft), ascent ceased. The balloon remained between 2400 m (8000 ft) and 3000 m (10 000 ft) for about $1\frac{1}{2}$ hours while moving due north of the launch site. (See figs. 23 and 24.) During this period all ballast had been dropped in an attempt to make the balloon continue its ascent. It is believed that the high humidity and weight of water and/or ice collected over the entire balloon system might have caused this balloon ascent performance. Finally, the balloon started a rather steady climb, probably as it dried off, and reached a float altitude of 26 800 m (88 000 ft) $3\frac{1}{2}$ hours after launch. A time history of its rise rate may be seen in figure 23. During the $3\frac{1}{2}$ hours, the balloon had drifted about 90 km (56 miles) to the north and by the time it had reached the westerly wind flow, it was north of the range boundary and passed over the range extension. Because this flight had no rockets, there was no advantage to abort the mission; therefore, a normal drop sequence was initiated. The ground track of the balloon is presented in figure 24. During the 6-hour period between AV-3 balloon launch and drop, several radars were reassigned to a higher priority mission and only two remained to track the AV-3 test vehicle. Because of the great distance and unfavorable tracking angle for these radars, the trajectory data were of lower quality than those for previous tests. The principal source of velocity data from this flight was obtained by trajectory reconstruction, using the radar position data and acceleration data from telemetry.

The launches and flights of AV-2 and AV-4 were nominal and good tracking data were obtained. The ground tracks and altitude histories for all flights from balloon launch to test-vehicle release are shown in figures 23 and 24, respectively. Comparison of the balloon performance data with that of similar tests from reference 6 show similar ground tracks and flight times except for AV-3. The float altitudes of the balloons from reference 6, however, were about 3000 m (10 000 ft) higher, as designed.

Impact Points

Impact points of the various components for all vehicles are shown in figure 25. Lines merely connect release points with impact points and do not represent the ground track during descent. In many cases, particularly for balloon components, the radar tracking was not continuous. Recovery was carried out as mentioned under "Launch Operations." Helicopters, vectored into position by tracking radars, aided in finding various components and also were in position to photograph the parachute and payload

during final descent. Typical photographs of the parachute, the aeroshell, the balloon load bar, and the balloon material are shown in figures 26, 27, 28, and 29, respectively.

Load Bar Pendulum

The preflight calibration photographs for AV-1 were very dark and load bar level could not be established. The motion of the ball (pendulum swing) at the time of drop was very small, being less than 0.3° half amplitude in either a longitudinal or a lateral direction. Swinging motion of the load bar under the balloon was also very small and measured less than 0.5° in a longitudinal direction and no motion was visible in a lateral direction. (See fig. 8.) Swinging in a longitudinal direction is motion in and out of the plane of the figure, and lateral motion is motion in the plane of the figure from left to right.

For AV-2 and AV-4 the swinging motion of the pendulum itself and the entire load bar were less than 0.5° half amplitude. Comparison of the average pendulum position at the time of drop with the preflight calibration showed a longitudinal load bar tilt of 0° and 0.1° lateral tilt for AV-2. The reading accuracy is estimated to be $\pm 0.2^{\circ}$. For AV-4 the load bar tilt measurements were 0° longitudinally and 0.3° laterally. Lateral tilt could be caused by more ballast being dropped from the hopper on one side than from the other side. Load bar swing under the balloon measured to be $\pm 0.1^{\circ}$ laterally and $\pm 0.3^{\circ}$ in a fore-and-aft direction. A view of the pendulum as seen in the load bar camera pictures is shown in figure 30.

Launch Opportunity

The presence of some factors other than weather make it impossible to make an accurate assessment of the launch probability plot shown in figure 21. These factors consisted largely of range support restrictions and at times waiver of some launch restrictions.

Vehicle AV-1 was available for launch on June 8 and was not launched until July 11 – a delay of 33 days. The remaining launches were made between July 25 and August 19. The only conclusion possible as to the adequacy of the probability curve of figure 21 is that it showed the likelihood of making the four launches during the summer of 1972 and they were accomplished.

Pointing System

The pointing systems incorporated in vehicles AV-1, AV-2, and AV-4 performed their mission as expected. The only anomaly was in AV-2 where a slow leak developed in the system about 30 minutes after lift-off. The leak was stopped about 1 hour and 40 minutes after launch by pulsing the system once in each direction. In order to insure suffi-

cient fuel for final pointing, the azimuth-hold operation for AV-2 was not initiated until 3 minutes before drop instead of the usual 10 minutes. The rotational amplitude at this time was very small and the motion was stopped on the desired heading for drop within 1 minute. A summary of the rotational motion of the test vehicles under the balloons for approximately $1\frac{1}{2}$ hours prior to drop is presented in figure 31. The torsional characteristics of the load bar and vehicle were very similar to that determined in the preflight tests. It may be noted, however, that in addition to the expected torsional oscillation, a slow oscillation or rotation of the entire system existed. This oscillation was particularly noticeable in the case of AV-4 (fig. 31(c)) where it had an average roll rate of 25 minutes per revolution up until the time ballast was dropped.

Basic Performance Data

The basic test vehicle performance data which include meteorological data, radar, and telemetered accelerations and angular rates are presented in figures 32 to 45 for AV-1, figures 46 to 59 for AV-2, figures 60 to 71 for AV-3 and figures 72 to 85 for AV-4. These data cover not only the period up to mortar fire but also through the period of parachute inflation and for about 80 seconds afterward. The discussion of data in figures 32 to 85 is confined to the period from drop to mortar fire except for the brief period during aeroshell separation. Discussion of data during mortar fire, parachute deployment, and the period following deployment is covered in reference 1. A tabulation of times for pertinent events and method of initiation is presented in table VIII. A summary of the flight Mach number and dynamic pressure attained are plotted on the envelope of Mars conditions in figure 86. Comparison of figure 86 with figure 3 shows that the required mortar fire and peak load test conditions were achieved for AV-2, AV-3, and AV-4. As previously mentioned, the mortar fire conditions for AV-1 were appreciably in excess of required conditions. Figure 86 also shows that aeroshell separation bracketed the desired test conditions.

Comparison of the meteorological data above 34 km (110 000 ft) for all vehicles shows that the air temperature for the AV-1 flight averages about 2° less than that for AV-2 or AV-4. However, this difference is well within the variation to be expected at this altitude. Comparison of the altitude time history of AV-1 and AV-4 shows clearly the lower altitude of AV-1 which was caused by the flight anomaly mentioned previously. This condition is also evident in comparing the flight-path angle of AV-1 in figure 38 with that of AV-4 in figure 78. A comparison of figure 52 with figure 78 shows the difference of flight-path angle history of the two-motor configuration, AV-2, and the four-motor configuration, AV-4. The attitude angle of drop was 65° for AV-2 and 55° for AV-4. This difference in drop angle allowed the flight-path angle during the test period to be approximately the same for both tests. The peak velocity and Mach number of AV-4 (figs. 75 and 76) are slightly higher than those for AV-1 (figs. 35 and 36), because of the lower total

drag at the slightly higher altitude. This condition is also noted in comparing figure 37 with figure 77 which shows that the peak dynamic pressure for AV-1 is greater than that for AV-4. Figure 37 shows that the dynamic pressure had not decayed to the required test level at the time the programers initiated mortar fire in the AV-1 flight. In extrapolating the AV-1 dynamic pressure prior to mortar fire to the required mortar fire value of 565 N/m^2 (11.8 lb/ft^2), it is noted that mortar fire would have been initiated at about 42 seconds if the computer had sent the signal. It was, however, preempted by tne back-up switch on the programer which closed at 38.31 seconds when the dynamic-pressure value was 670 N/m^2 (14 lb/ft^2) – an overload of 62 percent of the then defined worst expected case for Mars. It may be noted that the yaw rate assumes a small negative trim value for AV-1, AV-2, and AV-4 after spin-up and then effectively returns to zero after despin. This negative value is the result of the pitch-down moment caused by the drag-force vector not passing through the center of gravity. Such a pitch-down moment on a body rolling in a positive direction causes a negative yawing moment.

In figures 43, 57, and 83, it is noted that in all cases rocket thrust had ceased by 35 seconds, which is some 3 seconds before mortar fire. In no test was there evidence that afterburning from the rocket motors affected the bridles, base cover, or parachute. However, there were a few small holes (6.35 mm (0.25 in.) diameter) in each of the parachutes which probably came from particles jarred loose from the rocket motors by the mortar ignition shock.

In all plots the data from continuous telemetered channels has been smoothed by a 29-point least-squares method to remove noise. The data which was smoothed was sampled at 0.01-second intervals. However, during the period from just prior to mortar fire until after aeroshell separation, the data presented in all angular rate plots and acceleration plots are unfiltered in order to insure that all peak values are accurate.

The temperatures at 18 locations throughout the test vehicle were measured, as a possible aid in diagnosing anomalies in performance of the test vehicle, and are listed in table IX. A sketch showing these locations is presented as figure 87. The temperature readings for AV-1, AV-2, and AV-4 start at about 30 minutes after balloon launch; however, the first reading for AV-3 is over 2 hours after balloon launch. The temperatures of most AV-3 components were cooler than the corresponding temperatures on the other vehicles because of the long float time for AV-3. The thin aeroshell skin, however, in all cases reached a constant temperature in a comparatively short period of time. All temperatures were within the desired limits.

Aeroshell Separation

The aeroshells were separated from the payloads at about 9 seconds after mortar fire for AV-1, AV-2, and AV-4 and at about 14 seconds after mortar fire for the free-fall test

for AV-3. The separation hardware was the same as that to be used on Viking and these separation tests were to be proof tests of this hardware. The test conditions at aeroshell separation for all vehicles are shown in figure 86 and are compared with expected Mars conditions. A Viking specification was that a minimum separation of 15.24 m (50 ft) should be accomplished in 3 seconds. Figure 88 shows that the slowest separation (AV-3) was almost double the minimum requirement. The separation distances in figure 88 were determined by the extensiometers for the first 30.5 cm (12 in.) and from separation velocity. Separation velocity was determined from the size of the aeroshell in photographs taken by the forward-viewing camera, and by radar and, in some cases, theodolite tracking. The three extensiometers spaced 120^{o} apart as shown in figure 12 were used to give a measure of the angular displacement (cocking) of the aeroshell as it came off the guide rails. References 14, 15, 16, and 9 present detailed results of the aeroshell separation and angular misalinement. It will be noted in figures 40 and 41 for AV-1 and figures 80 and 81 for AV-4 that the angular velocity of the test vehicle has damped very little at the time of aeroshell separation. This condition causes relative angular motion between aeroshell and payload during the aeroshell separation. The angular velocities at the time of aeroshell separation are appreciably lower for AV-2 and AV-3 (figs. 54, 55, 66, and 68).

Vehicle Dynamics

A time history of the test-vehicle attitude angles and angles of attack are of interest throughout the entire rocket motor burning period because of the desire for the angle of attack at mortar ignition to be about the same as that expected for the Viking entry vehicle. Although there was no active system onboard the test vehicle to control angle of attack, it was expected that the test-vehicle angle of attack would be similar to that of the Viking entry vehicle if the rocket motors did not develop unexpected thrust misalinements. Read-up of data from the rearward-facing cameras gave test-vehicle attitude angles for a very short period of time during motor burning because they were not turned on until shortly before mortar fire. Near the time of mortar fire, the flight-path angle was very low so that the only landmarks visible to the camera are very far away. This distance made identification of landmarks very difficult. In the case of AV-1, AV-2, and AV-4, however, it was possible to obtain some attitude angle data from cameras. AV-3 was dropped with the longitudinal axis vertical so no landmarks were visible in the rearward-viewing cameras.

Time histories of Euler angles (θ, ψ, and ϕ), altitude, velocity, flight-path angle, and flight azimuth angle were obtained from the STEP program previously mentioned.

The initial conditions used in the STEP calculations, which started at drop, are presented in table X. Trajectory parameters were obtained from radar and attitude-angle data from load bar camera and magnetometer. The biases and scale factors used

for each of the test vehicles are also shown in table X. Figures 89 to 93 present the STEP data up to the time of mortar fire for AV-1. It may be noted that agreement with camera data is good for all quantities except for ψ where the difference is about 4^{o} at mortar fire. Variations of the biases and scale factors were tried in an attempt to better this agreement. In all cases, however, any changes which improved the agreement of the azimuth caused larger disagreement in the roll angle or pitch angle. Mean deviations and standard deviations from the mean deviation for AV-1, AV-2, and AV-4 are presented in table XI. The Euler angles and flight parameters in conjunction with the measured wind profile were used to compute time histories of α, β, and η shown in figures 94 to 96 for AV-1. In figure 93 the reason that the roll-attitude trace does not go completely out to $\pm 180^{o}$ before changing polarity is because STEP points are calculated every 0.01 second but they are printed every 0.2 second and the printer connects all points. Thus if it printed a point at 165^{o} while rolling at 200^{o} per second, it would be at 205^{o} at 0.2 second later so the printer would print the point at -155^{o}. In figure 95 it will be noted that the angle of sideslip trims about zero as expected but the angle-of-attack trim value as shown in figure 94 varies from about 9^{o} at 15 seconds out to about 8^{o} at rocket burnout because of the vehicle center of gravity not being on the vehicle axis of symmetry.

Figures 97 to 101 present the flight data for AV-2 and agreement in Euler angles with camera data is within about 1^{o} over the period that camera data are available. Time histories of angle of attack and sideslip for AV-2 are presented in figures 102 and 103. Comparison of the total angle-of-attack history for AV-2 (fig. 104) with the corresponding time history for AV-1 (fig. 96) shows that the total angle of attack for AV-2 took a much longer time to reach a point where it oscillated about its approximately 7^{o} trim value than did AV-1. This effect is partly because its value at rocket motor ignition is 10^{o} larger than AV-1 (because of difference in angle carried under the balloon) and partly because of its lower acceleration along the longitudinal axis. Even in the case of AV-2, however, the total angle of attack is reduced so that it oscillates about the trim value considerably in advance of despin. It may be noted in figure 104 that there is considerable increase in amplitude of the total angle-of-attack oscillations after despin (33.2 sec) which was predicted during preflight analysis. The low transonic damping coefficient is the primary cause of this large increase in total angle of attack.

Figures 105 to 109 present the flight data for AV-4 which is very similar in agreement with camera data as were the data from AV-1. The difference between STEP data and camera data in figure 107 is about 1^{o} in pitch and about 4^{o} in yaw. The damping of the angle-of-attack and angle-of-sideslip oscillations in figures 110 and 111 is also very similar to that for AV-1 and much more heavily damped than that for AV-2. As was the case for AV-1 and AV-2, the total angle of attack (fig. 112) increases appreciably after despin. The time history of total angle of attack for all three test vehicles (figs. 95, 104, and 112) shows how little control exists on the angle of the test vehicle with the free air-

stream at the time of mortar fire. The oscillation total amplitude at mortar fire is 10^{o} to 20^{o} with no way of predicting where on the cycle the test vehicle will be at the time of mortar fire. Fortunately, the angle of attack at mortar fire for each test was neither zero nor greatly in excess of that expected for the Viking entry vehicle and the parachute therefore was subjected to a valid test, especially since the tests were conducted at test conditions with margin. Similar STEP simulations and angle-of-attack determinations were not attempted for AV-3 because there was no correlative camera data.

CONCLUSIONS

Four flight qualification tests of the Viking parachute were conducted behind a simulated Viking spacecraft; these tests bracketed a range of Mach numbers and dynamic pressures postulated for the Viking '75 mission to Mars. Conclusions from these tests as to the performance of the balloon-launched test vehicles are as follows:

1. On the first test a shock load at balloon launch changed the pitch attitude at which the test vehicle was carried under the balloon and caused parachute test conditions to be exceeded.

2. In all cases the balloon system carried the test vehicle to the required altitude.

3. The required parachute test conditions for supersonic, transonic, and subsonic tests were achieved by using a ground command system coupled to a real-time computer to initiate parachute deployment.

4. In all cases the balloon load bar was within 1^{o} of level at the time the test vehicle was dropped. The swinging motion of the load bar under the balloon was less than 1^{o}.

5. A simple arrangement using aspect magnetometers and cold gas jets operated by ground command was successful in pointing the test vehicle at the required azimuth for release from the balloon.

6. Aeroshell separations took place in all tests with much greater than the minimum required separation velocity even though motion of the payload under the parachute at the time the separation was initiated was in most cases higher than expected.

7. Trajectory reconstruction methods combined with methods for reading vehicle attitude from onboard cameras were used to give a continuous history of test-vehicle Euler angles and angles to the airstream. The results up through the time of mortar firing show the test-vehicle performance and stability to be nominal.

Langley Research Center,
National Aeronautics and Space Administration,
Hampton, Va., June 10, 1974.

REFERENCES

1. Bendura, Richard J.; Lundstrom, Reginald R.; Renfroe, Philip G.; and LeCroy, Stewart R.: Flight Tests of Viking Parachute System in Three Mach Number Regimes. II – Parachute Test Results. NASA TN D-7734, 1974.

2. Steinberg, Sy; Siemers, Paul M., III; and Slayman, Robert G.: Development of the Viking Parachute Configuration by Wind Tunnel Investigation. AIAA Paper No. 73-454, May 1973.

3. Murrow, H. N.; Eckstrom, C. V.; and Henke, D. W.: Development Flight Tests of the Viking Decelerator System. AIAA Paper No. 73-455, May 1973.

4. Moog, R. D.; and Michel, F. C.: Balloon Launched Viking Decelerator Test Program Summary Report. TR-3720359 (Contract NAS 1-9000), Martin Marietta Corp., Mar. 1973. (Available as NASA CR-112288).

5. Henning, Allen B.; and Lundstrom, Reginald R. (With appendix A by James C. Young): Flight Test of an Erectable Spacecraft Used for Decelerator Testing at Simulated Mars Entry Conditions. NASA TN D-6910, 1972.

6. Lundstrom, Reginald R.; Darnell, Wayne L.; and Henning, Allen B.: Large-Scale Decelerator Flight Tests Simulating a Mars Environment. J. Spacecraft & Rockets, vol. 5, no. 9, Sept. 1968, pp. 1106-1108.

7. Brecht, John P.; Pleasants, James E.; and Mehring, Richard D.: The Viking Mortar: Design, Development, and Flight Qualification. AIAA Paper No. 73-458, May 1973.

8. Brown, Clarence A., Jr.; and Campbell, James F.: Experimental Wake Survey Behind a 140°-Included-Angle Cone at Angles of Attack of 0° and 5°, Mach Numbers From 1.60 to 3.95, and Longitudinal Stations Varying From 1.0 to 8.39 Body Diameters. NASA TM X-2409, 1971.

9. Dickinson, D.; Schlemner, J.; Hicks, F.; Michel, F.; and Moog, R. D.: Balloon Launched Decelerator Test Program – Post-Test Test Report (45 Day) – BLDT Vehicle AV-4. TR-3720295 (Contract NAS 1-9000), Martin Marietta Corp., Oct. 1972. (Available as NASA CR-112179.)

10. Darnell, Wayne L.: Use of a Magnetic Azimuth-Indicator System Developed for Balloon Payloads of the Planetary Entry Parachute Program. Proceedings AFCRL Scientific Balloon Symposium, Lewis A. Grass, ed., AFCRL 68-0661, U.S. Air Force, Dec. 1968, pp. 75-86. (Available from DDC as AD 685 726.)

11. Alley, V. L., Jr.: Analysis of Yarn Reinforced Laminate for Balloons and Other Structural Uses. Proceedings Seventh AFCRL Scientific Balloon Symposium, George F. Nolan, ed., AFCRL-TR-73-0071, U.S. Air Force, Jan. 3, 1973, pp. 415-448. (Available from DDC as AD 767 582.)

12. Wagner, William E.; and Serold, Arno C.: Formulation on Statistical Trajectory Estimation Programs. NASA CR-1482, 1970.

13. Bendura, Richard J.; and Renfroe, Philip, G.: A Data Reduction Technique and Associated Computer Program for Obtaining Vehicle Attitudes With a Single Onboard Camera. NASA TM X-3050, 1974.

14. Dickinson, D.; Schlemmer, J.; Hicks, F.; Michel, F.; and Moog, R. D.: Balloon Launched Decelerator Test Program – Post-Flight Test Report – BLDT Vehicle AV-1. TR 3720289 (Contract NAS 1-9000), Martin-Marietta Corp., Sept. 1972. (Available as NASA CR-112176.)

15. Dickinson, D.; Schlemmer, J.; Hicks, F.; Michel, F.; and Moog, R. D.: Balloon Launched Decelerator Test Program – Post-Flight Test Report – BLDT Vehicle AV-2. TR-3720291 (Contract NAS 1-9000), Martin-Marietta Corp., Dec. 1972. (Available as NASA CR-112177.)

16. Dickinson, D.; Schlemmer, J.; Hicks, F.; Michel, F.; and Moog, R. D.: Balloon Launched Decelerator Test Program – Post-Flight Test Report – BLDT Vehicle AV-3. TR-3720293 (Contract NAS 1-9000), Martin-Marietta Corp., Jan. 1973. (Available as NASA CR-112178.)

TABLE I.- SUMMARY OF QUALIFICATION TESTS

Test designation	Test condition	Launch date	Launch time, G.M.T.	Main balloon size, m^3 (ft^3)	Comment
AV-1	Supersonic	7/11/72	Balloon, 14 hr:35 min; test-vehicle drop, 17 hr:37 min:13.8 sec	979 500 (34 600 000)	Parachute damage due to excessive test condition
AV-2	Transonic	7/26/72	Balloon, 14 hr:03 min; test-vehicle drop, 16 hr:55 min:33.7 sec	979 500 (34 600 000)	Successful
AV-3	Subsonic	8/19/72	Balloon, 11 hr:45 min; test-vehicle drop, 17 hr:45 min:00.6 sec	118 000 (4 166 000)	Successful
AV-4 (repeat of AV-1)	Supersonic	8/13/72	Balloon, 13 hr:40 min; test-vehicle drop, 16 hr:24 min:30.8 sec	979 500 (34 600 000)	Successful

TABLE II.- MASS PROPERTIES

(a) AV-1

Condition	Mass, kg (lbm)	Center of gravity, cm (in.)			Moment and product of inertia, kg-m^2 (slug-ft^2)					
		x'*	y	z	I_{XX}	I_{YY}	I_{ZZ}	P_{XY}	P_{XZ}	P_{YZ}
At drop from load bar	1527.3 (3367)	88.70 (34.92)	0	-3.58 (-1.41)	782 (577)	668 (493)	552 (407)	0.58 (0.43)	2.35 (1.73)	0.34 (0.25)
At mortar fire	860.0 (1896)	86.31 (33.98)	0	-3.58 (-1.41)	595 (439)	473 (349)	456 (336)	.58 (.43)	2.35 (1.73)	.22 (.16)
With decelerator deployed	816.9 (1801)	83.41 (32.84)	0	-3.58 (-1.41)	592 (437)	454 (335)	437 (322)	.62 (.46)	2.36 (1.73)	.22 (.16)
With decelerator deployed and aeroshell dropped	655.9 (1446)	92.61 (36.46)	0	-4.47 (-1.76)	335 (262)	308 (227)	290 (214)	.58 (.43)	5.23 (3.86)	-.23 (-.17)

*Measured from test vehicle theoretical apex.

(b) AV-2

Condition	Mass, kg (lbm)	Center of gravity, cm (in.)			Moment and product of inertia, kg-m^2 (slug-ft^2)					
		x'*	y	z	I_{XX}	I_{YY}	I_{ZZ}	P_{XY}	P_{XZ}	P_{YZ}
At drop from load bar	1194.8 (2634)	87.05 (34.27)	0	-3.58 (-1.41)	685 (505)	561 (414)	500 (369)	0.46 (0.34)	1.48 (1.09)	35.5 (26.2)
At mortar fire	860.5 (1897)	85.22 (33.55)	0	-3.58 (-1.41)	590 (435)	462 (341)	449 (331)	.49 (.36)	1.48 (1.09)	-.24 (-.18)
With decelerator deployed	817.4 (1802)	82.25 (32.38)	0	-3.58 (-1.41)	588 (434)	446 (329)	433 (319)	.56 (.41)	1.48 (1.09)	-.24 (-.18)
With decelerator deployed and aeroshell dropped	655.5 (1445)	91.29 (35.92)	0	-4.47 (-1.76)	347 (256)	297 (219)	283 (209)	.76 (.56)	4.23 (3.12)	-.43 (-.52)

*Measured from test vehicle theoretical apex.

TABLE II.- MASS PROPERTIES - Concluded

(c) AV-3†

Condition	Mass, kg (lbm)	Center of gravity, cm (in.)			Moment and product of inertia, kg-m² (slug-ft²)					
		x'*	y	z	I_{XX}	I_{YY}	I_{ZZ}	P_{XY}	P_{XZ}	P_{YZ}
At drop from load bar	862.3 (1901)	84.68 (33.34)	0.15 (0.06)	-3.43 (-1.35)	555 (409)	460 (339)	401 (296)	-0.07 (-0.05)	1.33 (0.98)	1.45 (1.07)
At mortar fire	862.3 (1901)	84.68 (33.34)	.15 (.06)	-3.43 (-1.35)	555 (409)	460 (339)	401 (296)	-.07 (-.05)	1.33 (.98)	1.45 (1.07)
With decelerator deployed	819.2 (1806)	81.69 (32.16)	.15 (.06)	-3.43 (-1.35)	553 (408)	443 (327)	385 (284)	0	1.33 (.98)	1.45 (1.07)
With decelerator deployed and aeroshell dropped	659.5 (1454)	90.35 (34.57)	.13 (.05)	-4.29 (-1.69)	273 (201)	297 (219)	237 (175)	-.12 (-.09)	3.89 (2.87)	1.49 (1.10)

†Properties do not include ice which accumulated on and in this vehicle passing through rainstorms during ascent. This weight was estimated to be 12 kg ± 5 kg.

*Measured from test vehicle theoretical apex.

(d) AV-4

Condition	Mass, kg (lbm)	Center of gravity, cm (in.)			Moment and product of inertia, kg-m² (slug-ft²)					
		x'*	y	z	I_{XX}	I_{YY}	I_{ZZ}	P_{XY}	P_{XZ}	P_{YZ}
At drop from load bar	1527.7 (3368)	88.67 (34.91)	0	-3.58 (-1.41)	782 (577)	668 (493)	552 (407)	0.58 (0.43)	2.35 (1.73)	0.34 (0.25)
At mortar fire	860.5 (1897)	86.31 (33.98)	0	-3.58 (-1.41)	595 (439)	473 (349)	456 (336)	.58 (.43)	2.35 (1.73)	.22 (.16)
With decelerator deployed	817.4 (1802)	83.39 (32.83)	0	-3.58 (-1.41)	592 (437)	454 (335)	437 (322)	.62 (.46)	2.35 (1.73)	.22 (.16)
With decelerator deployed and aeroshell dropped	655.9 (1446)	92.63 (36.47)	0	-4.97 (-1.76)	355 (262)	308 (227)	290 (214)	.58 (.43)	5.23 (3.86)	-.23 (-.17)

*Measured from test vehicle theoretical apex.

TABLE III.- NOMINAL EVENT TIMES (SECONDS AFTER DROP)

(a) Flights AV-1, AV-2, and AV-4

Event	AV-1	AV-2	AV-4	Initiation method
(1) Drop from load bar Start programer	0	0	0	Command
(2) Ignite spin motors Arm rocket motors	1.0	1.0	1.0	Programer
(3) Ignite rocket motors	2.0	2.0	2.0	Programer
(4) Ignite despin motors Release camera lens covers Start rear Milliken camera	33.0	33.0	33.0	Programer
(5) Ignite parachute mortar Start Photosonics camera Start forward Milliken camera	33.5 to 38.5	33.5 to 42.0	33.5 to 39.5	Ground command
(6) Backup for items (5) Ignite parachute mortar Start Photosonics camera Start forward Milliken camera	38.0	41.0	39.0	Programer
(7) Separate aeroshell	47.6	48.0	47.0	Programer
(8) All current off	400.0	400.0	400.0	Programer

(b) Flight AV-3

Event	AV-3	Initiation method
(1) Drop from load bar Start programer	0	Command
(2) Start rear Milliken camera Arm mortar	12.0	Programer
(3) Ignite parachute mortar Start Photosonics camera Start forward Milliken camera	16.4	Ground command
(4) Backup for items (3) Ignite parachute mortar Start Photosonics camera Start forward Milliken camera	18.0	Programer
(5) Separate aeroshell	30.0	Programer
(6) All current off	400.0	Programer

TABLE IV.- CHANNELS USED ON TEST VEHICLE COMMAND SYSTEM

Command	IRIG* tones	Remarks
Point clockwise	1, 3, 6	Manual command
Point counterclockwise	1, 5, 6	Manual command
Arm	1, 2, 6	Manual command
Safe	1, 4, 6	Manual command
Radio frequency on	1, 2, 7	Manual command
Radio frequency off	1, 6, 7	Manual command
Drop	1, 3, 7	Manual command
Mortar fire	1, 4, 5	Computer generated command
Safe (backup)	1, 2, 4	Manual command
Point clockwise (backup)	1, 2, 3	Manual command
Point counterclockwise (backup)	1, 2, 5	Manual command

*Inter-Range Instrumentation Group.

TABLE V.- TELEMETRY MEASUREMENTS

(a) Continuous telemeter channels

IRIG channel	Function	Range
4	Magnetometer 2	$\pm 180^{o}$
5	Magnetometer 1	$\pm 180^{o}$
6	Aeroshell separation distance 3	0 to 30.5 cm (12 in.)
7	Aeroshell separation distance 2	0 to 30.5 cm (12 in.)
8	Aeroshell separation distance 1	0 to 30.5 cm (12 in.)
9	Angular rate, yaw	$\pm 300^{o}$/sec
10	Angular rate, pitch	$\pm 300^{o}$/sec
11	Angular rate, roll	$\pm 300^{o}$/sec
12	Linear acceleration, $\ddot{z}$	$\pm$1.0g
13	Linear acceleration, $\ddot{y}$	$\pm$1.0g
14	Linear acceleration, low range, $\ddot{x}$ (AV-1, AV-4)	-2.0 to 5.0g
14	Linear acceleration, low range, $\ddot{x}$ (AV-2, AV-3)	-2.0 to 3.0g
15	Linear acceleration, high range, $\ddot{x}$ (AV-1, AV-4)	-15 to 1.0g
15	Linear acceleration, high range, $\ddot{x}$ (AV-2, AV-3)	-7 to 1.0g
16	Tensiometer 3 (AV-1, AV-4)	0 to 80 000 N (18 000 lbf)
16	Tensiometer 3 (AV-2, AV-3)	0 to 53 400 N (12 000 lbf)
17	Tensiometer 2 (AV-1, AV-4)	0 to 80 000 N (18 000 lbf)
17	Tensiometer 2 (AV-2, AV-3)	0 to 53 400 N (12 000 lbf)
18	Tensiometer 1 (AV-1, AV-4)	0 to 80 000 N (18 000 lbf)
18	Tensiometer 1 (AV-2, AV-3)	0 to 53 400 N (12 000 lbf)
19	Camera time code generator	0 to 1.25 V dc
20	Commutator 1 (PAM 30 × 30)	----------
21	Commutator 2 (PAN 30 × 30)	----------

TABLE V.- TELEMETRY MEASUREMENTS – Continued

(b) Commutator channel assignment list; commutator 1

Commutator channel	Function	Range
1	Zero calibration	0 V dc
2	Full-scale calibration	5 V dc
3	Spare	----------
4	Rate gyro temperature, T-1	-18° to 52° C (0° to 125° F)
5	Boost motor 1 temperature, T-2	-74° to 66° C (-100° to 150° F)
6	Equipment ballast temperature, T-3	-18° to 79° C (0° to 175° F)
7	S-band transmitter temperature, T-4	-18° to 79° C (0° to 175° F)
8	Equipment beam 1 temperature, T-5	-18° to 52° C (0° to 125° F)
9	Bridle 1 temperature, T-6	-68° to 99° C (-90° to 210° F)
10	Command decoder 1, tone 1	0 to 5 V dc
11	Command receiver AGC	0 to 4 V dc
12	Arm command, A	0 to 4 V dc
13	Safe command, A	0 to 4 V dc
14	Clockwise pointing command	0 to 4 V dc
15	Counterclockwise pointing command	0 to 4 V dc
16	Arm command, B	0 to 4 V dc
17	Safe command, B	0 to 4 V dc
18	Mortar command	0 to 28 V dc
19	Programer A reset	0 to 14 V dc
20	Programer B reset	0 to 14 V dc
21	Programer A TM out	0 to 14 V dc
22	Programer B TM out	0 to 14 V dc
23	Transient battery voltage	0 to 33.5 V dc
24	Pointing pressure	0 to 170 atmospheres
25	Main battery current	0 to 16 A
26	Main battery voltage	0 to 36 V dc
27	Pyro. battery A voltage	0 to 37 V dc
28	Pyro. battery B voltage	0 to 37 V dc
29	Frame synchronization	----------
30	Frame synchronization	----------

TABLE V.- TELEMETRY MEASUREMENTS – Concluded

(c) Commutator channel assignment list; commutator 2

Commutator channel	Function	Range
1	Zero calibration	0 to 5 V
2	Full-scale calibration	0 to 5 V
3	Spare	
4	Aeroshell 1 temperature, T-7	-74° to 66° C (-100° to 150° F)
5	Boost motor 2 temperature, T-8	-74° to 66° C (-100° to 150° F)
6	Mortar canister 1 temperature, T-9	-68° to 99° C (-90° to 210° F)
7	Mortar breech temperature, T-10	-4° to 66° C (25° to 150° F)
8	Spare	----------
9	Equipment beam 2 temperature, T-11	-18° to 52° C (0° to 125° F)
10	Bridle 2 temperature, T-12	-68° to 99° C (-90° to 210° F)
11	Command decoder 2, tone 1	0 to 5 V dc
12	Command decoder 2, tone 2	0 to 5 V dc
13	Spare	----------
14	Command decoder 1, tone 3	0 to 5 V dc
15	Command decoder 2, tone 4	0 to 5 V dc
16	Command decoder 2, tone 5	0 to 5 V dc
17	Command decoder 1, tone 6	0 to 5 V dc
18	Spare	----------
19	Command decoder 2, tone 7	0 to 5 V dc
20	Full-scale calibration 3	0 to 5 V dc
21	Aeroshell 2 temperature, T-13	-74° to 66° C (-100° to 150° F)
22	Motor support structure temperature, T-14	-74° to 66° C (-100° to 150° F)
23	Spare	----------
24	Mortar canister 2 temperature, T-15	-68° to 99° C (-90° to 210° F)
25	Mortar breech flange temperature, T-16	-4° to 66° C (25° to 150° F)
26	Main battery temperature, T-17	-18° to 79° C (0 to 175° F)
27	Bridle 3 temperature, T-18	-68° to 99° C (-90° to 210° F)
28	Spare	----------
29	Frame synchronization	----------
30	Frame synchronization	----------

TABLE VI.- MASS BREAKDOWN AT BALLOON LAUNCH

(a) AV-1

Balloon masses	kg	lb	Parachute(s) masses	kg	lb
Strobe light (on valve)	3.2	(7.00)	Test vehicle	1525.9	(3364.00)
Balloon valve(s)	5.9	(13.00)	Interface structure	47.6	(105.00)
EV-13 modified valve plate	7.3	(16.00)	Pointing system with gas	55.3	(122.00)
Launch balloon	421.8	(930.00)	Instrumentation package A	25.4	(56.00)
Transfer duct	75.3	(166.00)	Instrumentation package B	25.4	(56.00)
Mainstay cable 2.54 cm (1 in.) Hi-Shear	2.3	(5.00)	Instrumentation bar cable	1.4	(3.00)
Main balloon	3105.0	(6647.00)	Milliken down camera 1	16.3	(36.00)
Clevis 2.2 cm (7/8 in.)	1.6	(3.5)	Radiosonde	5.4	(12.00)
Korn multiple parachute release	5.9	(13.00)	Payload strobe light	2.7	(6.00)
Radar reflector	2.7	(6.00)	Ballast hopper 1	8.2	(18.00)
Total balloon masses	3541.2	(7807.00)	Ballast hopper 2	8.2	(18.00)
Chute masses less ballast	2116.0	(4665.00)	Loadbar with brackets	87.1	(192.00)
Total pourable ballast	544.3	(1200.00)	Loadbar cables	26.3	(58.00)
Maximum parachute descent load	2660.3	(5865.00)	Clevis 2.54 cm (1 in.)	2.3	(5.00)
Gross mass	6201.5	(13 672.00)	Heavy load release plate	2.7	(6.00)
Free lift (10 percent of gross mass)	620.1	(1367.00)	Clevis 2.9 cm $\left(1\frac{1}{8}\text{ in.}\right)$	3.2	(7.00)
Gross lift	6821.5	(15 039.00)	Parachute, 0.48 m (100 ft), no. 3	81.6	(180.00)
Allowance (leakage and so forth, 3 percent)	204.6	(451.00)	Parachute, 30.48 m (100 ft), no. 2	81.6	(180.00)
Total lift at launch	6617.0	(14 588.00)	Parachute, 30.48 m (100 ft), no. 1*	108.9	(240.00)
			Total mass on recovery parachutes (less ballast)	2116.0	(4665.00)

(b) AV-2

Balloon masses	kg	lb	Parachute(s) masses	kg	lb
Strobe light (on valve)	3.2	(7.00)	Test vehicle	1205.2	(2657.00)
Balloon valve(s)	5.9	(13.00)	Interface structure	39.9	(88.00)
EV-13 modified valve plate	7.3	(16.00)	Pointing system with gas	55.3	(122.00)
Launch balloon	423.2	(933.00)	Instrumentation package A	25.4	(56.00)
Transfer duct	76.2	(168.00)	Instrumentation package B	25.4	(56.00)
Transfer duct blanket	2.3	(5.00)	Instrumentation bar cable	1.4	(3.00)
Mainstay cable 2.54 cm (1 in.) Hi-Shear	2.3	(5.00)	Milliken DBM-54 Dw cam 1	16.3	(36.00)
Main balloon	2989.6	(6591.00)	Milliken DBM-54 Dw cam 2	20.0	(44.00)
Clevis 2.2 cm (7/8 in.)	1.8	(4.00)	Radiosonde	2.7	(6.00)
Korn multiple parachute release	5.9	(13.00)	Payload strobe light	1 8	(4.00)
Radar reflector	2.7	(6.00)	Ballast hopper 1	8.2	(18.00)
Total balloon masses	3520.3	(7761.00)	Ballast hopper 2	8.2	(18.00)
Parachute masses less ballast	819.9	(3985.00)	Loadbar with brackets	91.2	(201.00)
Total pourable ballast	544.3	(1200.00)	Loadbar cables	26.3	(58.00)
Maximum parachute descent load	2351.9	(5185.00)	Clevis 2.54 cm (1 in.)	2.3	(5.00)
Gross mass	5872.2	(12 946.00)	Heavy load release plate	2.7	(6.00)
Free lift (10 percent of gross mass)	587.4	(1295.00)	Clevis 2.9 cm $\left(1\frac{1}{8}\text{ in.}\right)$	3.2	(7.00)
Gross lift	6459.6	(14 241.00)	Parachute, 30.48 m (100 ft), no. 3	81.6	(180.00)
Allowance (leakage and so forth, 3 percent)	193.7	(427.00)	Parachute, 30.48 m (100 ft), no. 2	81.6	(180.00)
Total lift at launch	6265.9	(13 814.00)	Parachute, 30.48 m (100 ft), no. 1*	108.9	(240.00)
			Total mass on recovery parachutes (less ballast)	1807.6	(3985.00)

*Includes mass of electric cables up to valves, mainstay release, etc.

TABLE VI.- MASS BREAKDOWN AT BALLOON LAUNCH – Concluded

(c) AV-3

Balloon masses	kg	lb
Strobe light (on valve)	3.2	(7.00)
Balloon valve(s)	5.9	(13.00)
EV-13 modified valve plate	7.3	(16.00)
Launch balloon	263.1	(580.00)
Transfer duct	75.3	(166.00)
Transfer duct blanket	3.6	(8.00)
Mainstay cable 2.54 cm (1 in.) Hi-Shear	6.8	(15.00)
Main balloon	915.3	(2018.00)
Clevis 2.2 cm (7/8 in.)	1.8	(4.00)
Korn multiple parachute release	5.9	(13.00)
Radar reflector	2.7	(6.00)
Total balloon masses	1290.9	(2846.00)
Parachute masses less ballast	1326.8	(2925.00)
Total pourable ballast	226.8	(500.00)
Maximum parachute descent load	1553.5	(3425.00)
Gross mass	2844.5	(6271.00)
Free lift (10 percent of gross mass)	284.4	(627.00)
Gross lift	3128.9	(6898.00)
Allowance (leakage and so forth, 3 percent)	93.9	(207.00)
Total lift at launch	3035.0	(6691.00)

Parachute(s) masses	kg	lb
Test vehicle	866.4	(1910.00)
Interface structure	34.0	(75.00)
Instrumentation package A	25.4	(56.00)
Instrumentation package B	25.4	(56.00)
Instrumentation bar cable	1.4	(3.00)
Milliken DBM-54 Dw cam 1	16.3	(36.00)
Milliken DBM-54 Dw cam 2	20.0	(44.00)
Radiosonde	2.7	(6.00)
Payload strobe light	1.8	(4.00)
Ballast hopper 1	8.2	(18.00)
Ballast hopper 2	8.2	(18.00)
Loadbar with brackets	92.1	(203.00)
Loadbar cables	26.3	(58.00)
Clevis 2.54 cm (1 in.)	2.3	(5.00)
Heavy load release plate	2.7	(6.00)
Clevis 2.9 cm $\left(1\frac{1}{8}\text{ in.}\right)$	3.2	(7.00)
Parachute, 30.48 m (100 ft), no. 3	81.6	(180.00)
Parachute, 30.48 m (100 ft), no. 2	81.6	(180.00)
Parachute, 30.48 m (100 ft), no. 1*	108.9	(240.00)
Total mass on recovery parachutes (less ballast)	1326.8	(2925.00)

(d) AV-4

Balloon masses	kg	lb
Strobe light (on valve)	3.2	(7.00)
Balloon valve(s)	5.9	(13.00)
EV-13 modified valve plate	7.3	(16.00)
Launch balloon	421.4	(929.00)
Transfer duct	75.3	(166.00)
Transfer duct blanket	3.6	(8.00)
Mainstay cable 2.54 cm (1 in.) Hi-Shear	6.8	(15.00)
Main balloon	3004.6	(6624.00)
Clevis 2.2 cm (7/8 in.)	1.8	(4.00)
Korn multiple parachute release	5.9	(13.00)
Radar reflector	2.7	(6.00)
Total balloon masses	3538.5	(7801.00)
Parachute masses less ballast	2153.2	(4747.00)
Total pourable ballast	544.3	(1200.00)
Maximum parachute descent load	2697.5	(5947.00)
Gross mass	6236.0	(13 748.00)
Free lift (10 percent of gross mass)	623.7	(1375.00)
Gross lift	6859.6	(15 123.00)
Allowance (leakage and so forth, 3 percent)	205.9	(454.00)
Total lift at launch	6653.7	(14 669.00)

Parachute(s) masses	kg	lb
Test vehicle	1543.1	(3402.00)
Interface structure	47.6	(105.00)
Pointing system with gas	55.3	(122.00)
Instrumentation package A	25.4	(56.00)
Instrumentation package B	25.4	(56.00)
Instrumentation bar cable	1.4	(3.00)
Milliken DBM-54 Dw cam 1	16.3	(36.00)
Milliken DBM-54 Dw cam 2	20.0	(44.00)
Radiosonde	2.7	(6.00)
Payload strobe light	1.8	(4.00)
Ballast hopper 1	8.2	(18.00)
Ballast hopper 2	8.2	(18.00)
Loadbar with brackets	91.2	(201.00)
Loadbar cables	26.3	(58.00)
Clevis 2.54 cm (1 in.)	2.3	(5.00)
Heavy load release plate	2.7	(6.00)
Clevis 2.9 cm $\left(1\frac{1}{8}\text{ in.}\right)$	3.2	(7.00)
Parachute, 30.48 m (100 ft), no. 3	81.6	(180.00)
Parachute, 30.48 m (100 ft), no. 2	81.6	(180.00)
Parachute, 30.48 m (100 ft), no. 1*	108.9	(240.00)
Total mass on recovery parachutes (less ballast)	2153.2	(4747.00)

*Includes mass of electric cables up to valves, mainstay release, etc.

TABLE VII.- ESTIMATED ACCURACIES

Pitch rate	$\pm 12^{o}$/sec
Yaw rate	$\pm 12^{o}$/sec
Roll rate	$\pm 12^{o}$/sec
Longitudinal acceleration:	
High-range accelerometer AV-1, AV-4	±0.32g
AV-2, AV-3	±0.16g
Low-range accelerometer AV-1, AV-4	±0.14g
AV-1, AV-3	±0.10g
Transverse acceleration	±0.04g
Normal acceleration	±0.04g
Distance	±7.6 m (25 ft)
Velocity – above 550 m/sec (1800 ft/sec)	±12.2 m/sec (40 ft/sec)
Velocity – below 550 m/sec (1800 ft/sec)	±2 percent
Atmospheric temperature	$\pm 3^{o}$ C
Atmospheric density	±3 percent
Angles from camera data:	
ψ and θ	$\pm 2^{o}$
ϕ	$\pm 4^{o}$
Flight-path angles from radar	1^{o}
Tensiometers:	
AV-1 and AV-4 (each unit)	±1600 N (360 lbf)
AV-2 and AV-3 (each unit)	±1070 N (240 lbf)
Pointing azimuth	$\pm 5^{o}$

TABLE VIII.- TIMES FOR EVENTS FROM RELEASE

[Seconds unless otherwise noted]

Event	AV-1	AV-2	AV-3	AV-4
Balloon launch	-3 hr:2 min:14 sec	-2 hr:52 min:52 sec	-6 hr:0 min:01 sec	-2 hr:44 min:31 sec
Spacecraft release	0	0	0	0
Spin rocket fire	1.020	1.013	----------	1.020
Rocket ignition	2.024	2.022	----------	2.040
Despin	33.270	33.214	----------	33.070
Mortar fire	38.310	38.216	16.472	40.423
Line stretch (parachute)	39.368	39.201	17.422	41.429
First peak load (parachute)	39.97	39.84	18.247	41.995
Aeroshell separation	47.989	47.300	30.239	48.073
Telemeter off	403.08	401.80	403.05	400.52

TABLE IX.- MEASURED TEMPERATURES (K) ON TEST VEHICLE

[See figure 87 for location of measurements]

(a) AV-1; drop time is 3:02:14 after balloon launch; atmospheric temperature at drop 248 K

Time after balloon launch, hr:min:sec	Bridle			Mortar canister		Mortar breech T-10	Mortar flange T-16	Aeroshell		S-band transmitter	Rate gyro T-1	Main battery T-17	Instrument beam		Equipment ballast T-3	Rocket support structure T-14	Rocket motor	
	1 T-6	2 T-12	3 T-18	1 T-9	2 T-15			1 T-7	2 T-13	1 T-4			1 T-5	2 T-11			1 T-2	2 T-8
0:25:36	287.59	288.15	287.59	293.15	289.82	294	290	277	278	306	303	290	295	296	302	291	292	290
0:30:01	287.04	284.82	283.71	292.04	291.48	292	292	274	274	307	301	290	295	294	301	287	291	291
0:39:54	280.93	278.15	278.71	290.93	290.37	293	291	264	263	304	302	289	291	292	301	283	292	291
0:44:50	277.59	274.82	273.71	290.37	289.16	291	291	259	257	304	302	286	292	291	300	285	291	290
1:09:52	269.82	267.59	265.93	288.15	286.48	291	289	251	248	306	299	281	291	291	300	280	289	288
1:19:49	269.26	267.04	267.04	287.04	285.93	290	288	251	249	307	299	280	291	290	299	279	288	289
1:39:56	269.82	270.93	269.82	285.93	283.71	289	286	259	253	308	299	279	290	290	300	279	291	288
1:44:50	270.37	270.37	270.37	284.82	283.15	289	285	261	254	308	299	279	290	290	300	279	291	289
2:10:01	271.48	272.59	272.59	283.71	281.37	286	284	269	260	310	299	278	290	289	301	280	289	287
2:15:00	271.48	274.26	273.71	283.71	282.59	287	284	271	261	308	298	279	290	289	300	280	291	286
2:25:02	273.71	274.82	274.26	283.15	282.04	286	284	273	264	312	299	280	290	289	301	281	291	288
2:30:01	273.15	275.37	274.82	282.59	282.04	286	284	275	264	309	299	279	290	289	300	280	288	286
2:37:00	274.82	276.48	276.48	282.59	282.04	285	284	276	265	311	297	280	290	289	301	281	287	288
3:02:14	274.82	279.26	278.15	283.71	282.59	286	284	269	260	313	298	280	290	289	301	281	289	288
3:02:34	274.26	278.71	277.59	283.15	282.04	285	284	269	260	310	297	281	289	289	300	281	287	288
3:02:53	275.37	278.15	277.59	284.82	284.82	284	283	272	264	315	298	281	290	288	302	282	311	323
3:03:02	275.37	278.15	277.59	302.59	300.37	288	293	273	264	314	298	280	290	289	300	282	344	349
3:08:57	287.04	288.15	286.48	297.04	295.37	331	305	---	---	301	299	280	289	287	298	307	375	371

(b) AV-2; drop time is 2:52:52 after balloon launch; atmospheric temperature at drop 240 K

Time after balloon launch, hr:min:sec	Bridle			Mortar canister		Mortar breech T-10	Mortar flange T-16	Aeroshell		S-band transmitter	Rate gyro T-1	Main battery T-17	Instrument beam		Equipment ballast T-3	Rocket support structure T-14	Rocket motor	
	1 T-6	2 T-12	3 T-18	1 T-9	2 T-15			1 T-7	2 T-13	1 T-4			1 T-5	2 T-11			1 T-2	2 T-8
0:07:23	287.59	284.26	282.59	289.82	288.15	289	288	278	275	303	301	290	294	293	298	287	291	289
0:36:18	283.71	279.26	277.59	289.82	288.71	290	289	271	268	303	301	290	294	293	298	285	290	289
0:57:24	267.04	262.04	259.82	287.04	284.82	289	286	249	248	303	299	286	293	292	298	278	289	288
1:02:22	265.37	260.93	259.26	285.93	284.26	289	285	246	247	304	300	285	293	292	299	275	290	287
1:07:34	268.71	265.37	264.26	283.15	281.48	287	283	249	248	304	299	283	292	291	299	275	288	286
1:32:23	269.26	265.93	265.37	282.04	280.93	286	283	250	247	305	299	281	292	290	299	276	288	286
1:57:21	274.82	271.48	270.93	281.48	279.82	285	281	259	252	305	300	279	291	289	299	276	288	285
2:02:15	275.37	272.59	272.04	281.48	280.37	285	281	260	254	305	299	279	291	289	299	276	287	286
2:42:55	280.37	279.26	279.26	281.48	280.37	283	280	275	265	305	298	279	290	288	299	278	286	285
2:52:52	280.93	280.93	280.37	282.04	280.37	283	280	276	266	306	299	280	289	288	300	279	288	285
2:53:12	281.48	280.93	280.93	282.04	280.93	283	280	279	266	305	298	280	290	288	299	279	286	285
2:53:29	282.04	280.93	280.93	281.48	280.93	283	280	279	267	306	299	279	290	288	299	279	312	308
2:53:38	282.04	281.48	281.48	302.59	301.48	304	289	279	267	307	299	280	290	288	300	280	348	344
2:59:34	284.26	283.71	280.93	294.82	294.82	342	301	---	---	299	296	276	285	284	296	276	368	371

TABLE IX.- MEASURED TEMPERATURES (K) ON TEST VEHICLE – Concluded

(c) AV-3; drop time is 6:00:01 after balloon launch; atmospheric temperature at drop 225 K

Time after balloon launch, hr:min:sec	Bridle			Mortar canister		Mortar breech	Mortar flange	Aeroshell		S-band transmitter	Rate gyro	Main battery	Instrument beam		Equipment ballast	Rocket support structure	Rocket motor	
	1 T-6	2 T-12	3 T-18	1 T-9	2 T-15	T-10	T-16	1 T-7	2 T-13	1 T-4	T-1	T-17	1 T-5	2 T-11	T-3	T-14	1 T-2	2 T-8
2:05: 0	273	272	272	285	284	286	284	272	273	296	294	281	286	284	294	278		
2:09:55	272	270	270	284	284	286	283	269	270	296	293	280	285	283	295	276		
2:35:01	254	252	252	279	279	281	278	253	252	294	287	273	279	275	292	265		
2:40:00	251	251	249	278	278	281	276	251	250	295	285	271	278	274	291	264		
3:06:27	249	263	249	272	273	277	271	250	250	293	283	264	274	271	290	262		
3:12:27	250	250	249	274	273	278	271	251	251	291	283	263	274	270	291	262		
3:35:01	254	250	254	272	271	287	271	255	254	291	281	262	272	270	289	263		
4:05:03	254	258	254	271	270	278	269	257	259	290	281	261	271	270	288	263		
4:10:01	255	259	254	271	270	276	269	257	260	291	280	261	271	270	288	264		
4:35:00	251	259	260	270	270	289	270	258	262	291	281	262	271	270	288	265		
4:40:03	251	259	261	270	270	286	270	257	263	290	280	262	271	270	287	265		
5:05:53	256	260	259	269	269	278	269	260	263	290	280	262	271	270	287	265		
5:11:01	255	261	261	269	269	276	269	260	264	290	280	262	271	270	288	265		
5:50:01	255	265	263	269	269	284	270	259	265	290	281	263	271	270	288	267		
6:00:00	255	265	263	269	270	280	270	259	266	289	281	264	271	270	286	268		
6:00:16	255	265	262	269	269	280	270	259	266	290	281	263	271	270	287	267		
6:00:30	255	264	261	289	293	306	281	259	266	289	281	263	271	270	287	267		
6:06:43	243	248	244	281	281	329	290	---	---	281	277	256	263	255	280	233		

(d) AV-4; drop time is 2:44:31 after balloon launch; atmospheric temperature at drop, 245 K

Time after balloon launch hr:min:sec	Bridle			Mortar canister		Mortar breech	Mortar flange	Aeroshell		S-band transmitter	Rate gyro	Main battery	Instrument beam		Equipment ballast	Rocket support structure	Rocket motor	
	1 T-6	2 T-12	3 T-18	1 T-9	2 T-15	T-10	T-16	1 T-7	2 T-13	1 T-4	T-1	T-17	1 T-5	2 T-11	T-3	T-14	1 T-2	2 T-8
0:16:33	289	288	288	289	290	289	290	282	283	308	300	290	294	293	300	289	290	289
0:24:58	287	285	285	289	290	289	290	276	276	308	300	290	294	293	301	288	290	289
0:50:01	274	269	270	286	287	288	288	251	249	308	300	287	293	291	300	280	290	287
0:54:59	271	267	267	286	286	287	287	248	245	308	299	286	293	291	300	279	288	286
1:20:01	268	265	266	283	283	285	285	246	246	307	299	282	292	290	300	277	286	286
2:01:00	269	266	267	286	283	285	284	248	246	308	299	282	292	290	300	278	287	286
2:05:04	271	271	272	280	281	284	282	260	259	309	299	280	291	289	299	279	286	285
2:10:02	272	271	273	280	281	284	282	261	259	310	299	280	291	289	300	279	288	285
2:34:31	274	274	275	280	280	283	281	273	259	310	299	280	290	288	300	279	287	285
2:44:31	274	275	276	280	281	283	282	279	257	311	299	281	290	288	301	280	287	285
2:44:51	275	275	276	280	281	283	281	278	257	309	299	281	290	288	300	280	286	285
2:45:11	275	275	276	280	281	283	281	281	261	311	299	281	290	288	301	280	310	306
2:45:18	275	275	276	300	303	284	293	282	261	310	298	281	290	288	300	280	324	328
2:51:11	291	282	284	293	294	296	303	---	---	303	299	282	288	287	298	293	375	370

TABLE X.- STEP INITIAL CONDITIONS, BIASES, AND SCALE FACTORS

	AV-1	AV-2	AV-4
Initial conditions:			
Latitude, deg	33.2334	33.4528	33.2871
Longitude, deg	-106.2351	-106.2327	-106.2322
Altitude, m	36 739.0	36 705.0	36 808.0
Altitude, ft	120 536.0	120 424.0	120 762.0
Velocity, m/sec	29.75	28.99	30.51
Velocity, ft/sec	97.6	95.1	100.1
γ_p, deg	-8.24	-7.46	1.4
γ_y, deg	279.12	83.73	-126.00
ψ, deg	-13.00	210.00	137.00
θ, deg	*53.45	65.00	55.00
ϕ, deg	0	0	0
Time (from) drop	0	0	0
Biases:			
p, radians/sec	-0.02466248	0	-0.01745
q, radians/sec	0.007296768	0	-0.010646
r, radians/sec	0.00373606	0	-0.06108
a_x	0.1283	0	0
a_y	0	0	0
a_z	0	0	0
Scale factors:			
p, radians/sec	1.0	0.9808	0.9835
q, radians/sec	1.0	1.0	1.0
r, radians/sec	1.0	1.0	1.0
a_x	1.0	1.0	1.0
a_y	1.0	1.0	1.0
a_z	1.0	1.0	1.0

*Determined from trajectory reconstruction.

TABLE XI.- MEAN DEVIATIONS AND STANDARD DEVIATIONS FROM THE MEAN DEVIATION OF STEP AND RADAR OR CAMERA DATA

(a) Radar data

Flight	Range, m		Azimuth, deg		Elevation, deg	
	$\overline{\Delta R}$	σ_R	$\overline{\Delta AZ}$	σ_{AZ}	$\overline{\Delta EL}$	σ_{EL}
AV-1	6.79	4.08	0.041	0.026	0.022	0.010
AV-2	3.47	2.62	.017	.011	.017	.009
AV-4	14.21	9.53	.085	.038	.012	.007

(b) Camera data

Flight	Yaw		Pitch		Roll	
	$\overline{\Delta\psi}$	σ_ψ	$\overline{\Delta\theta}$	σ_θ	$\overline{\Delta\phi}$	σ_ϕ
AV-1	4.79	0.59	0.82	0.44	1.52	0.99
AV-2	1.56	1.03	1.61	.73	3.93	3.00
AV-4	3.02	1.26	1.07	.36	2.64	1.32

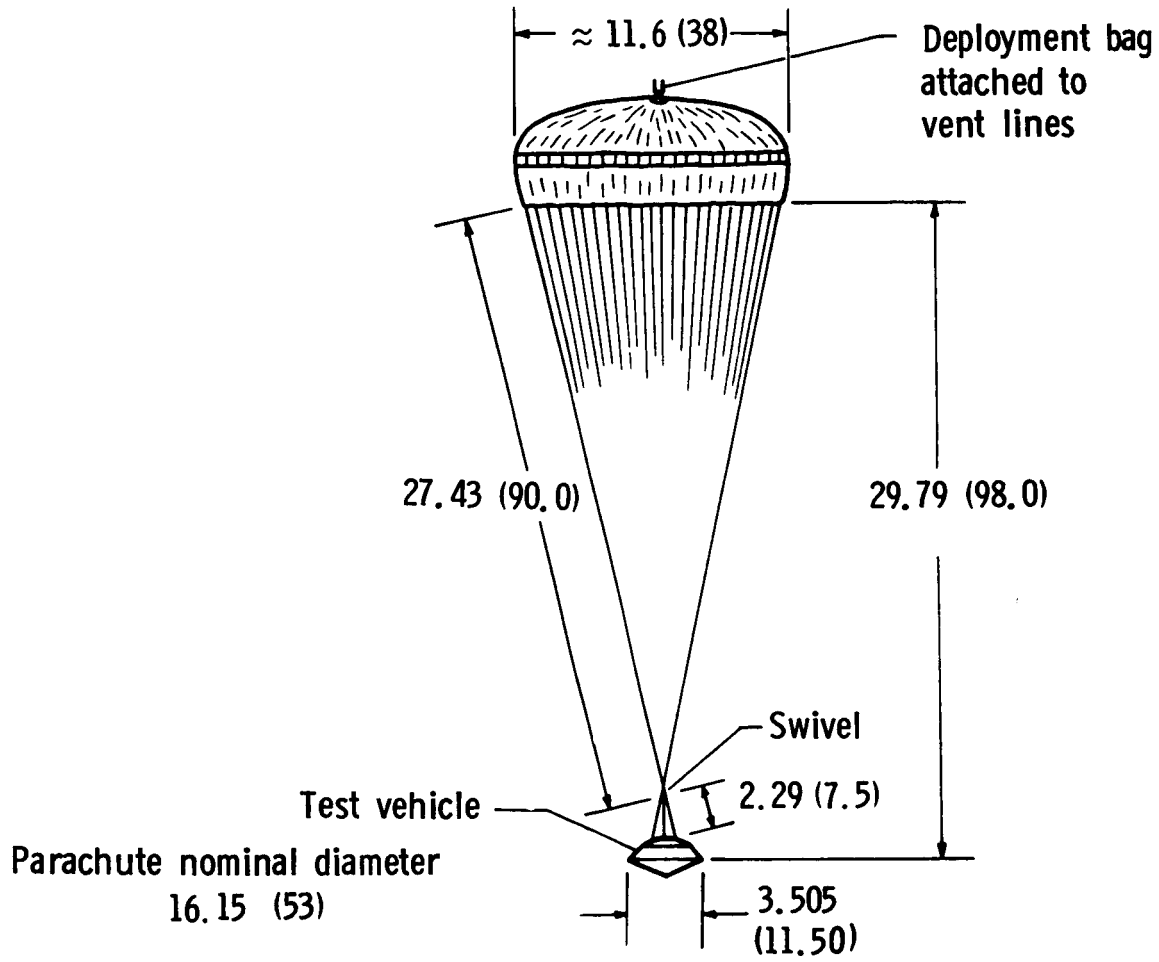


Figure 1.- Disk-gap-band parachute system. Dimensions are in meters (feet).

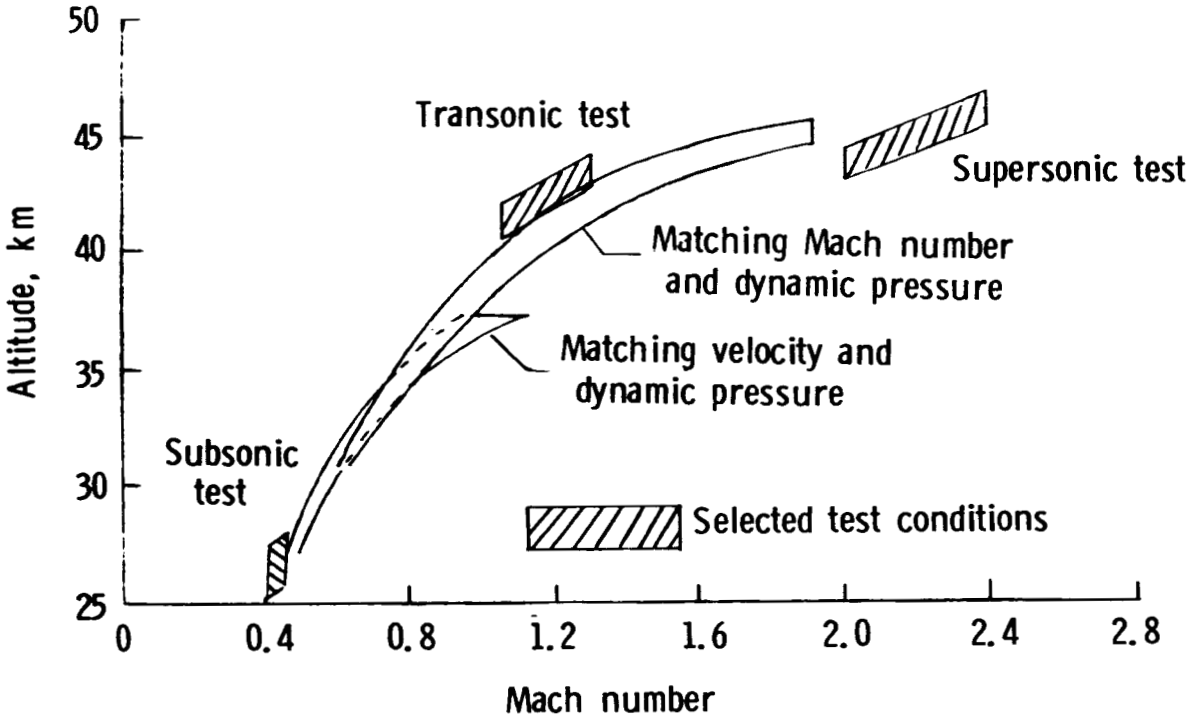


Figure 2.- Comparison between Earth conditions to match Mars parachute deployment conditions when using dynamic pressure-velocity, and dynamic pressure-Mach number.

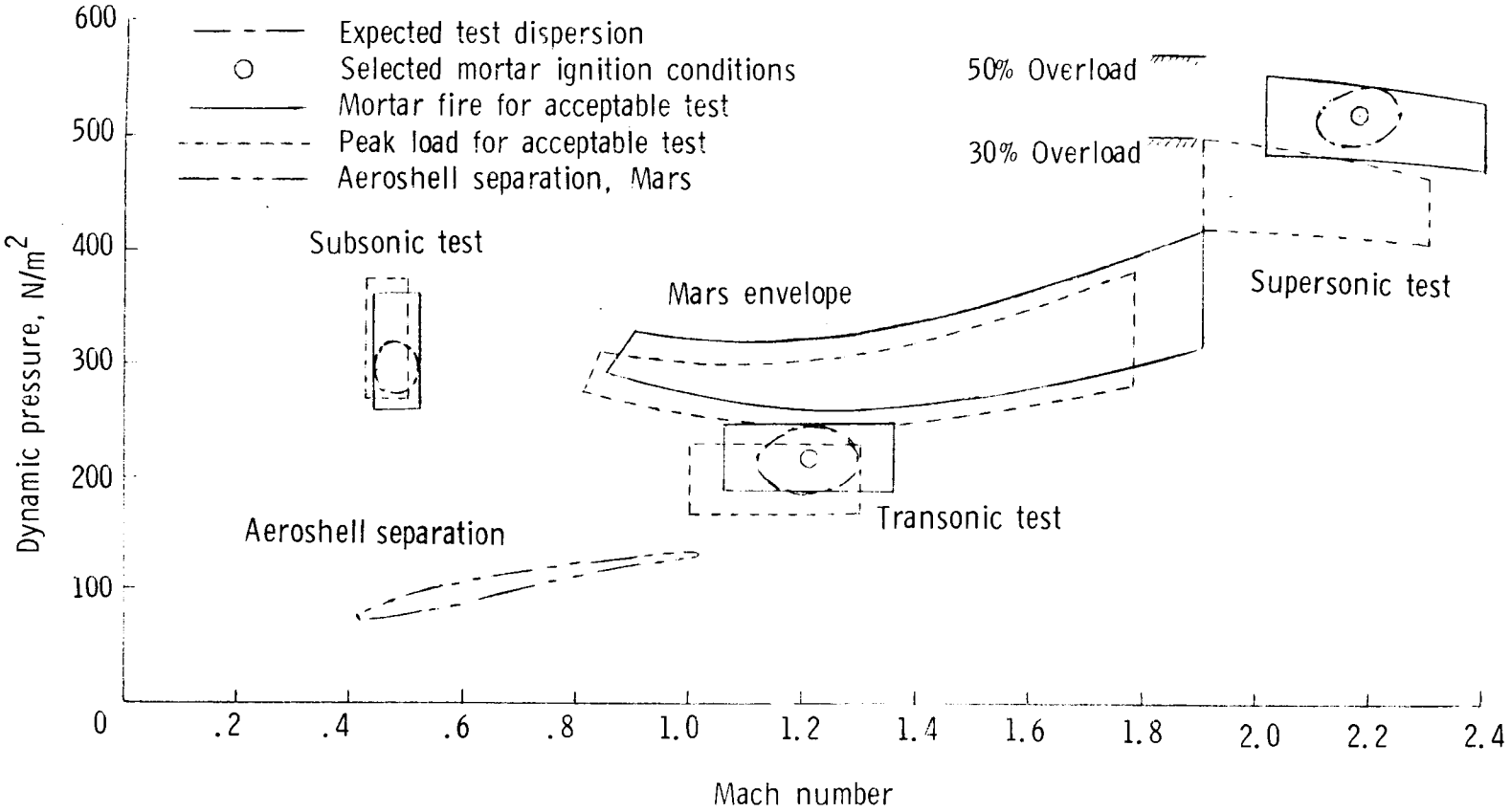
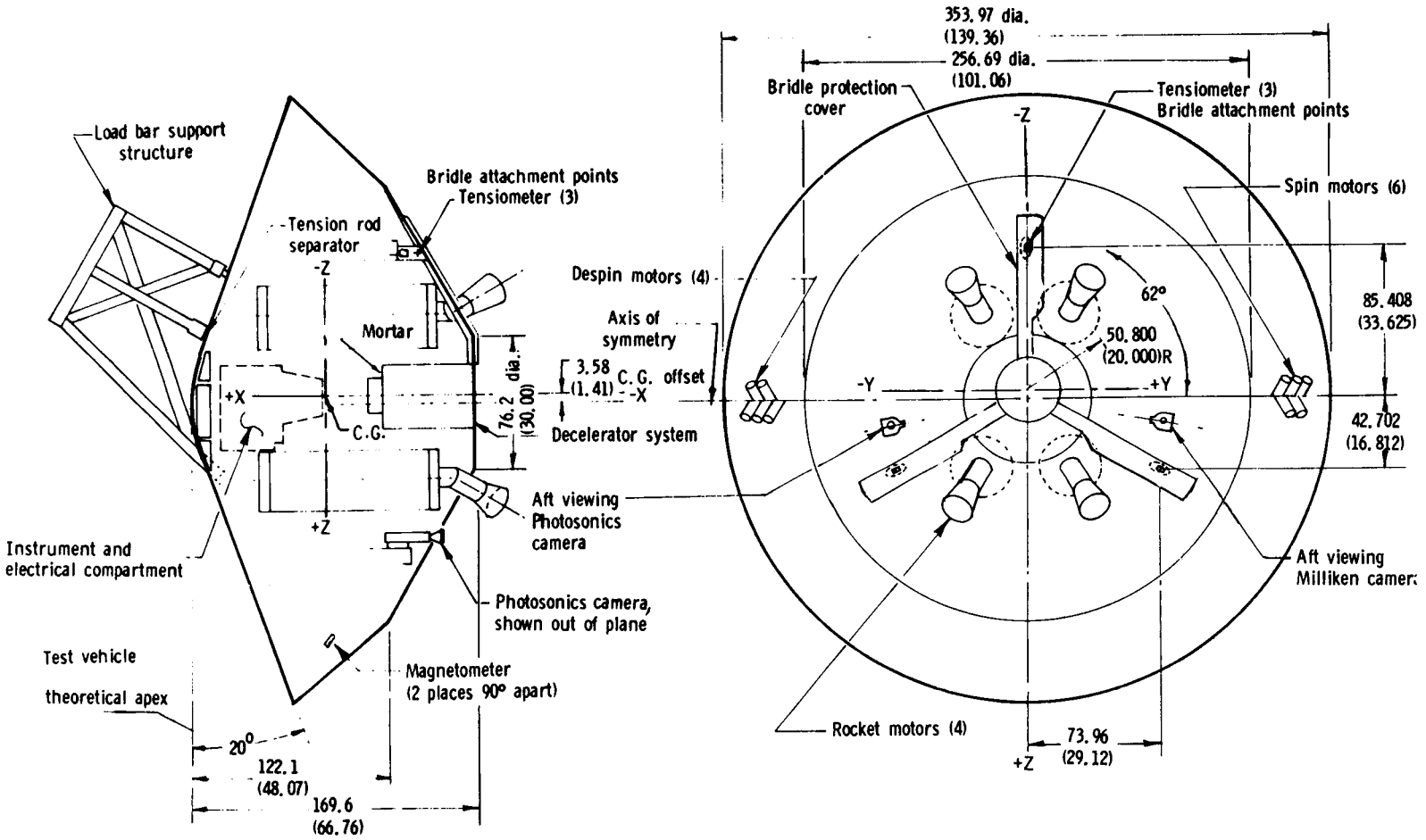
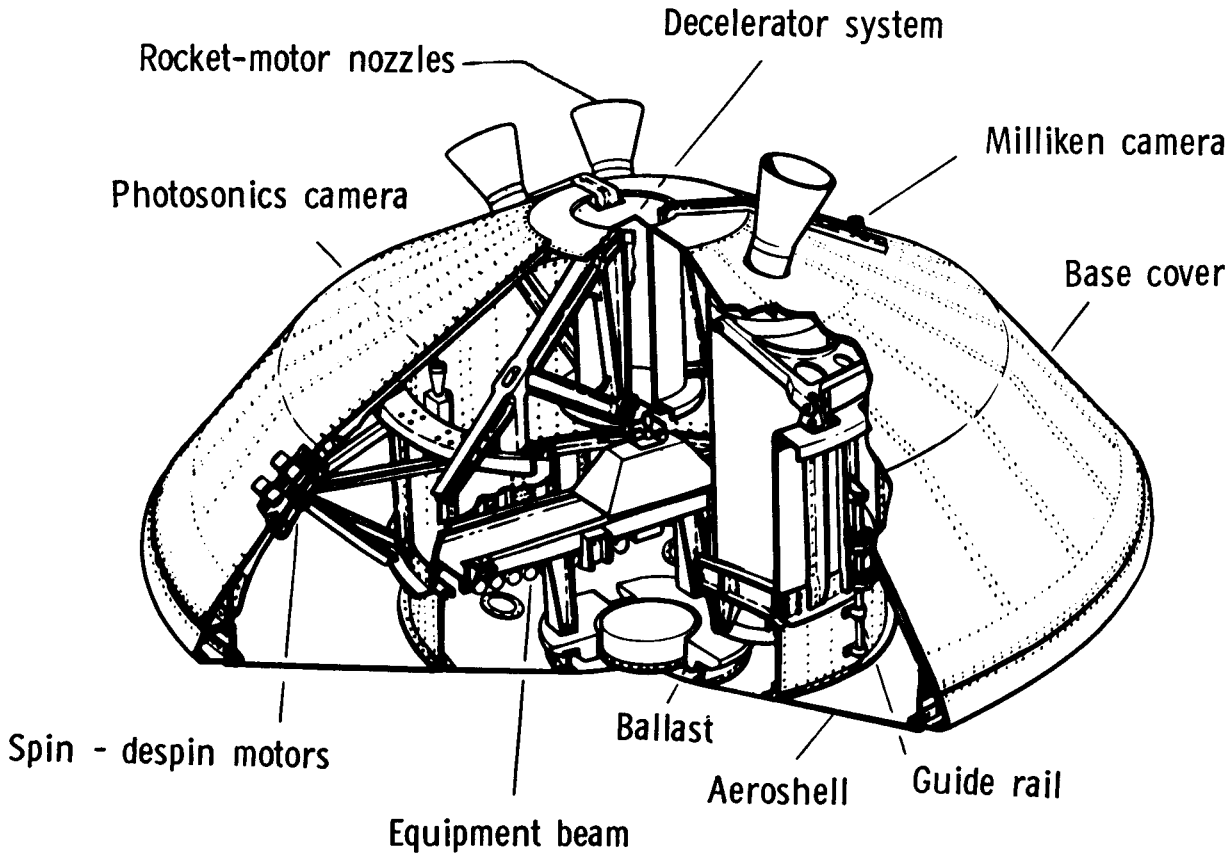


Figure 3.- Designed test conditions referenced to expected conditions at Mars.



(a) General arrangement.

Figure 4.- Test vehicle for supersonic test. Dimensions are in cm (in.).



(b) Three-dimensional sketch of test vehicle for supersonic test.

Figure 4.- Concluded.

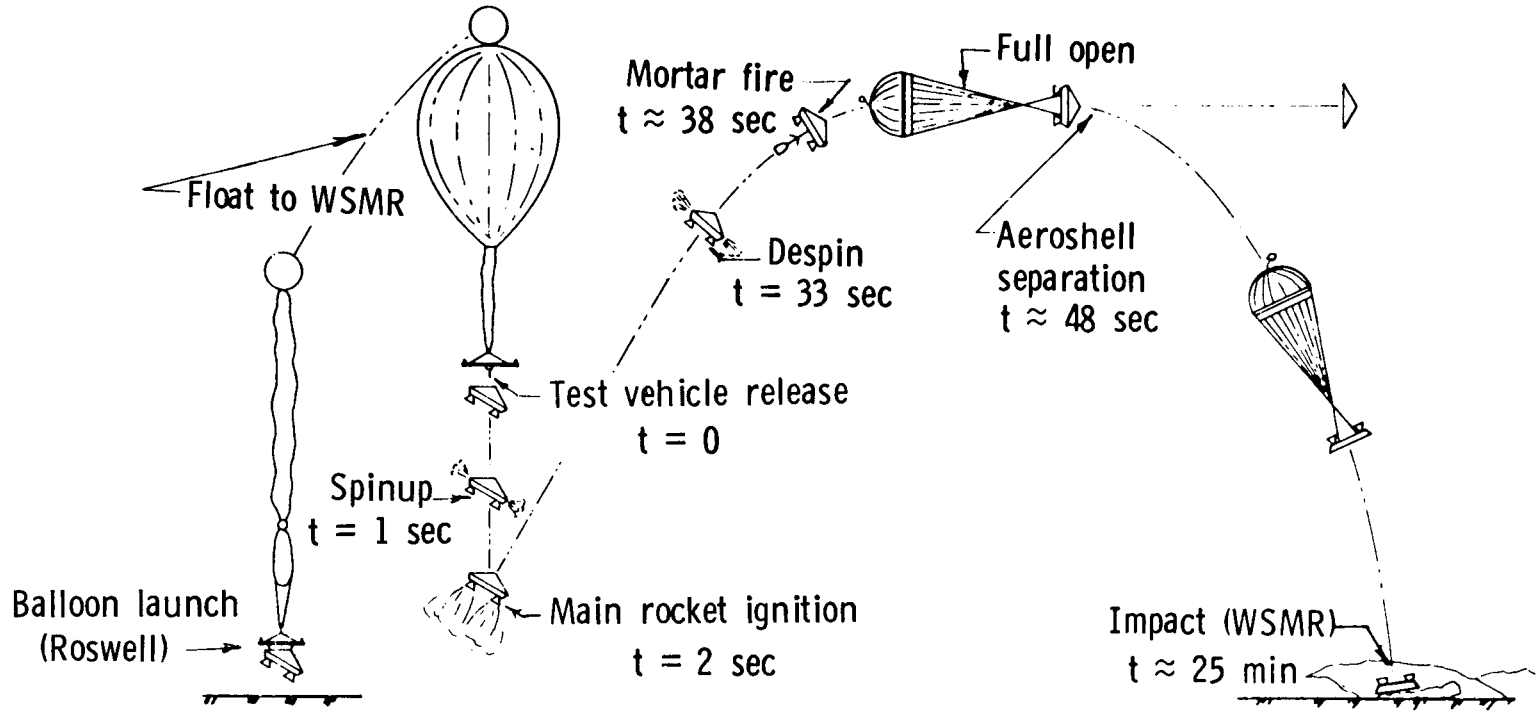


Figure 5.- Typical sequence of events, powered flight.

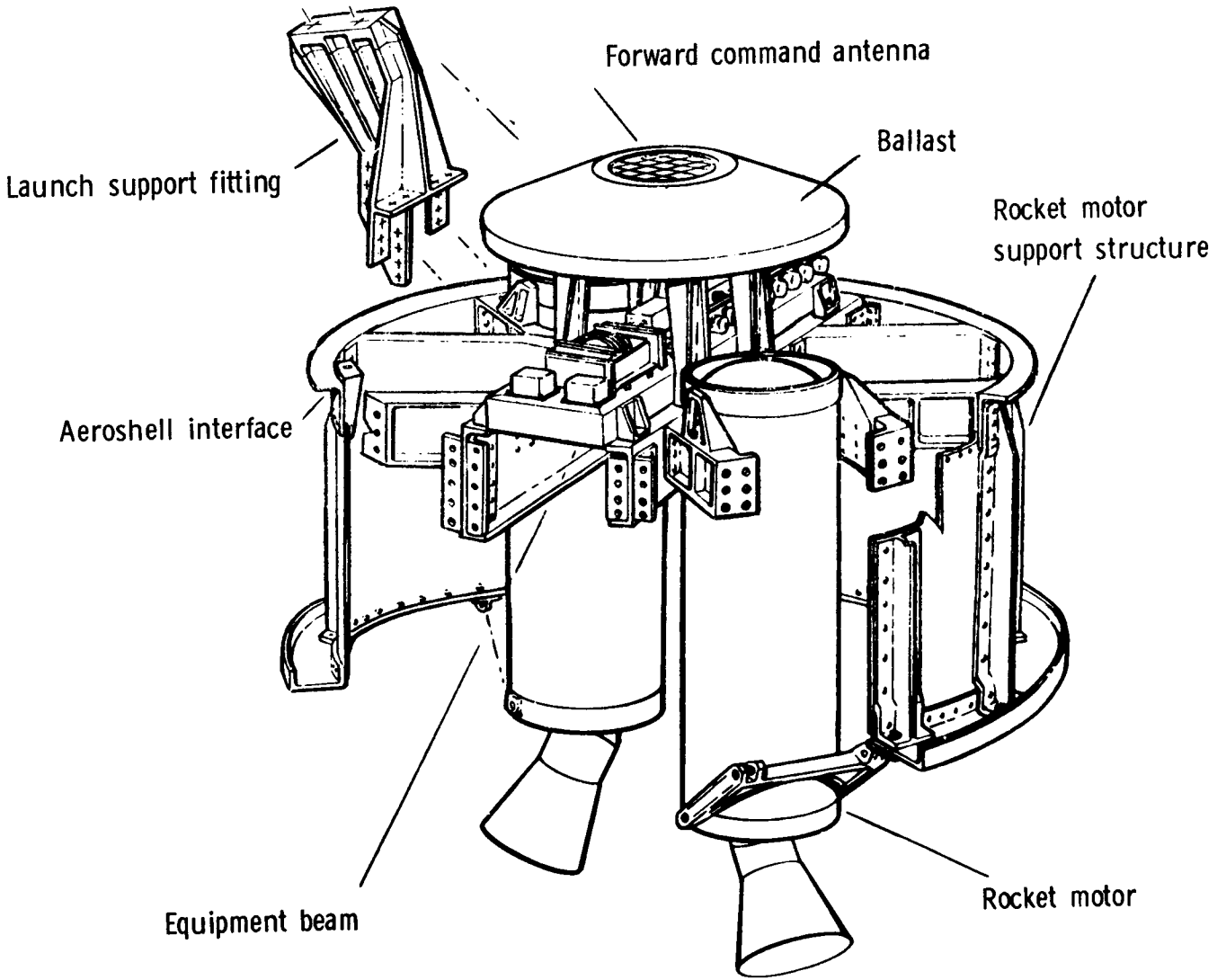


Figure 6.- Rocket-motor support structure assembly.

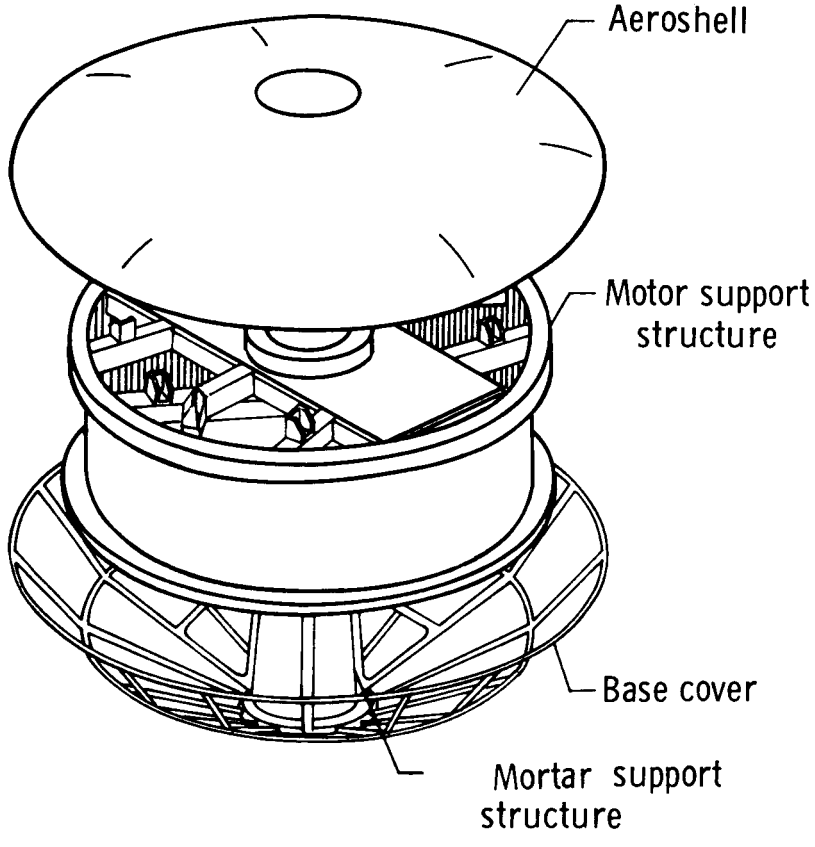
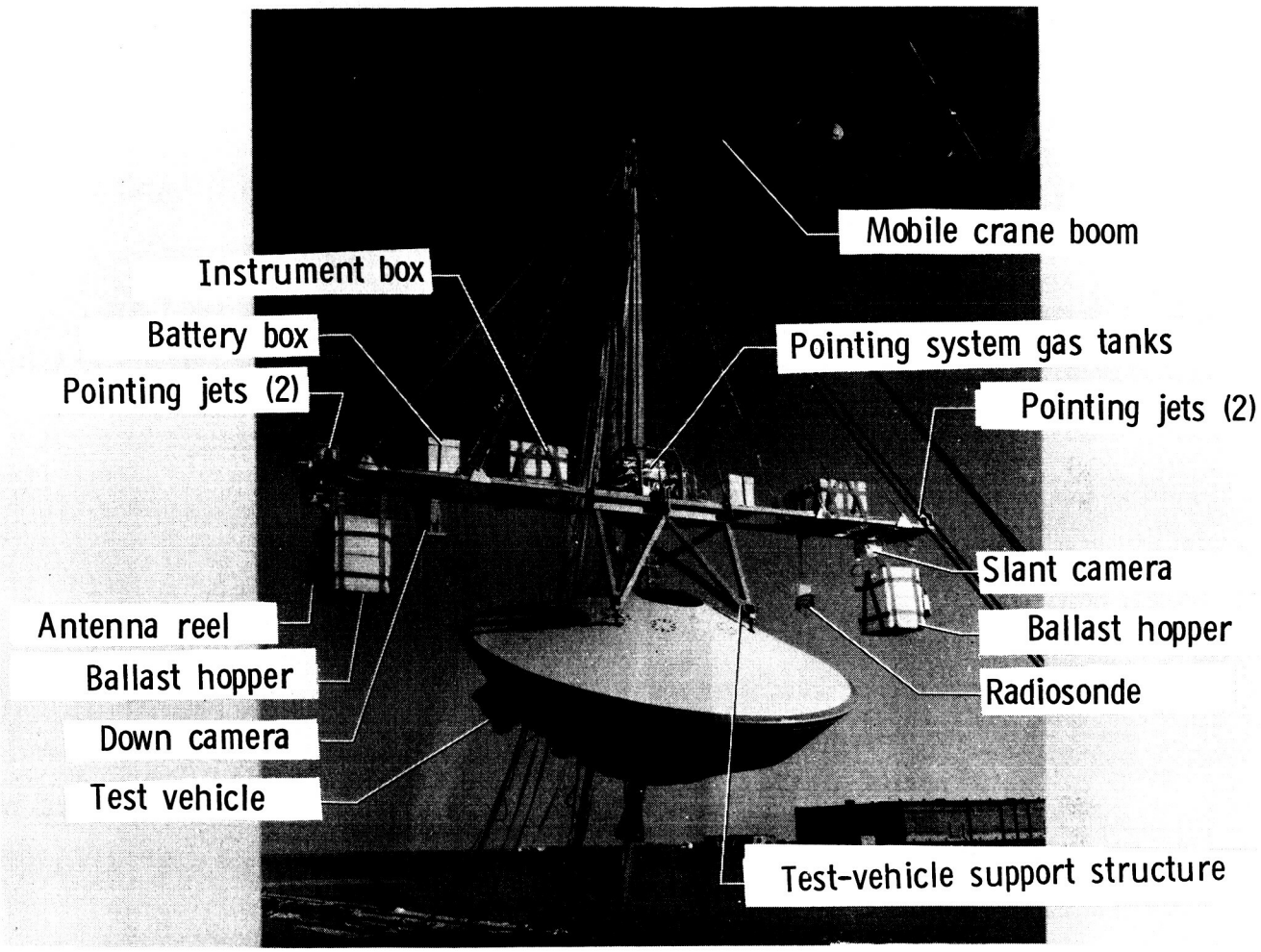


Figure 7.- Schematic showing assembly of three major components.



L-74-1121

Figure 8.- Photograph of test vehicle suspended from load bar.

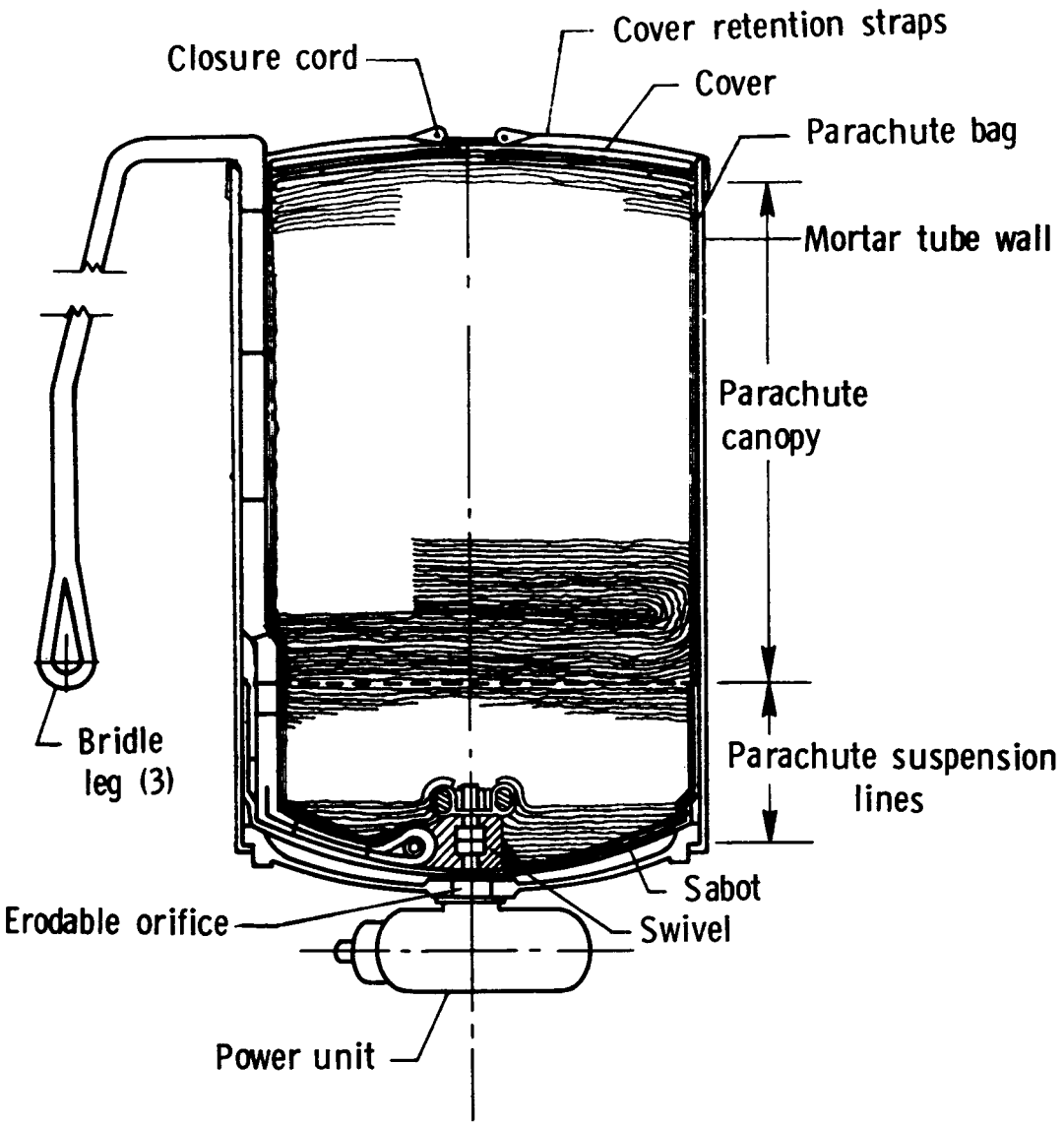


Figure 9.- Sketch of mortar with parachute pack.

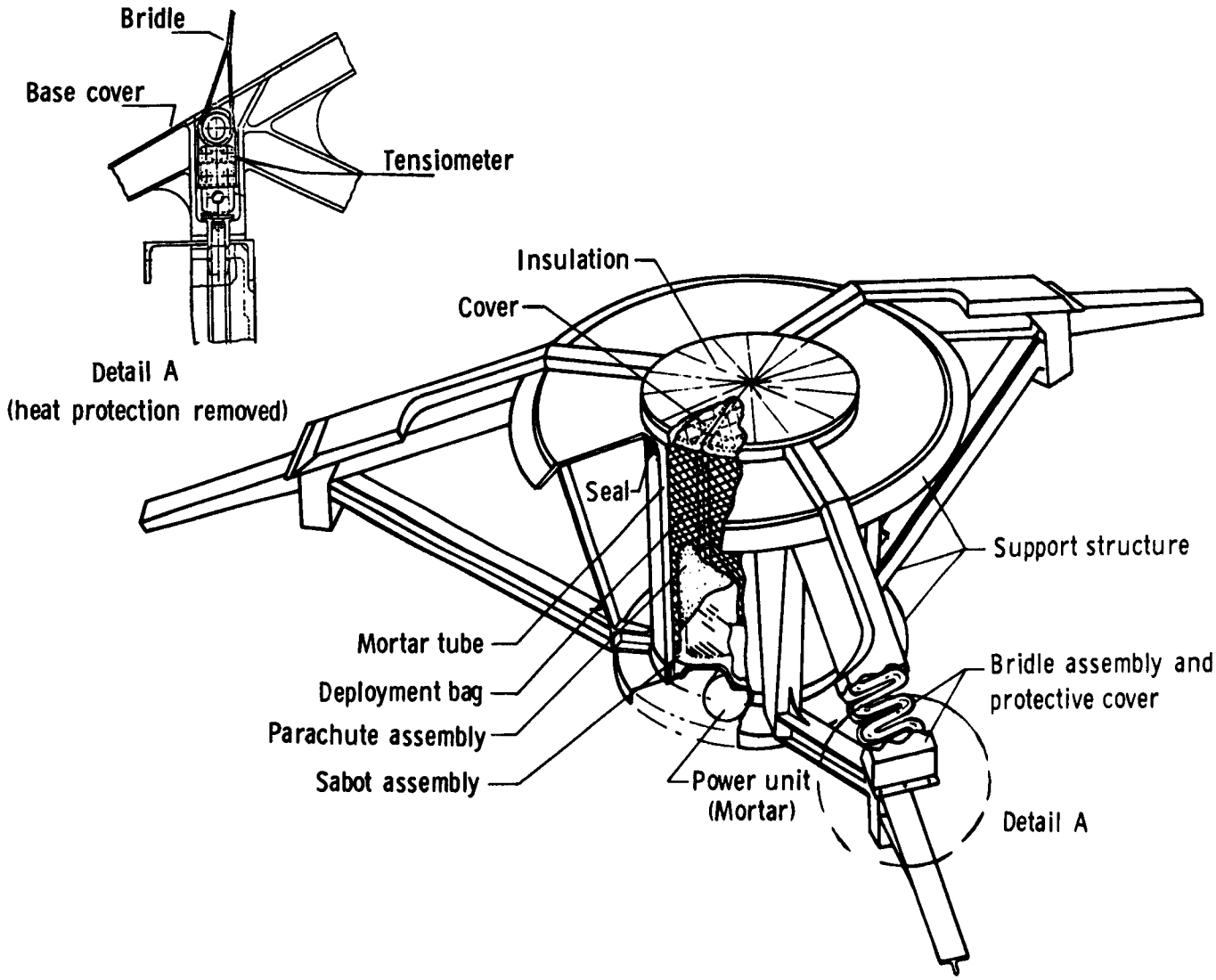
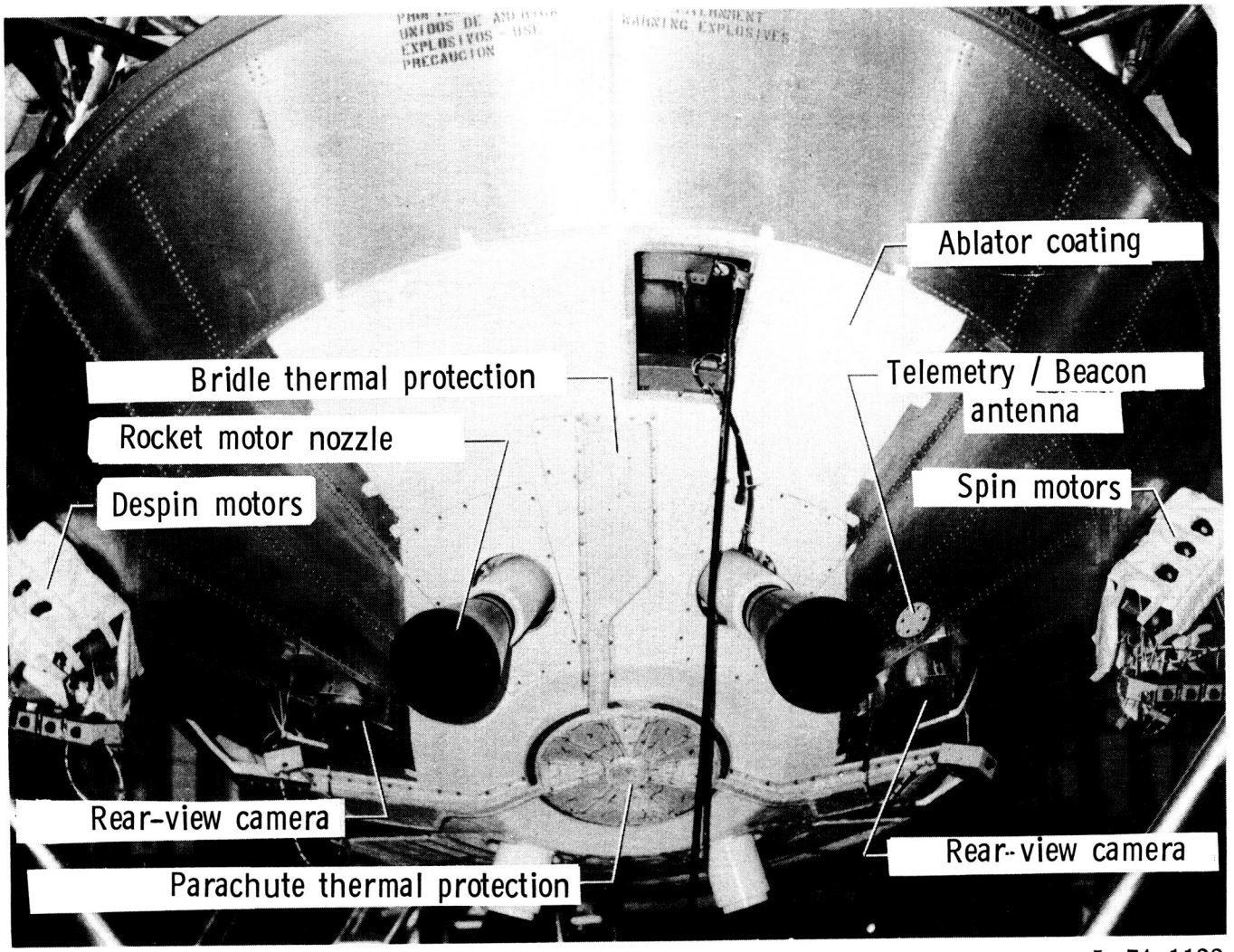
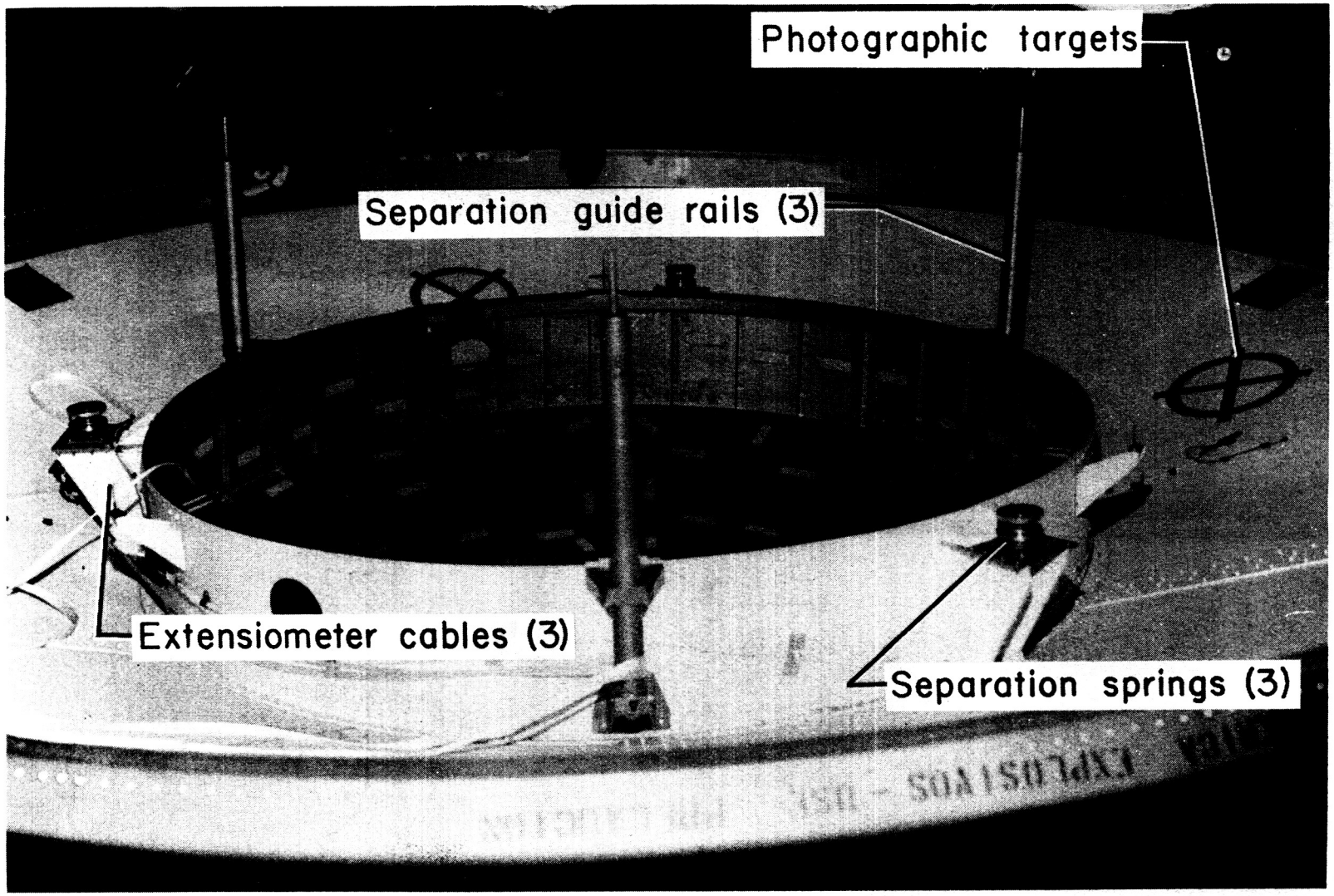


Figure 10.- Sketch of mortar support structure.



L-74-1122

Figure 11.- Photograph of base of test vehicle.



L-74-1123

Figure 12.- Photograph of interior of aeroshell.

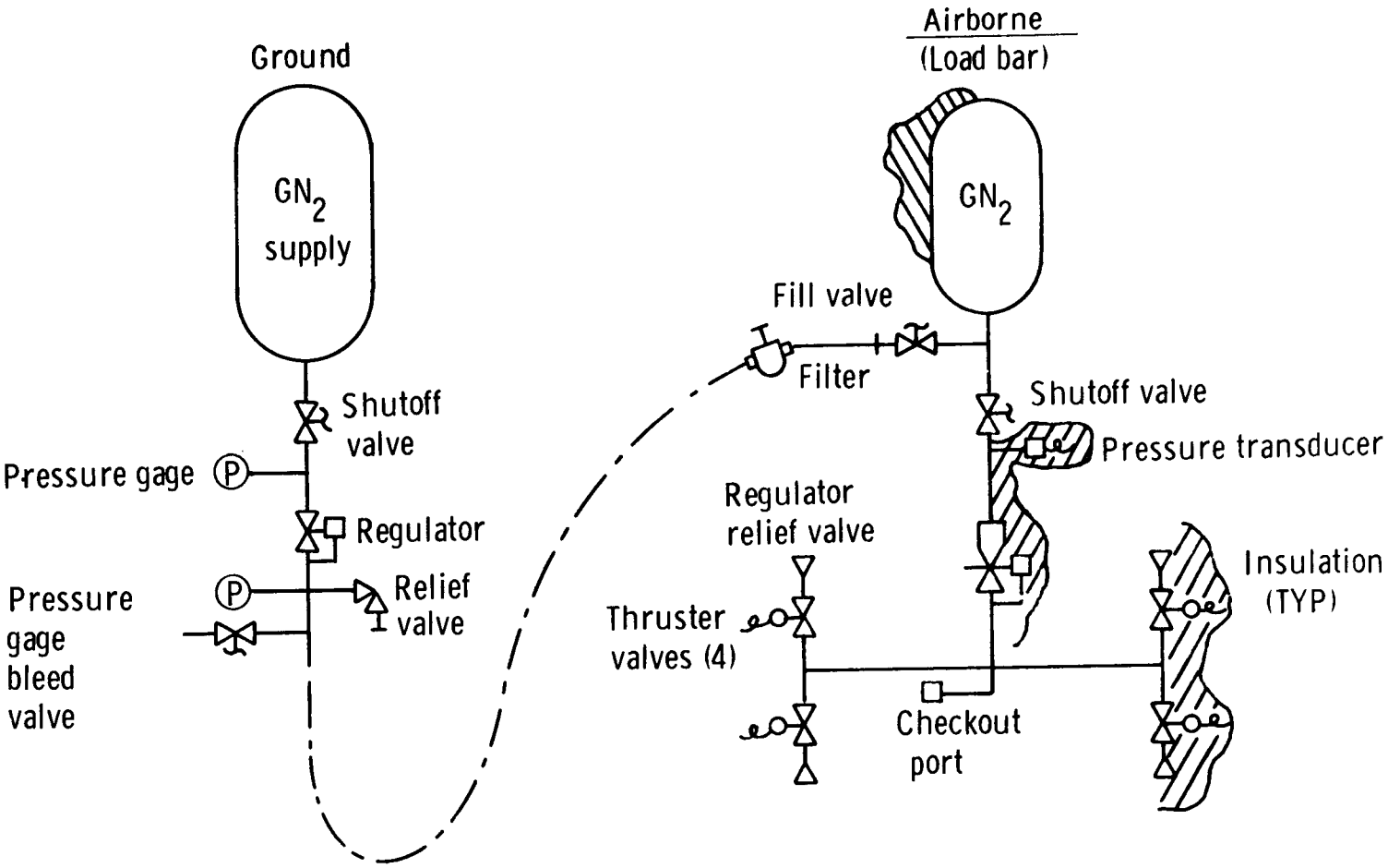


Figure 13.- Schematic of pointing system.

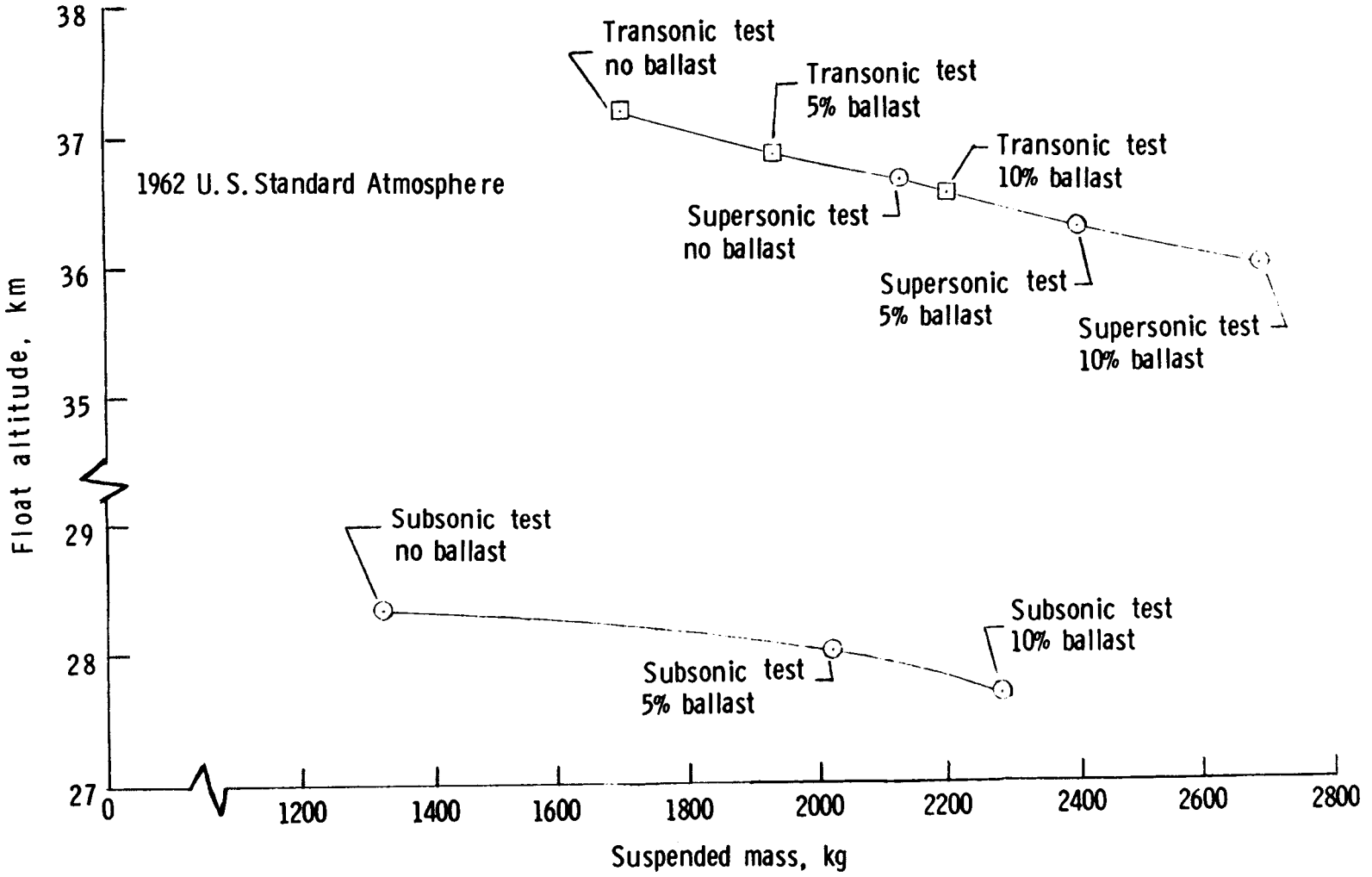
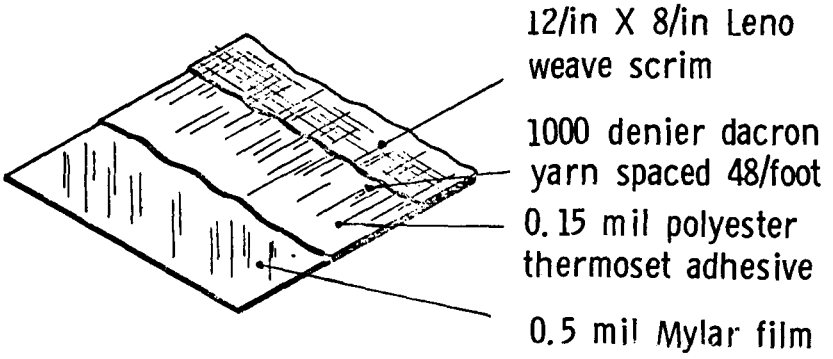
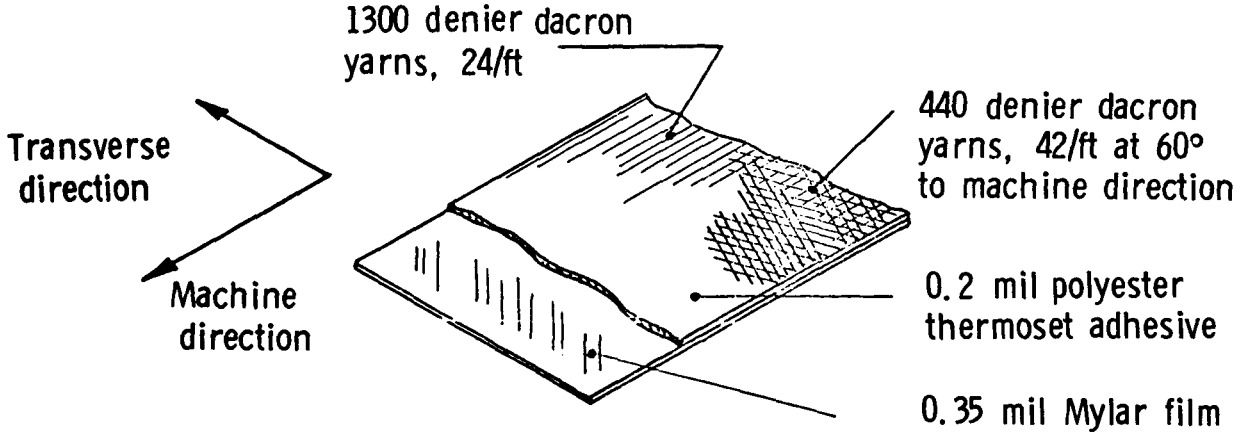


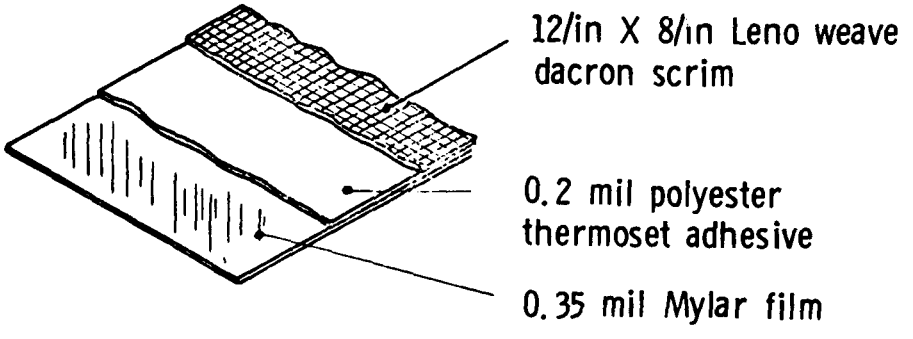
Figure 14.- Variation of balloon float altitude with suspended weight.



(a) Launch balloon material.

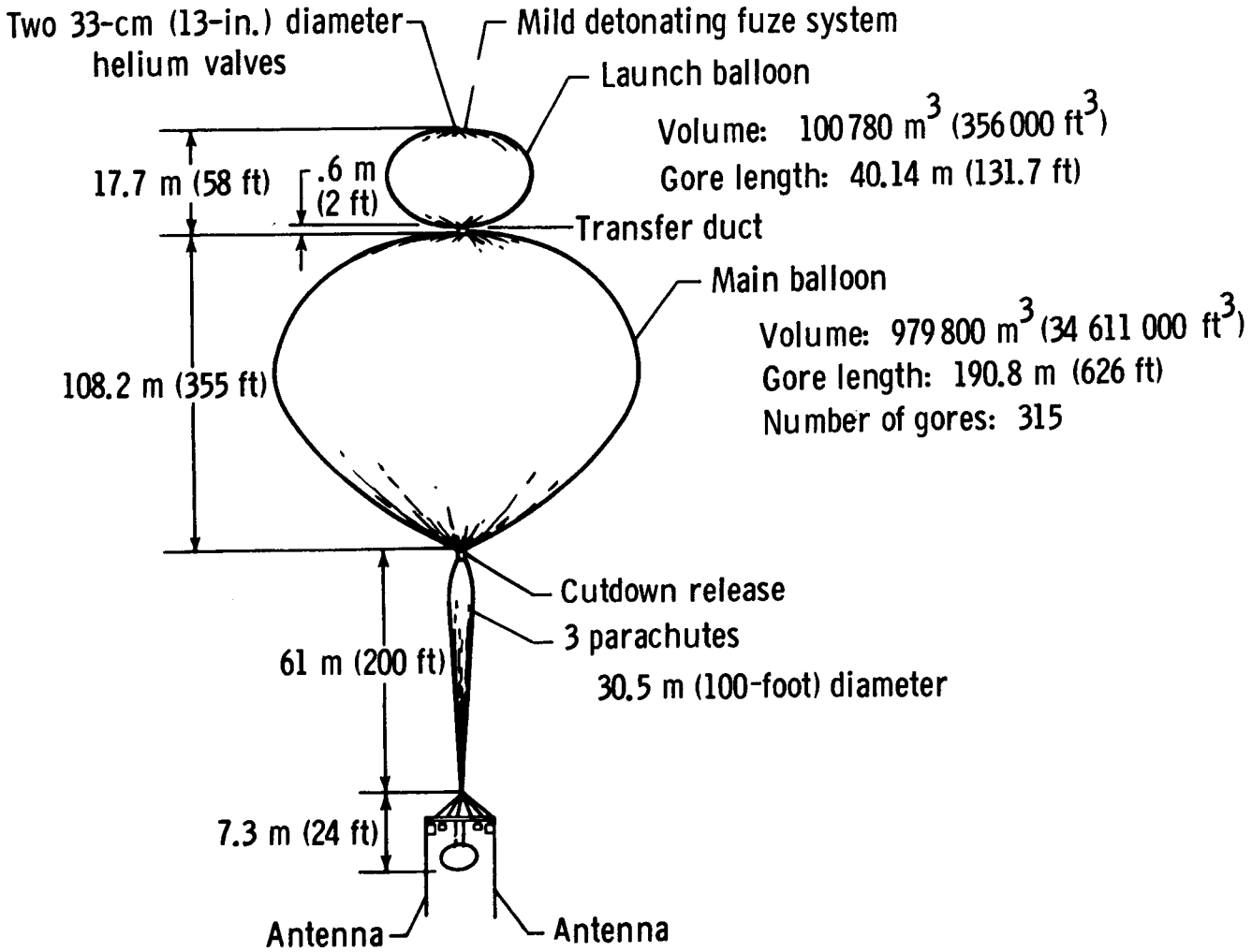


(b) Supersonic/transonic balloon material.



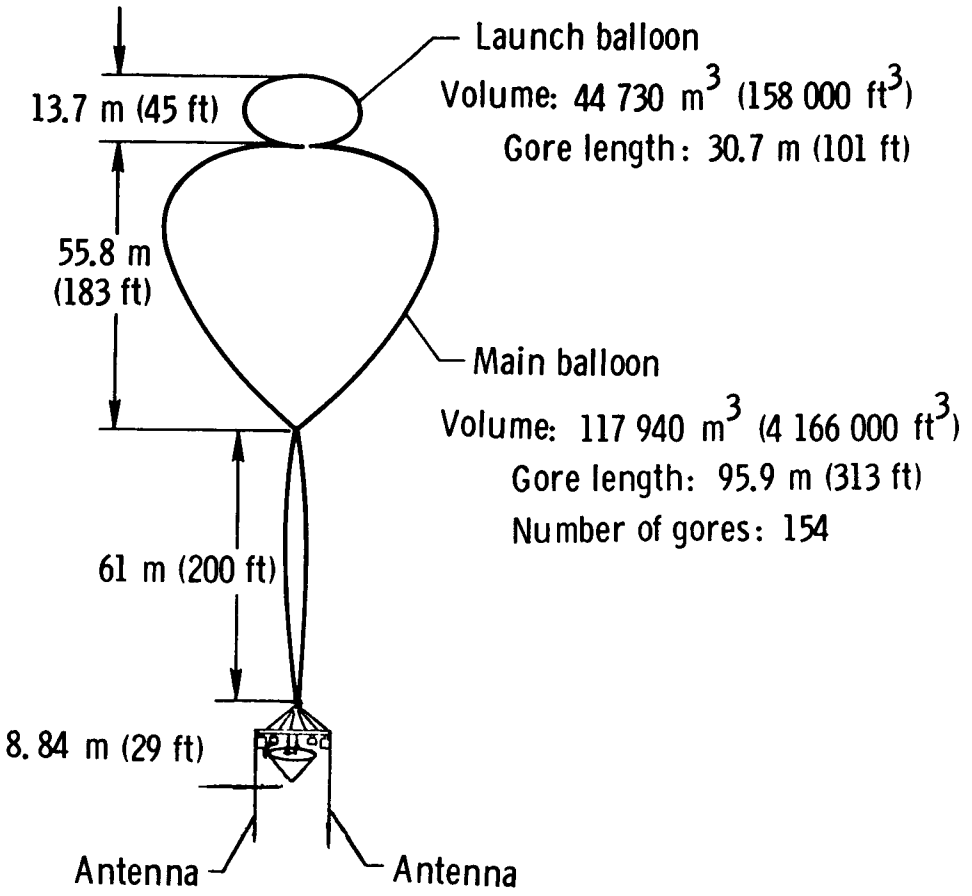
(c) Subsonic main balloon material.

Figure 15.- Balloon material construction.



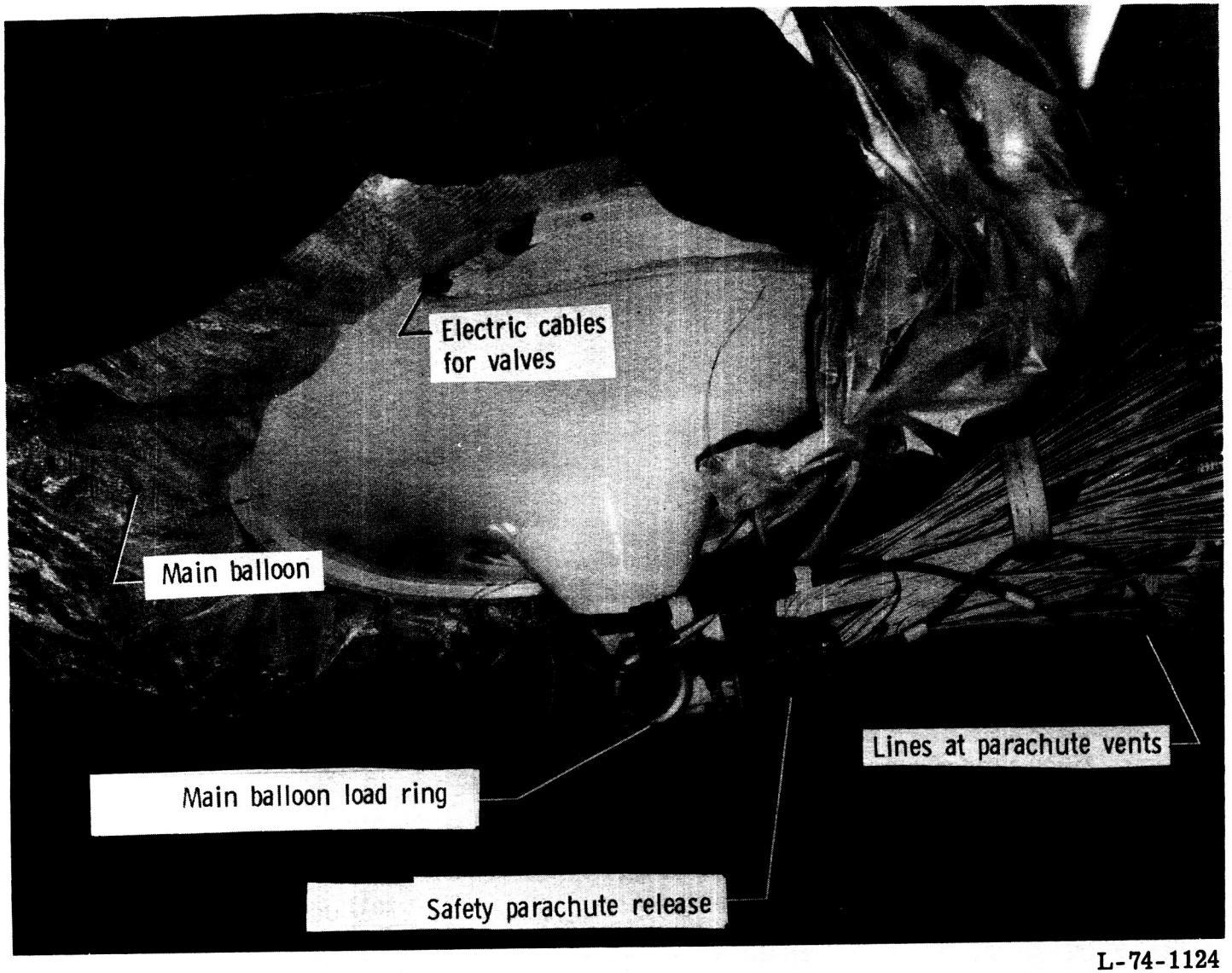
(a) Transonic and supersonic flight.

Figure 16.- Balloon system at float altitude.



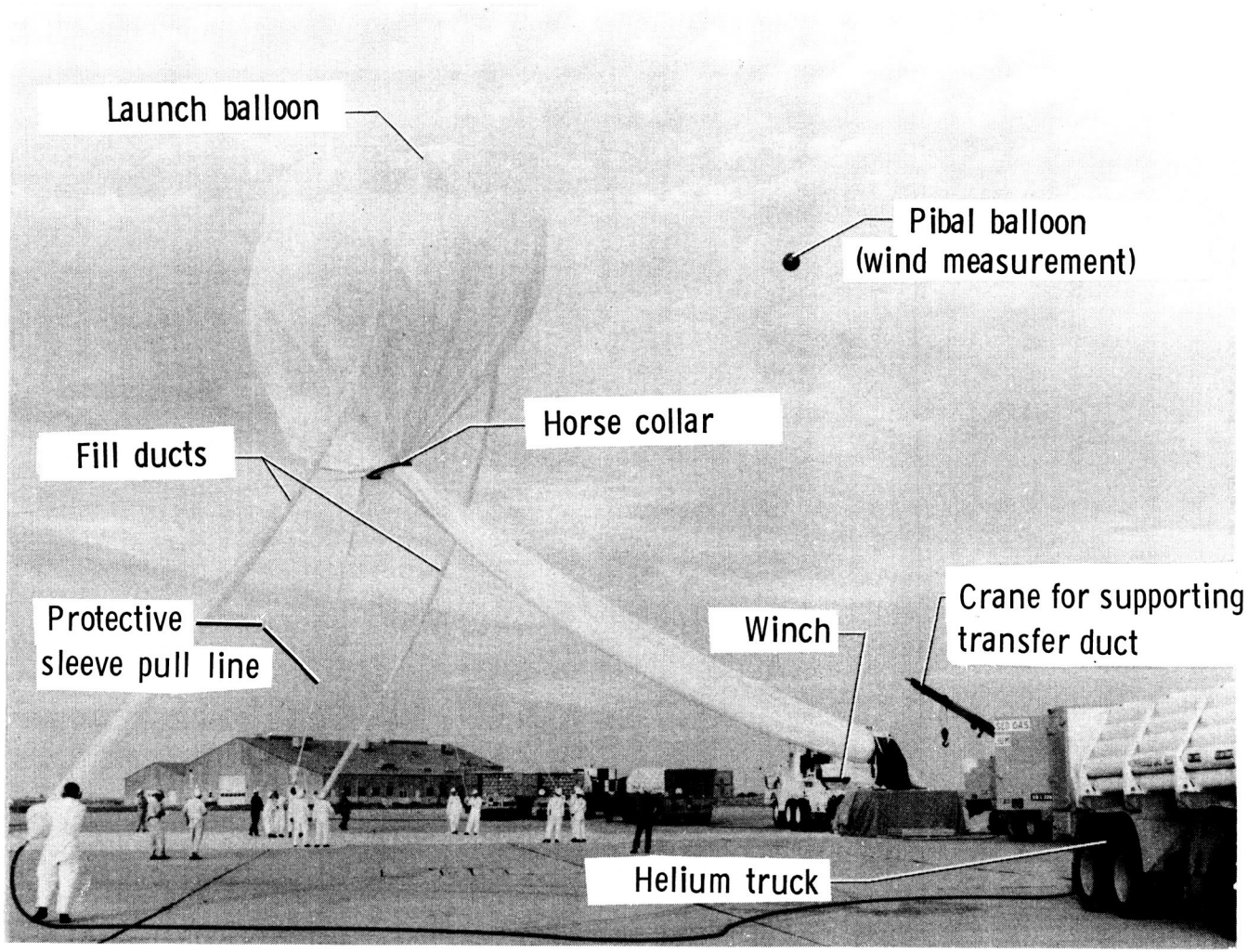
(b) Subsonic flight.

Figure 16.- Concluded.



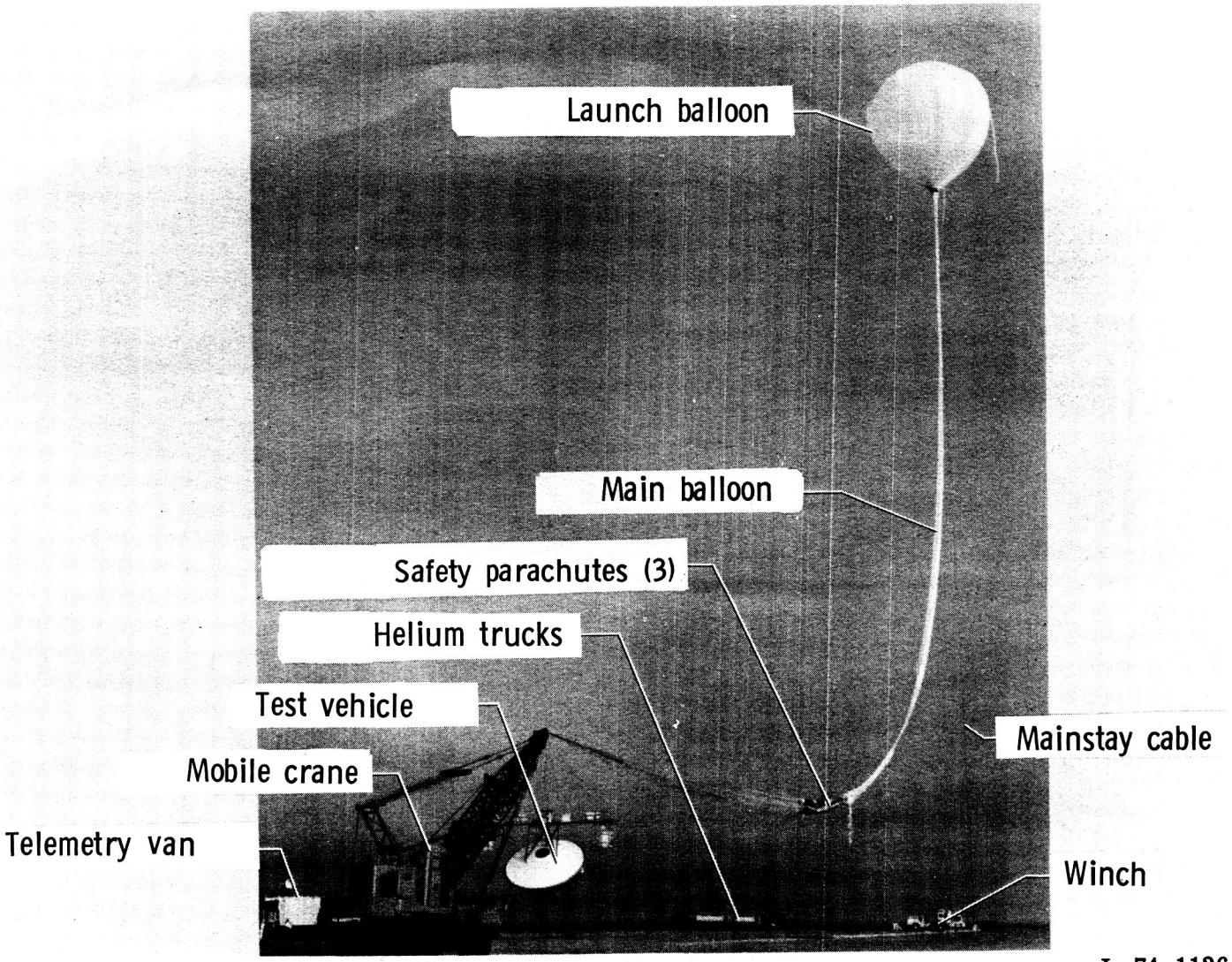
L-74-1124

Figure 17.- Photograph of balloon load ring and cut down release. AV-4.



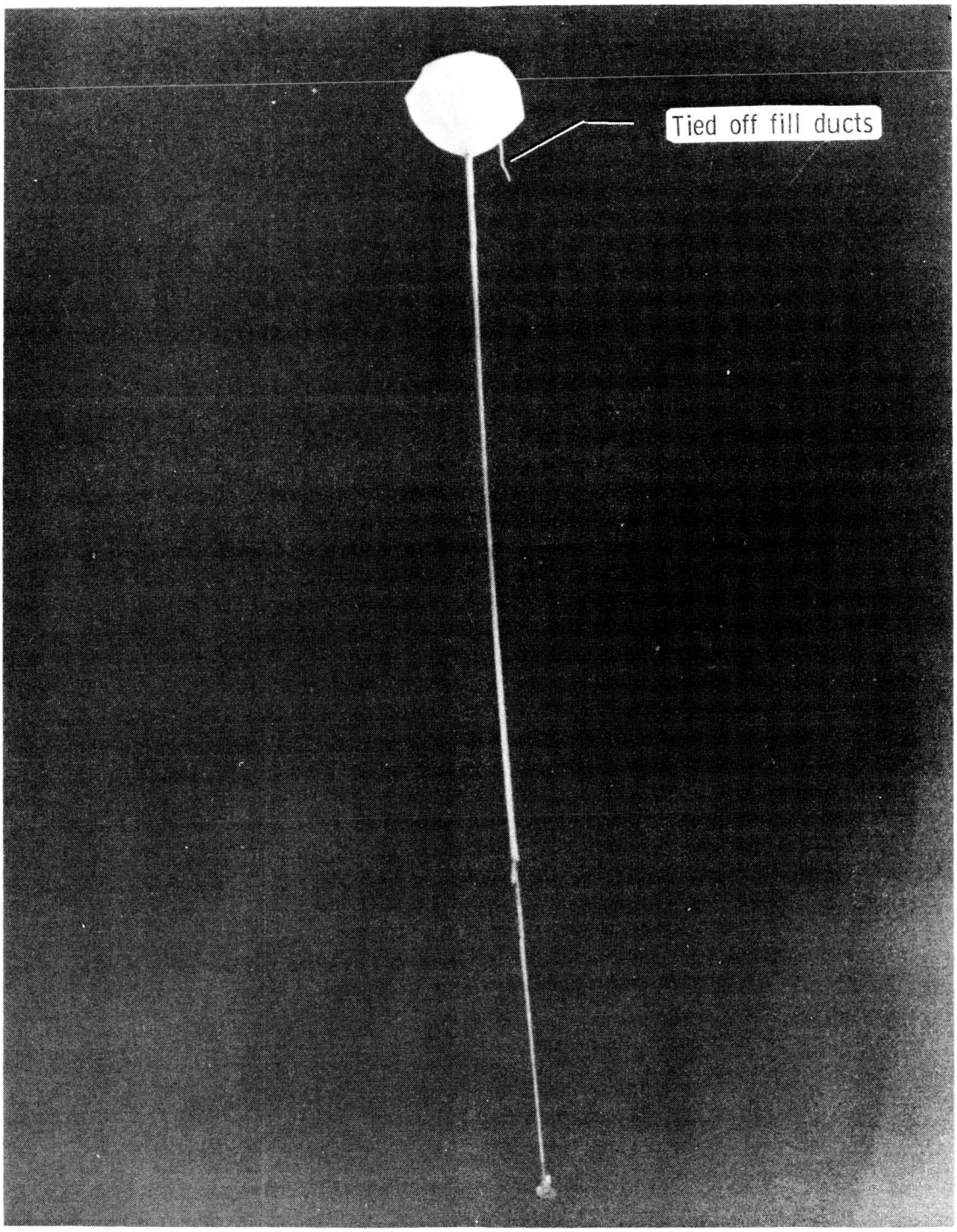
L-74-1125

Figure 18.- Balloon helium filling operations.



L-74-1126

Figure 19.- Reel up of balloon in preparation for launch.



L-74-1127

Figure 20.- Photograph of balloon directly after release.

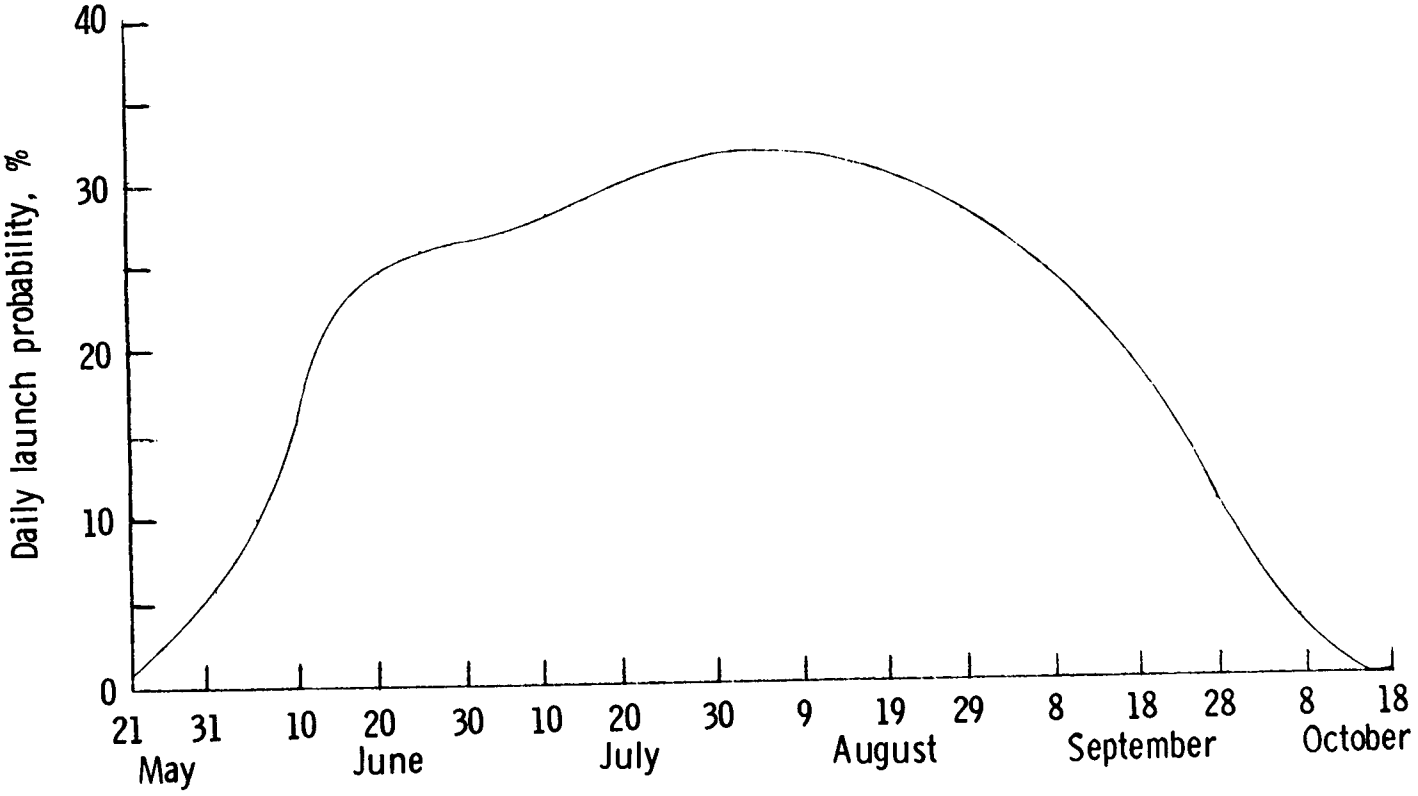
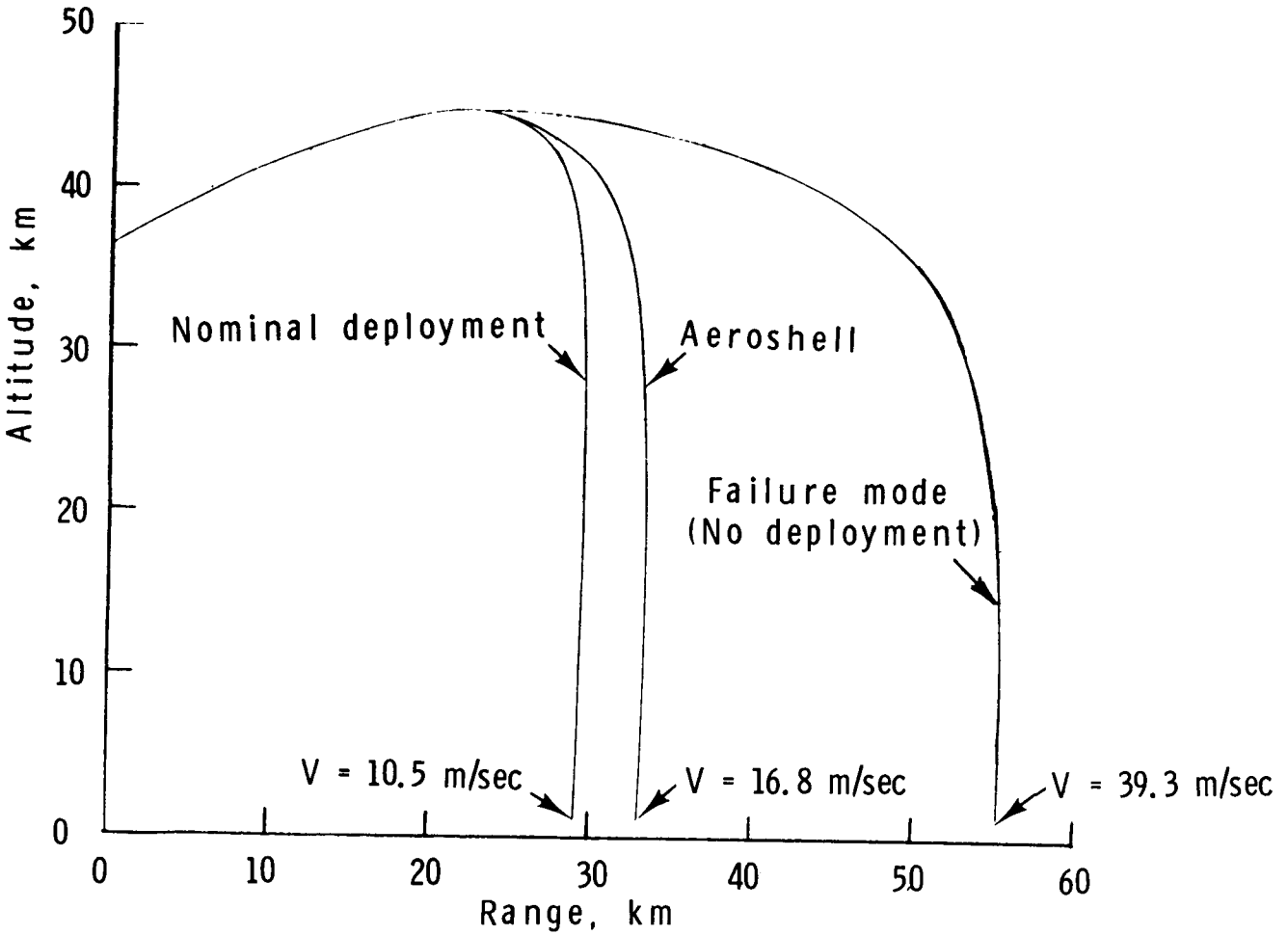
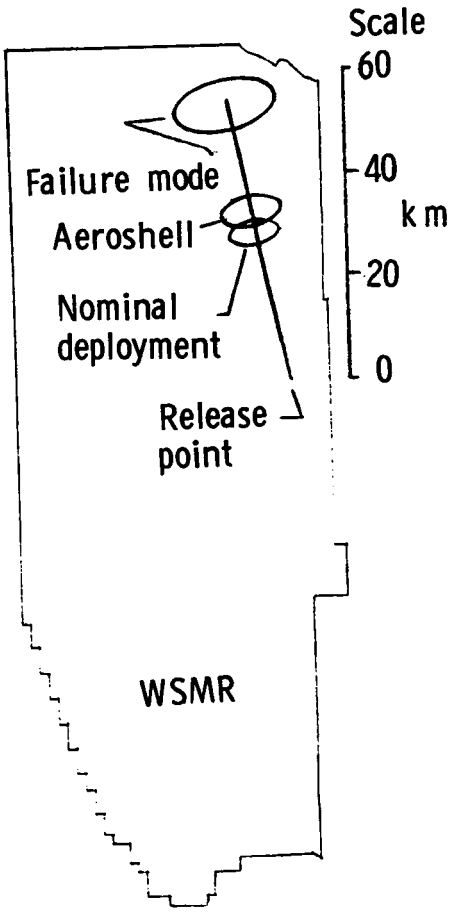


Figure 21.- Balloon launch probability.



(a) Altitude against horizontal range.

Figure 22.- Nominal and no deployment trajectories, supersonic flight.



(b) Ground track and dispersions.

Figure 22.- Concluded.

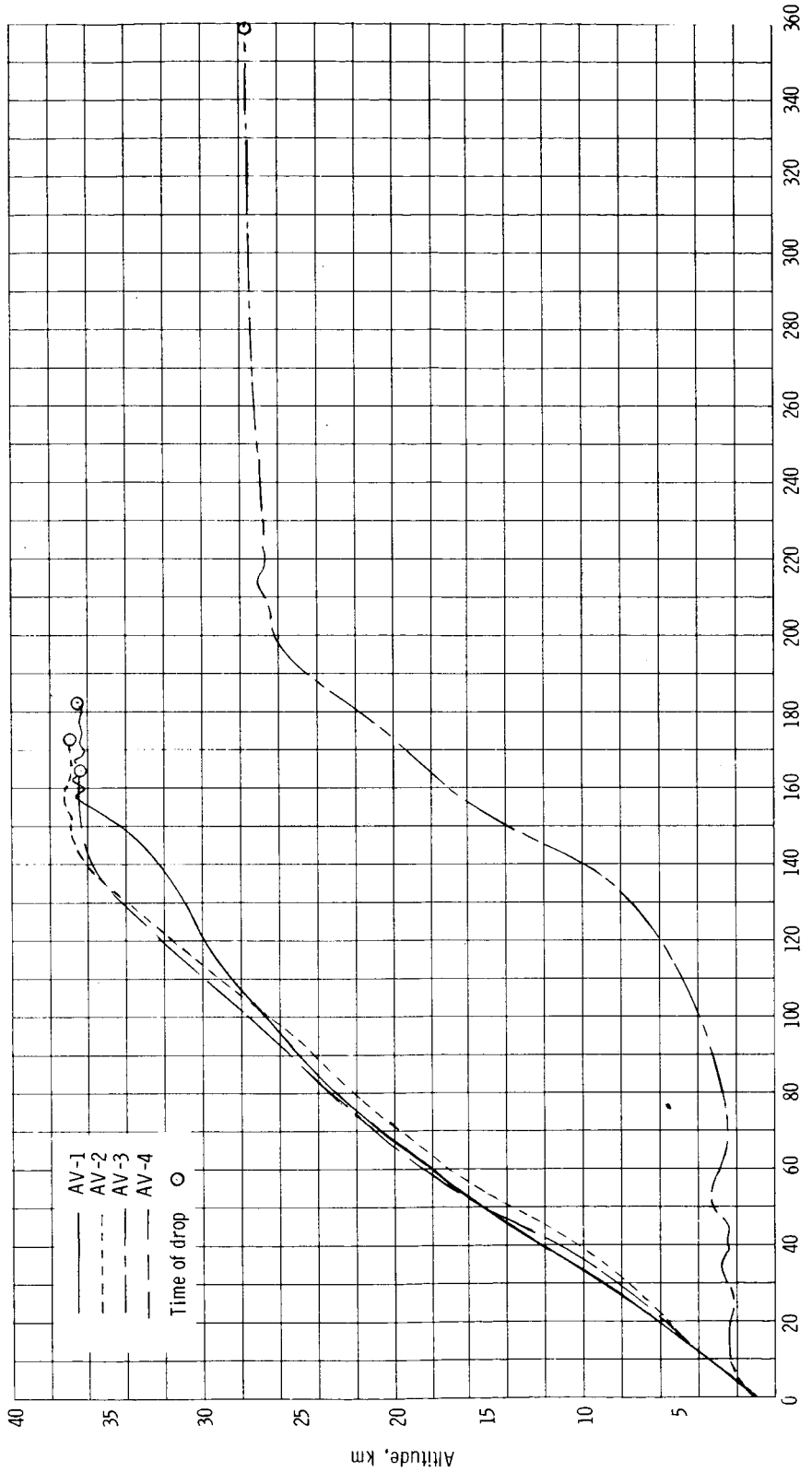


Figure 23.- Altitude time history for the balloons.

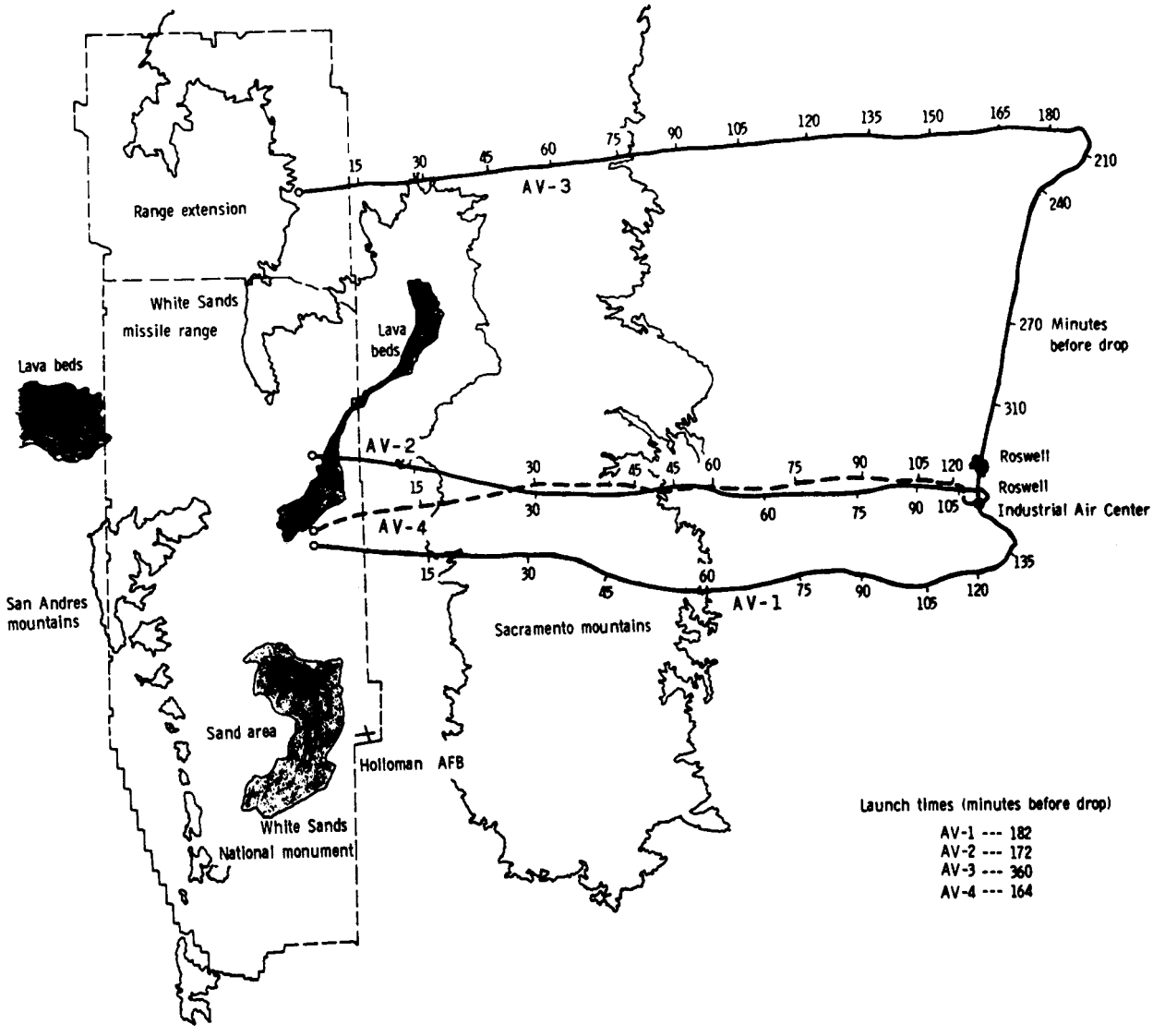


Figure 24.- Ground tracks of balloons. Time marks are minutes before drop.

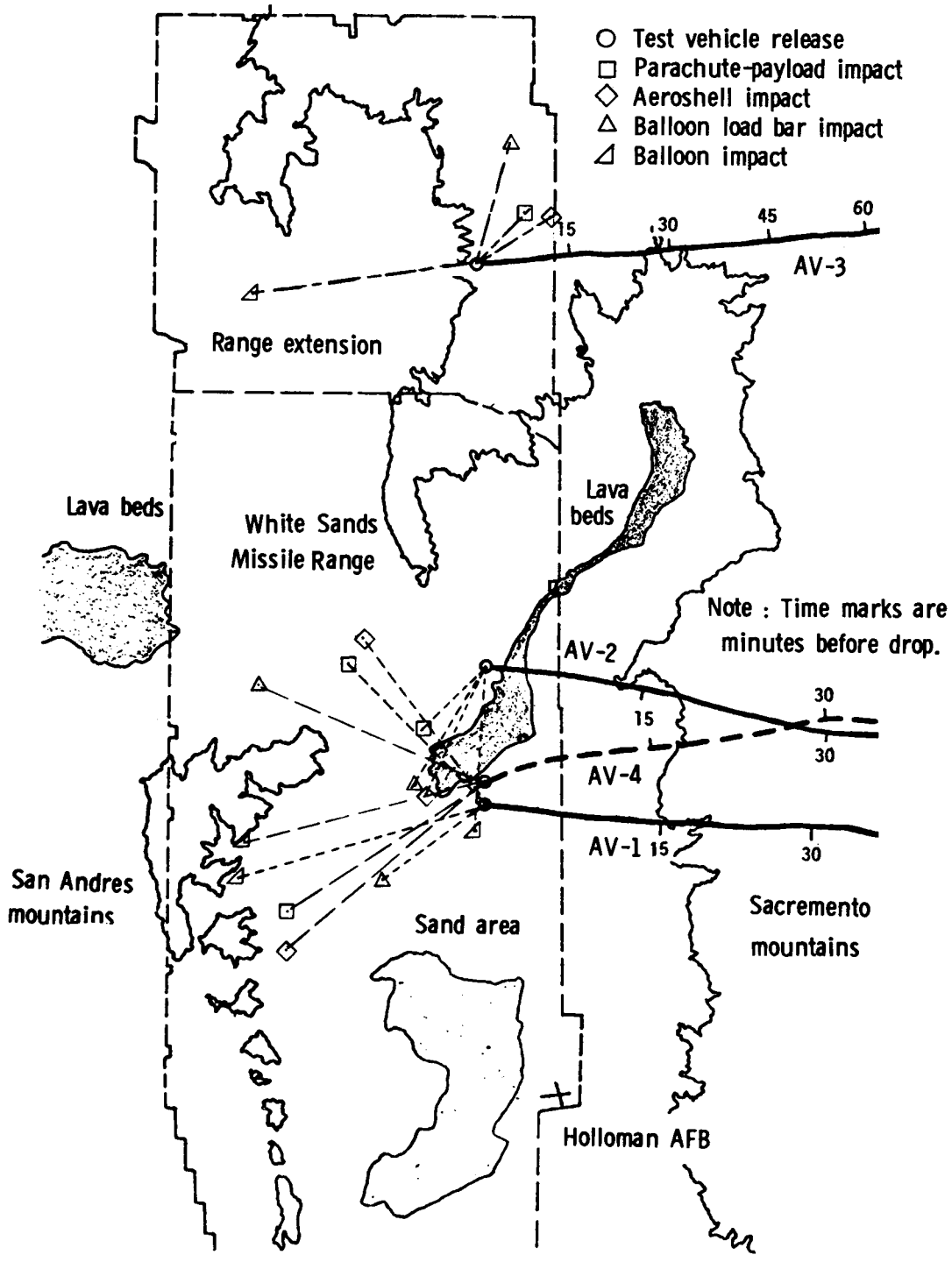
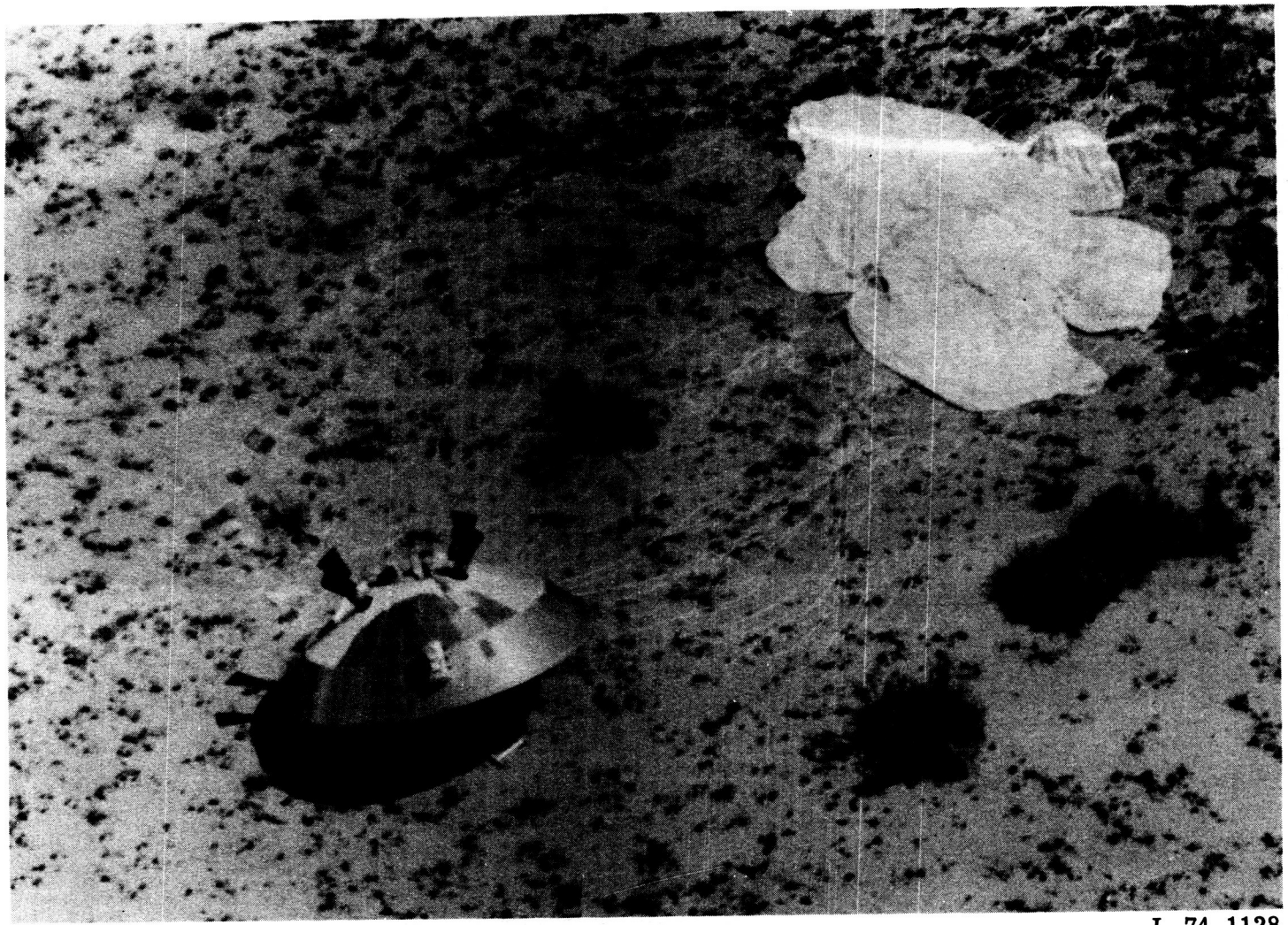
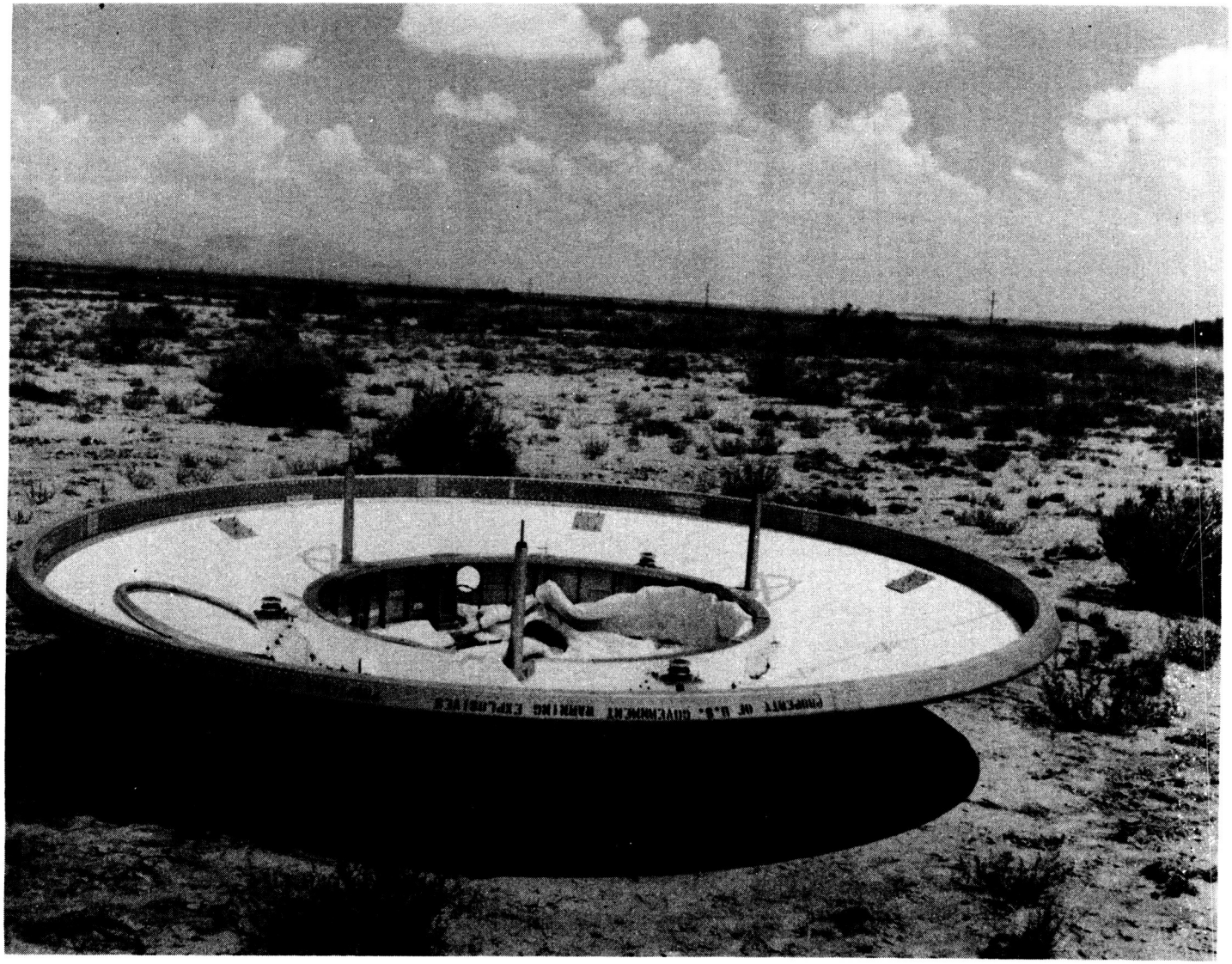


Figure 25.- Impact points for various components. Lines do not show ground track but merely connect release point with impact point.



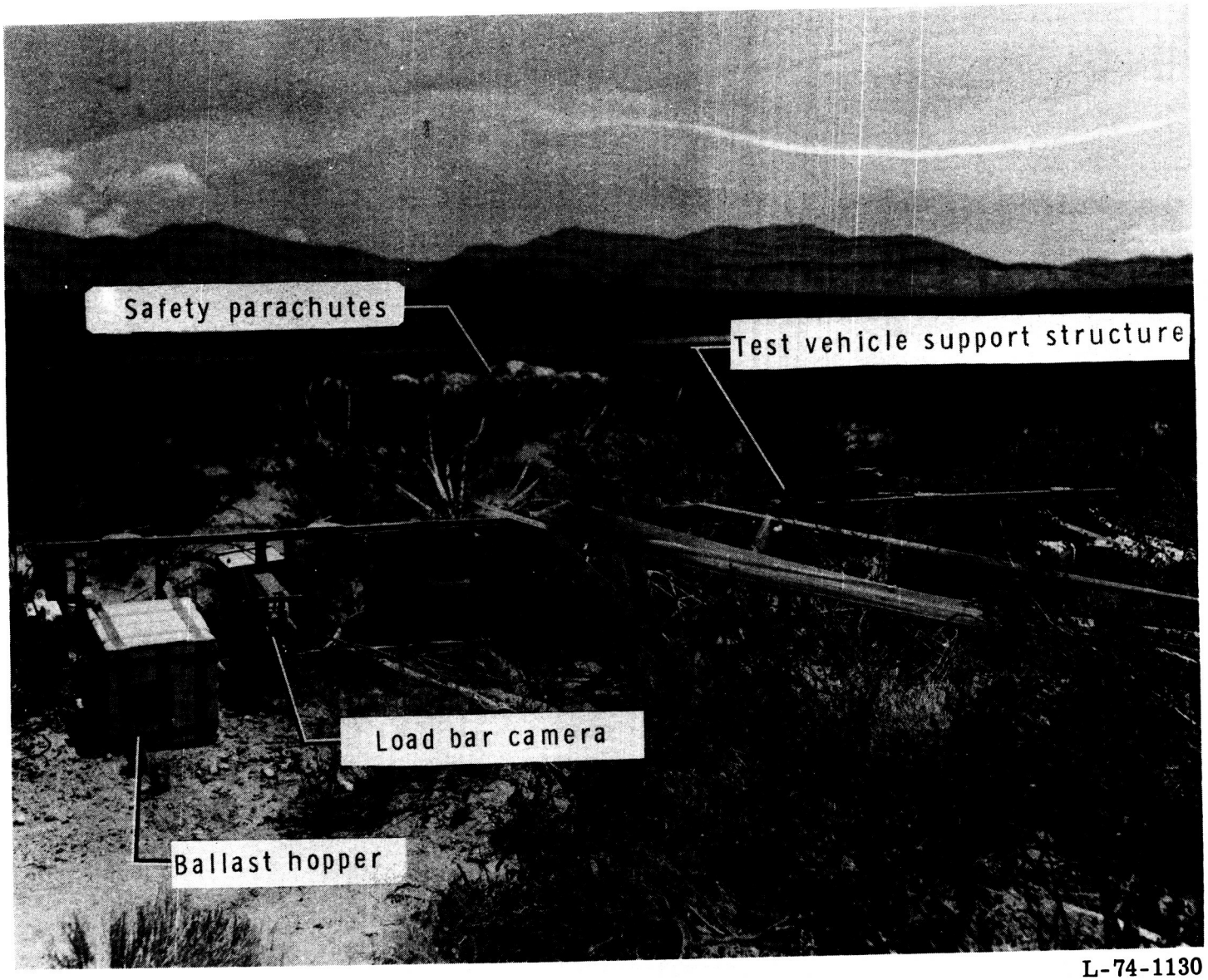
L-74-1128

Figure 26.- Photograph of payload parachute after impact.



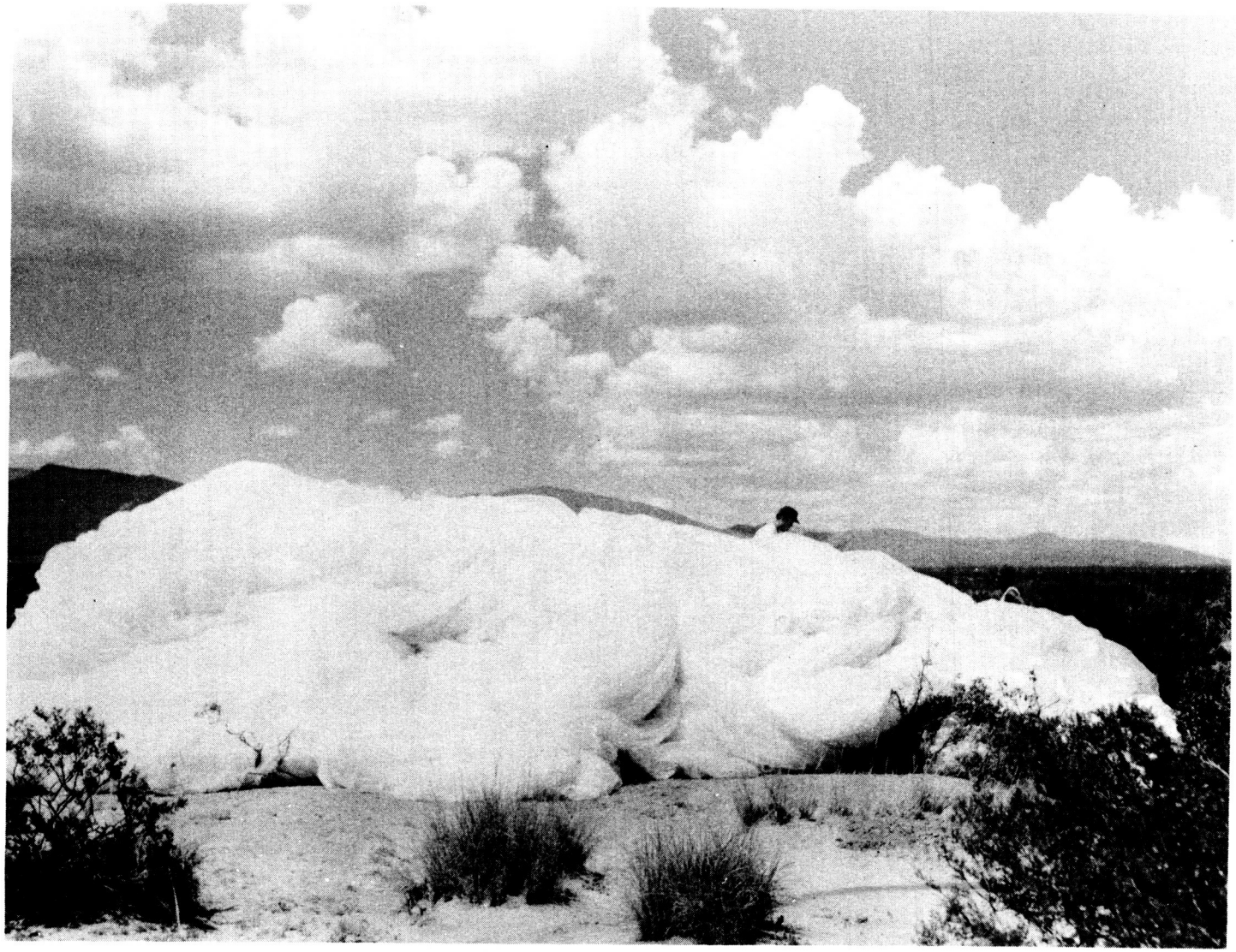
L-74-1129

Figure 27.- Photograph of aeroshell after impact.



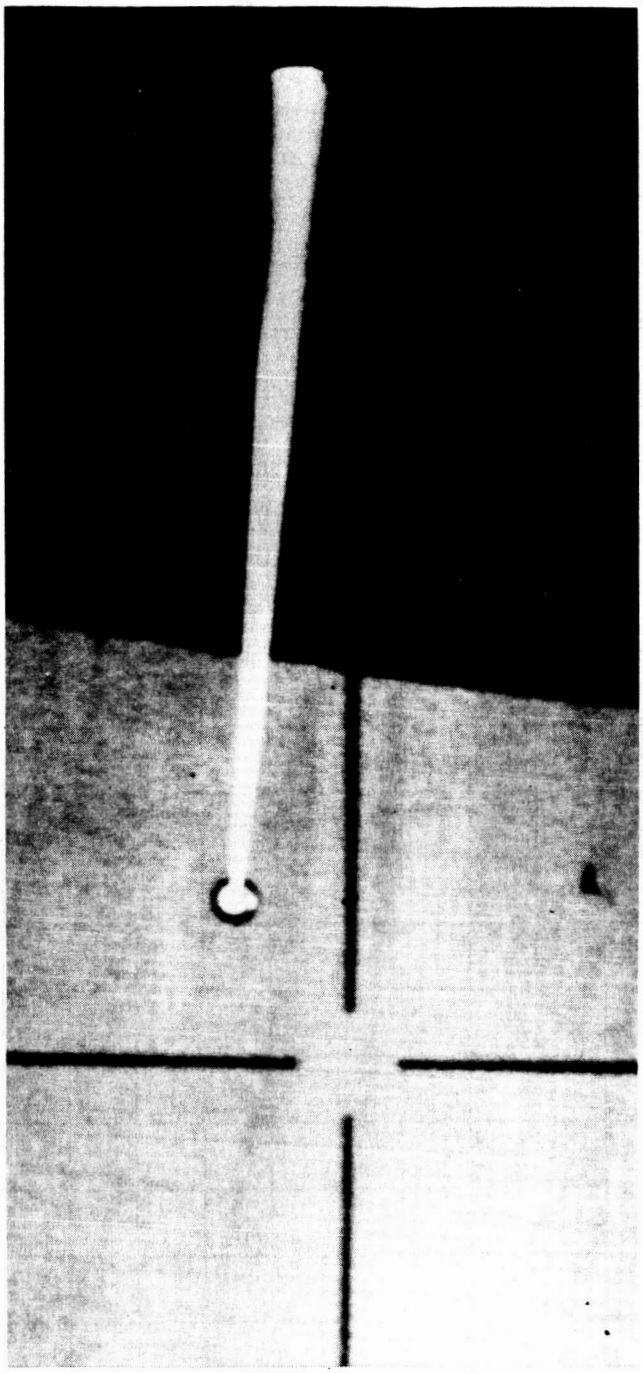
L-74-1130

Figure 28.- Photograph of balloon load bar after impact.



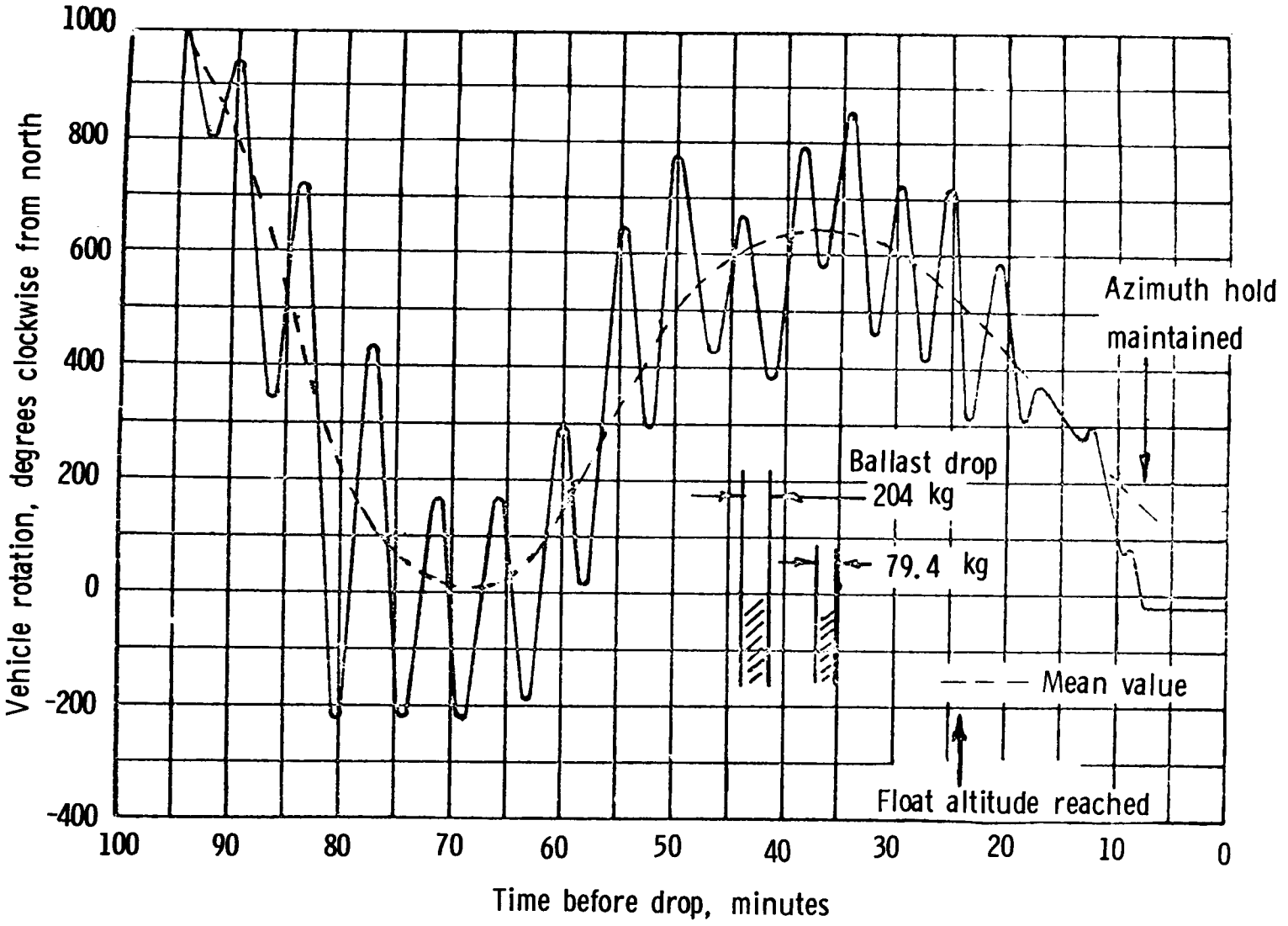
L-74-1131

Figure 29.- Photograph of balloon after impact.



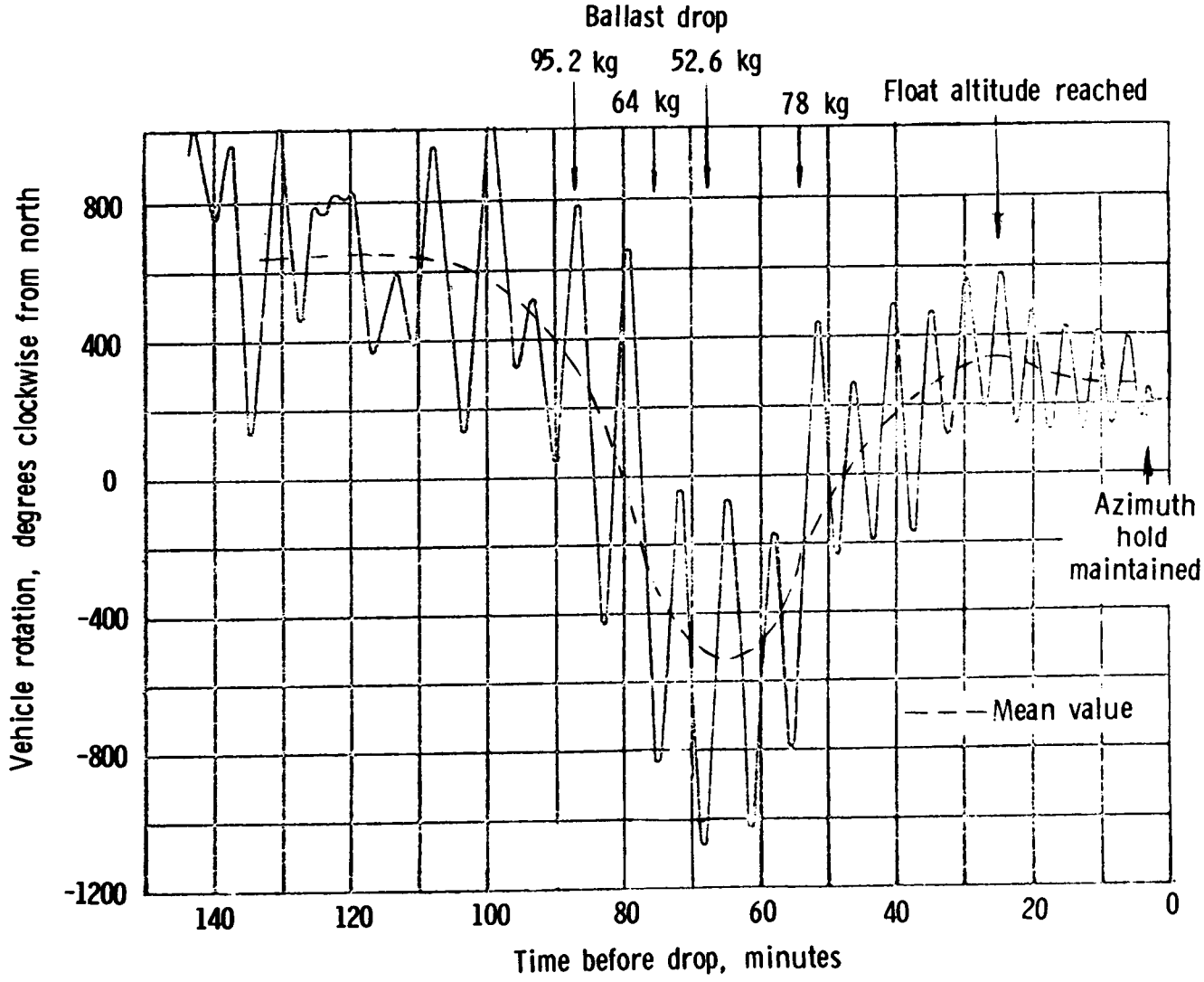
L-74-1132

Figure 30.- Calibration photograph of load bar pendulum.



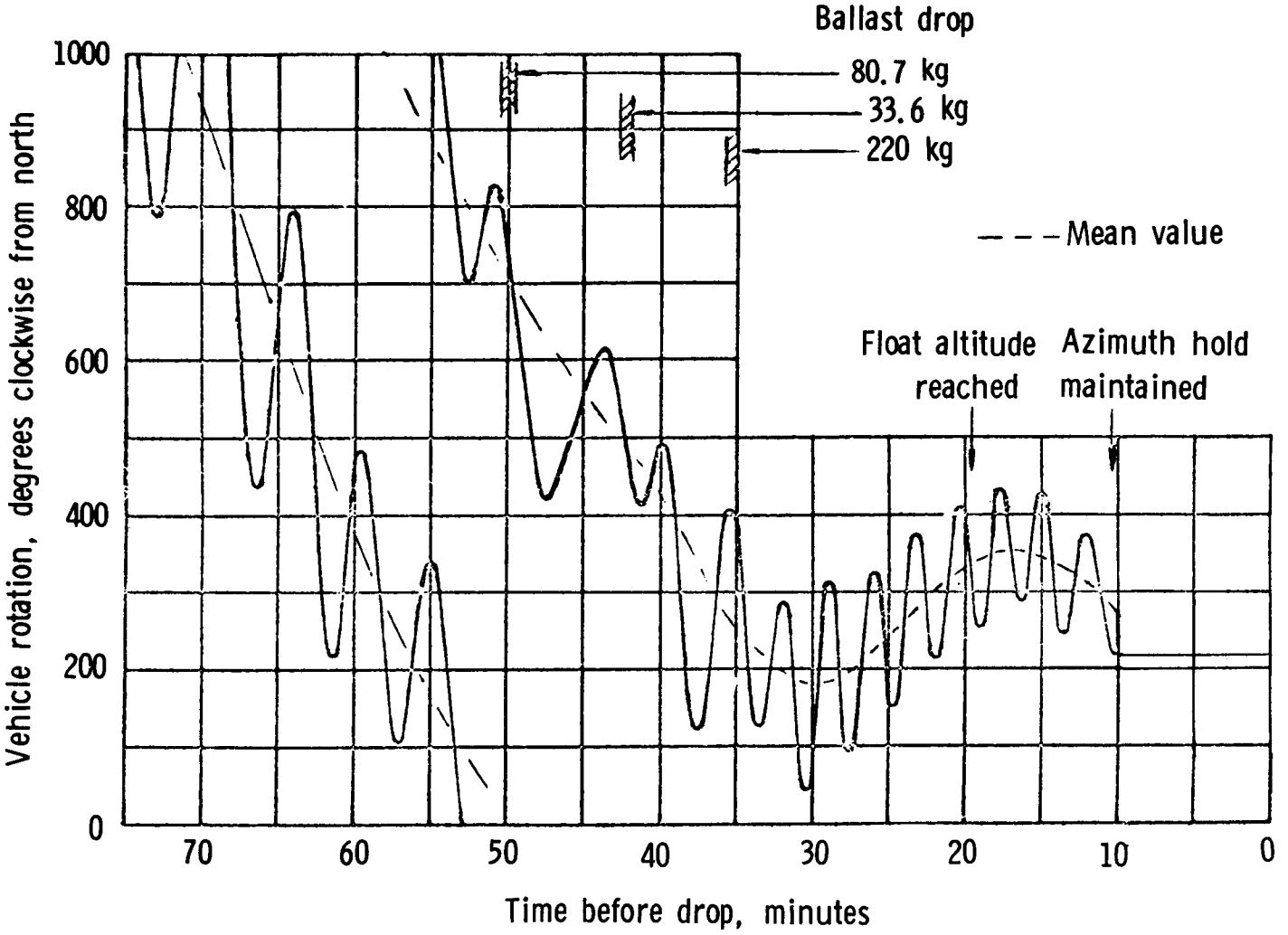
(a) AV-1 flight.

Figure 31.- Performance of pointing system.



(b) AV-2 flight.

Figure 31.- Continued.



(c) AV-4 flight.

Figure 31.- Concluded.

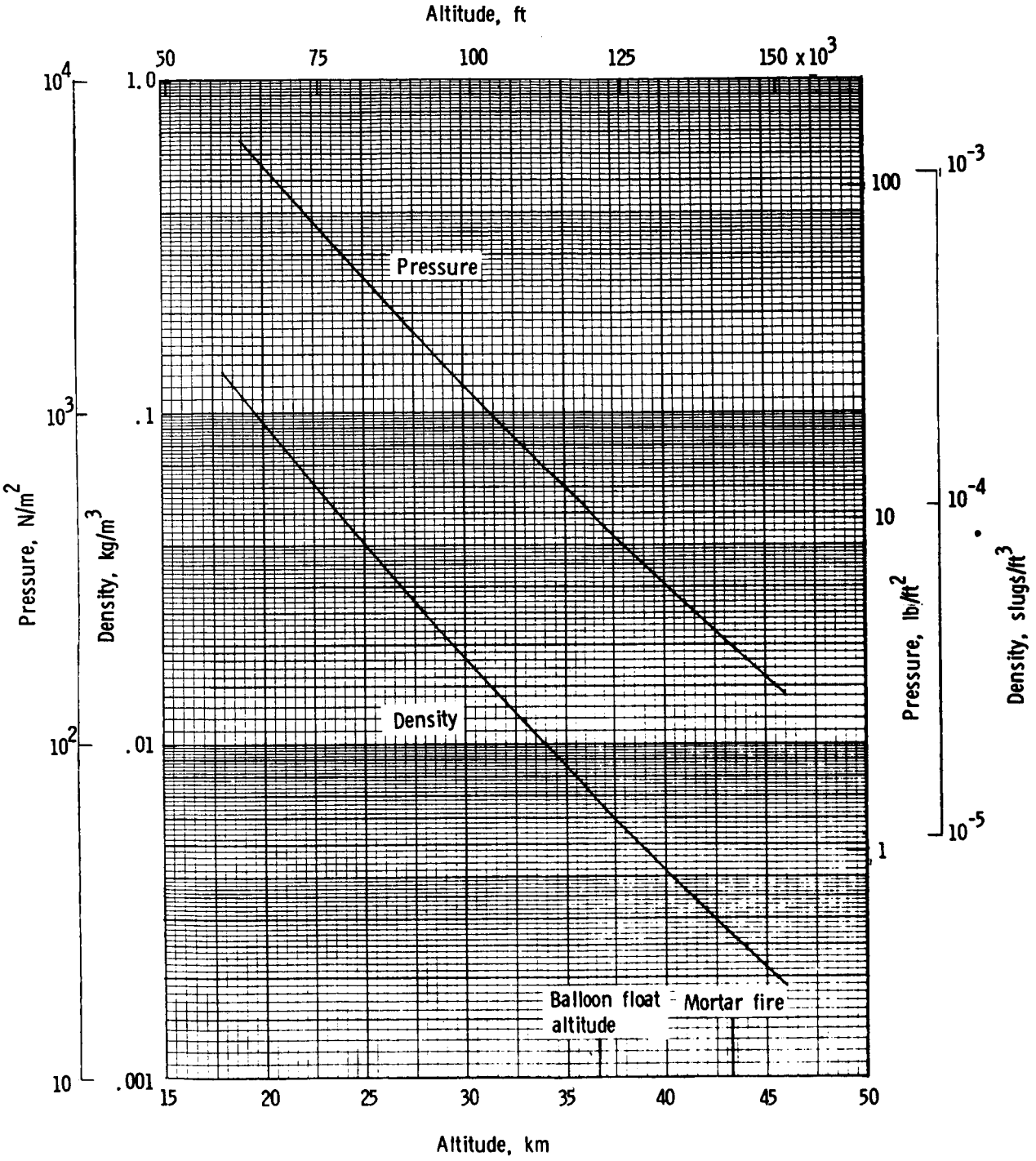


Figure 32.- Variation of ambient pressure and density with altitude. AV-1.

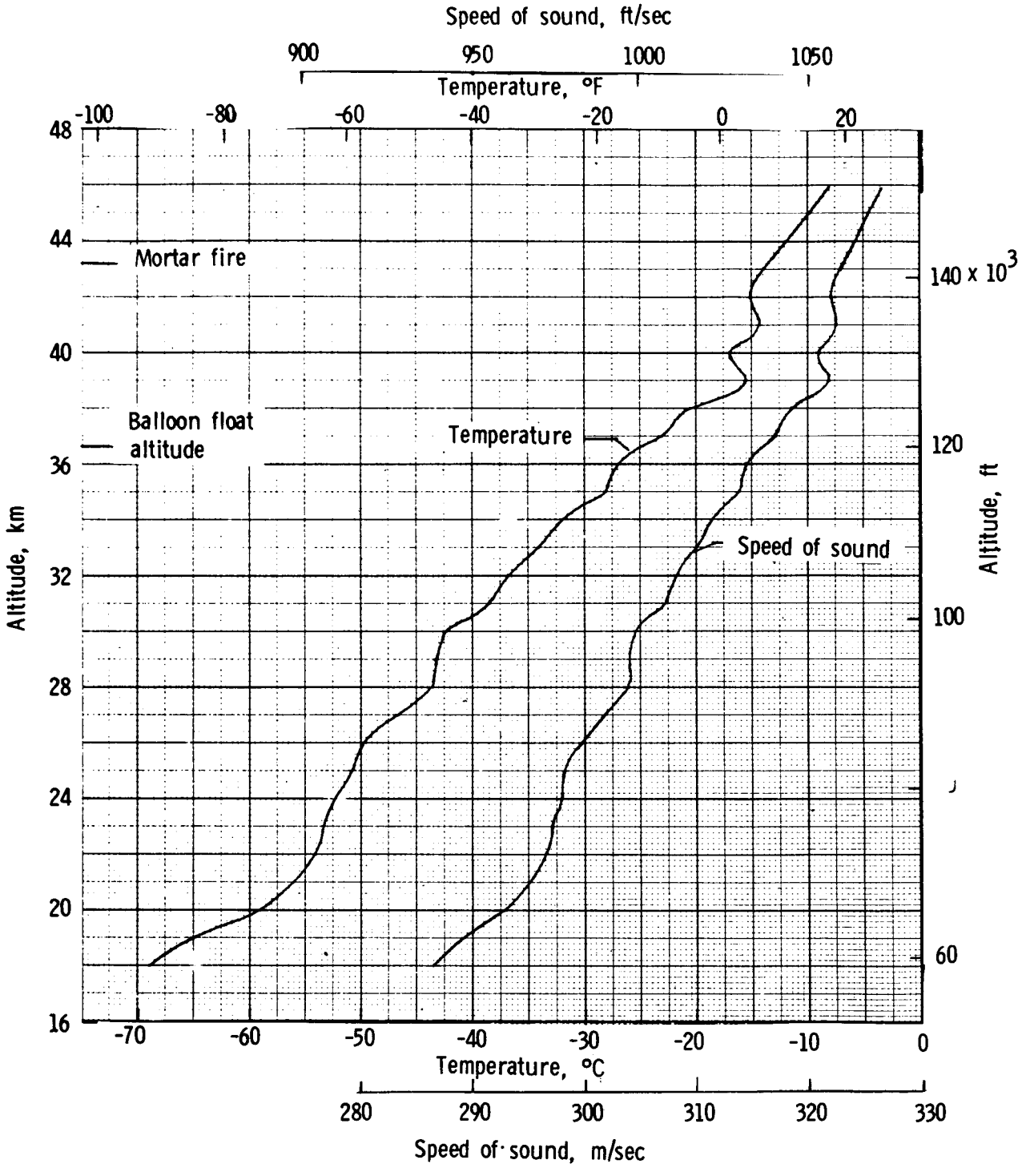


Figure 33.- Variation of ambient temperature and speed of sound with altitude. AV-1.

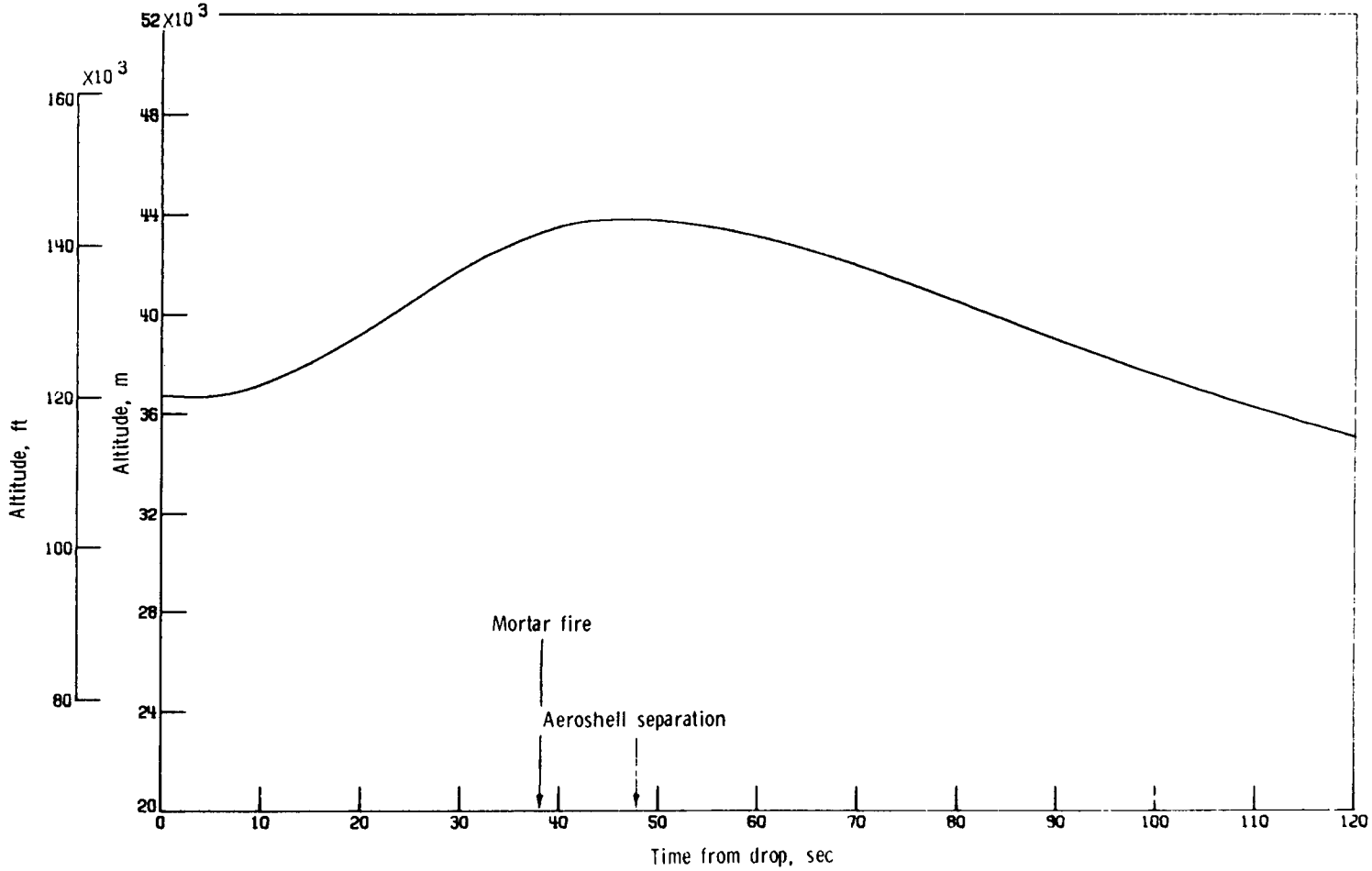


Figure 34.- Time history of altitude. AV-1.

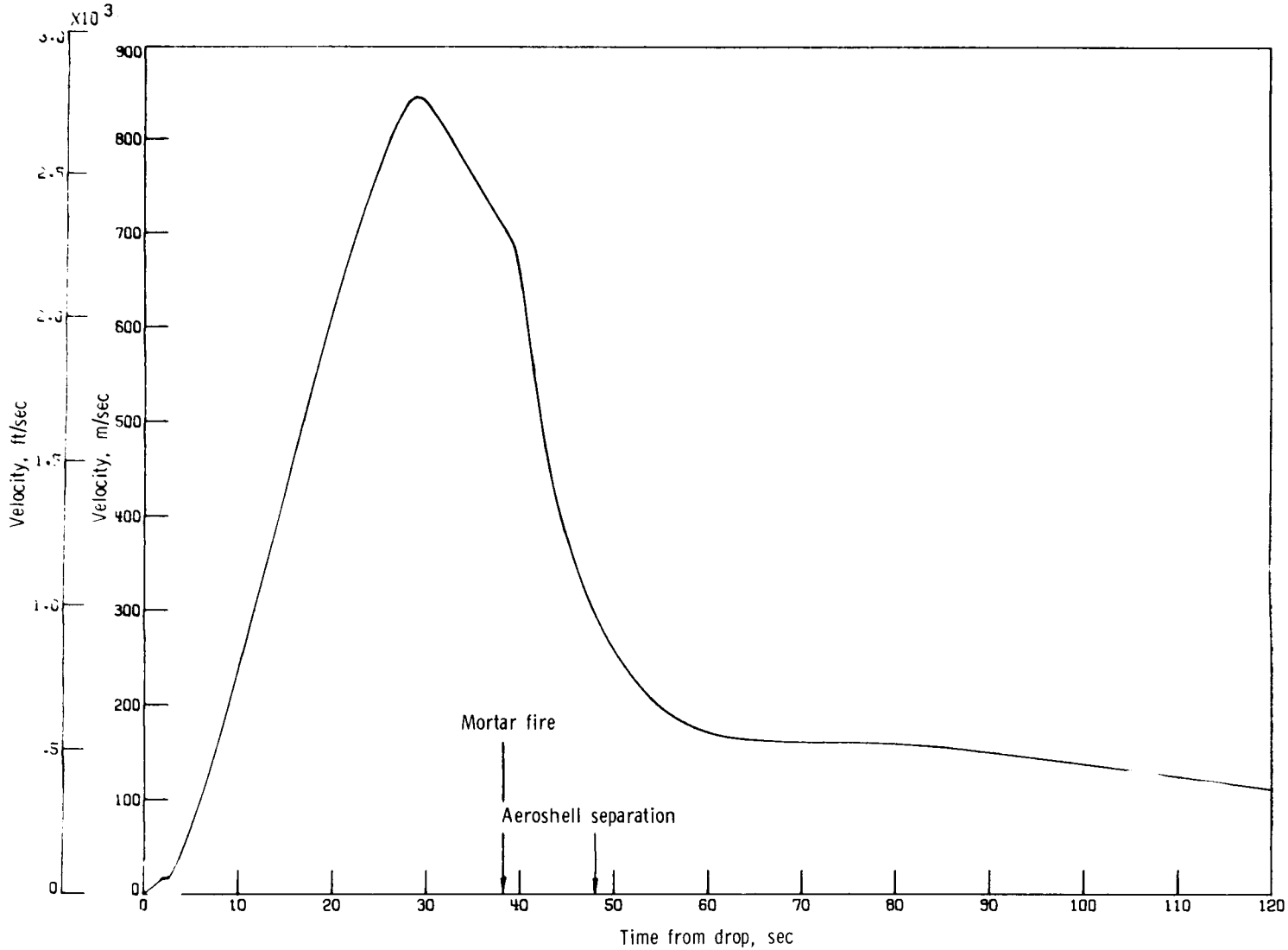


Figure 35.- Time history of velocity. AV-1.

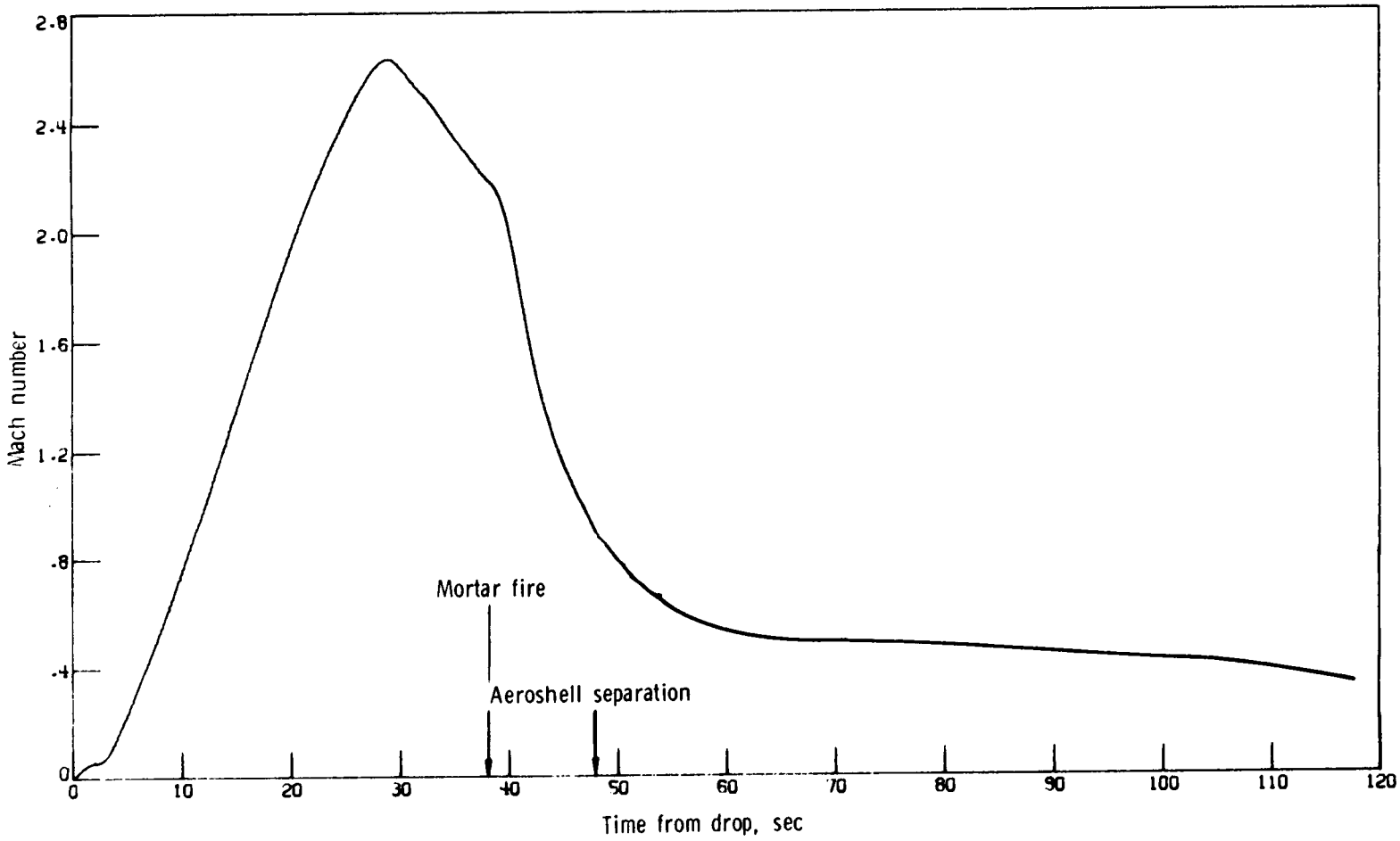


Figure 36.- Time history of Mach number. AV-1.

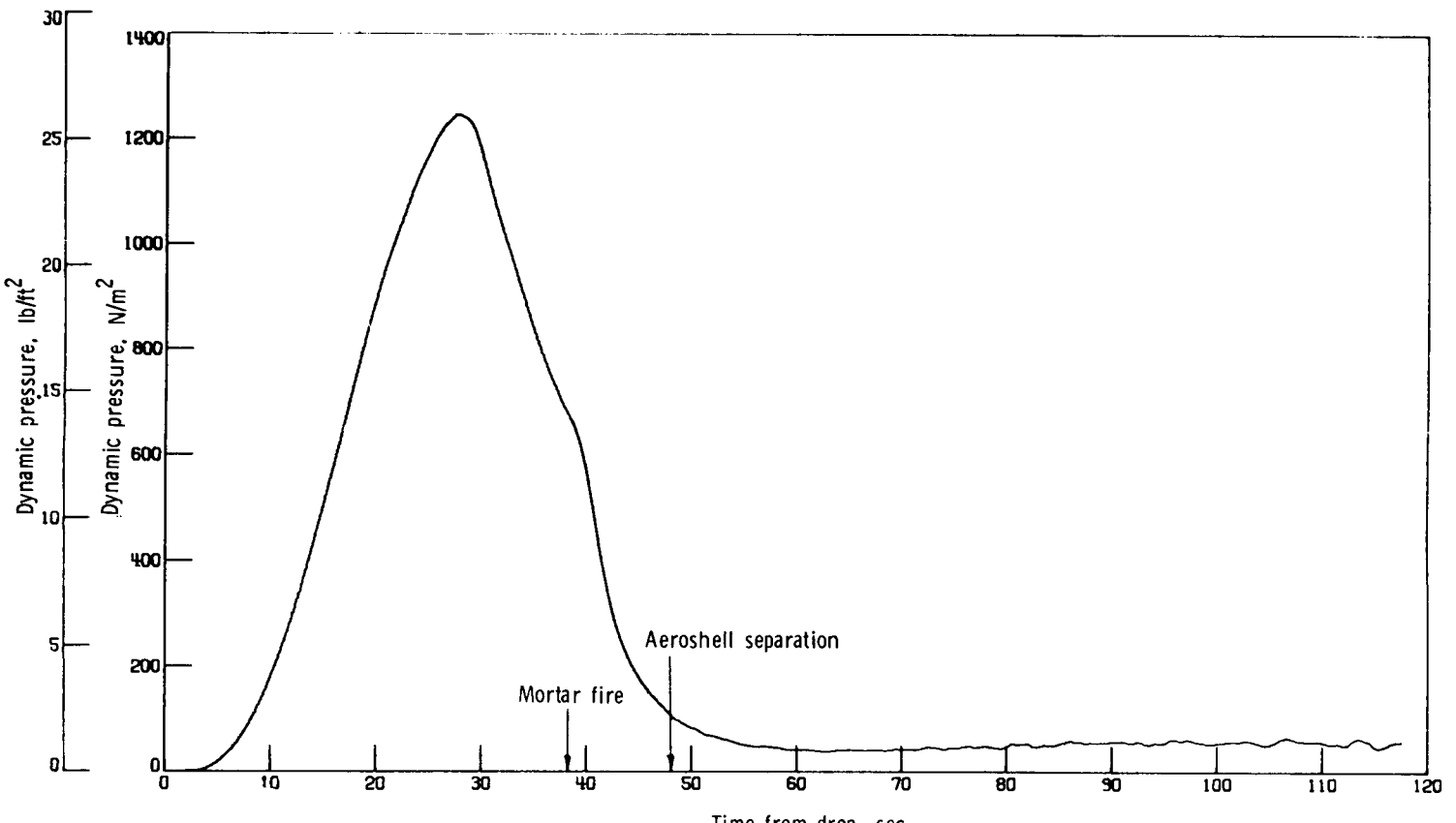


Figure 37.- Time history of dynamic pressure. AV-1.

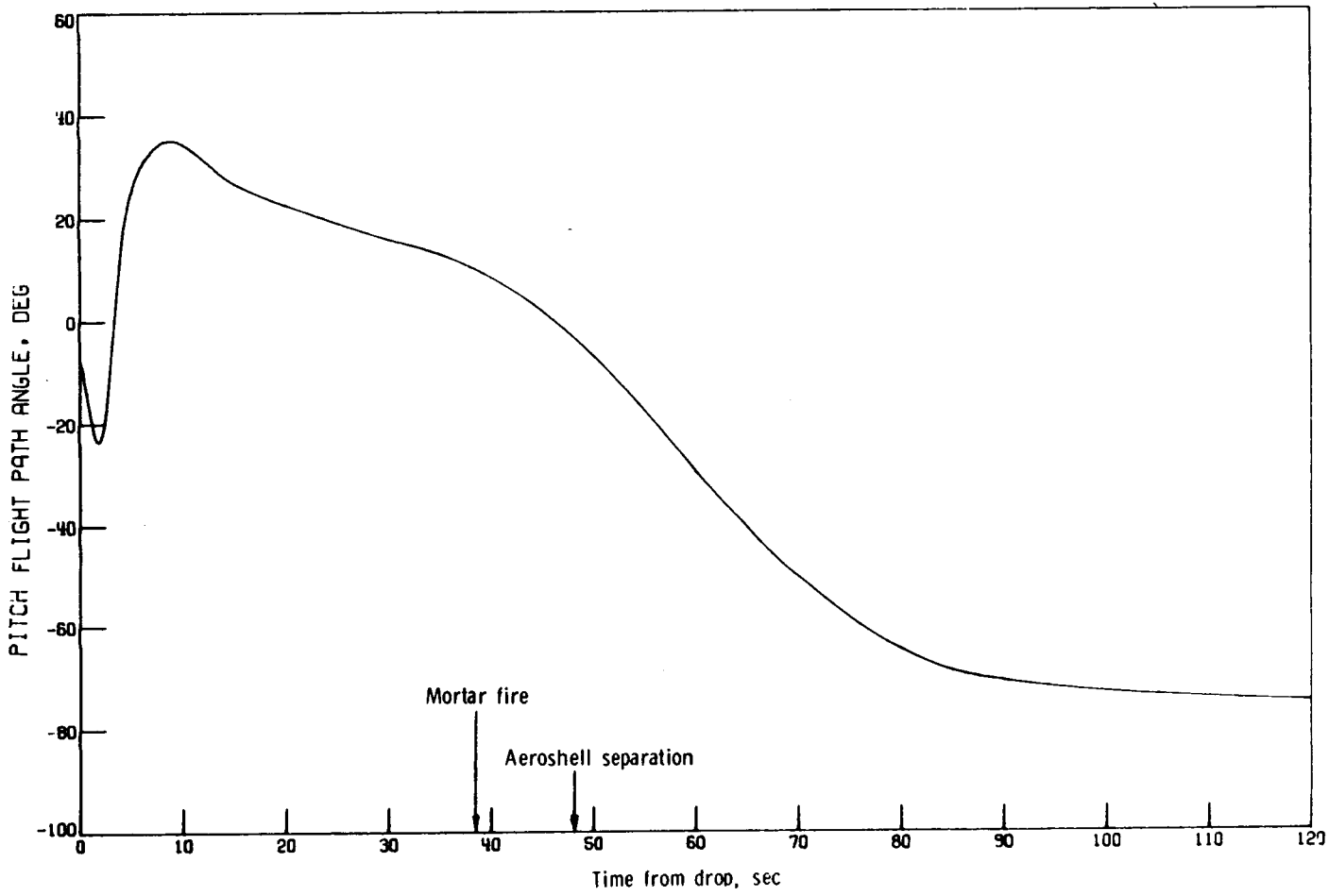


Figure 38.- Time history of vehicle flight path angle. AV-1.

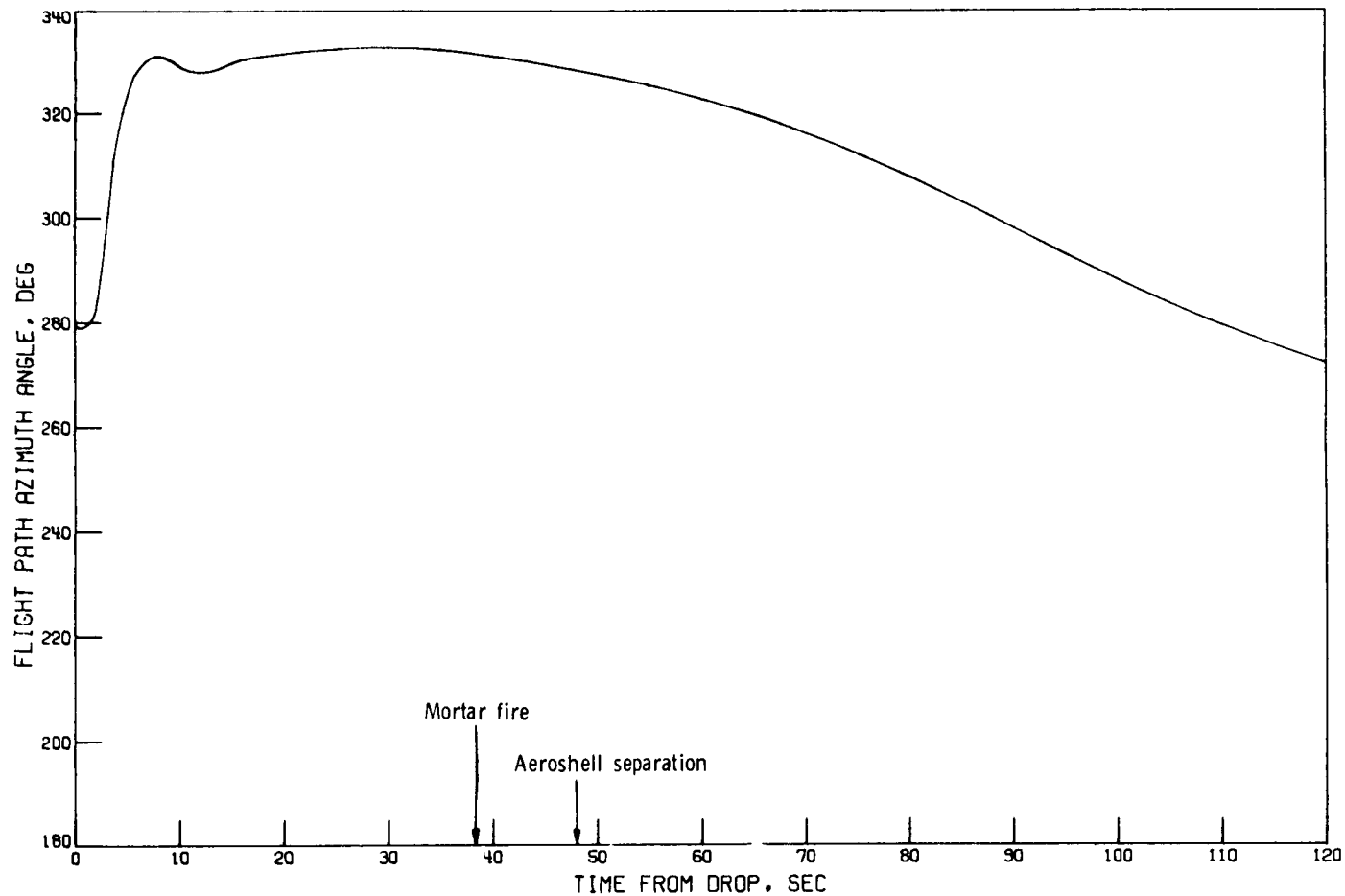


Figure 39.- Time history of flight azimuth angle. AV-1.

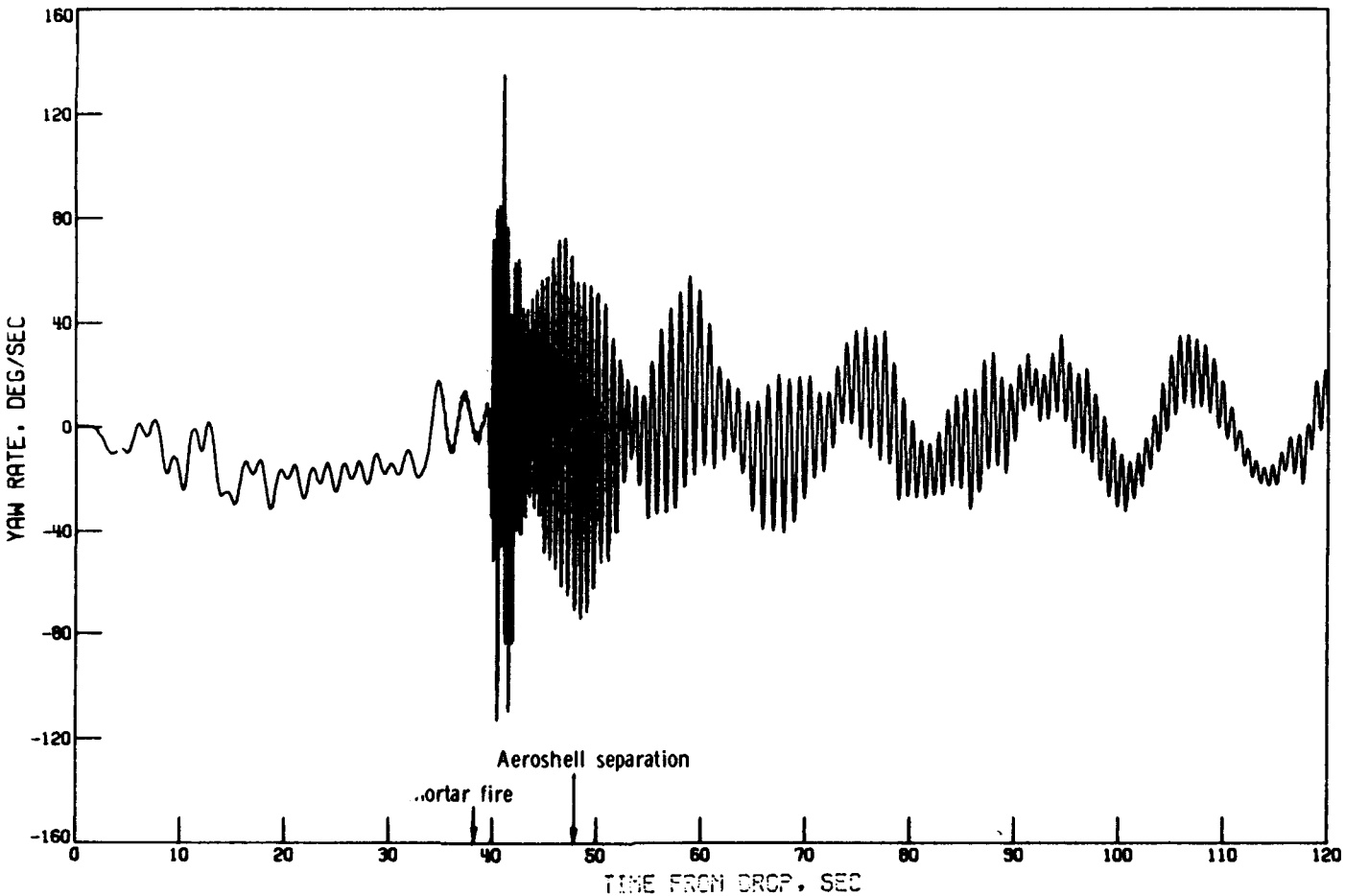


Figure 40.- Time history of yaw rate. AV-1.

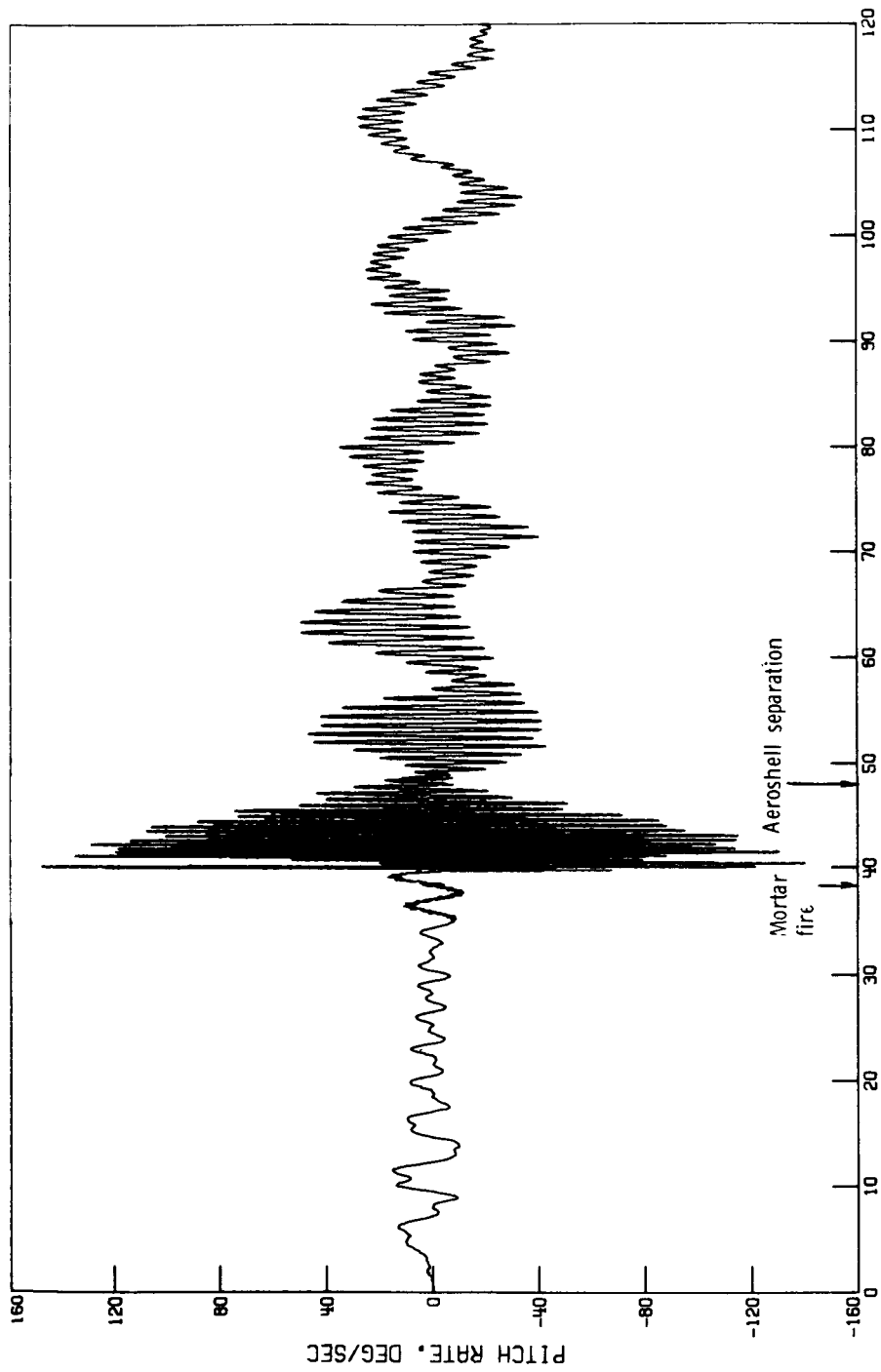


Figure 41.- Time history of pitch rate. AV-1.

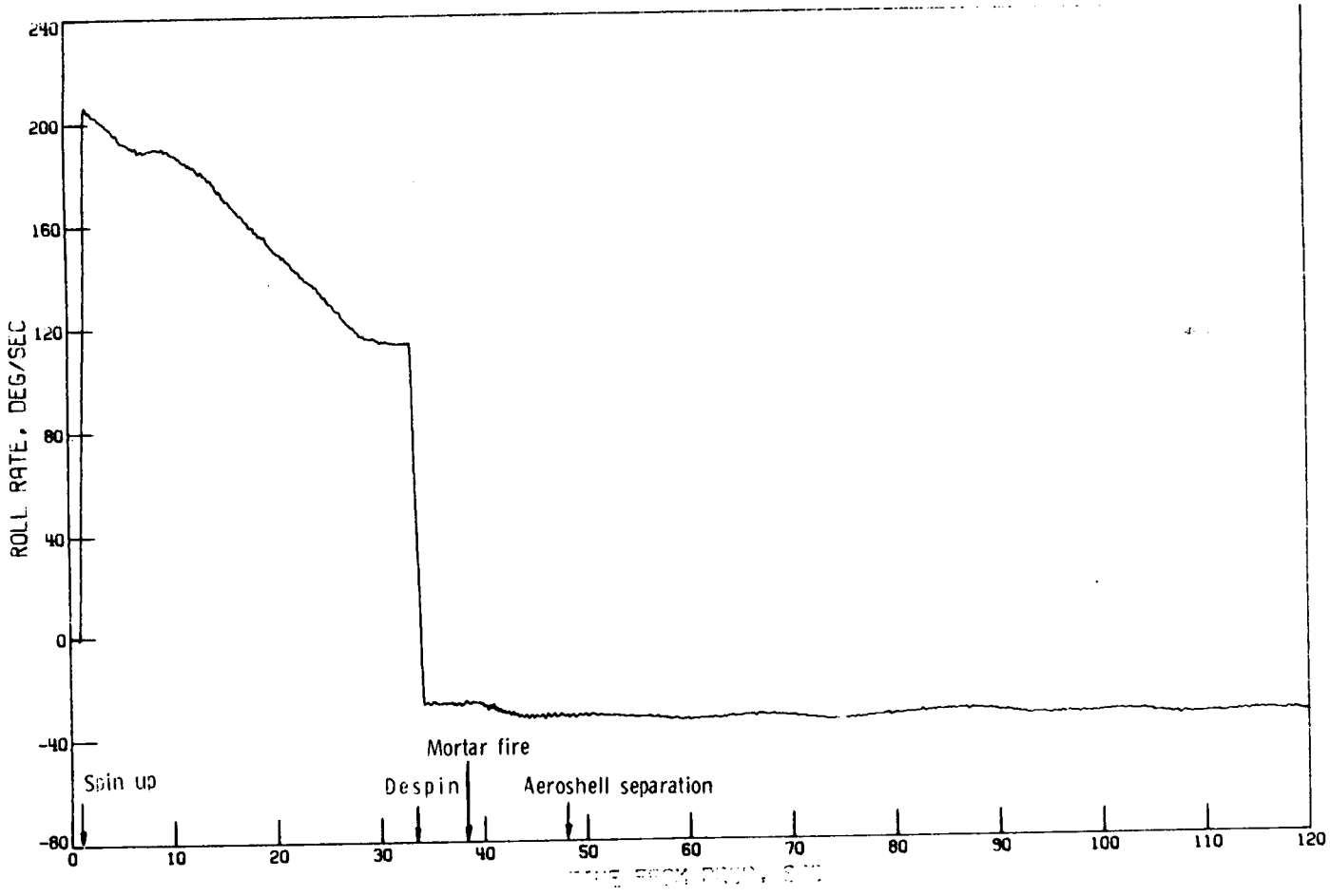


Figure 42.- Time history of roll rate. AV-1.

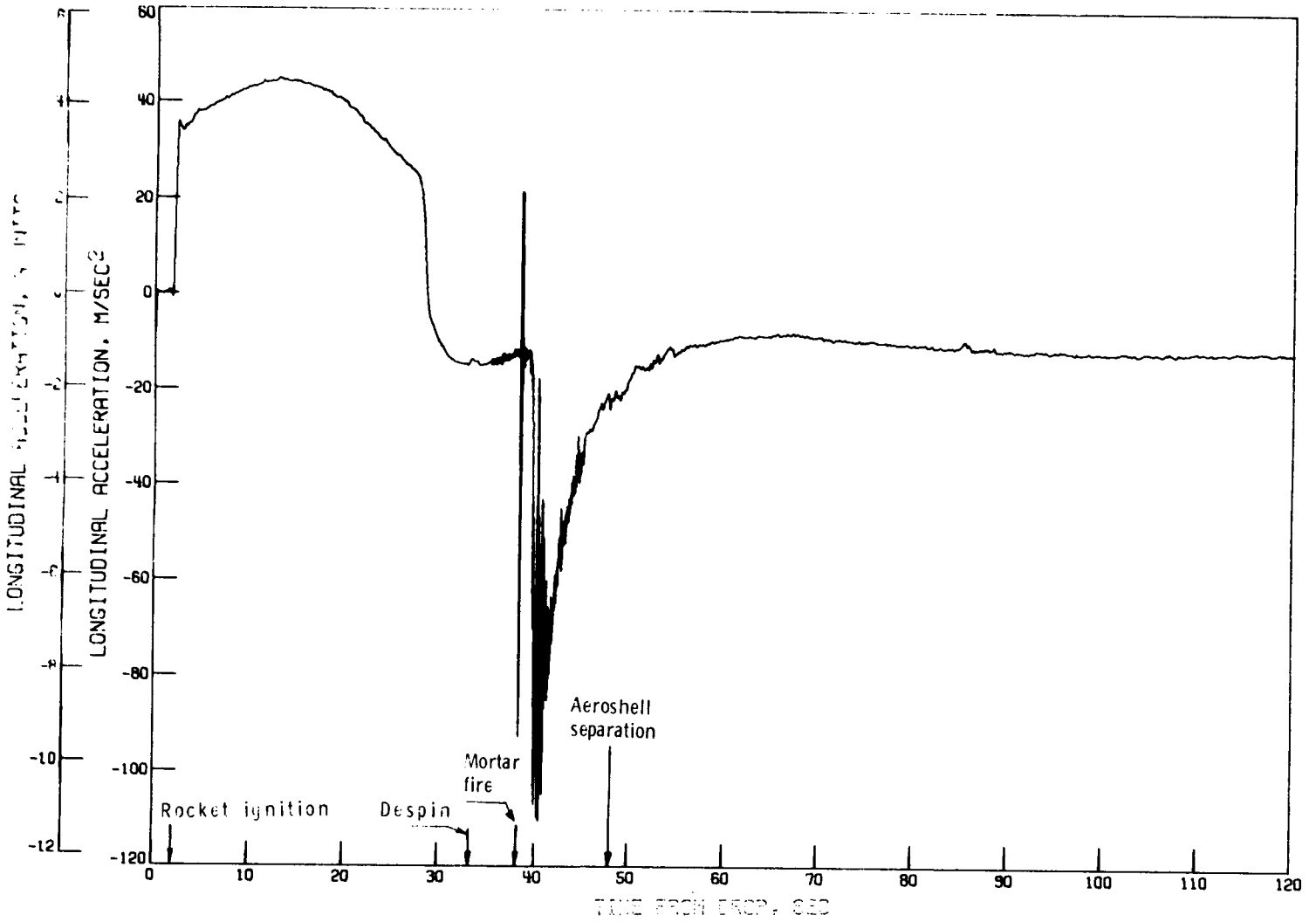


Figure 43.- Time history of longitudinal acceleration. AV-1.

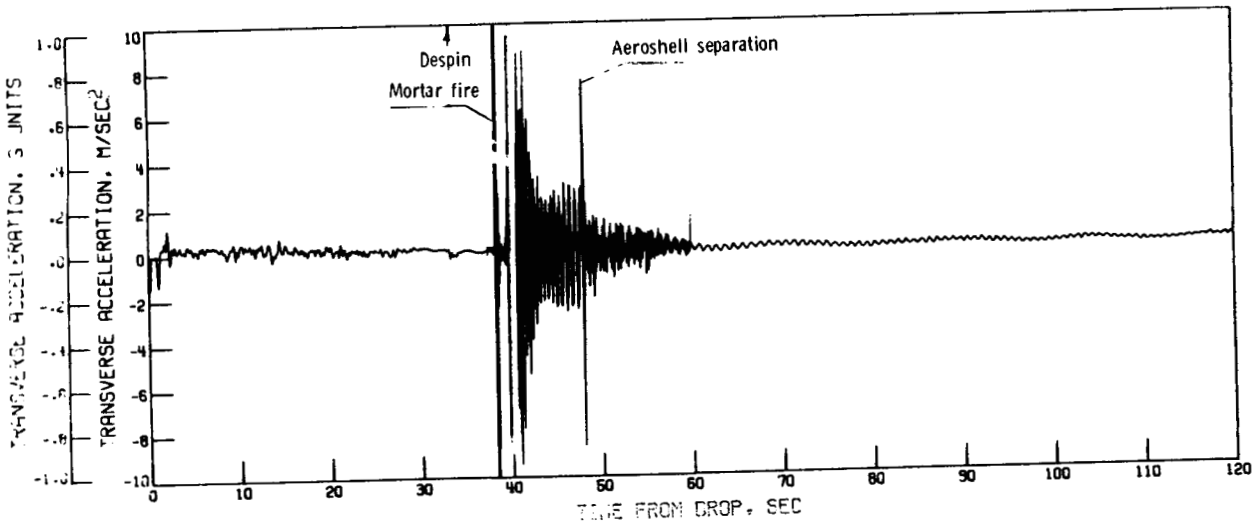


Figure 44.- Time history of transverse acceleration. AV-1; instrument limit, ±1g.

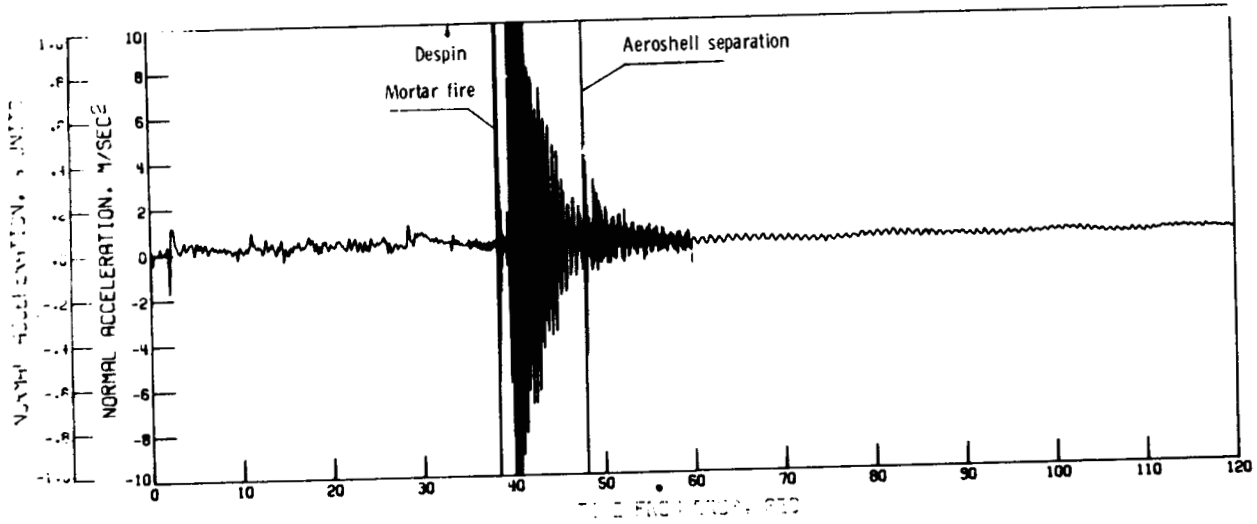


Figure 45.- Time history of normal acceleration. AV-1; instrument limit ±1g.

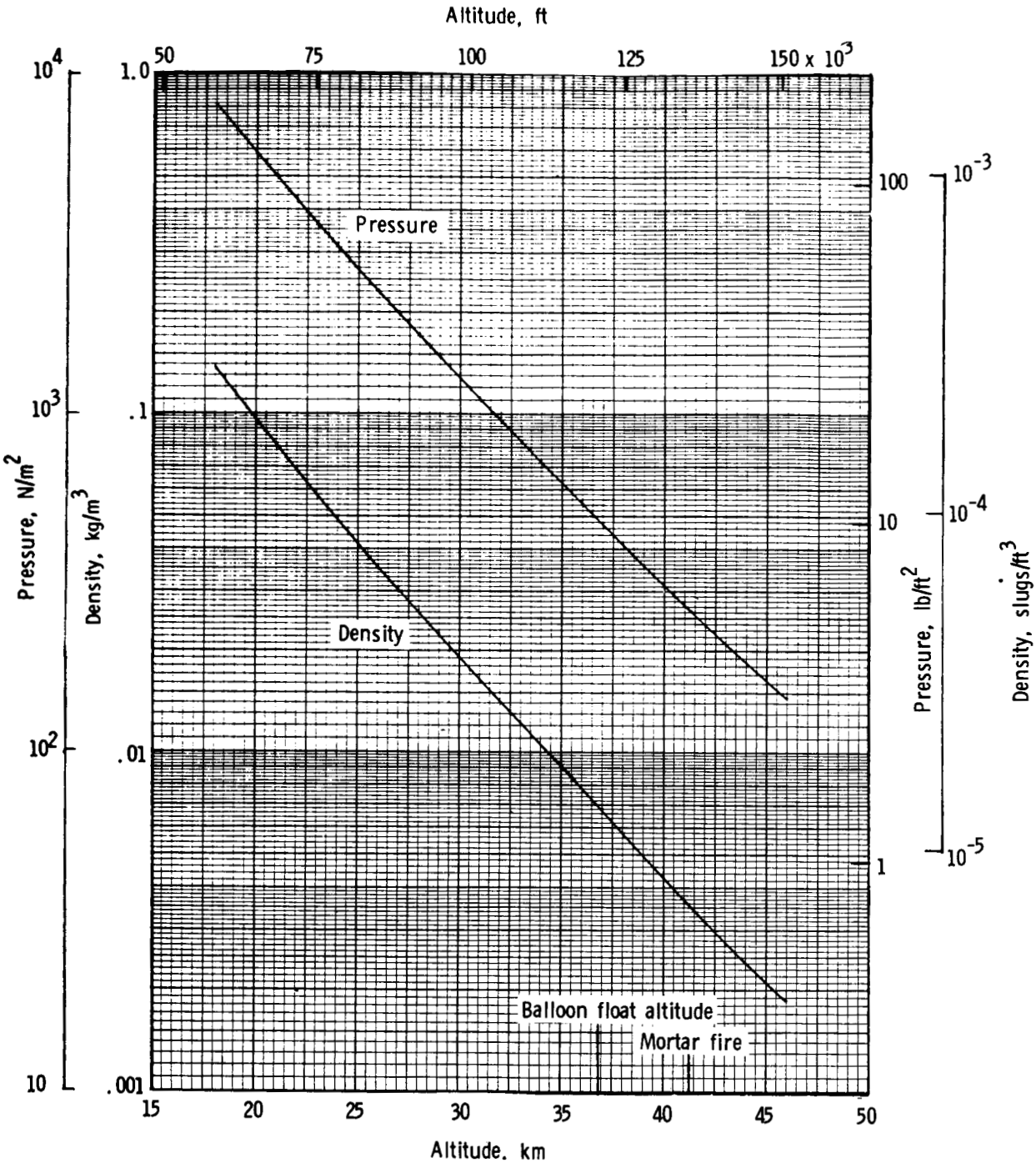


Figure 46.- Variation of ambient pressure and density with altitude. AV-2.

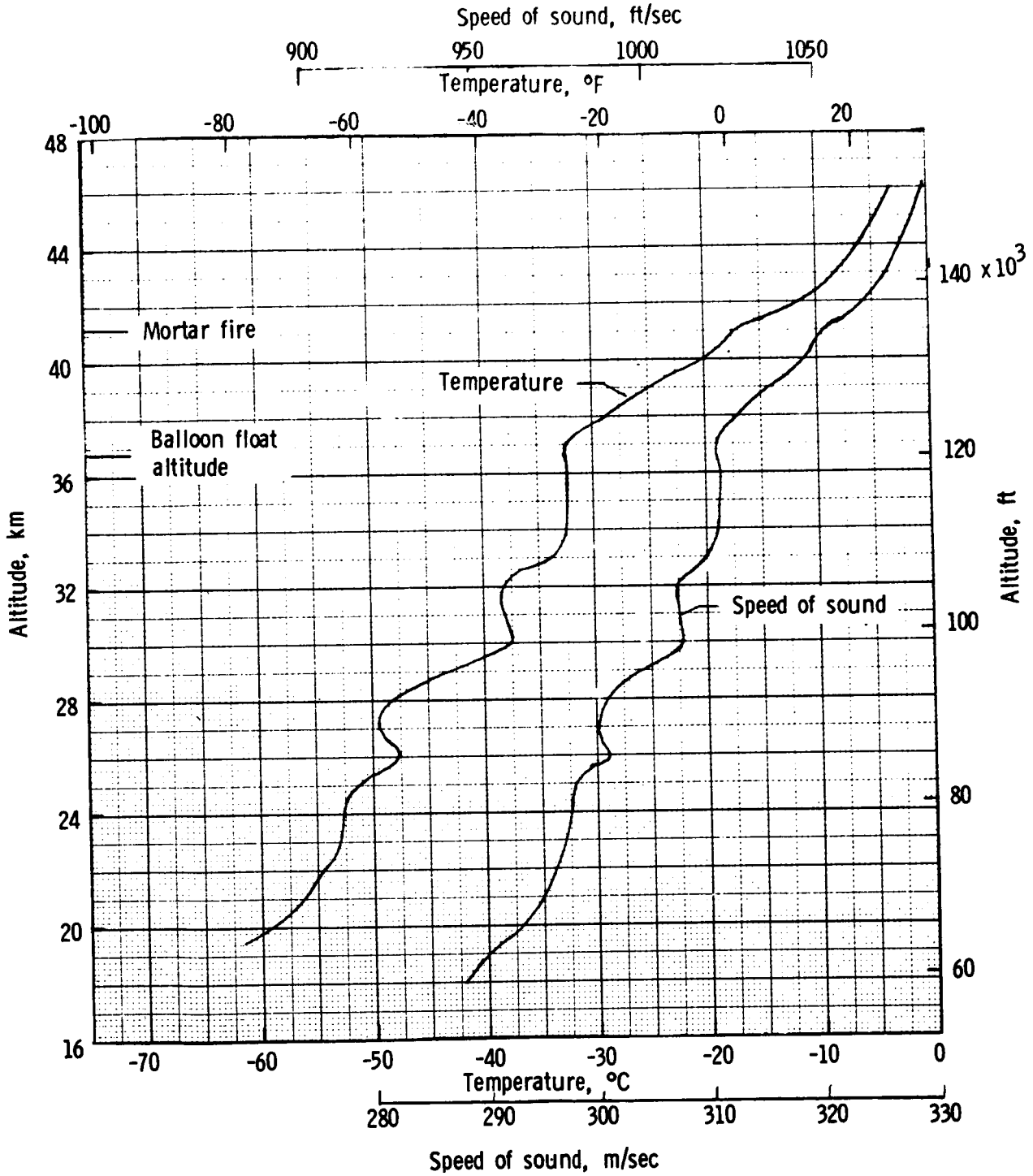


Figure 47.- Variation of ambient temperature and speed of sound with altitude. AV-2.

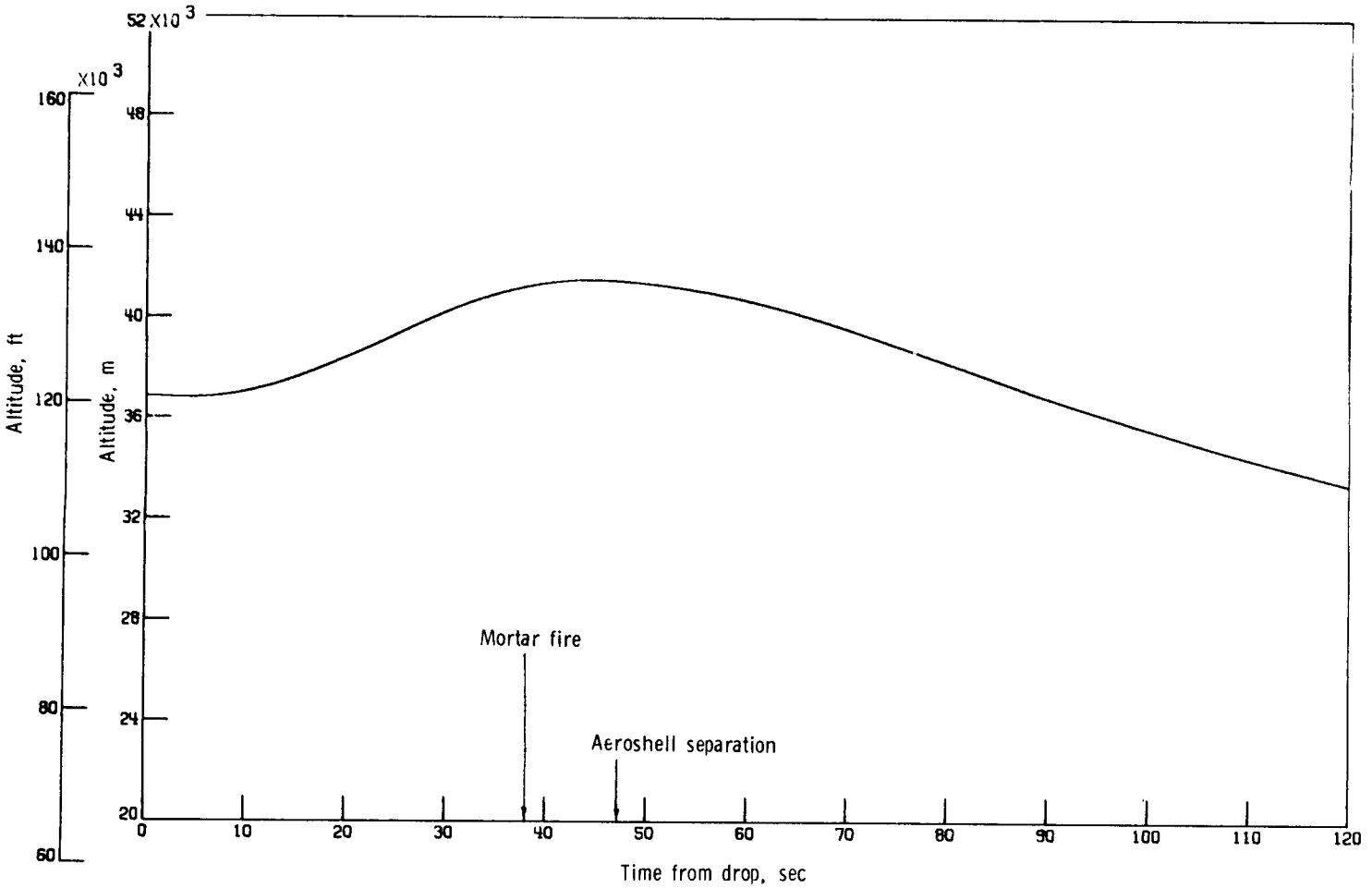


Figure 48.- Time history of altitude. AV-2.

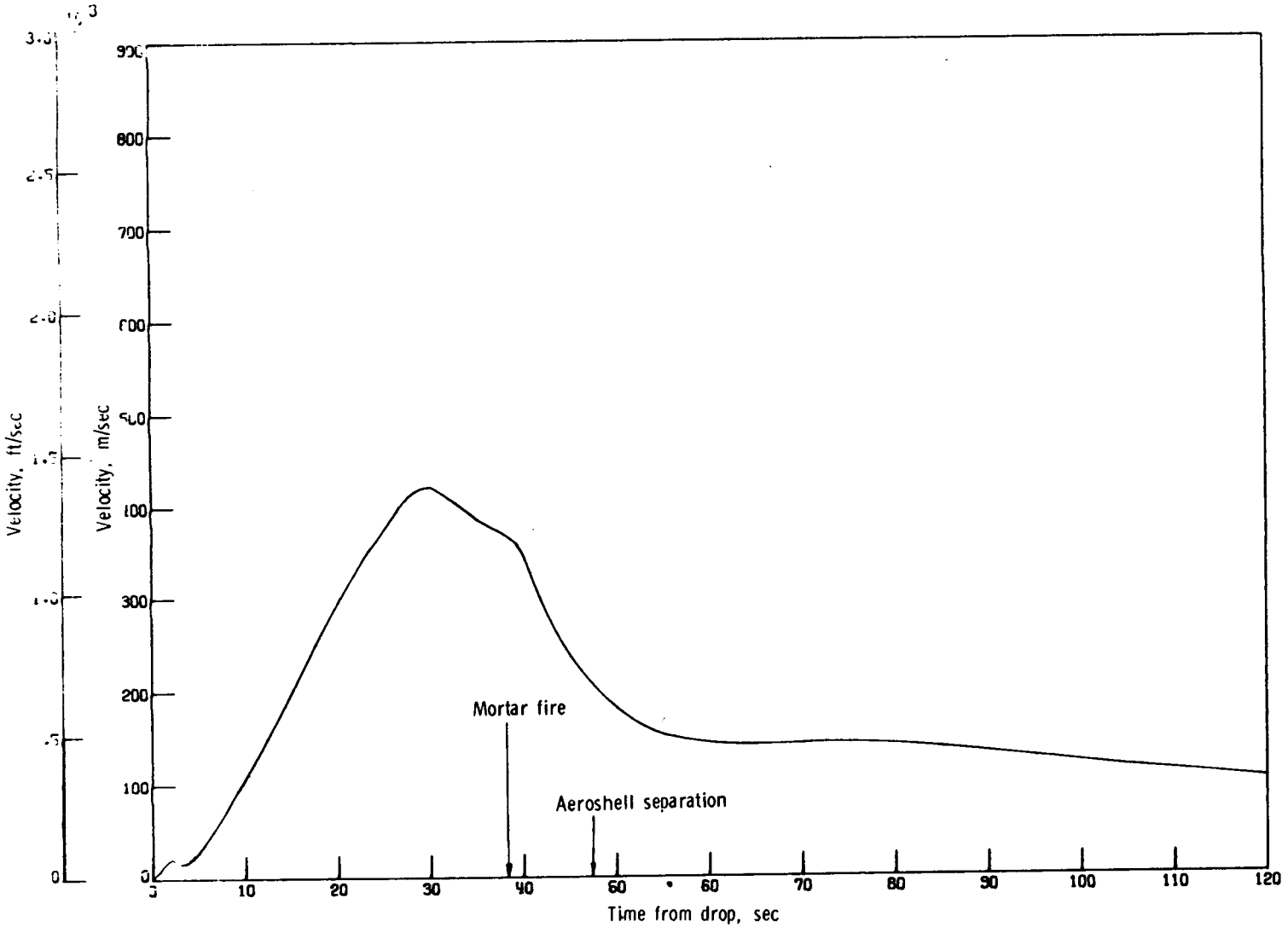


Figure 49.- Time history of velocity. AV-2.

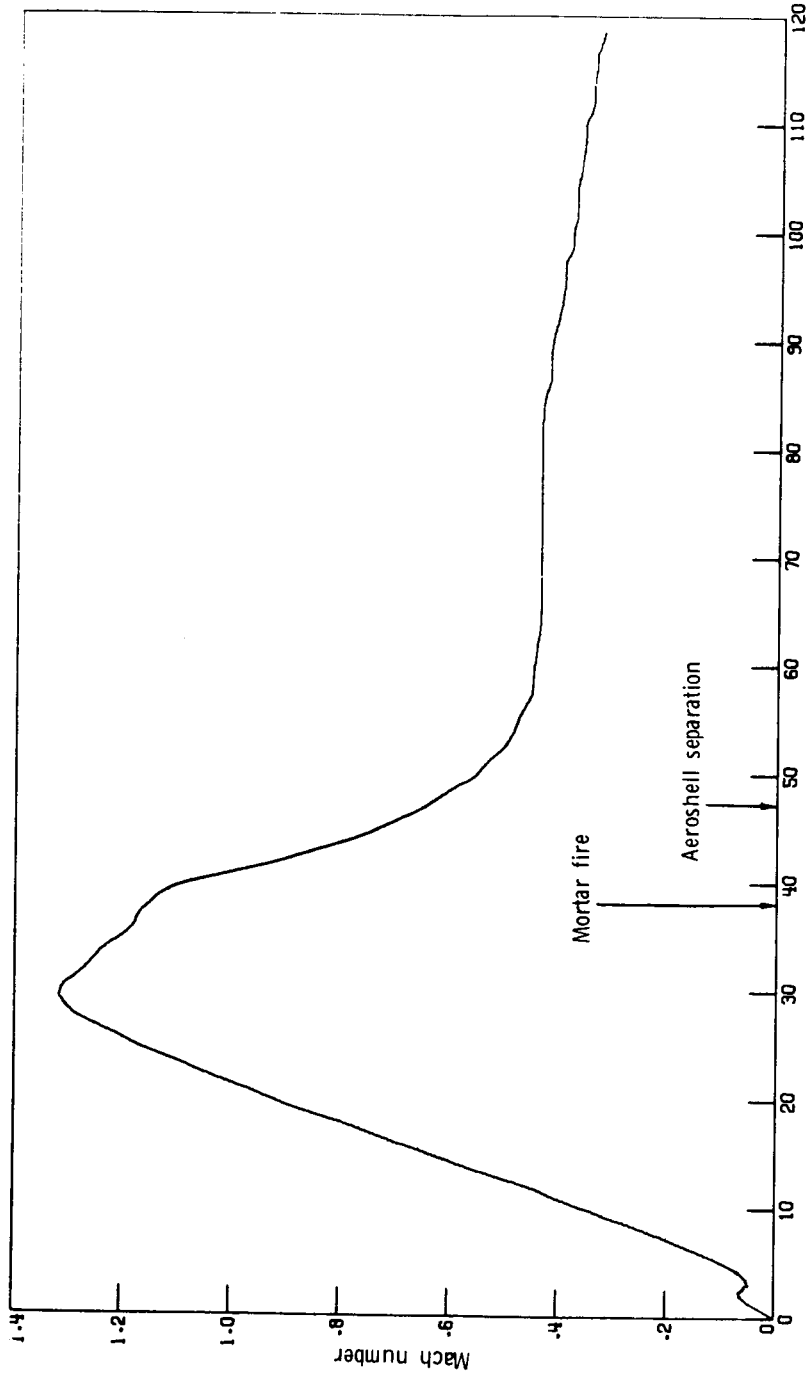


Figure 50.- Time history of Mach number. AV-2.

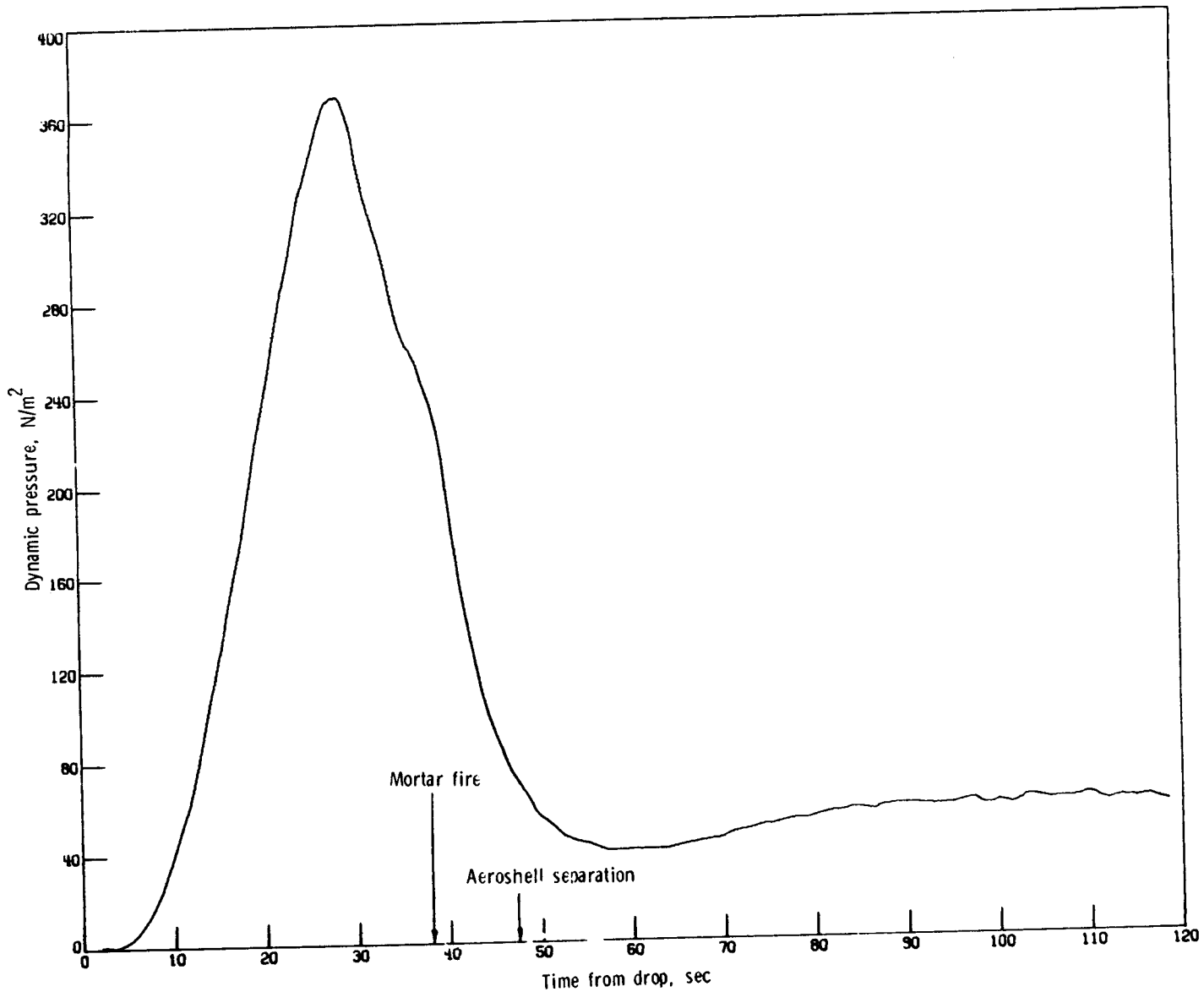


Figure 51.- Time history of dynamic pressure. AV-2.

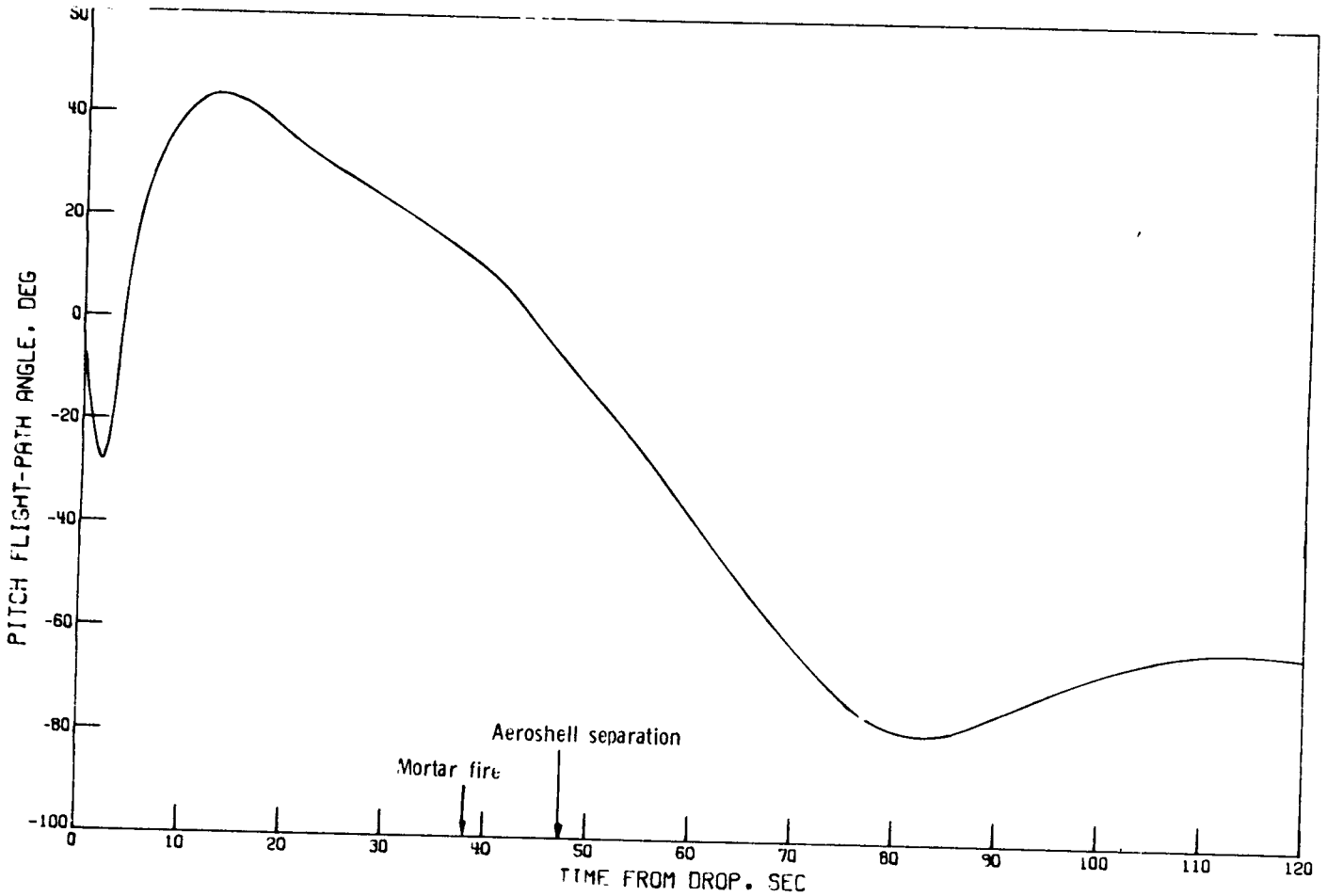


Figure 52.- Time history of vehicle pitch flight-path angle. AV-2.

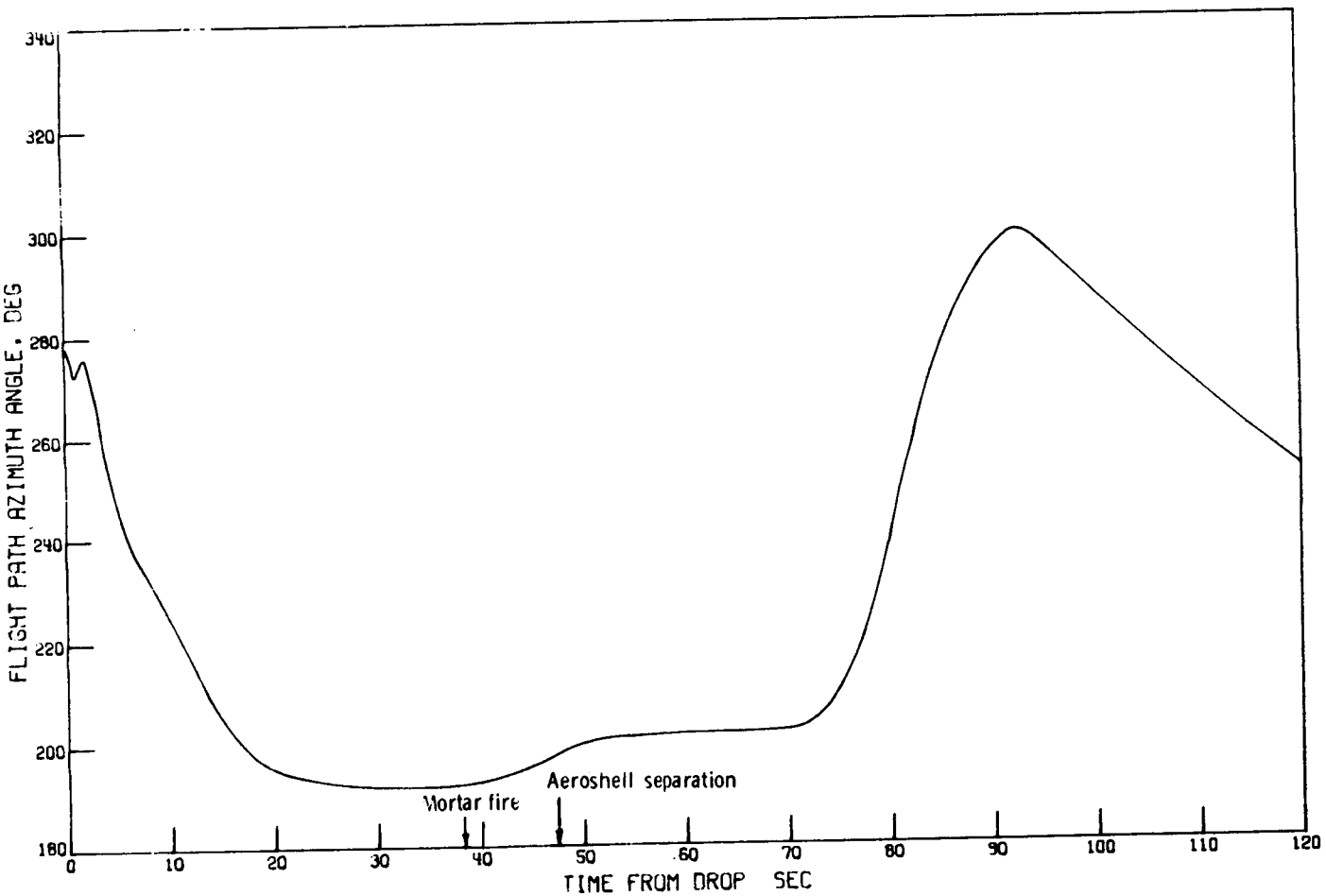


Figure 53.- Time history of flight-path azimuth angle. AV-2.

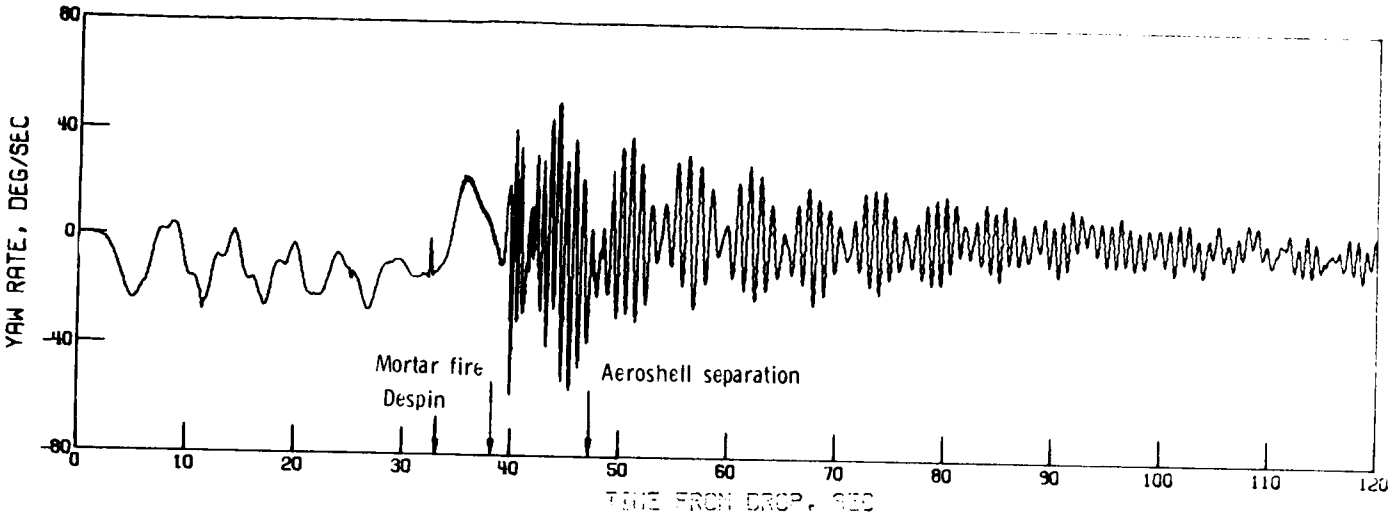


Figure 54.- Time history of yaw rate. AV-2.

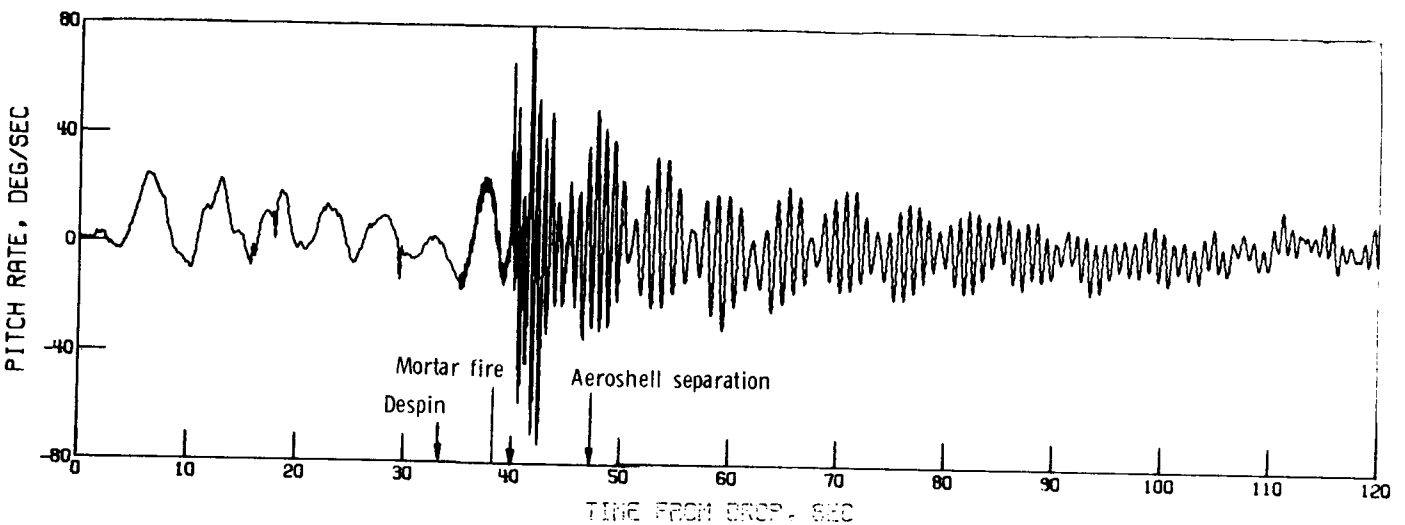


Figure 55.- Time history of pitch rate. AV-2.

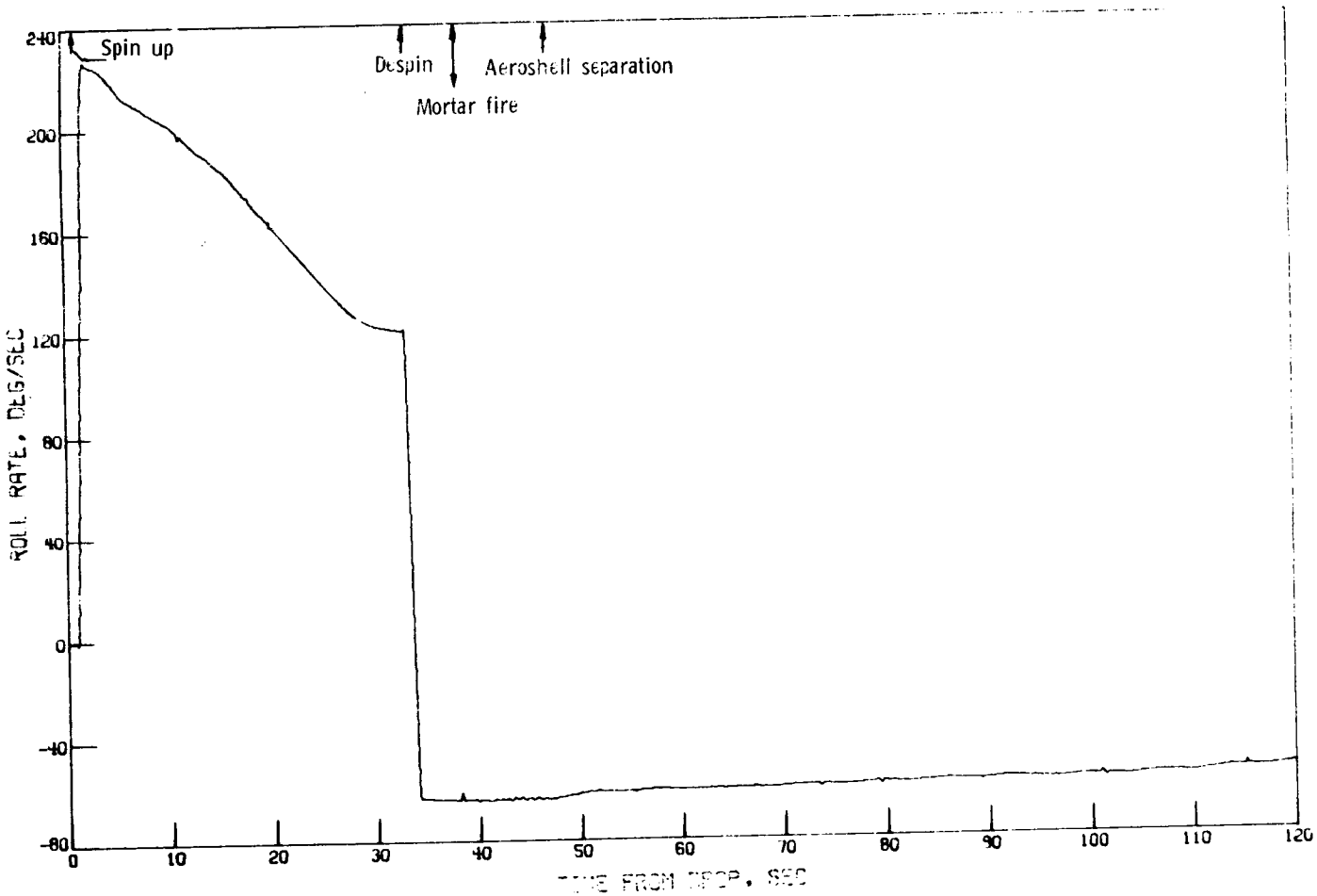


Figure 56.- Time history of roll rate. AV-2.

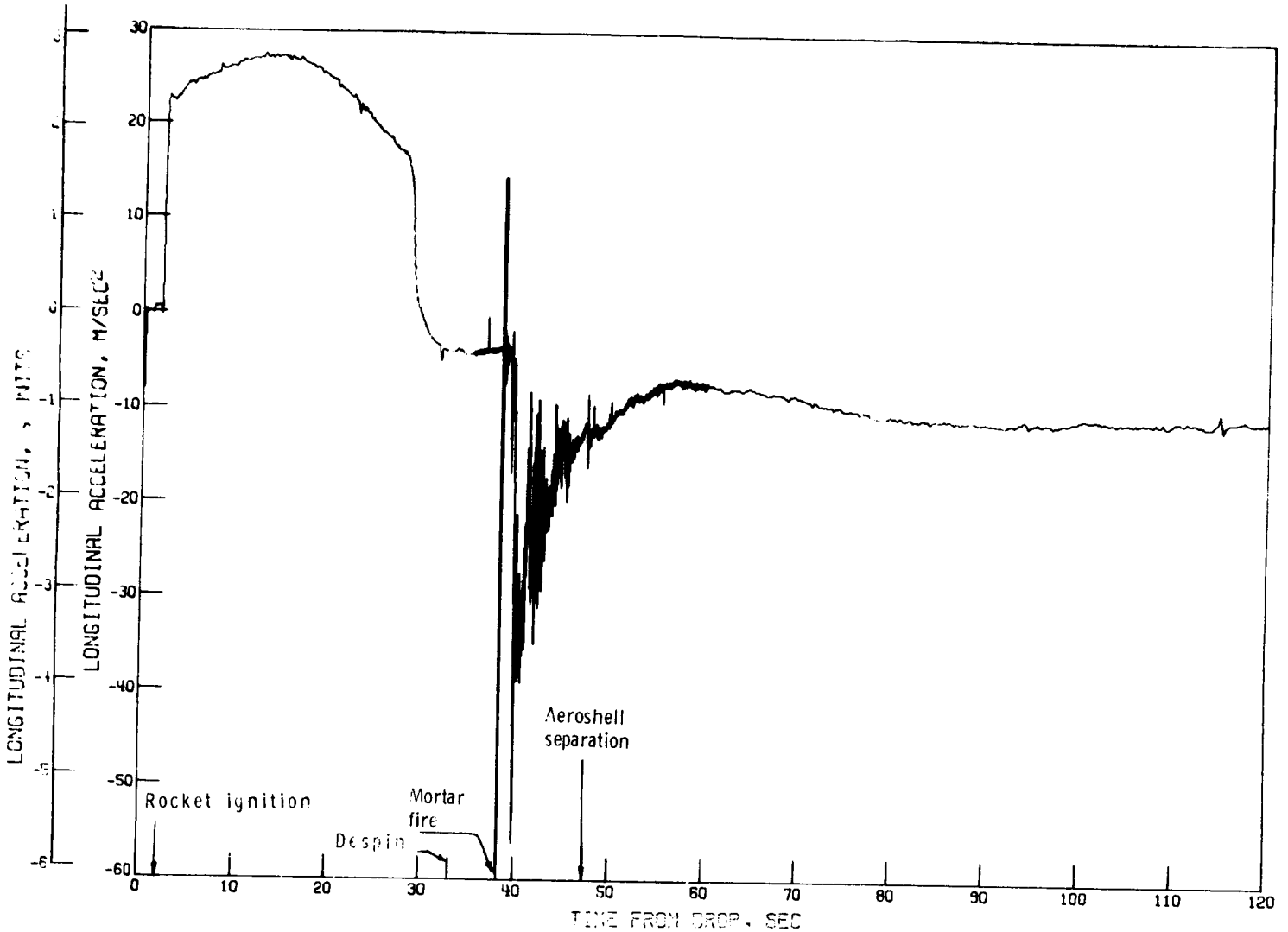


Figure 57.- Time history of longitudinal acceleration from accelerometer. AV-2.

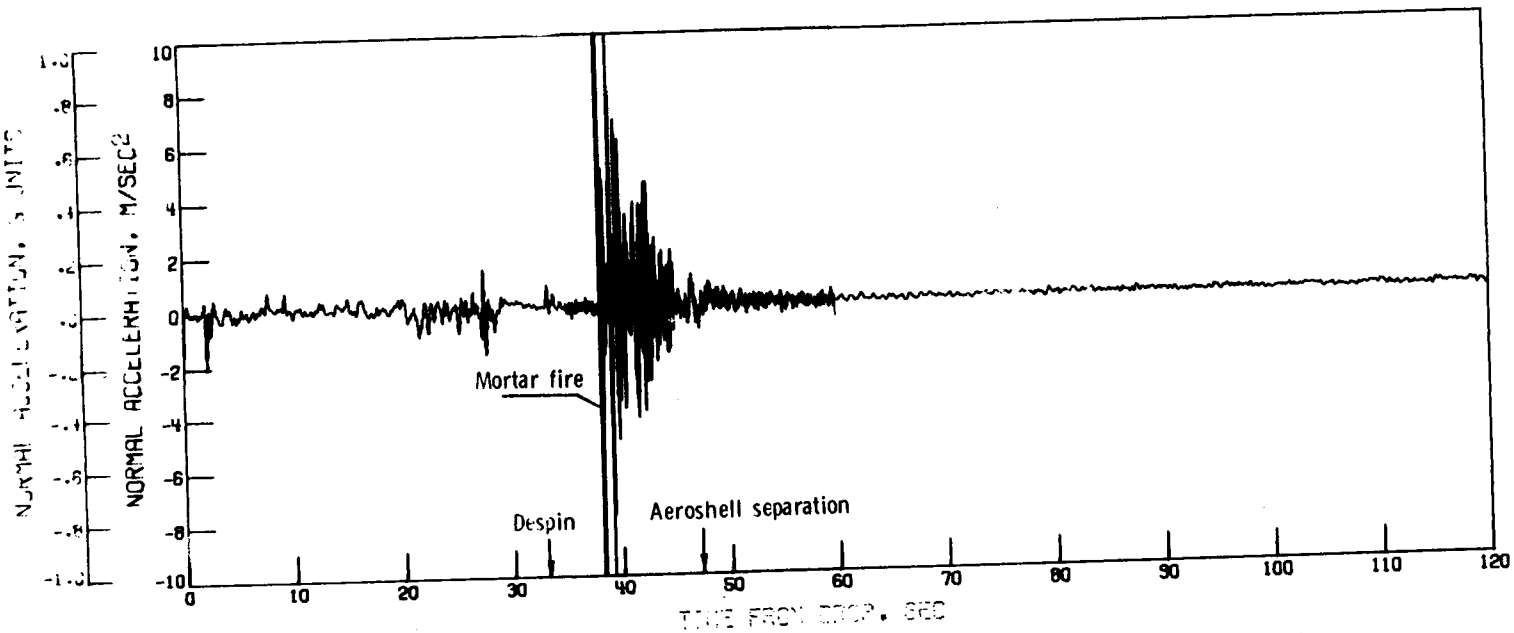


Figure 58.- Time history of normal acceleration. AV-2; instrument limit ±1g.

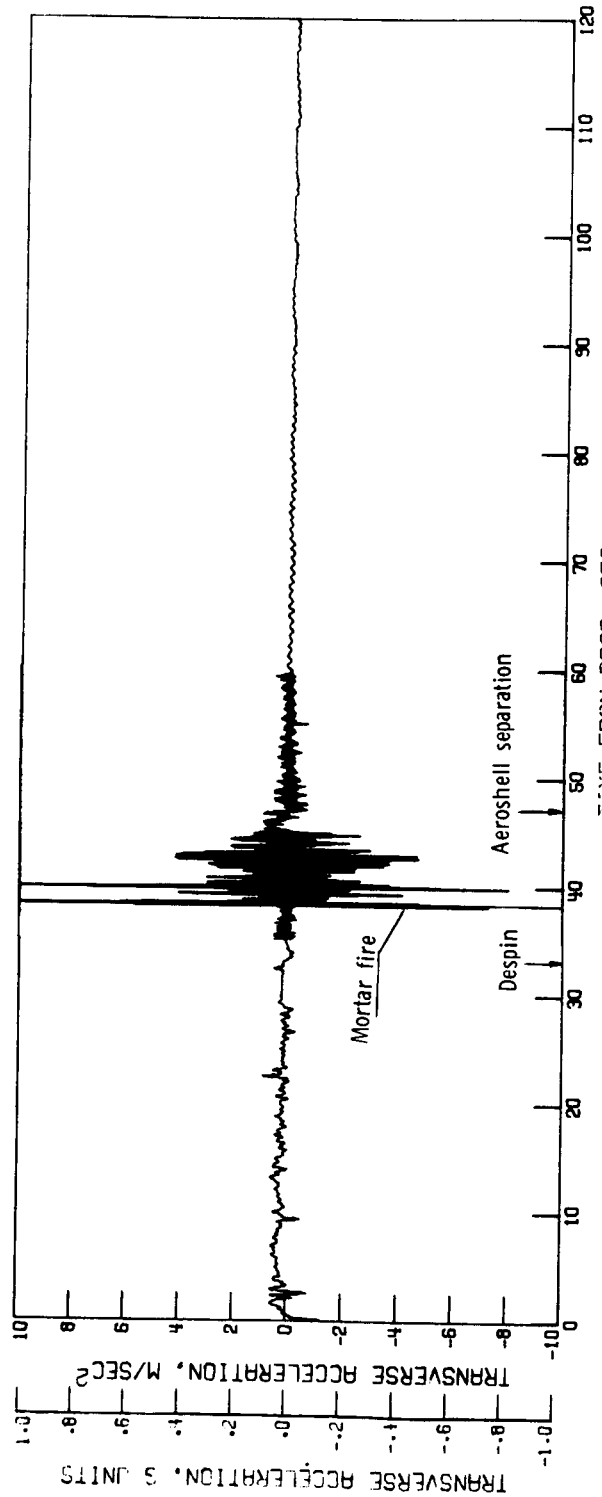


Figure 59.- Time history of transverse acceleration. AV-2; instrument limit ±1g.

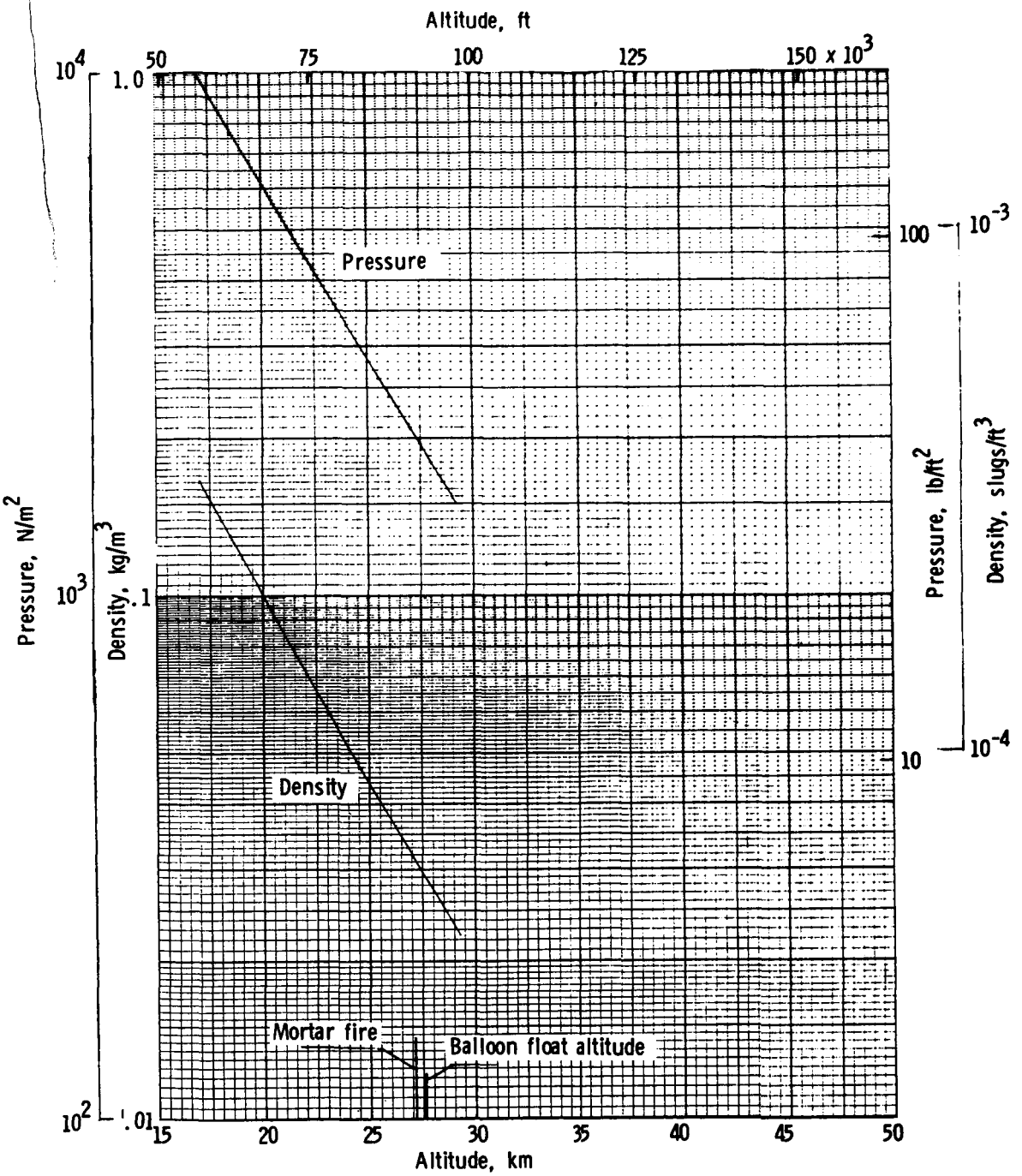


Figure 60.- Variation of ambient pressure and density with altitude. AV-3.

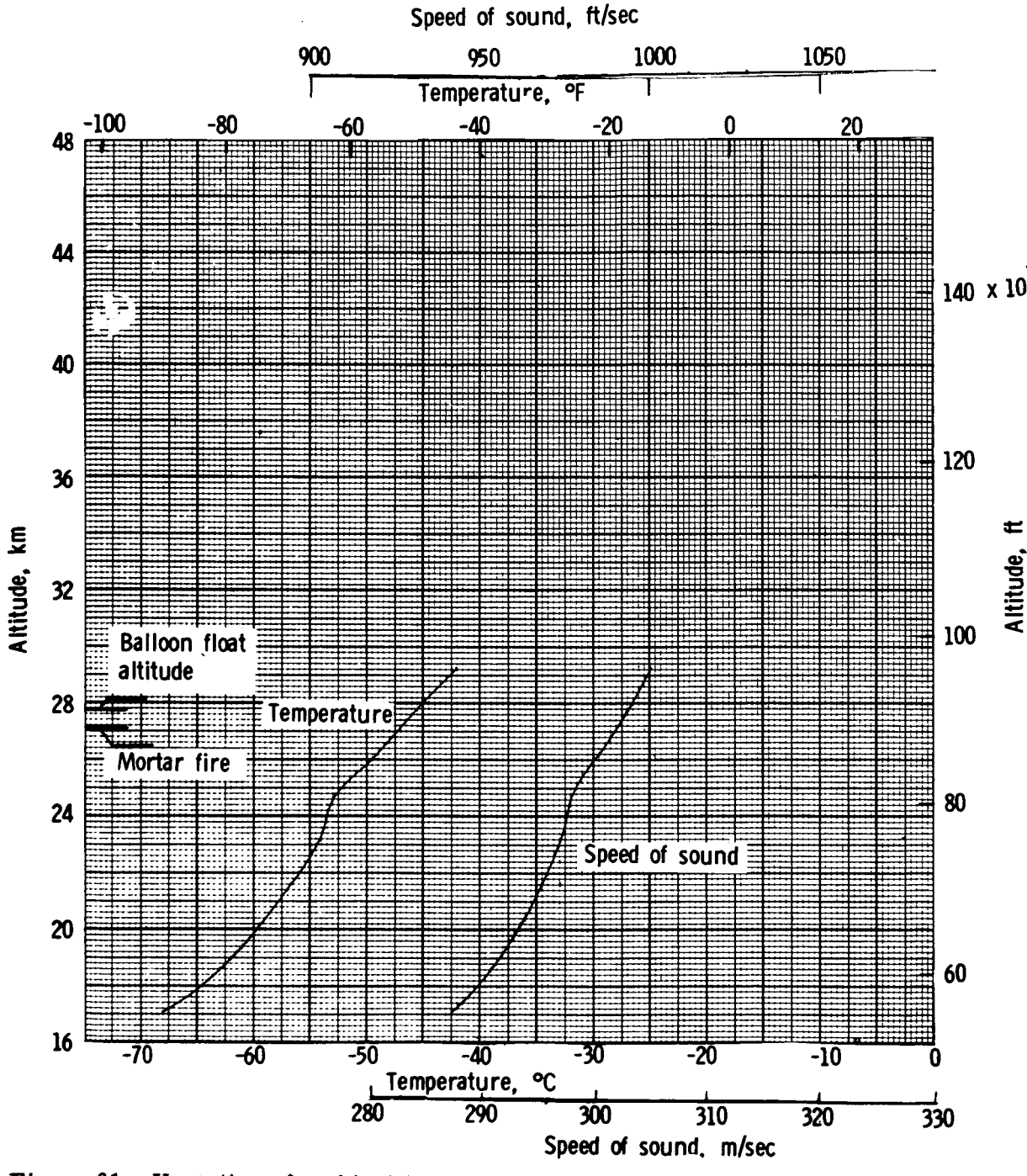


Figure 61.- Variation of ambient temperature and speed of sound with altitude. AV-3.

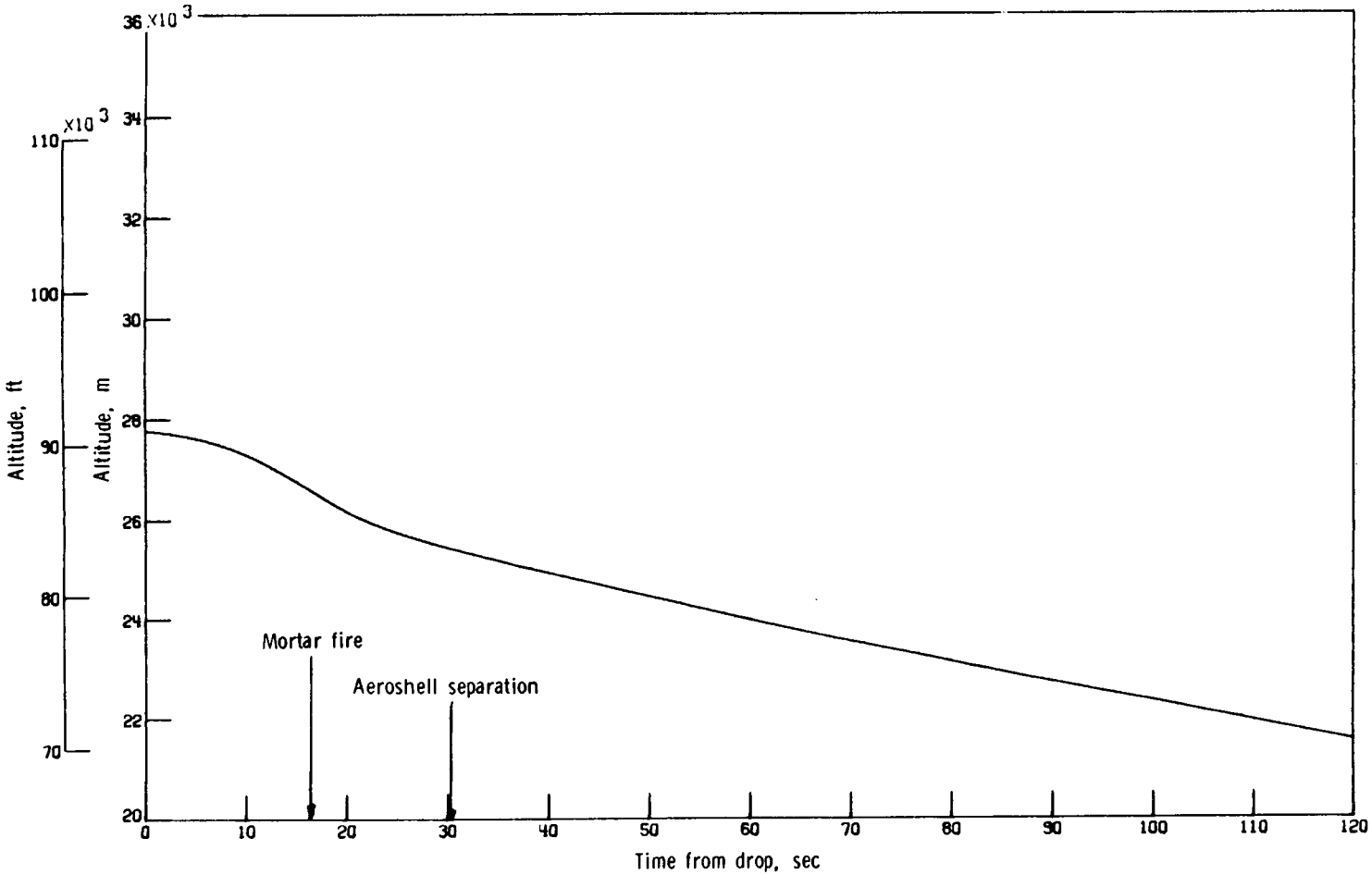


Figure 62.- Time history of altitude. AV-3.

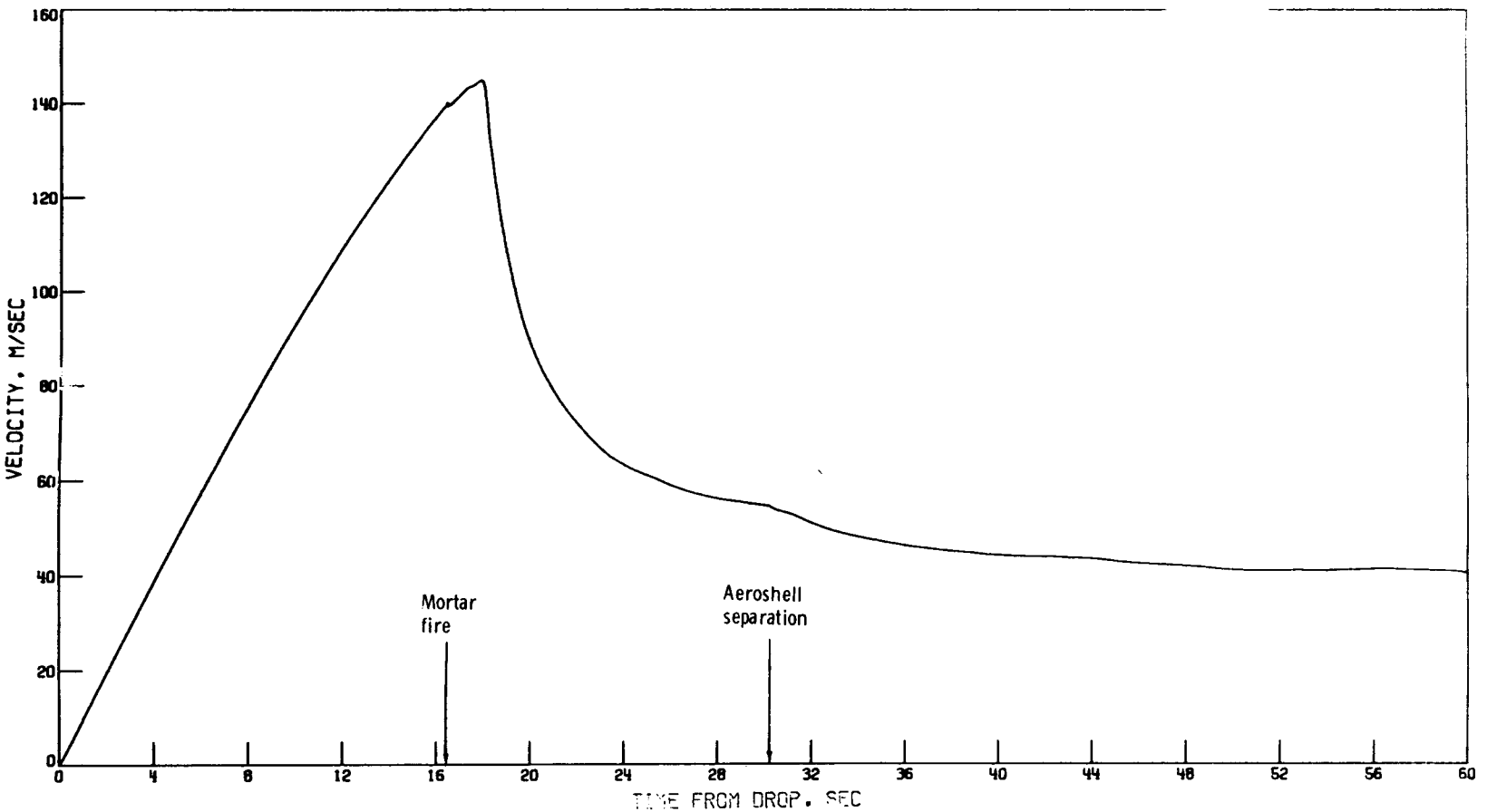


Figure 63.- Time history of velocity. AV-3.

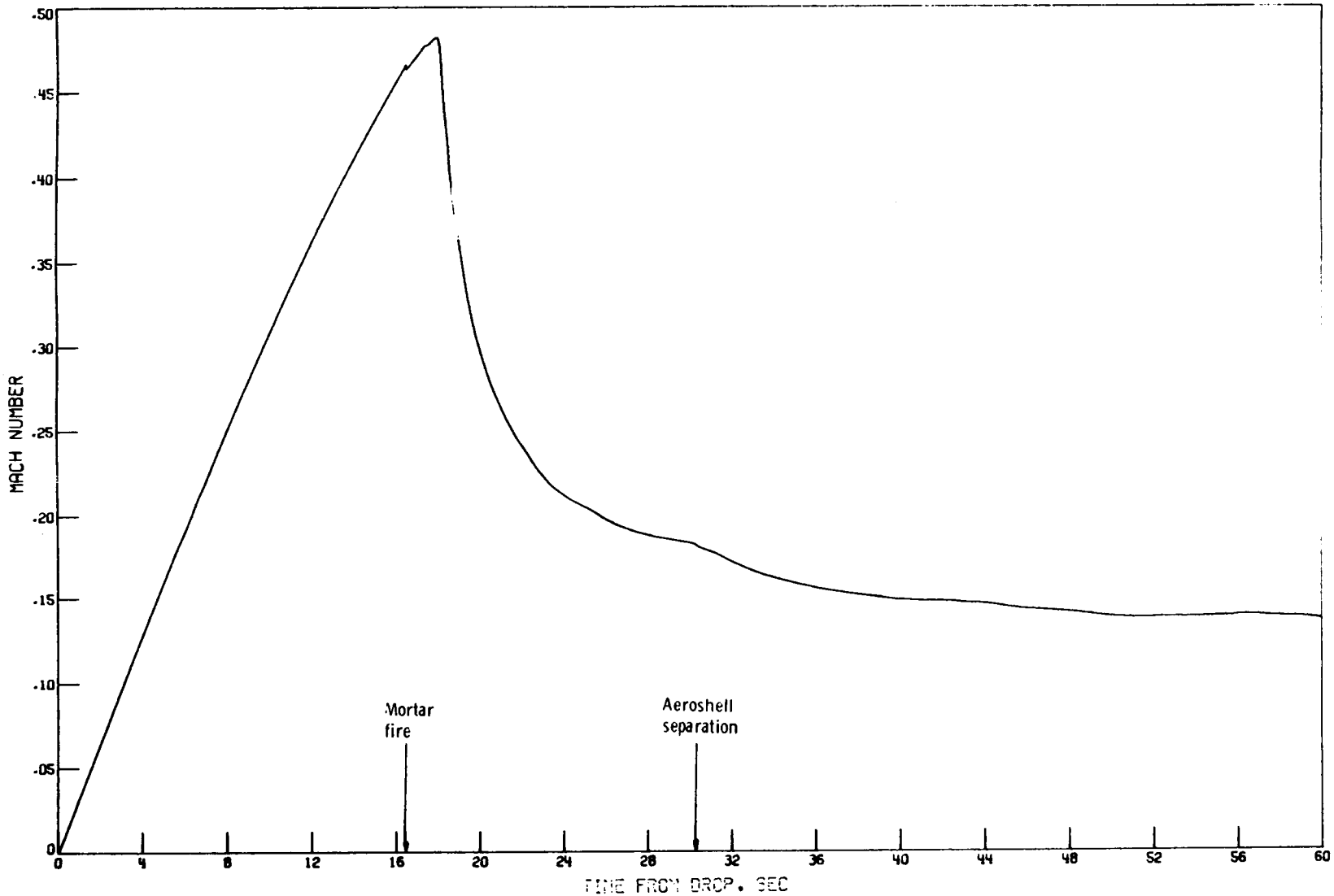


Figure 64.- Time history of Mach number. AV-3.

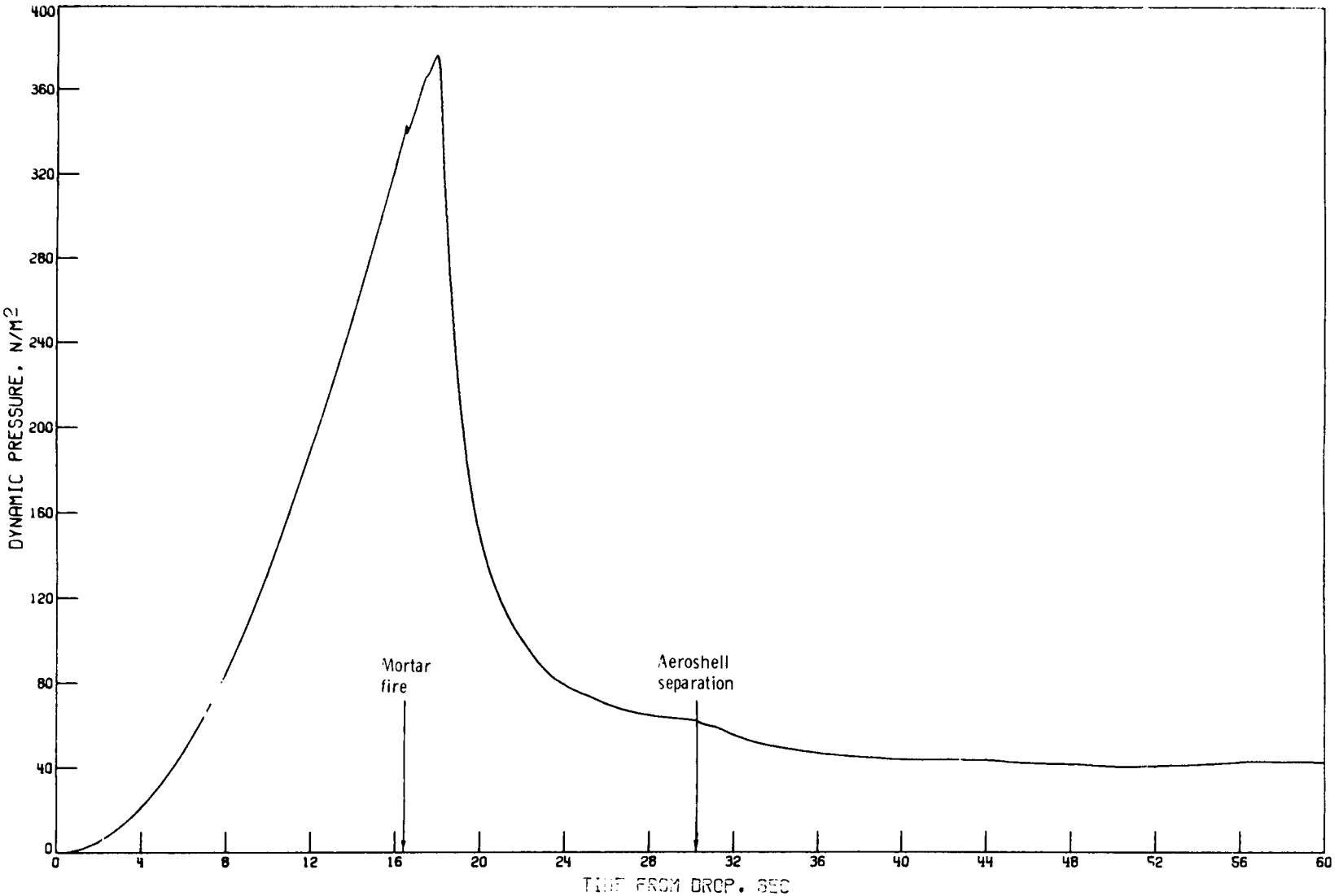


Figure 65.- Time history of dynamic pressure. AV-3.

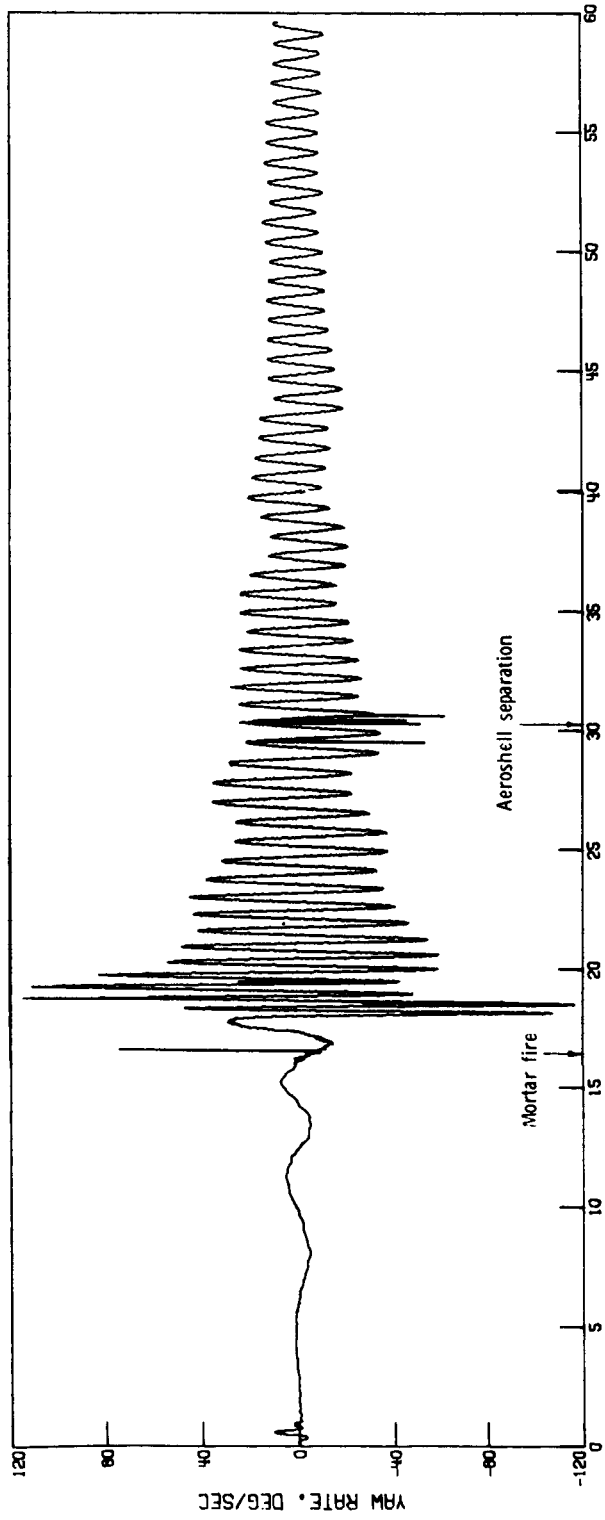


Figure 66.- Time history of yaw rate. AV-3.

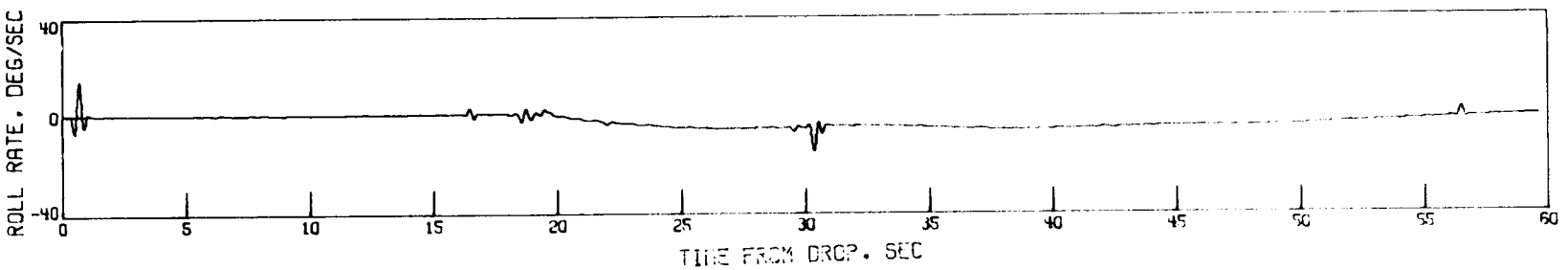


Figure 67.- Time history of roll rate. AV-3.

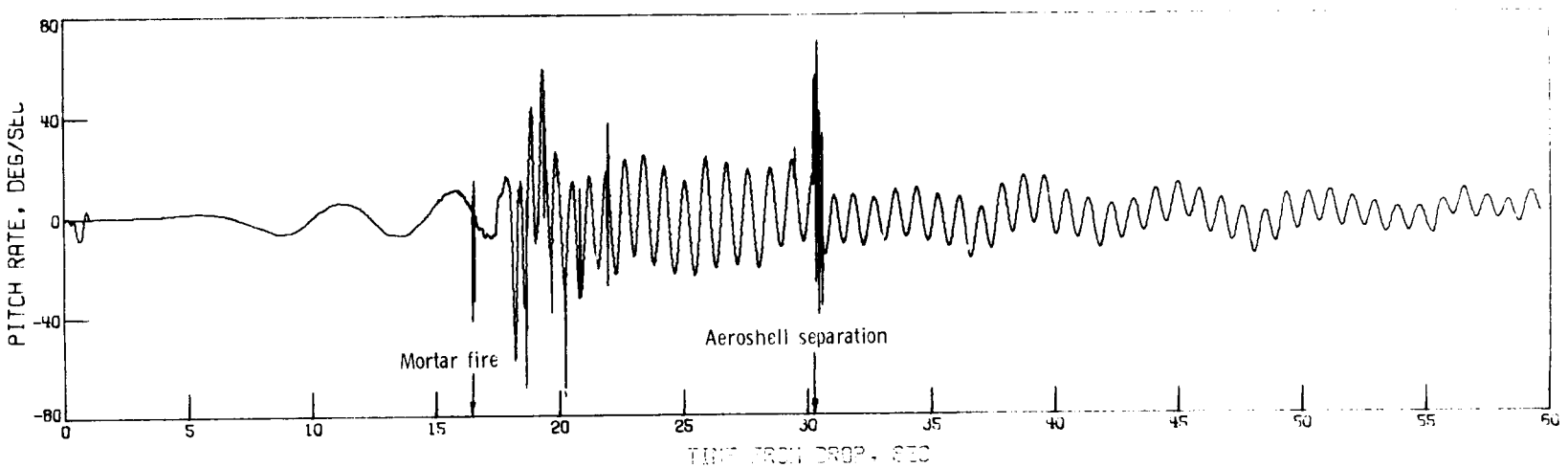


Figure 68.- Time history of pitch rate. AV-3.

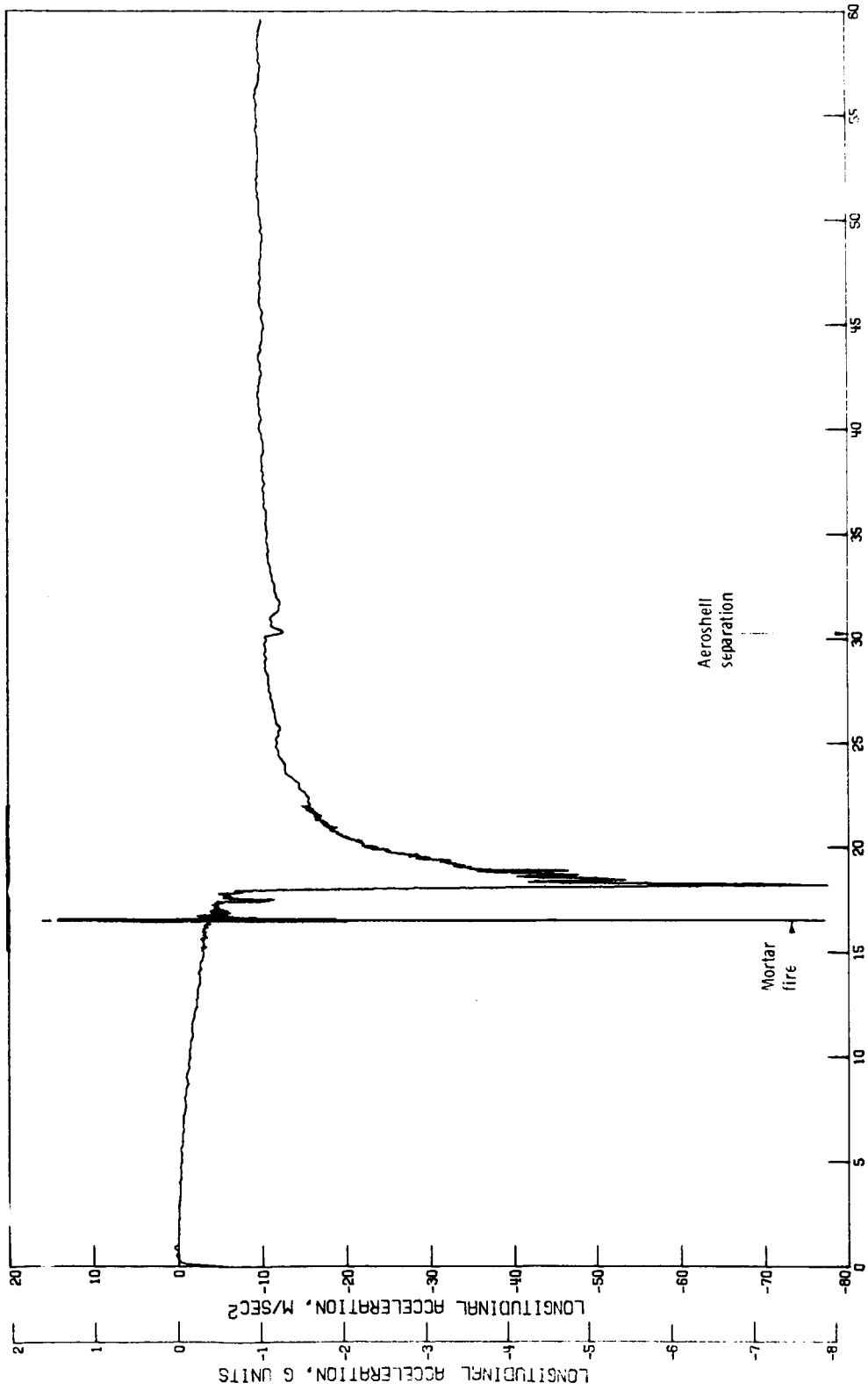


Figure 69.- Time history of longitudinal acceleration. AV-3.

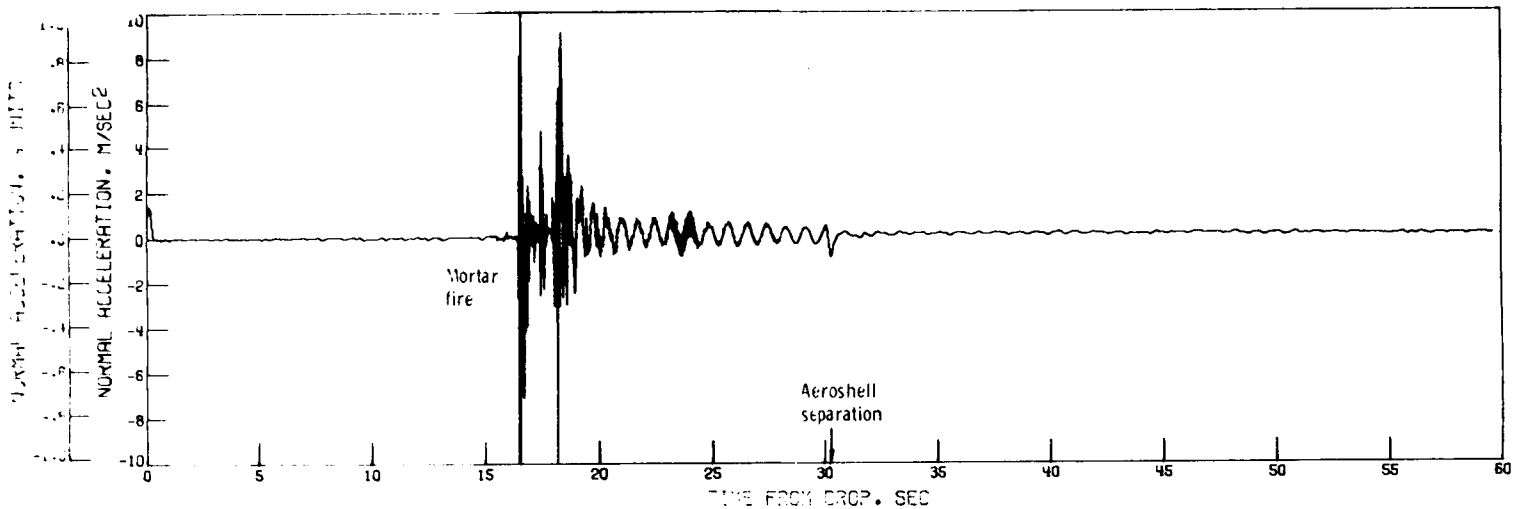


Figure 70.- Time history of normal acceleration. AV-3; instrument limit ±1g.

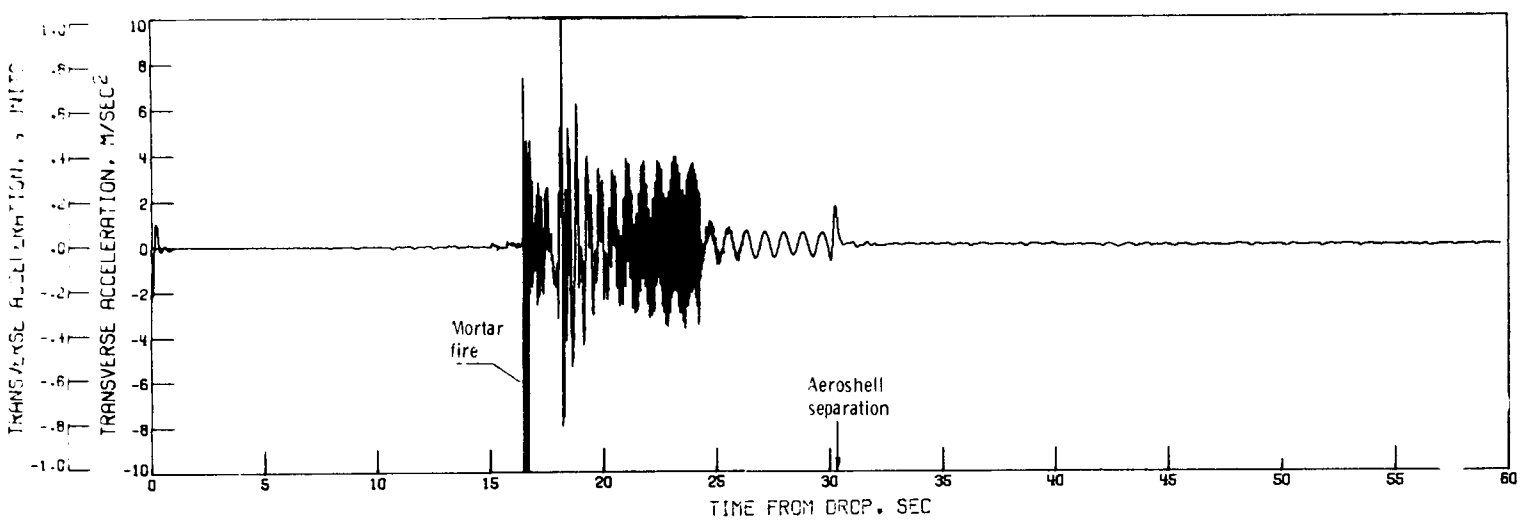


Figure 71.- Time history of transverse acceleration. AV-3; instrument limit ±1g.

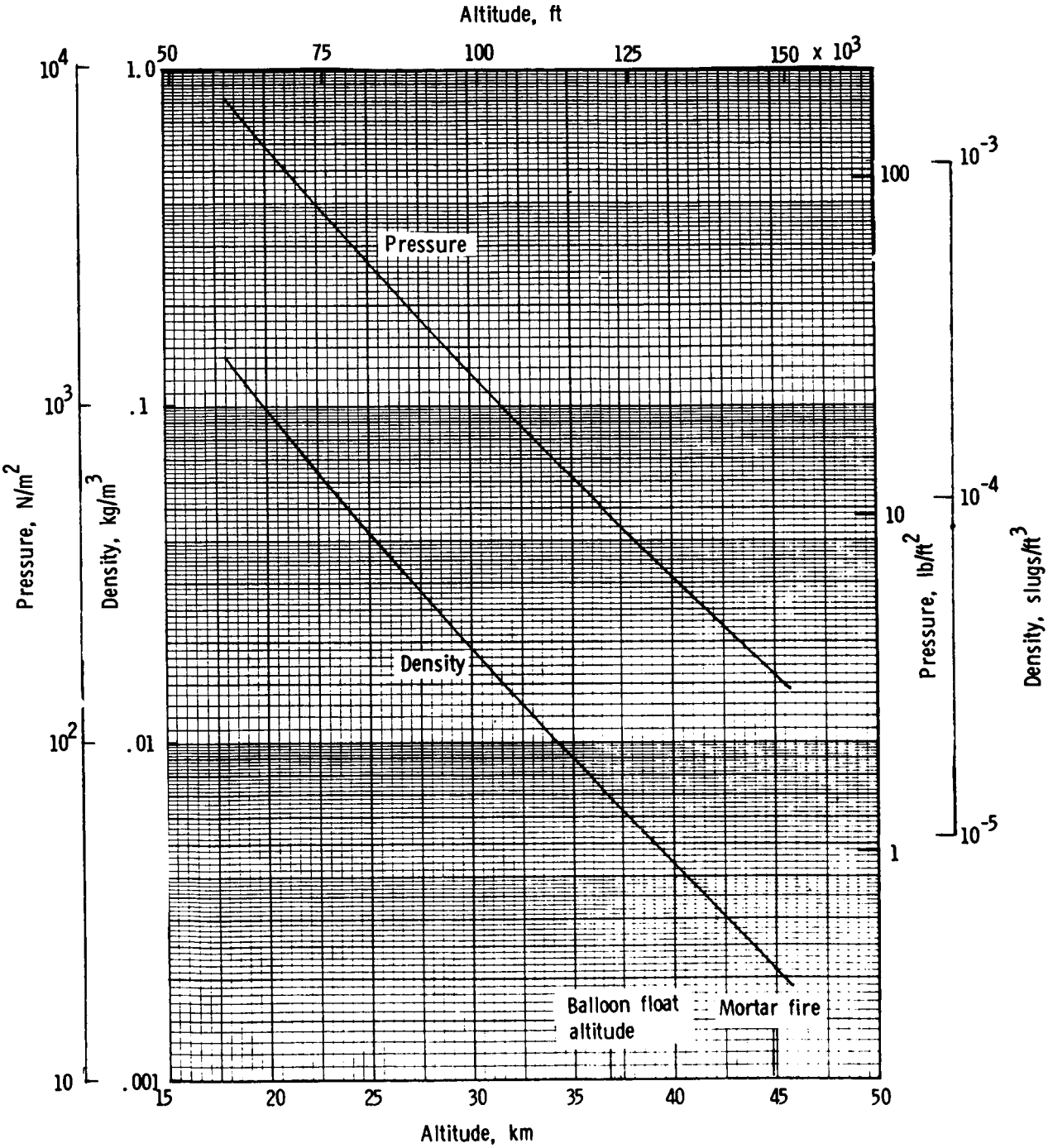


Figure 72.- Variation of ambient pressure and density with altitude. AV-4.

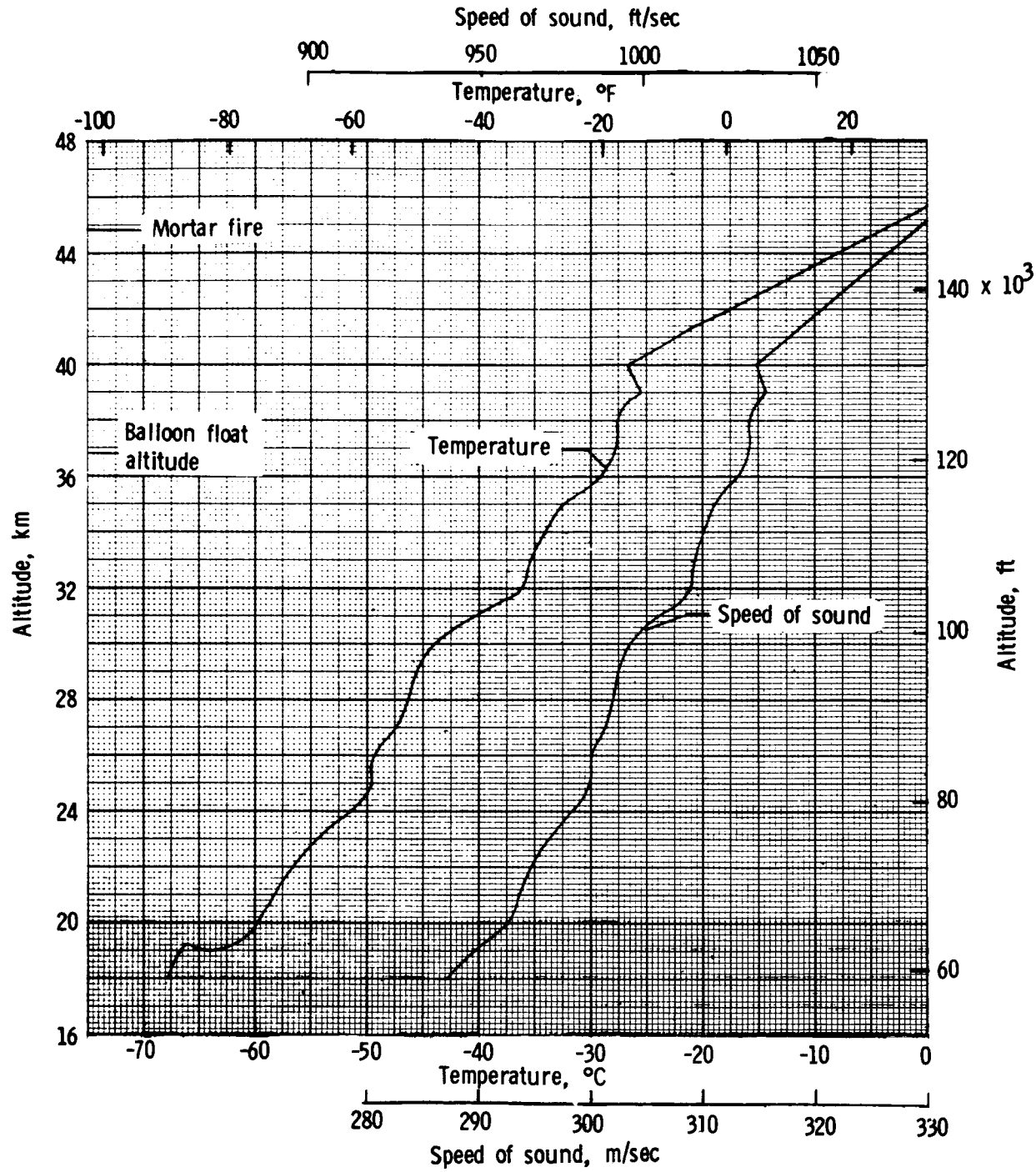


Figure 73.- Variation of ambient temperature and speed of sound with altitude. AV-4.

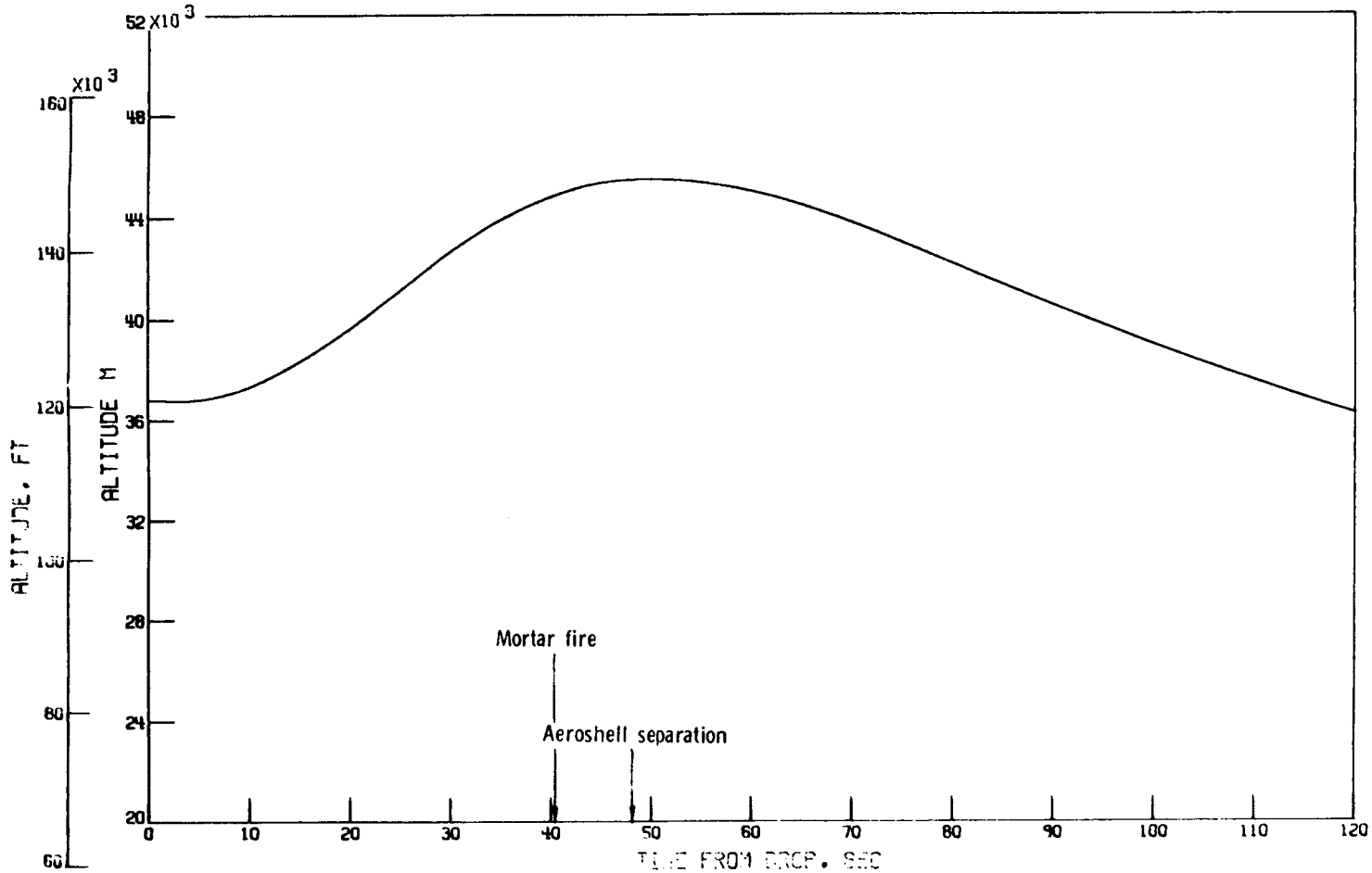


Figure 74.- Time history of altitude. AV-4.

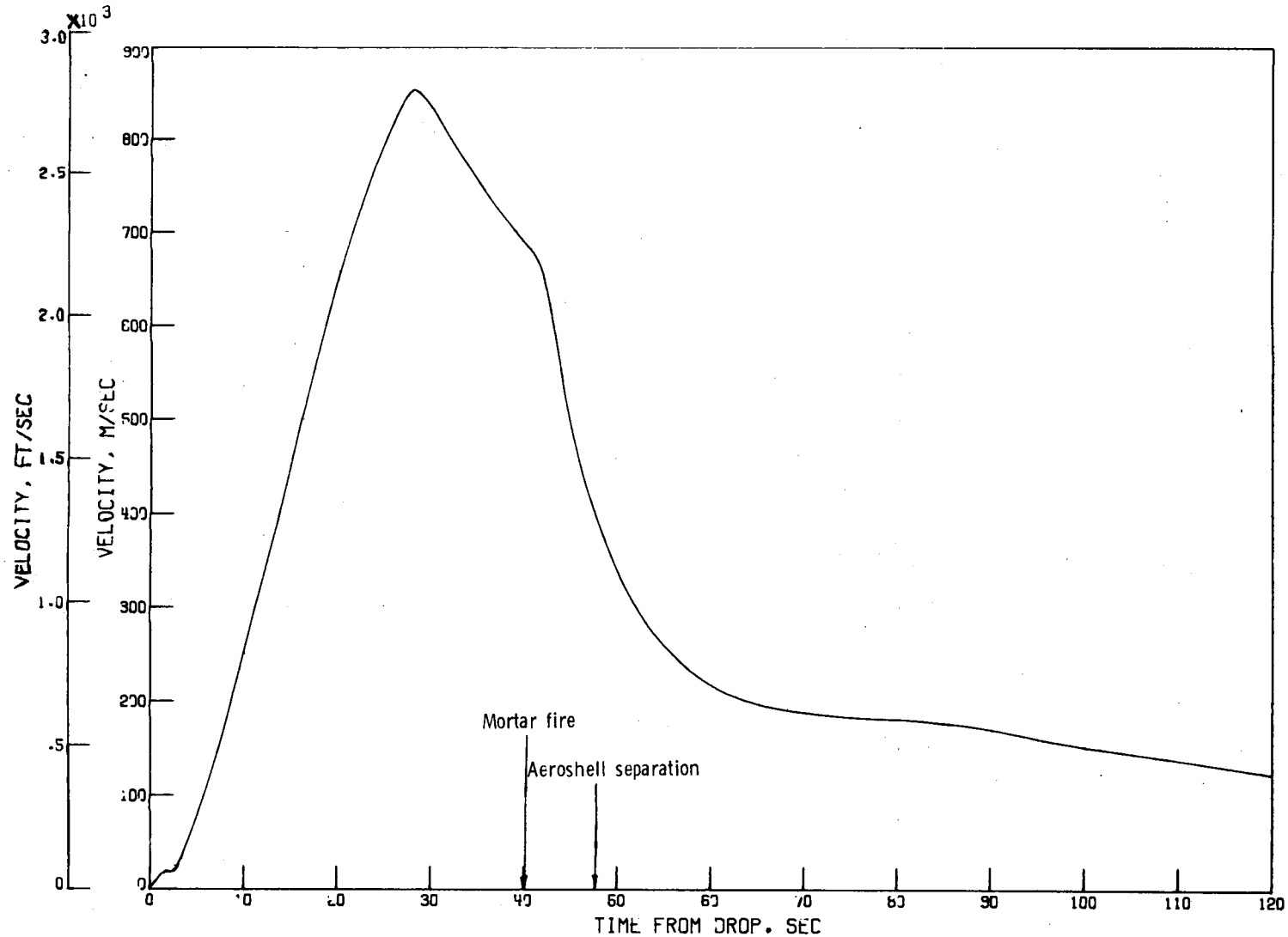


Figure 75.- Time history of velocity. AV-4.

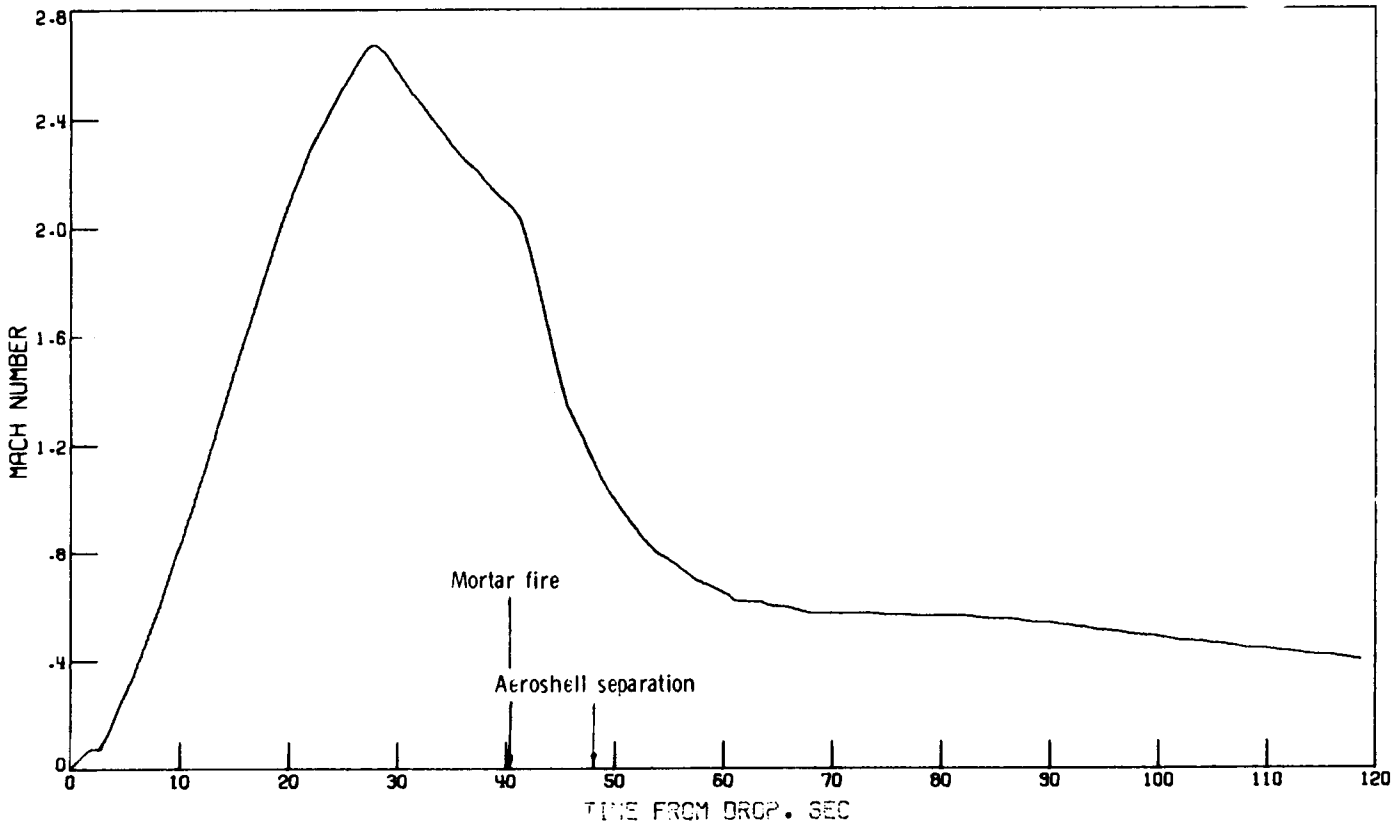


Figure 76.- Time history of Mach number. AV-4.

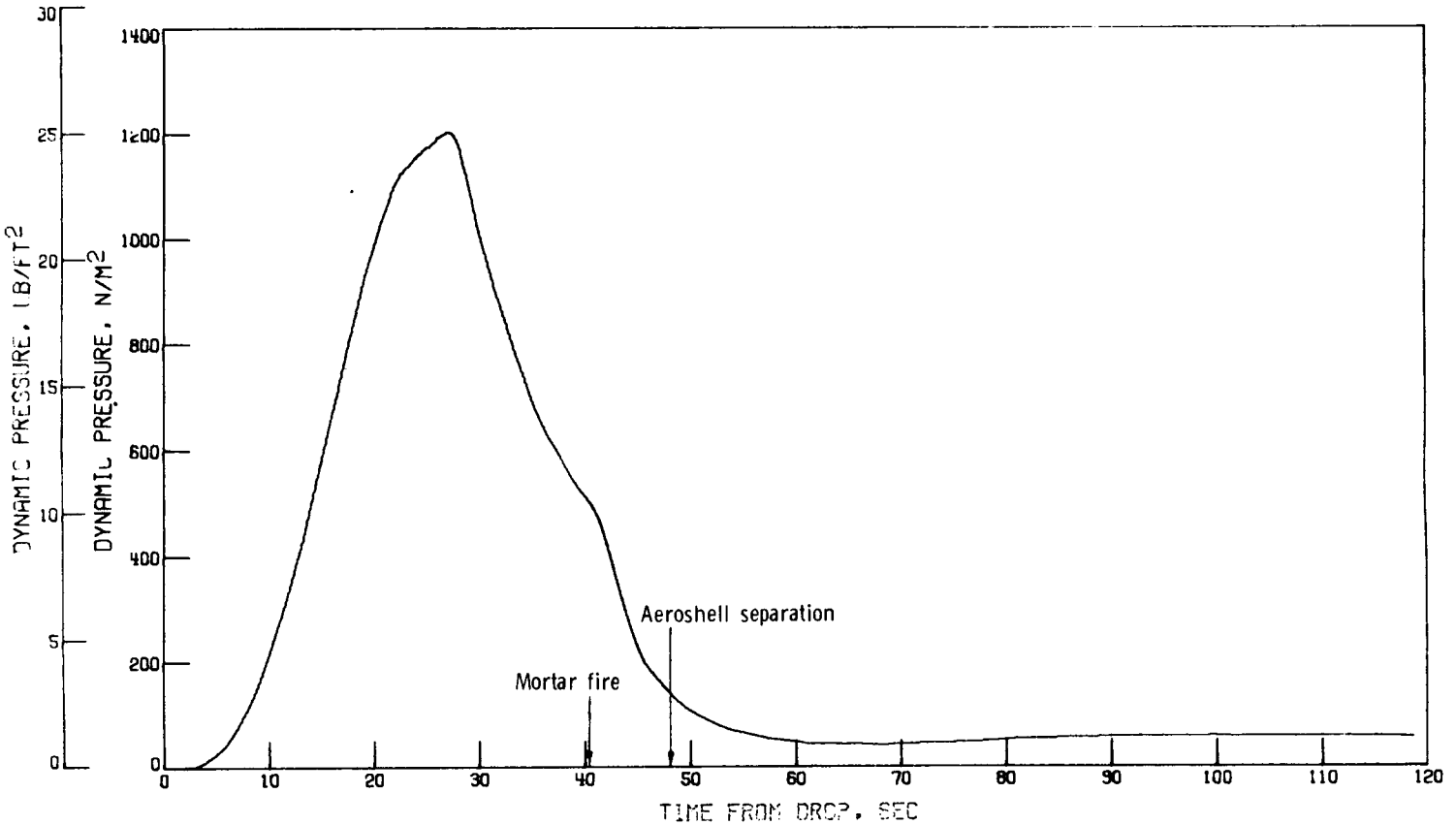


Figure 77.- Time history of dynamic pressure. AV-4.

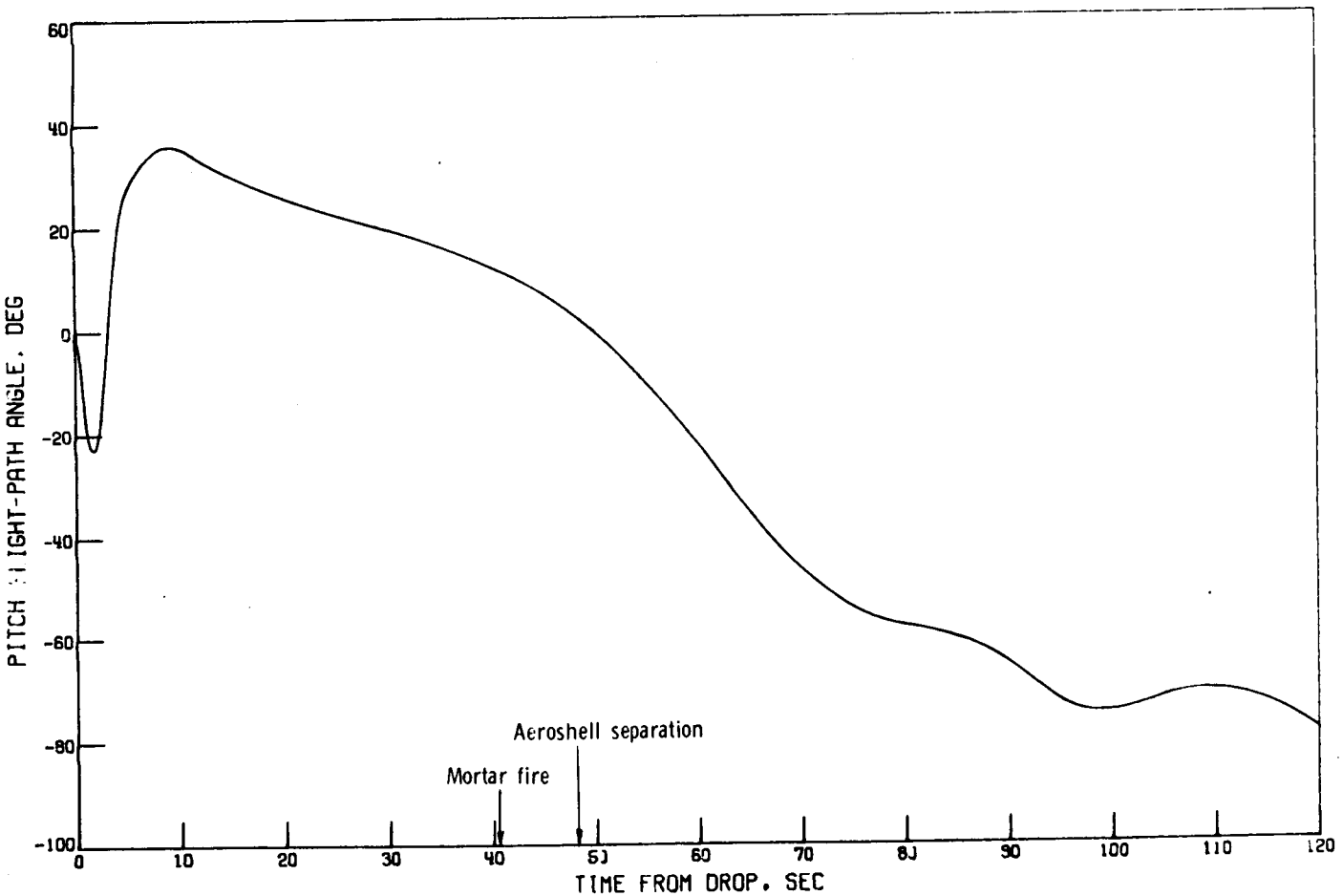


Figure 78.- Time history of vehicle pitch flight-path angle. AV-4.

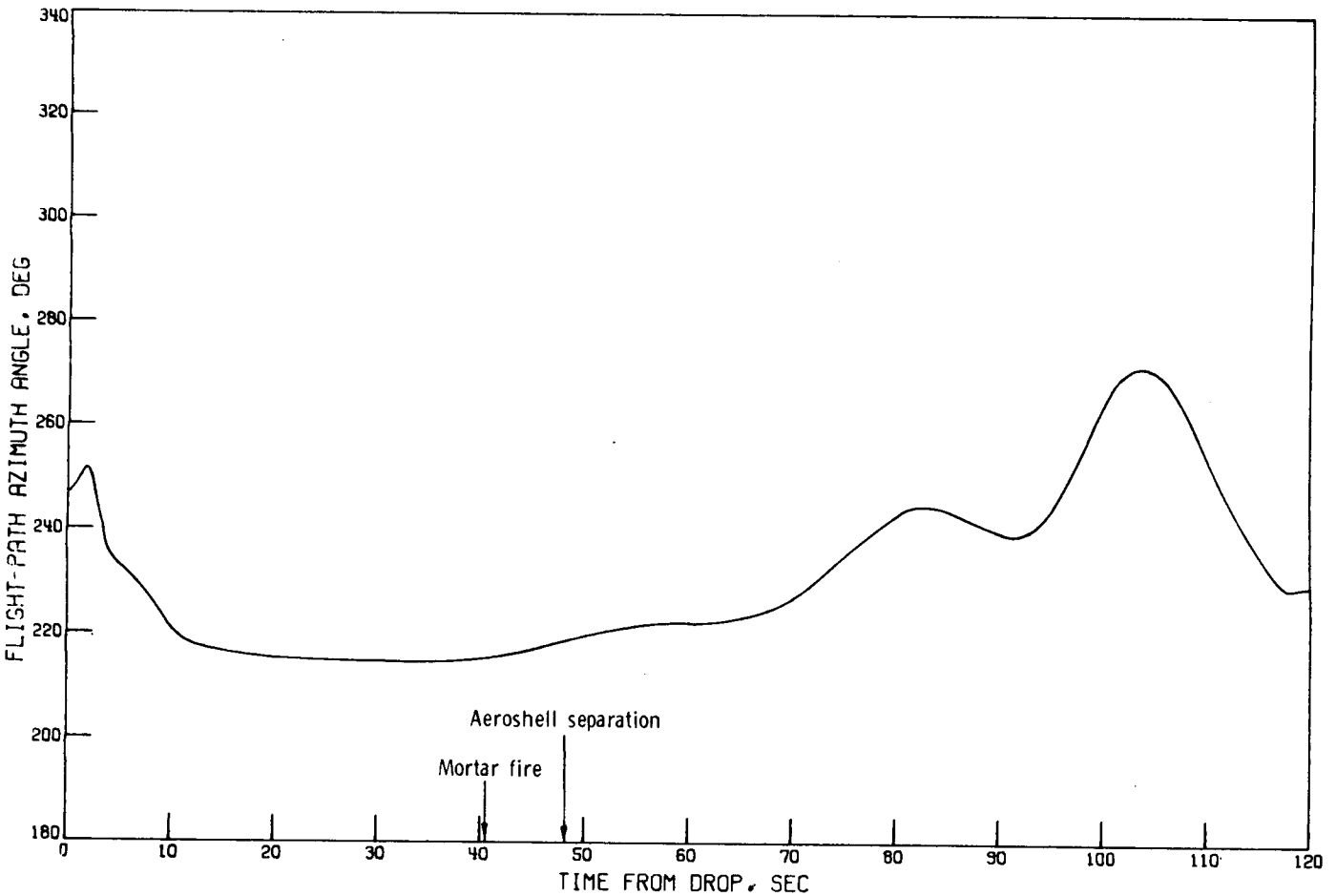


Figure 79.- Time history of flight-path azimuth angle. AV-4.

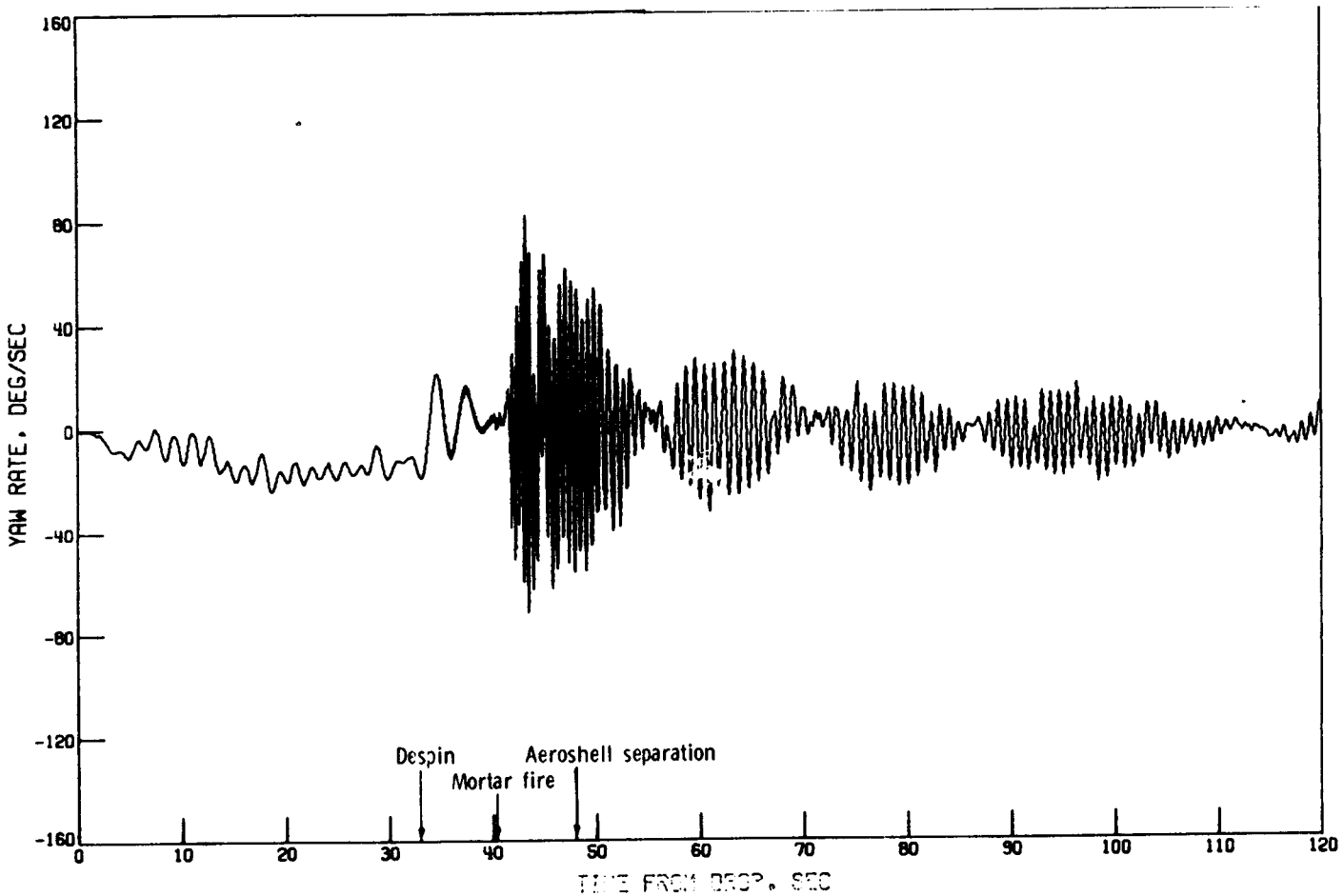


Figure 80.- Time history of yaw rate. AV-4.

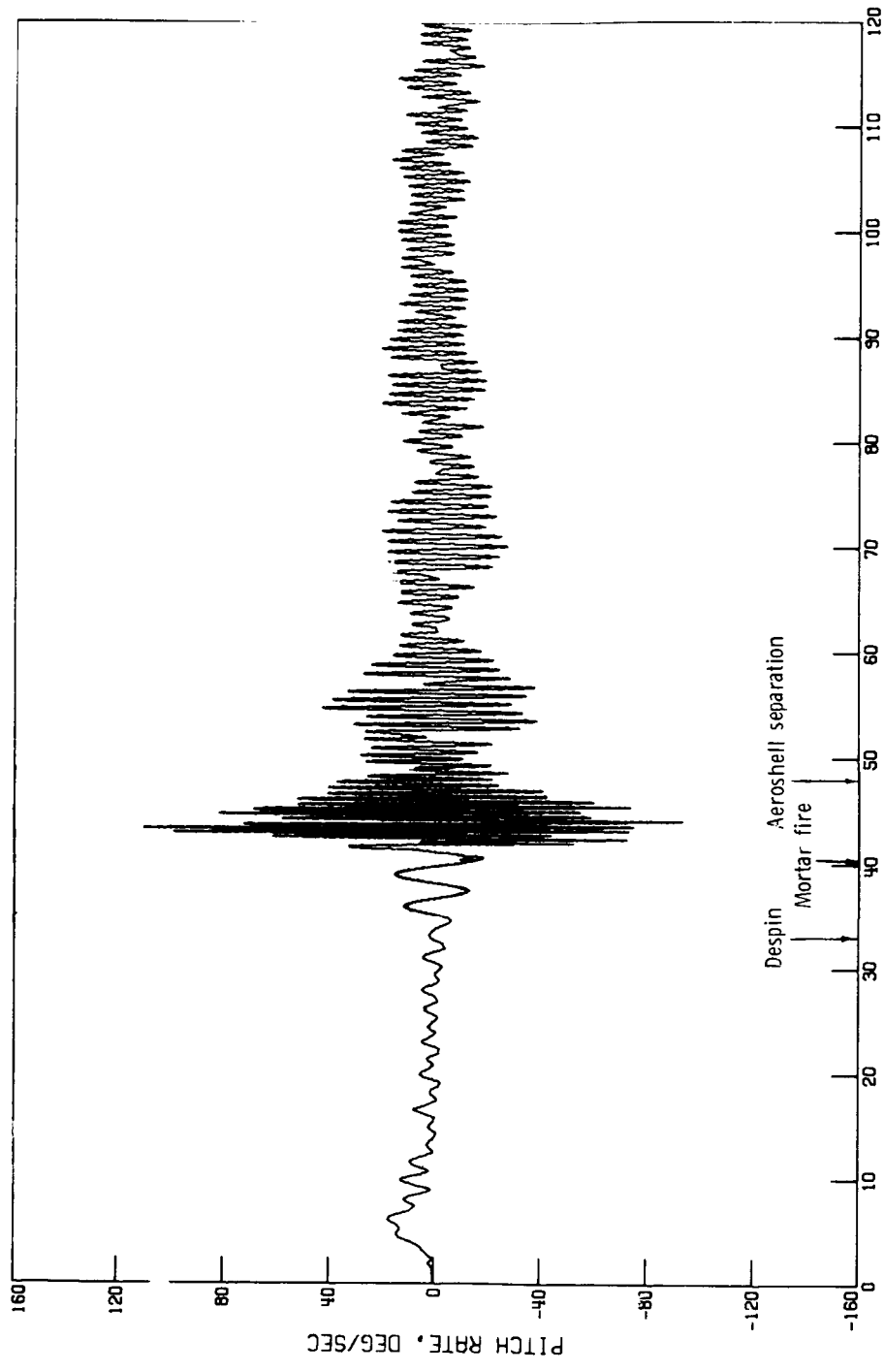


Figure 81.- Time history of pitch rate. AV-4.

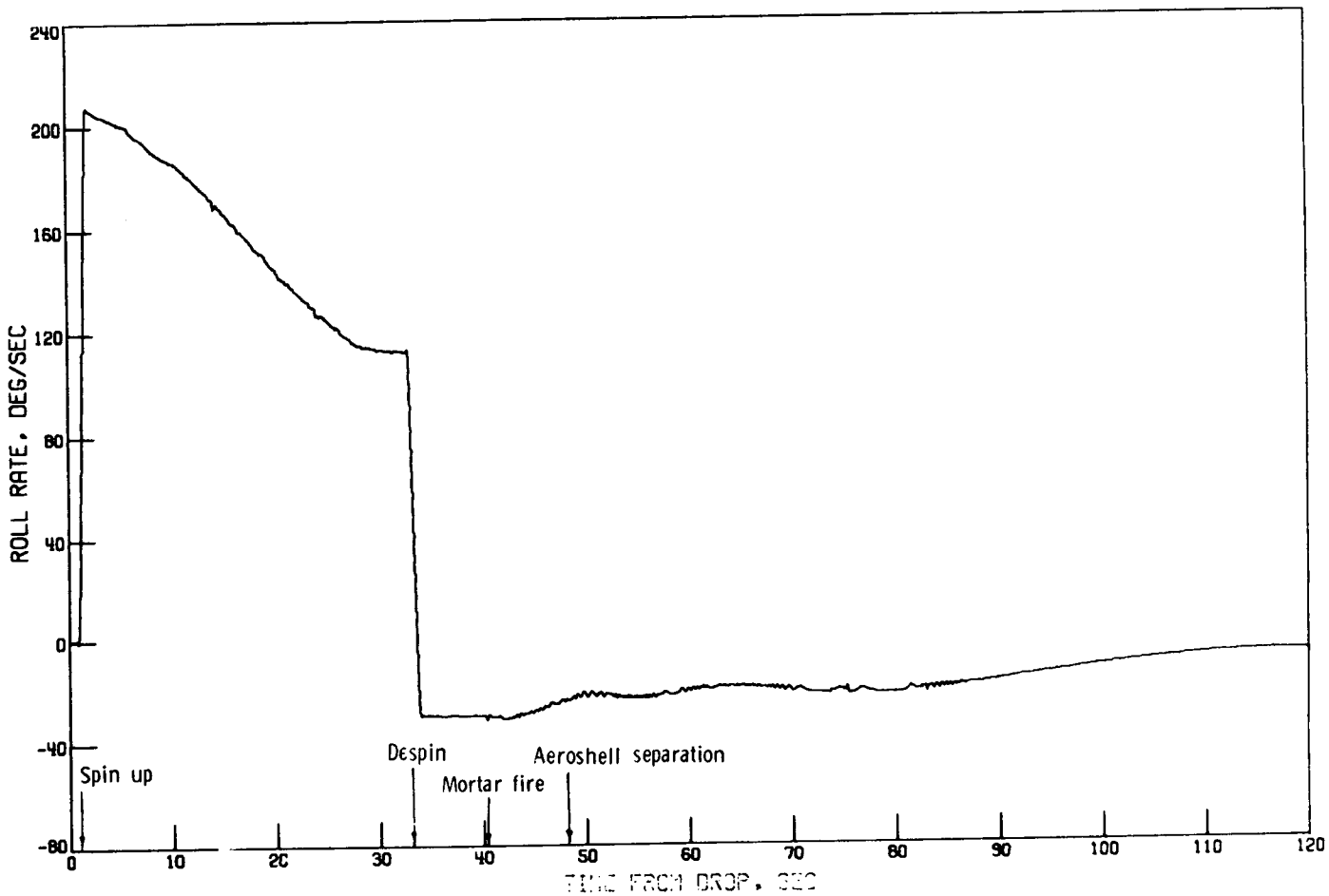


Figure 82.- Time history of roll rate. AV-4.

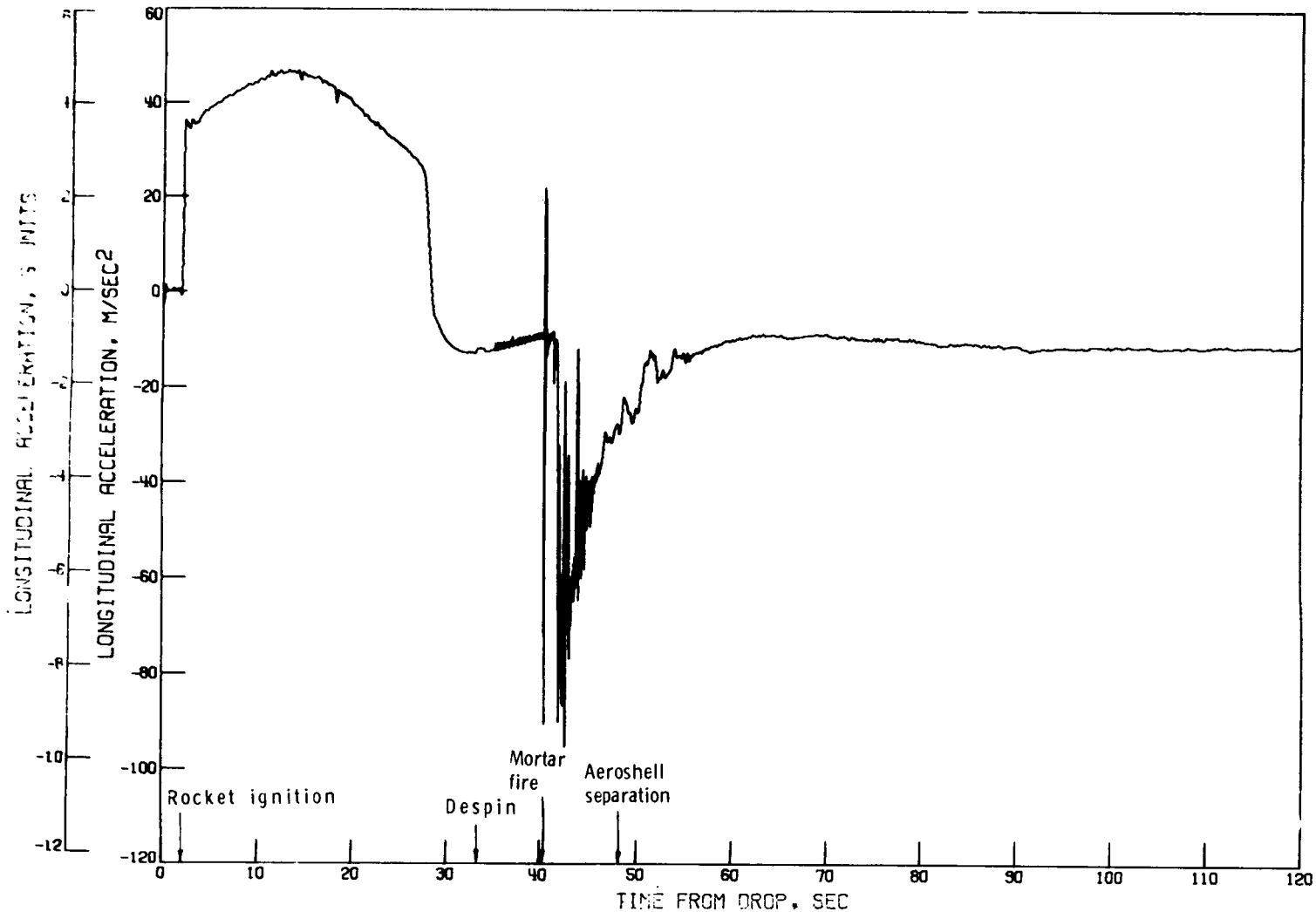


Figure 83.- Time history of longitudinal acceleration. AV-4.

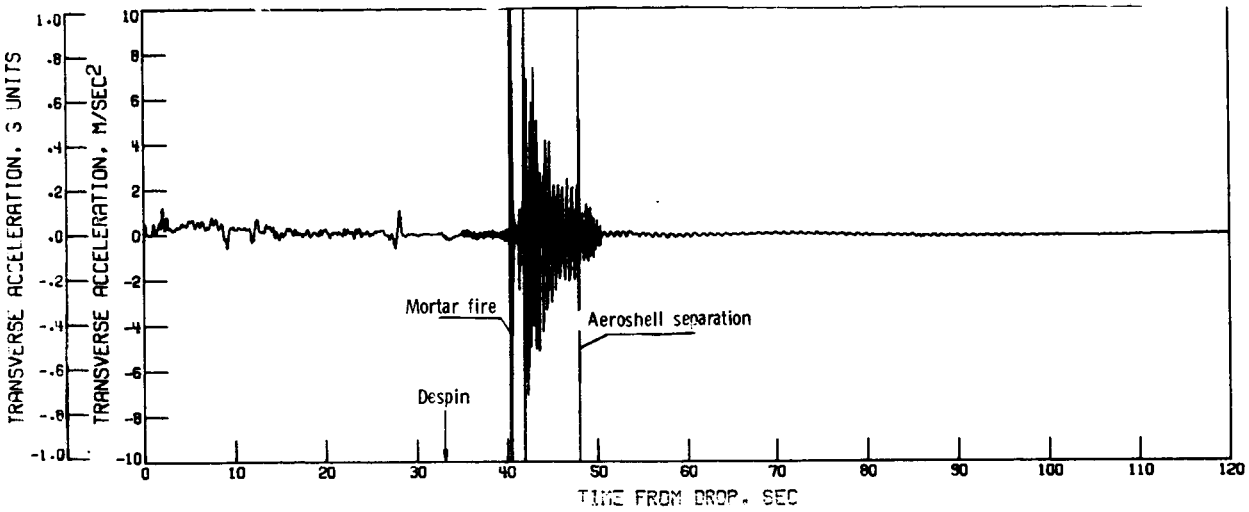


Figure 84.- Time history of transverse acceleration. AV-4; instrument limit ±1g.

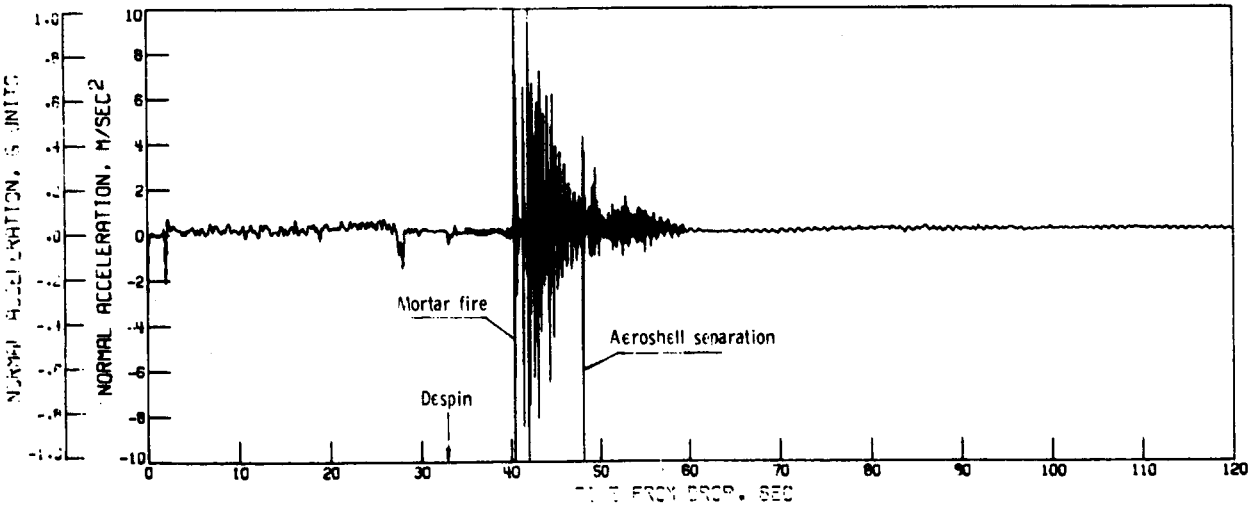


Figure 85.- Time history of normal acceleration. AV-4; instrument limit ±1g.

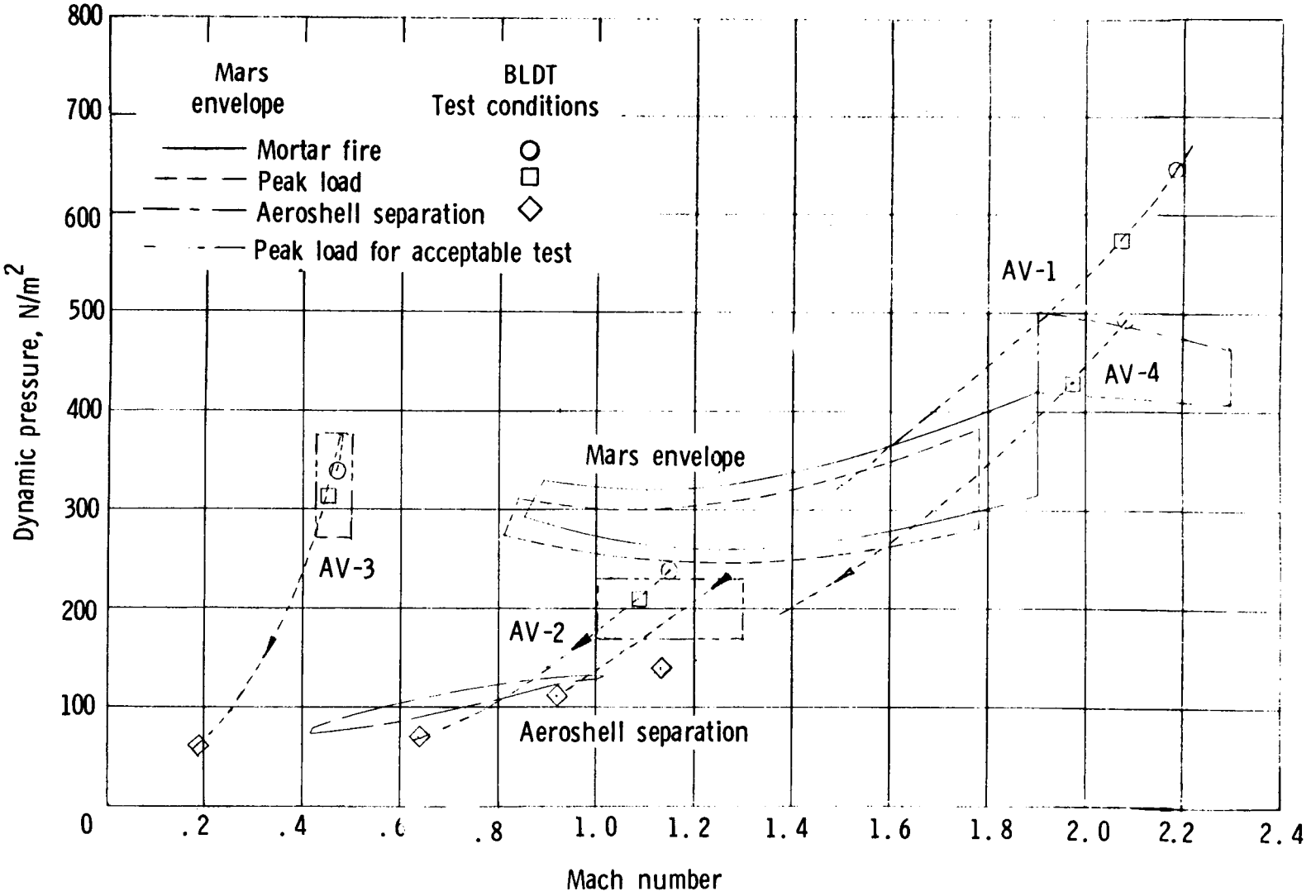


Figure 86.- Test conditions referenced to expected conditions at Mars.

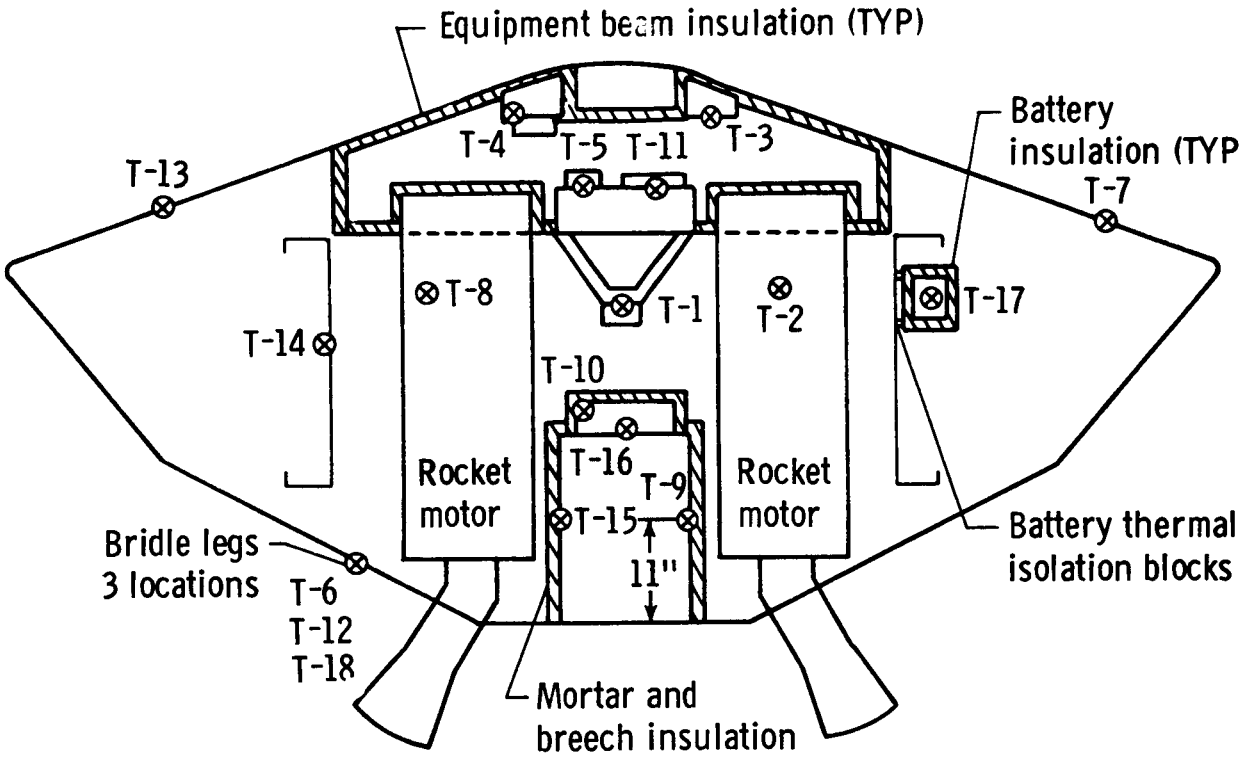


Figure 87.- Temperature measurement locations in test vehicle.

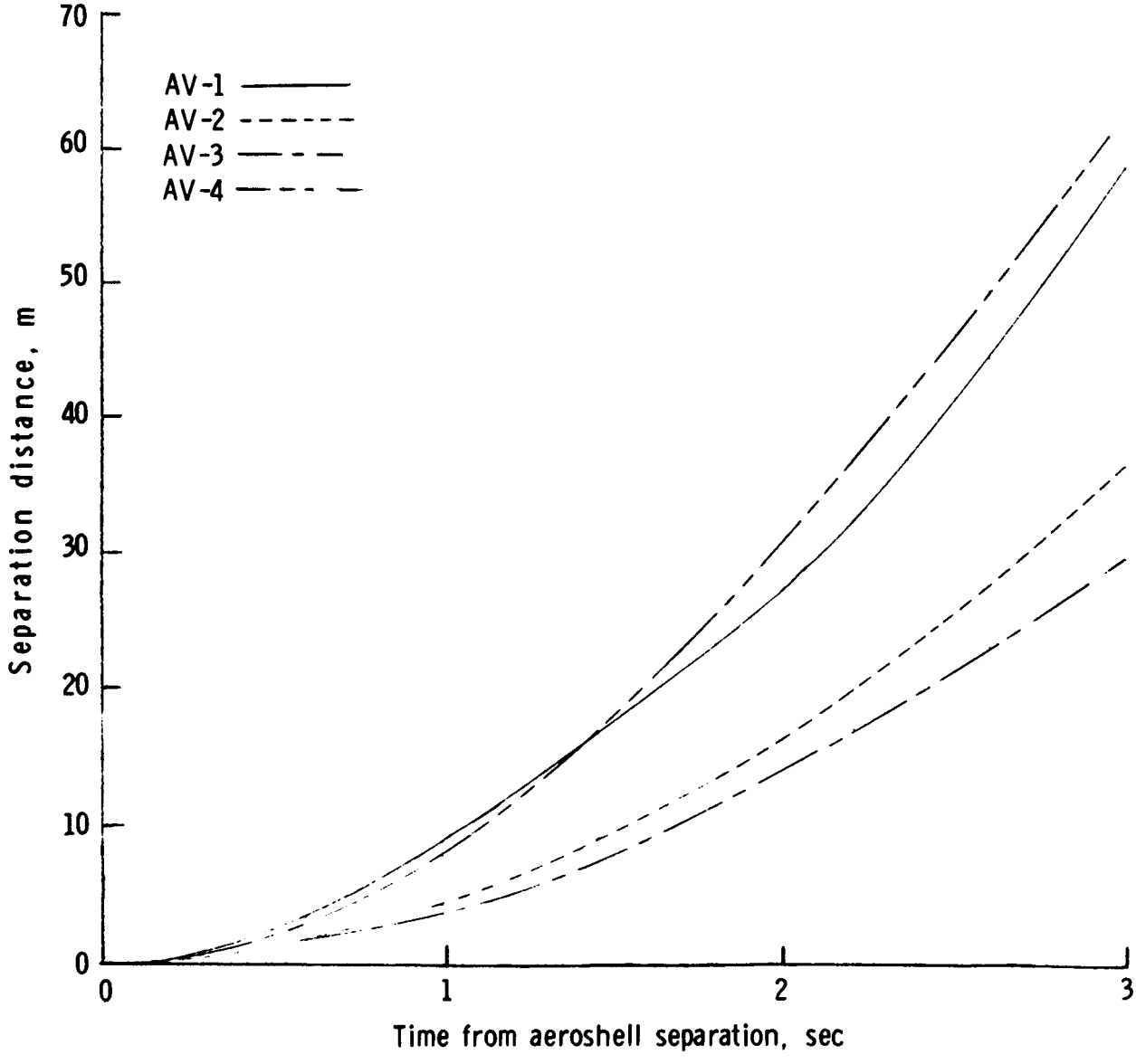


Figure 88.- Aeroshell separation distance.

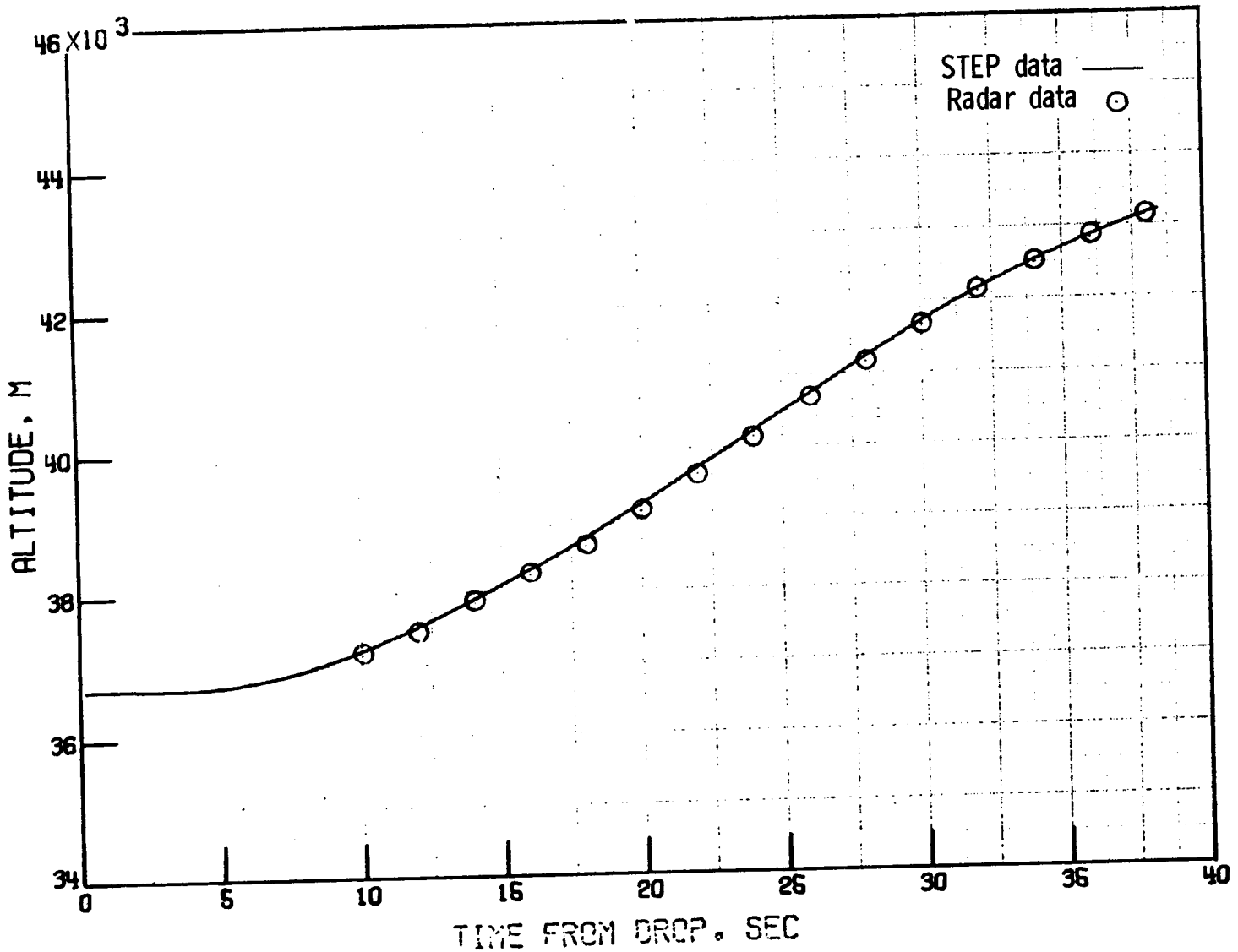


Figure 89.- History of test vehicle altitude. AV-1.

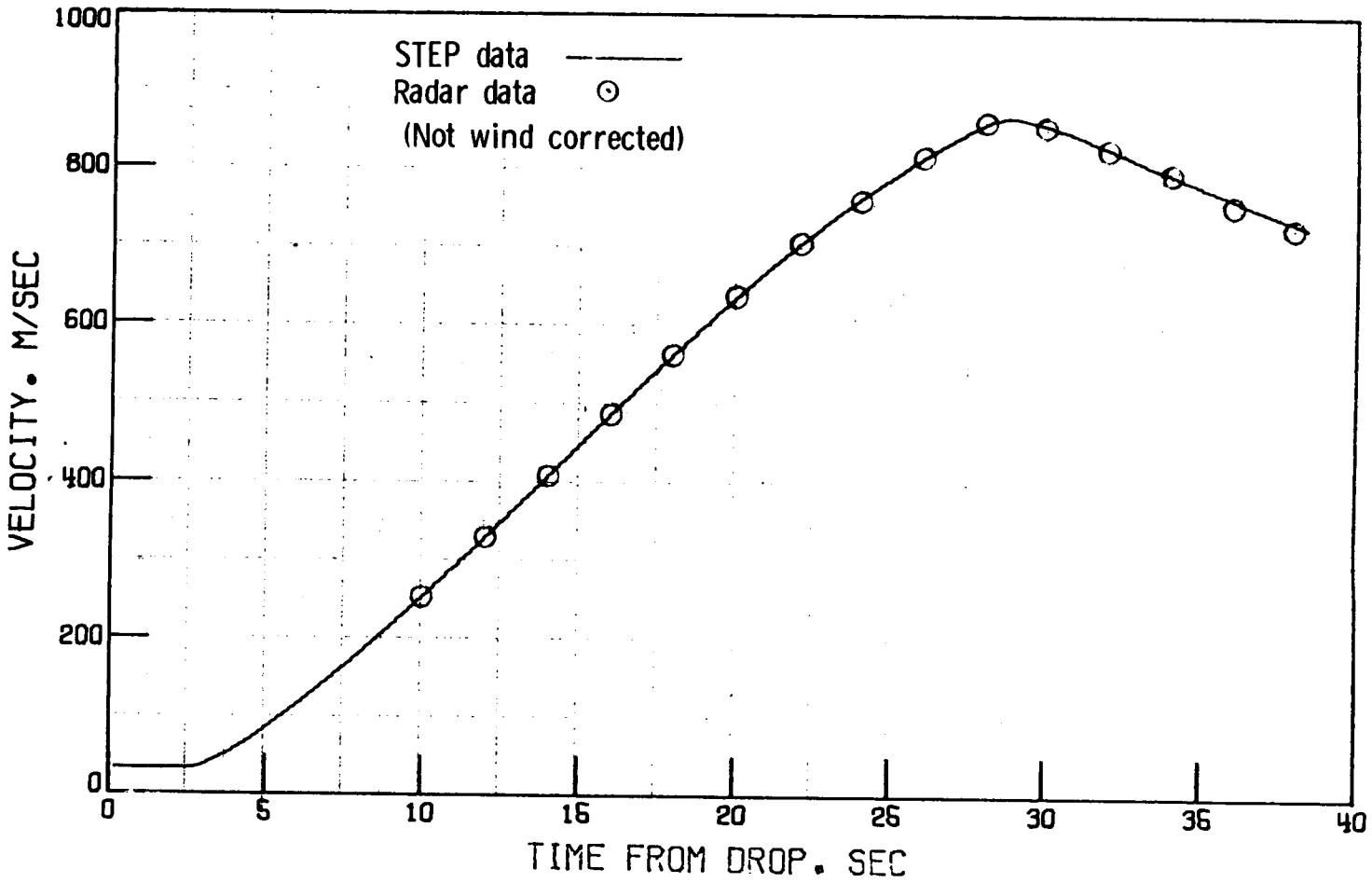


Figure 90.- History of test vehicle velocity. AV-1.

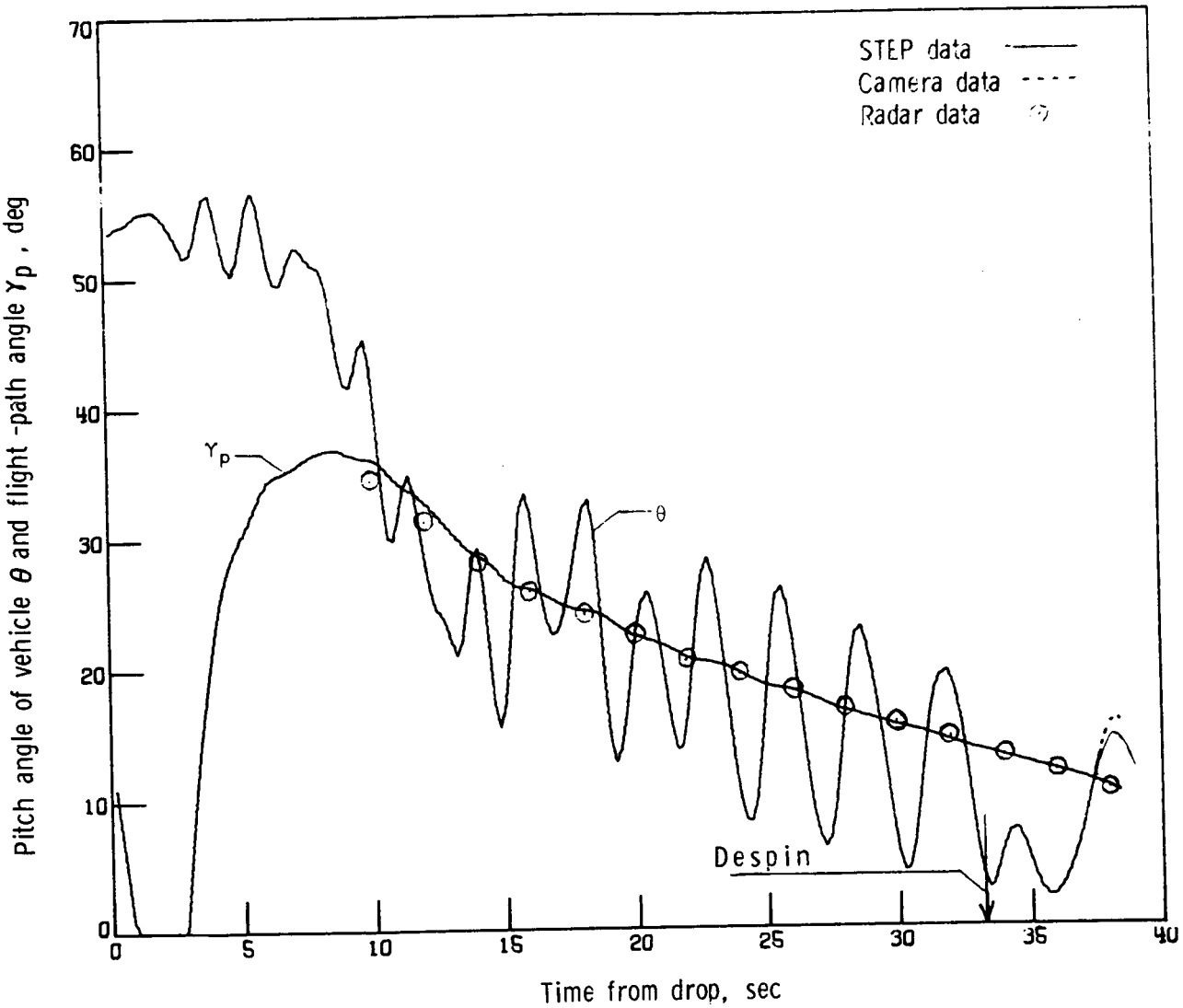


Figure 91.- History of test vehicle pitch attitude θ and flight-path angle γ_p. AV-1.

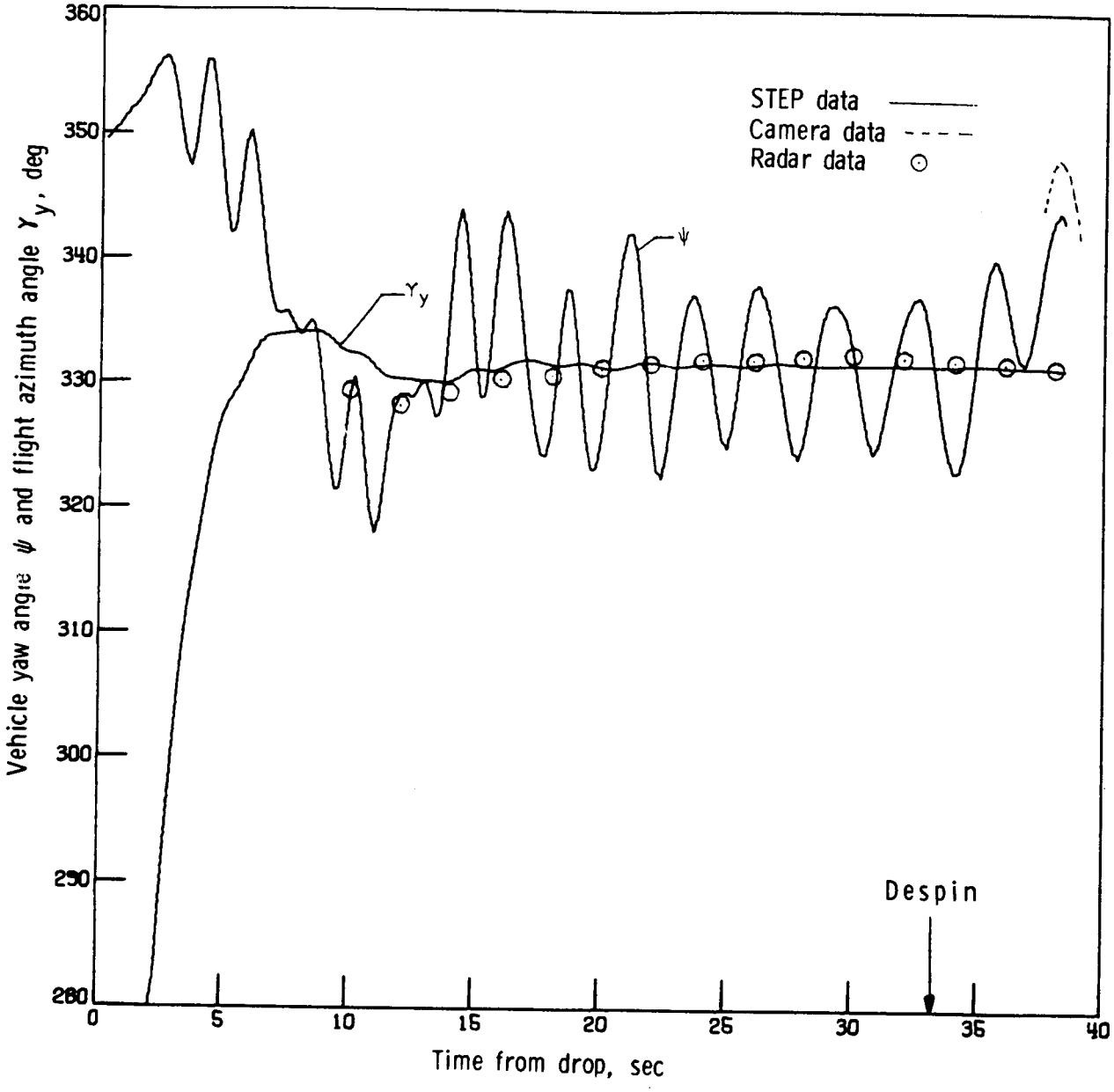


Figure 92.- History of test vehicle heading ψ and flight azimuth γ_y. AV-1.

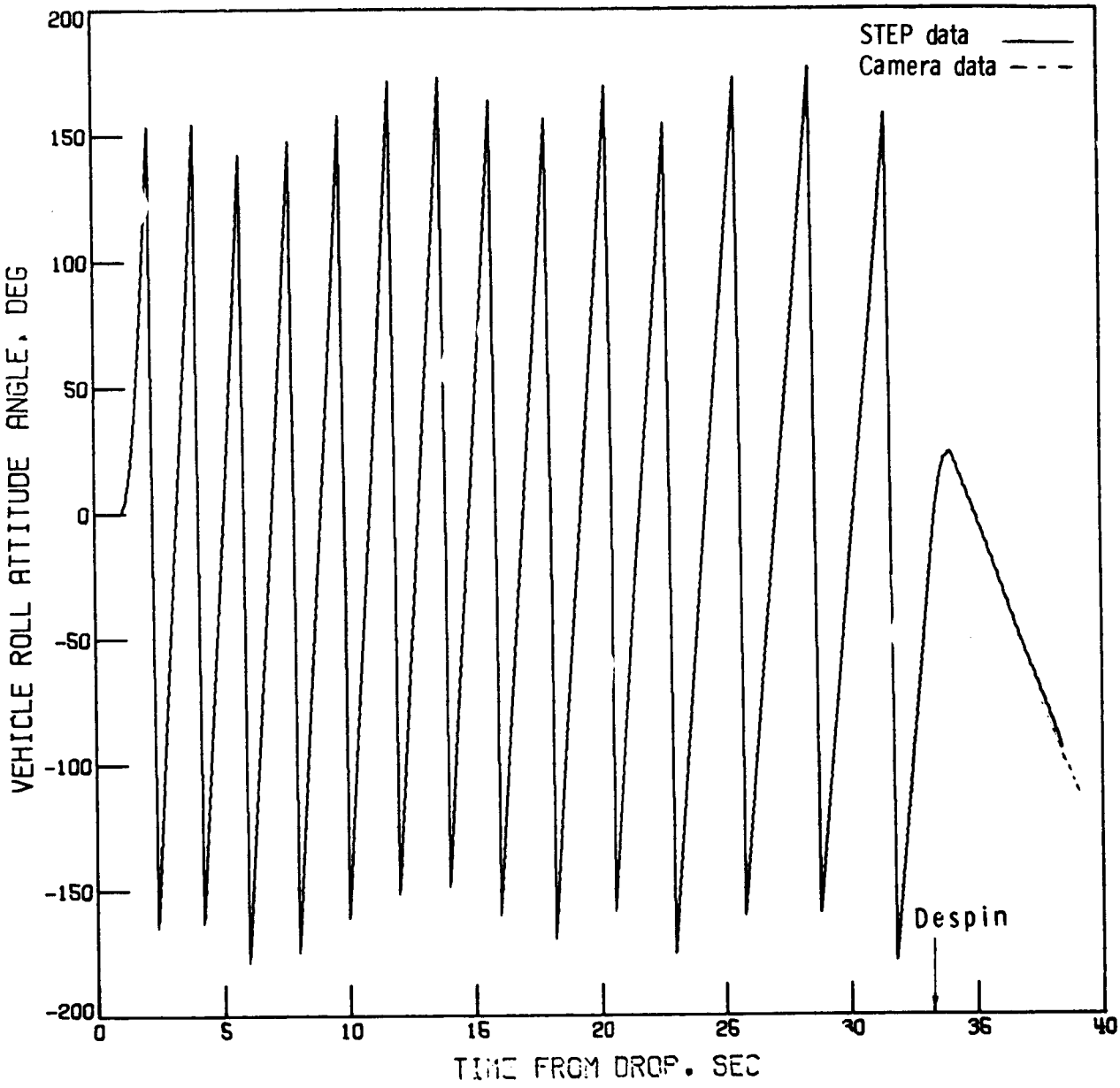


Figure 93.- Test vehicle roll attitude history. AV-1.

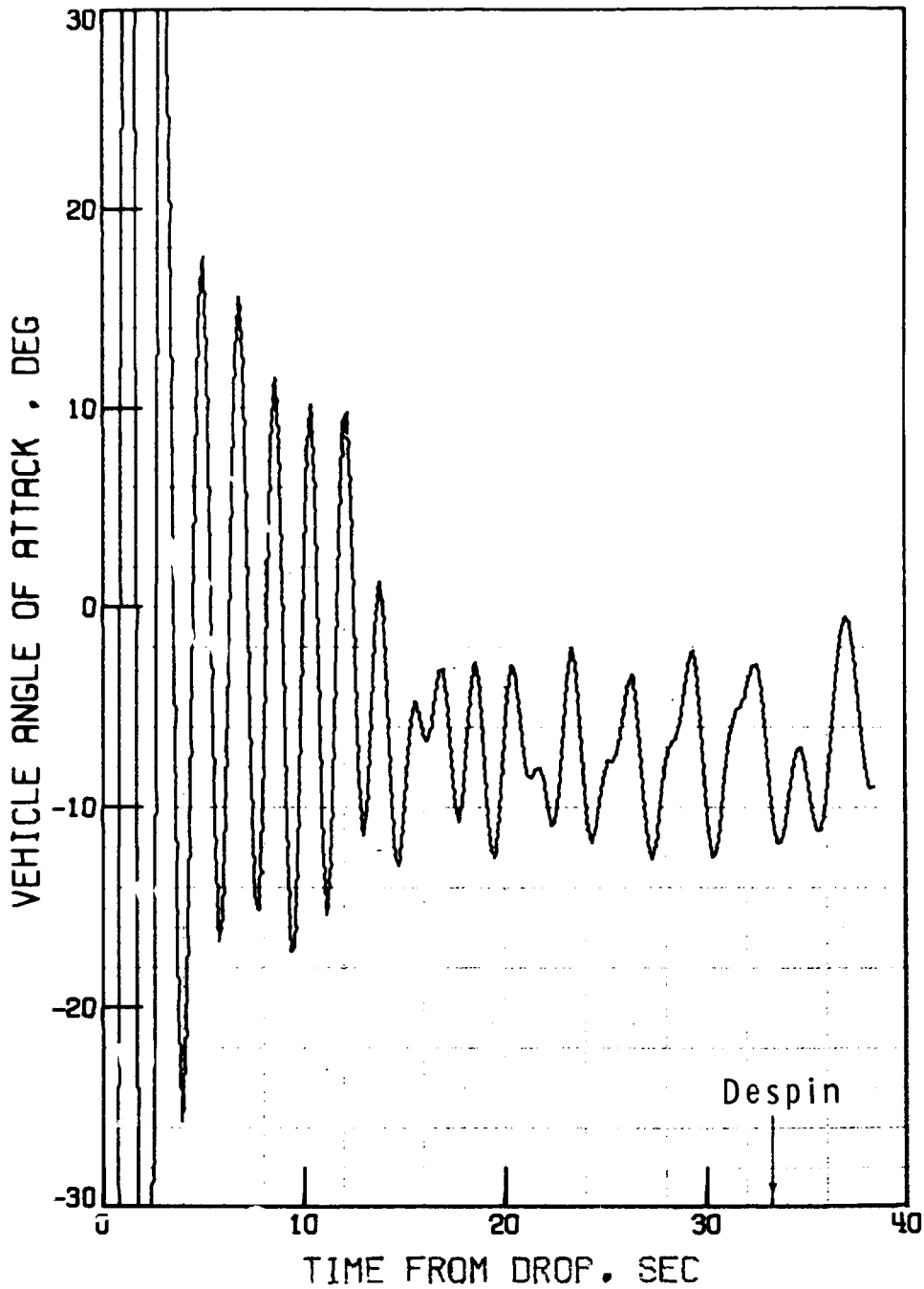


Figure 94.- Time history of angle of attack. AV-1.

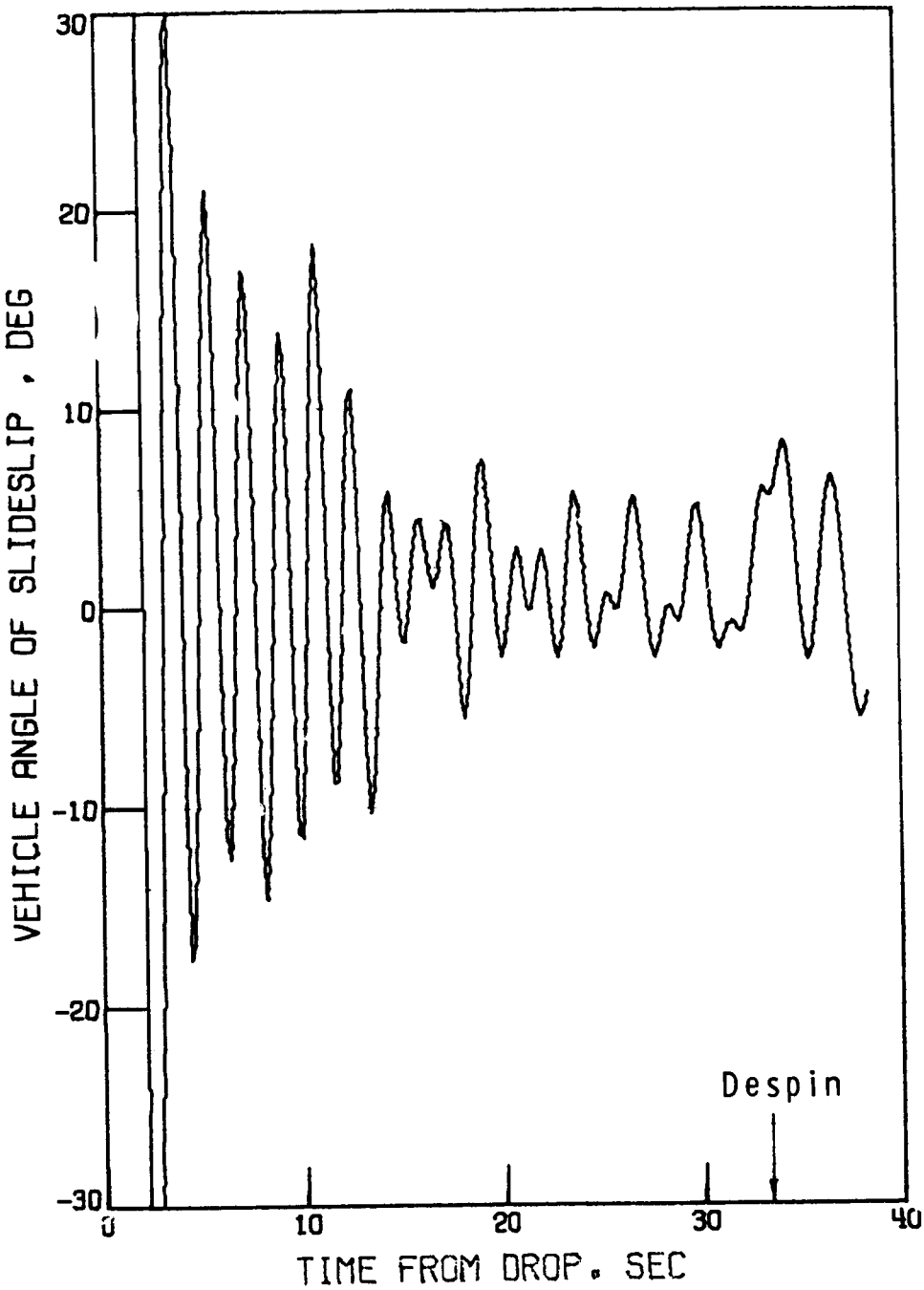


Figure 95.- Time history of angle of sideslip. AV-1.

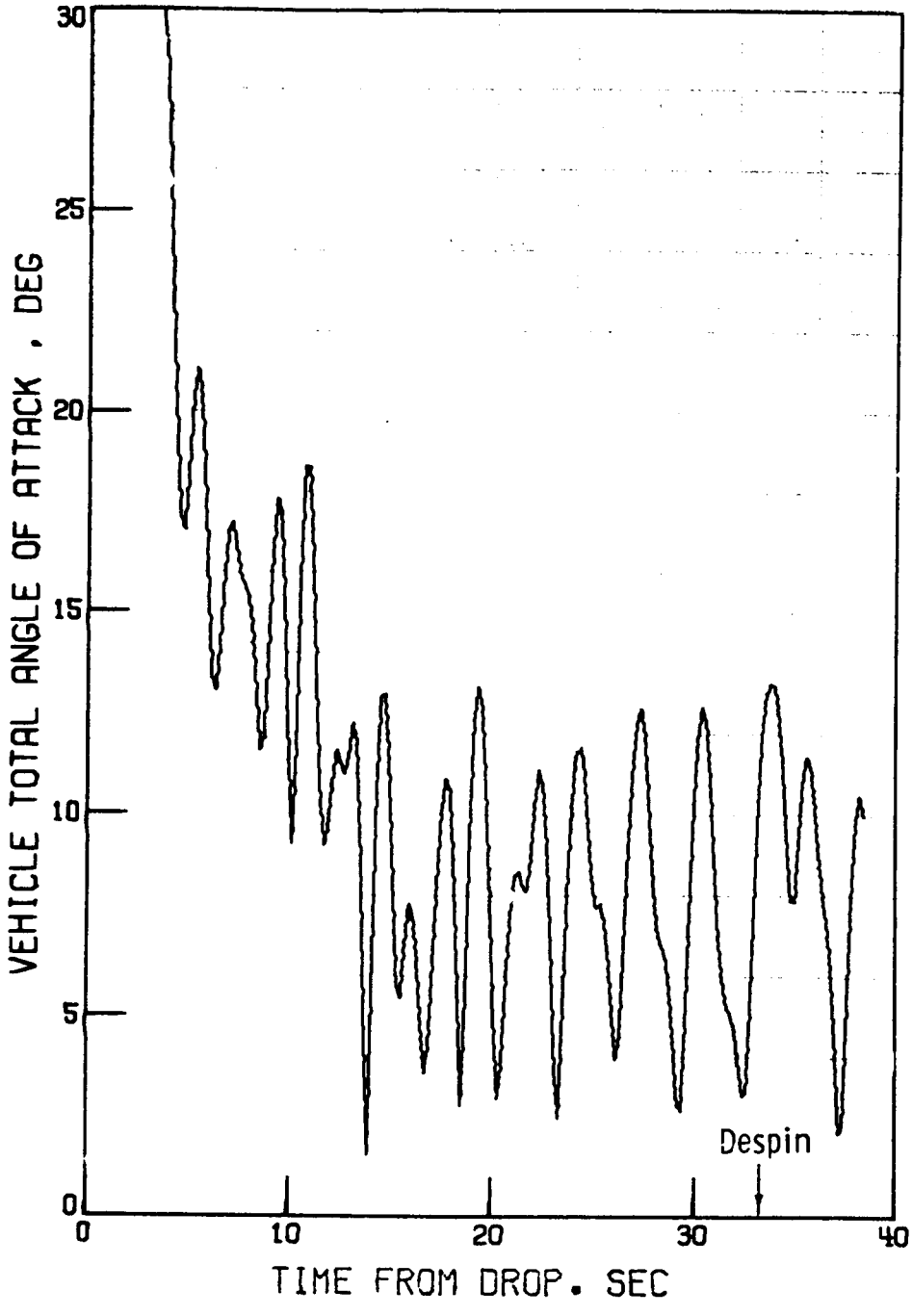


Figure 96.- Time history of total angle of attack. AV-1.

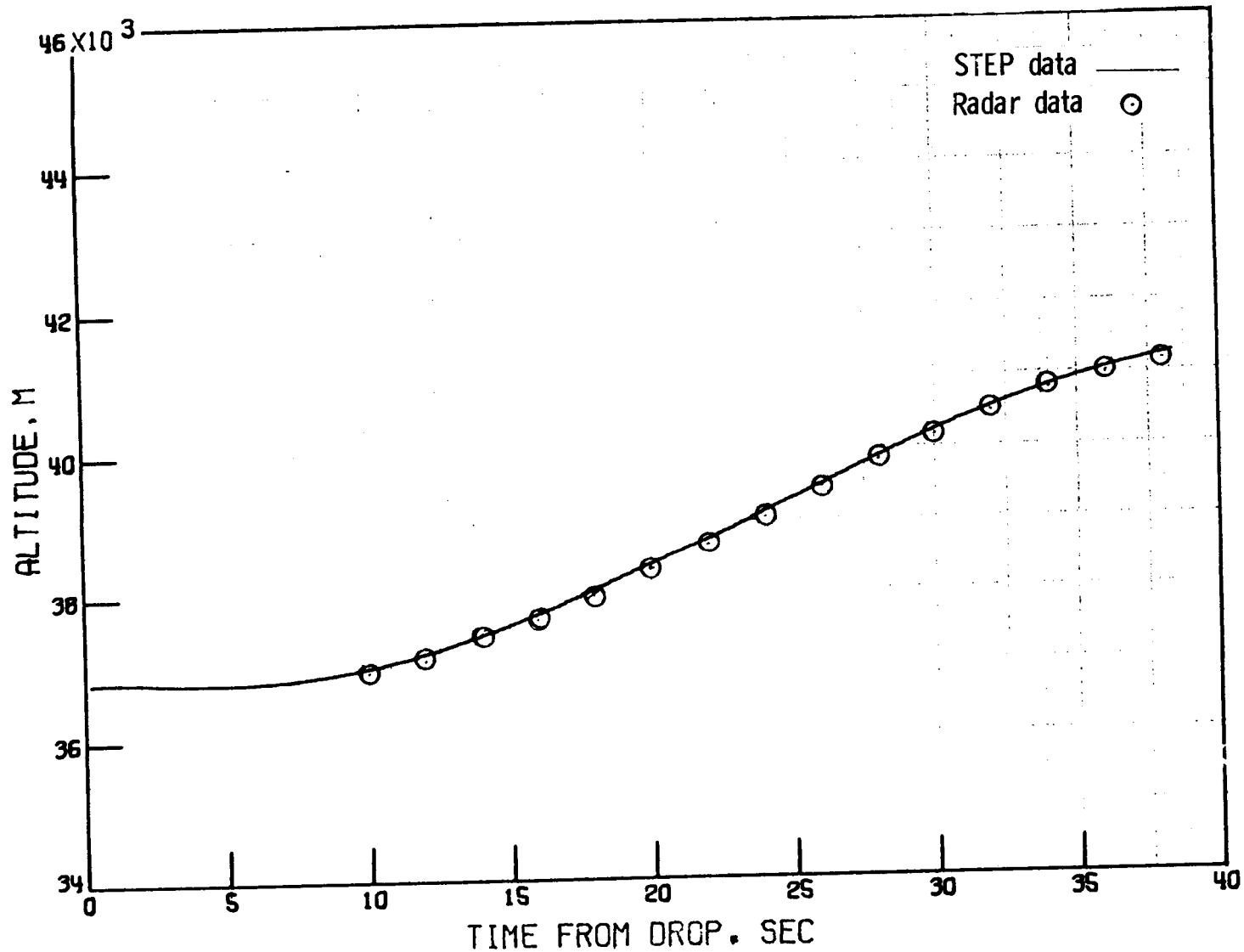


Figure 97.- History of test vehicle altitude. AV-2.

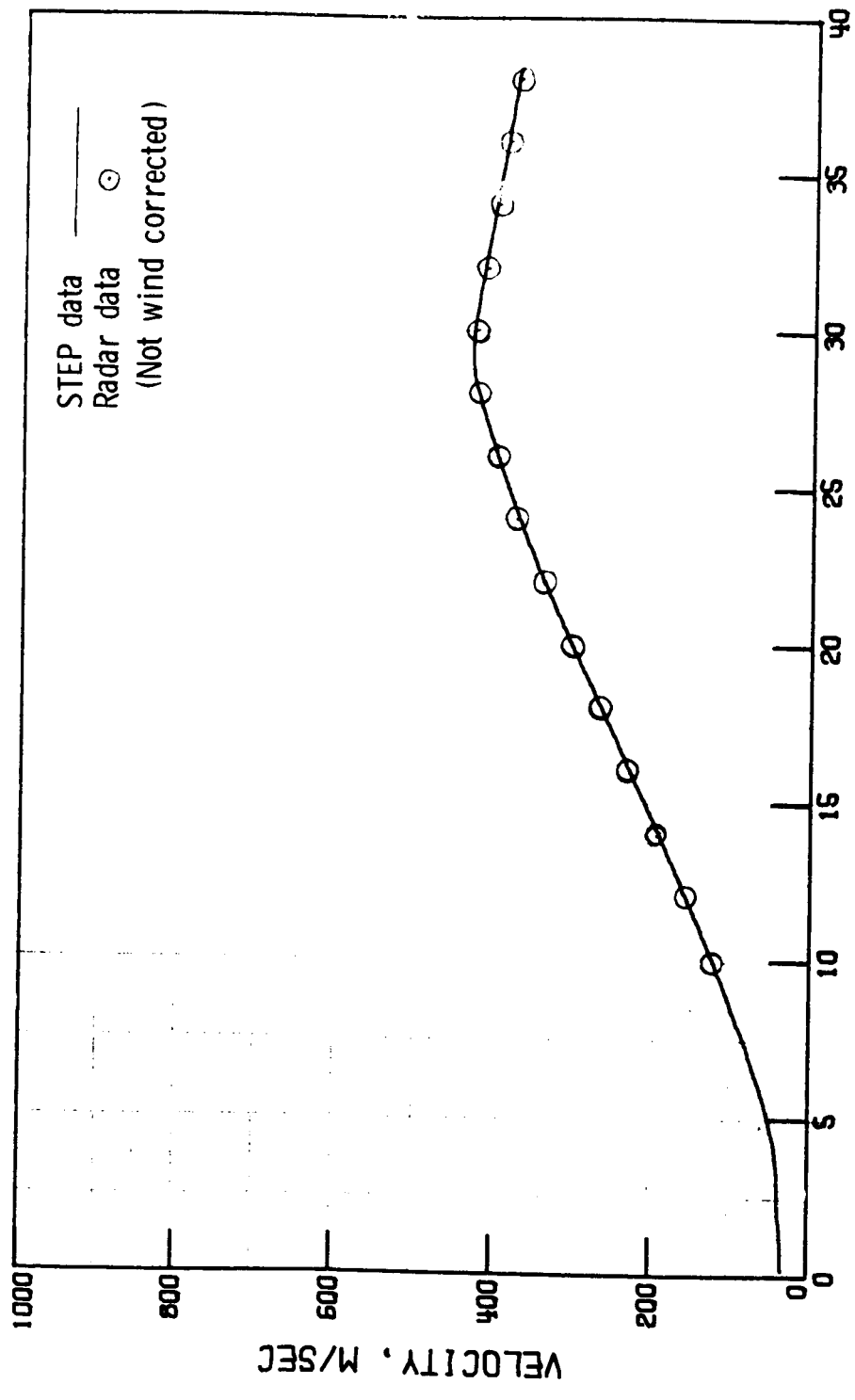


Figure 98.- History of test vehicle velocity. AV-2.

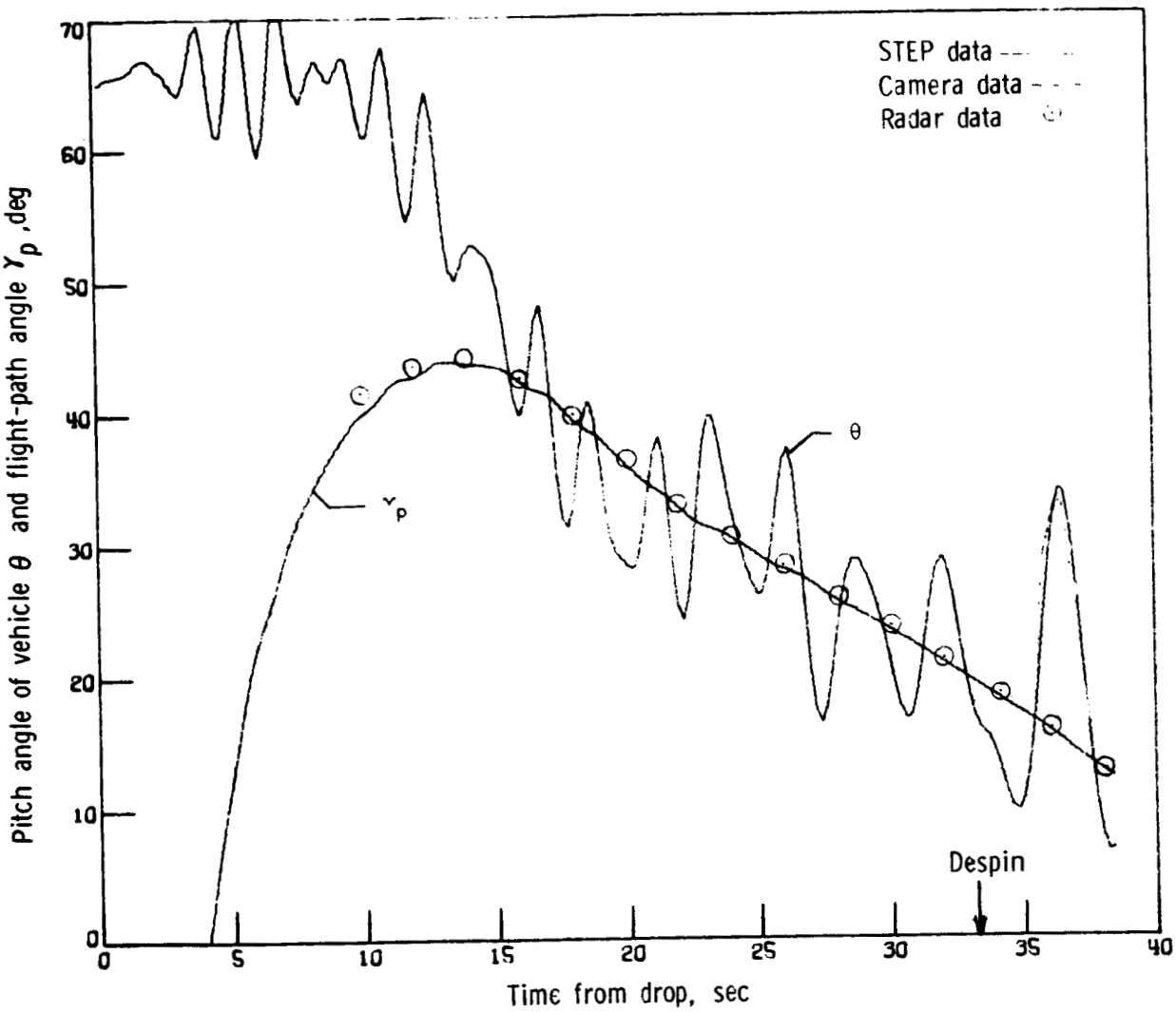


Figure 99.- History of test vehicle pitch attitude θ and flight-path angle γ_p. AV-2.

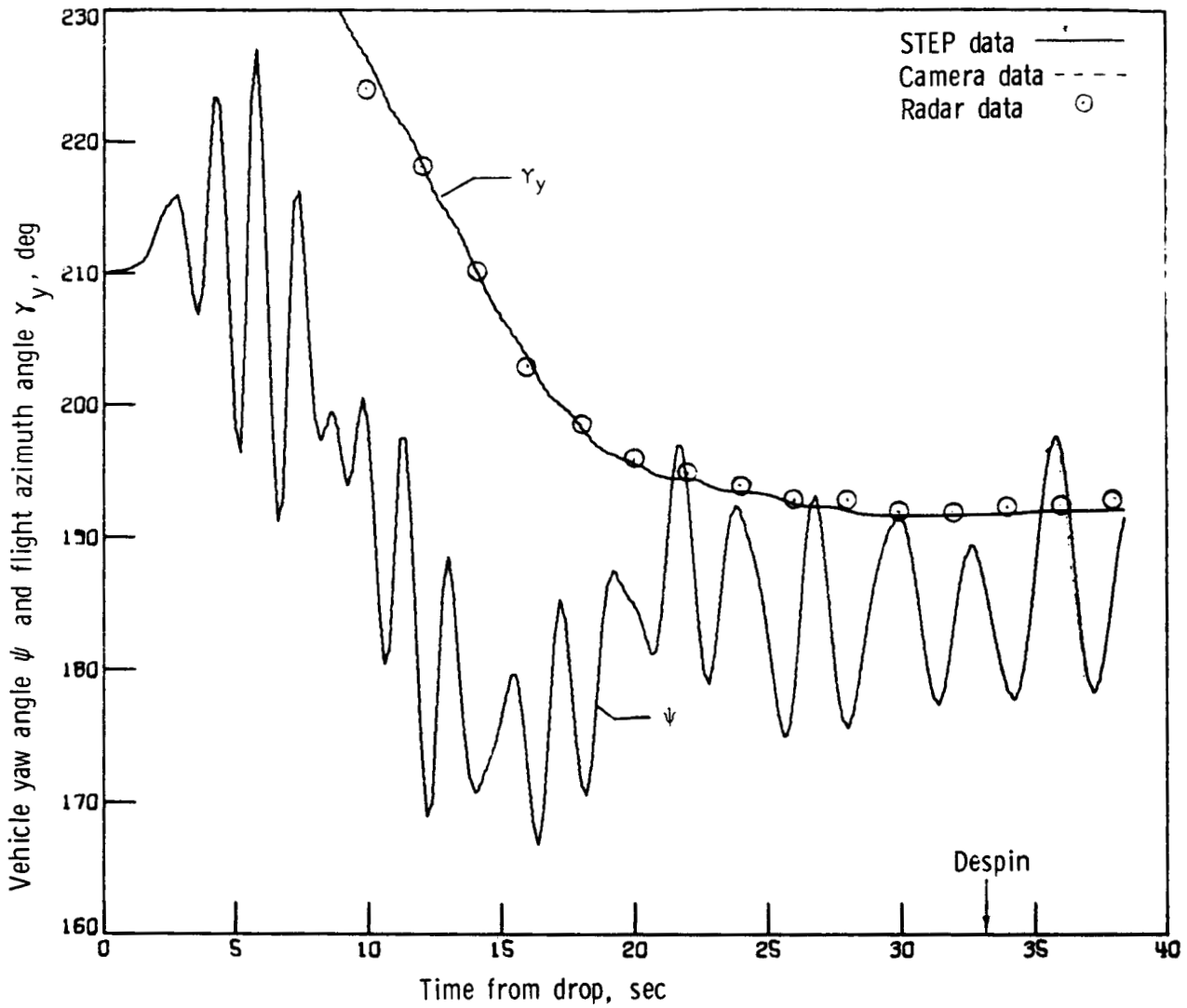


Figure 100.- History of test vehicle heading ψ and flight azimuth γ_y. AV-2.

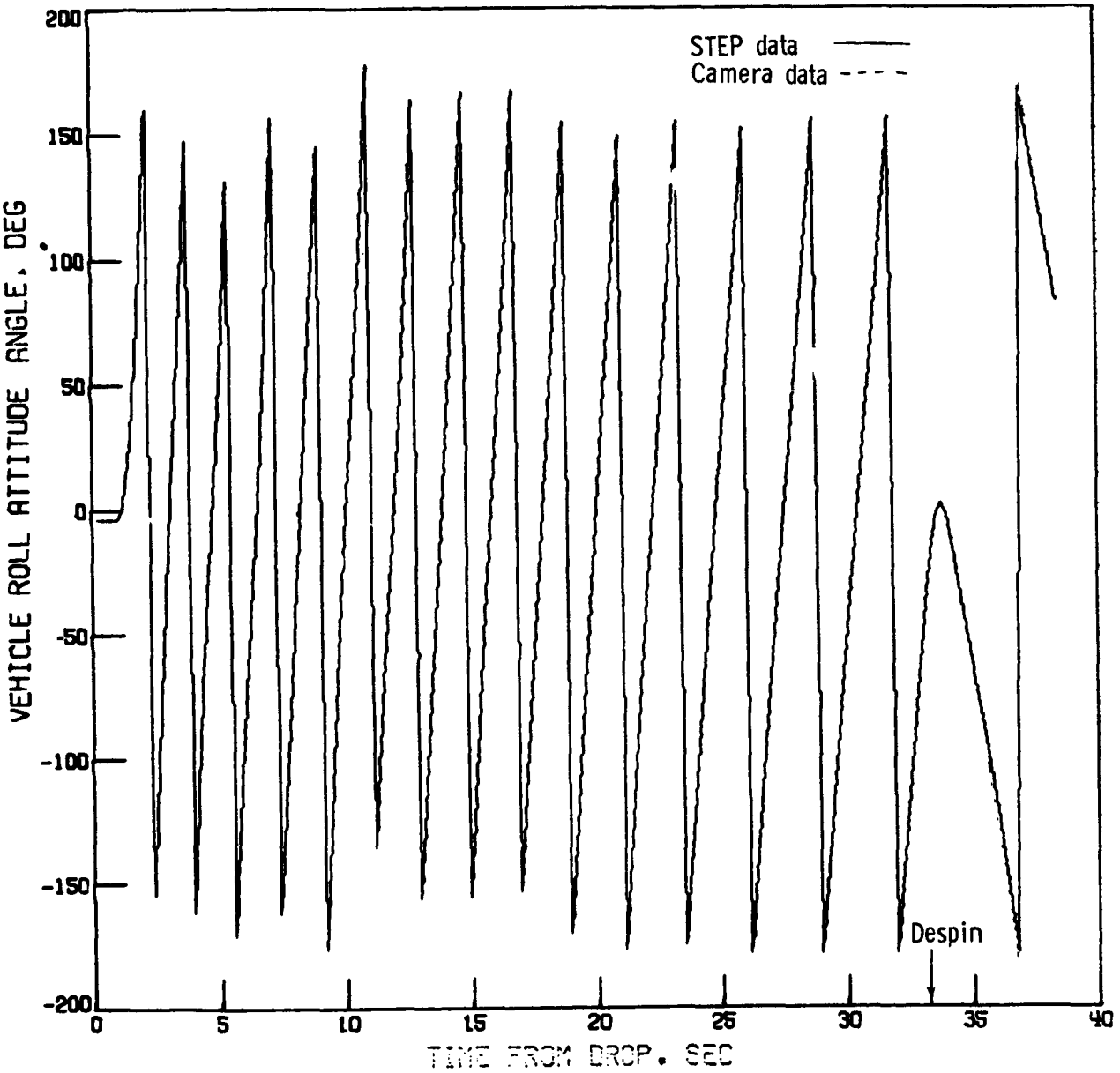


Figure 101.- Test vehicle roll attitude history. AV-2.

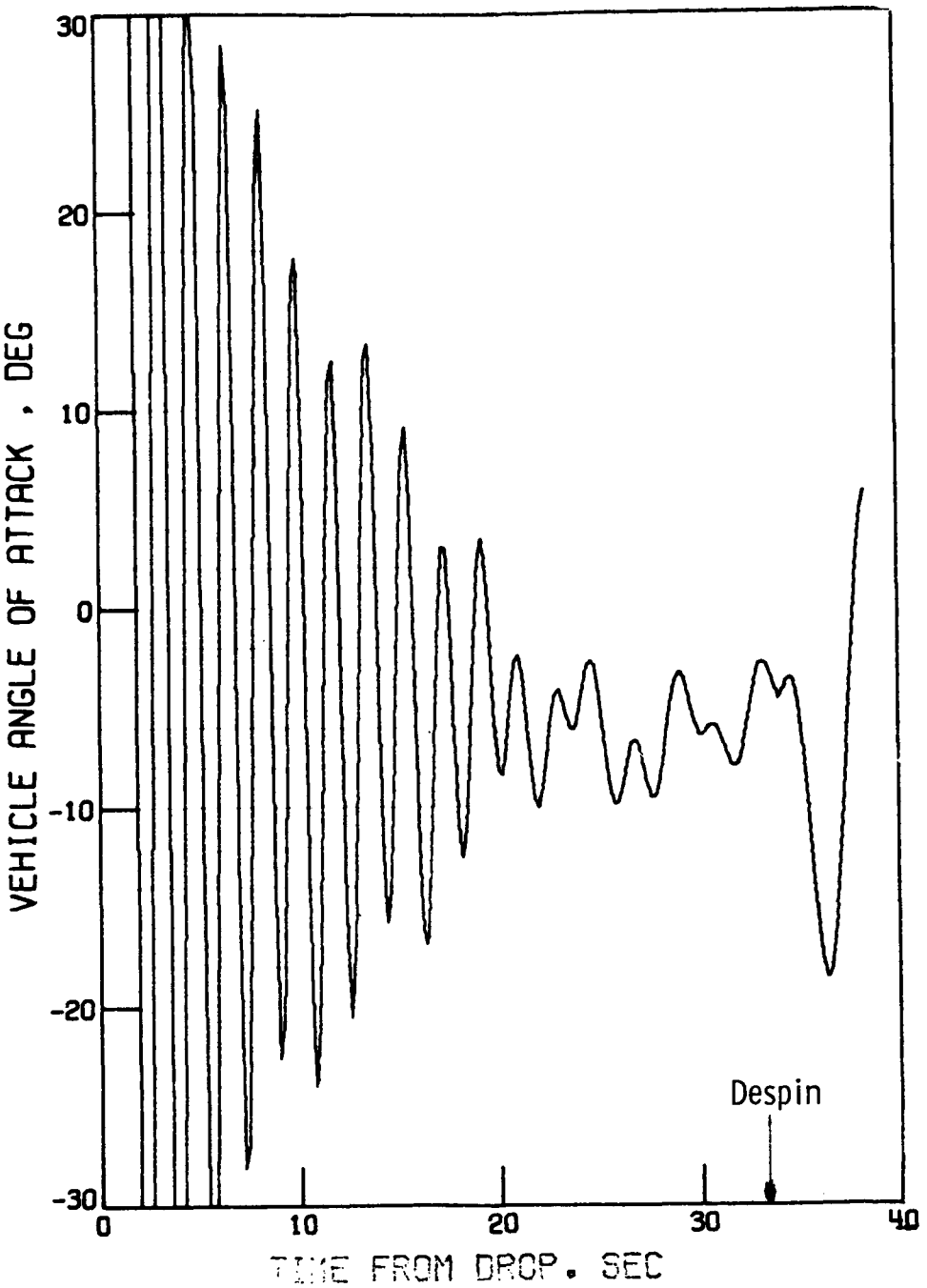


Figure 102.- Time history of angle of attack. AV-2.

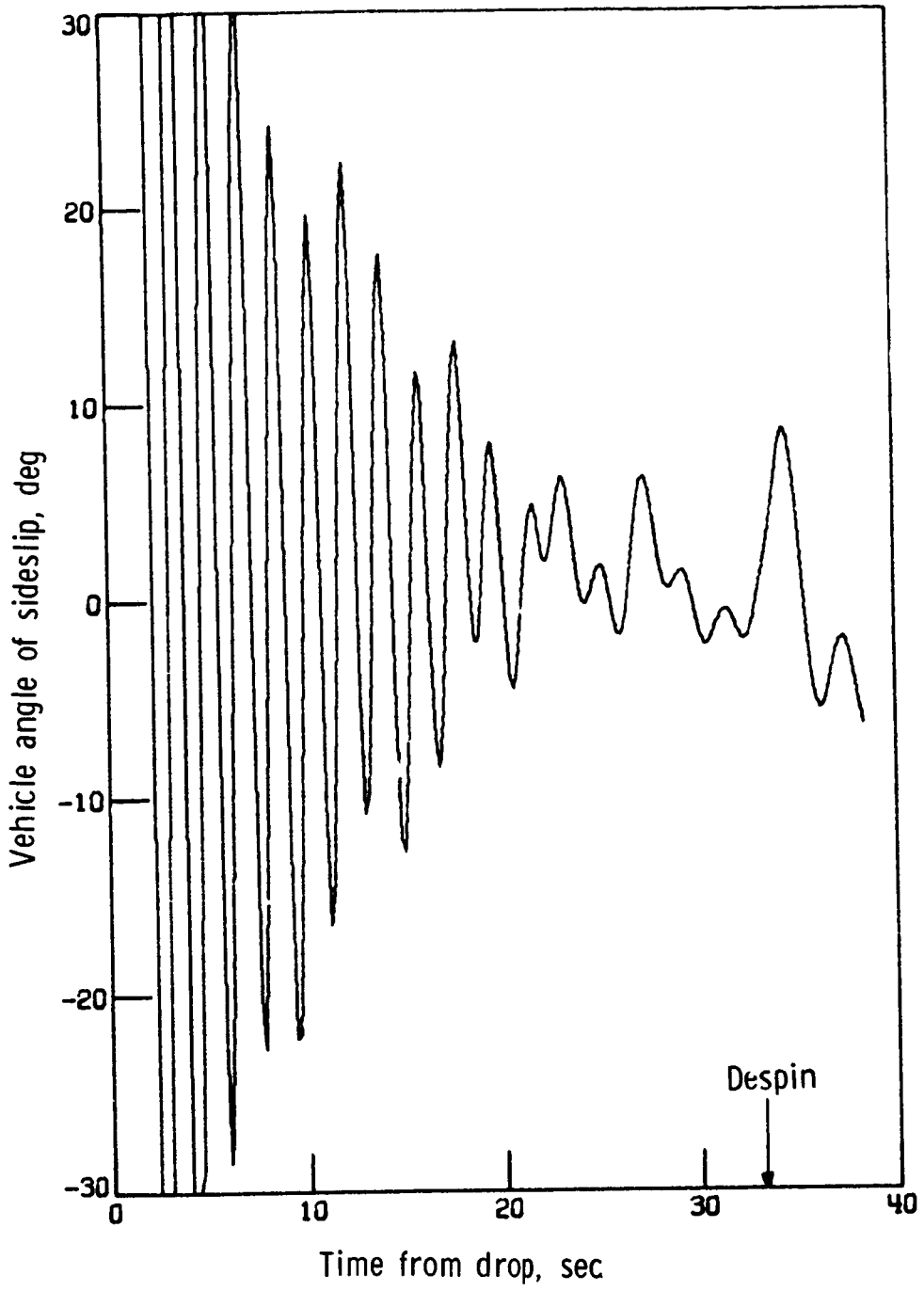


Figure 103.- Time history of angle of sideslip. AV-2.

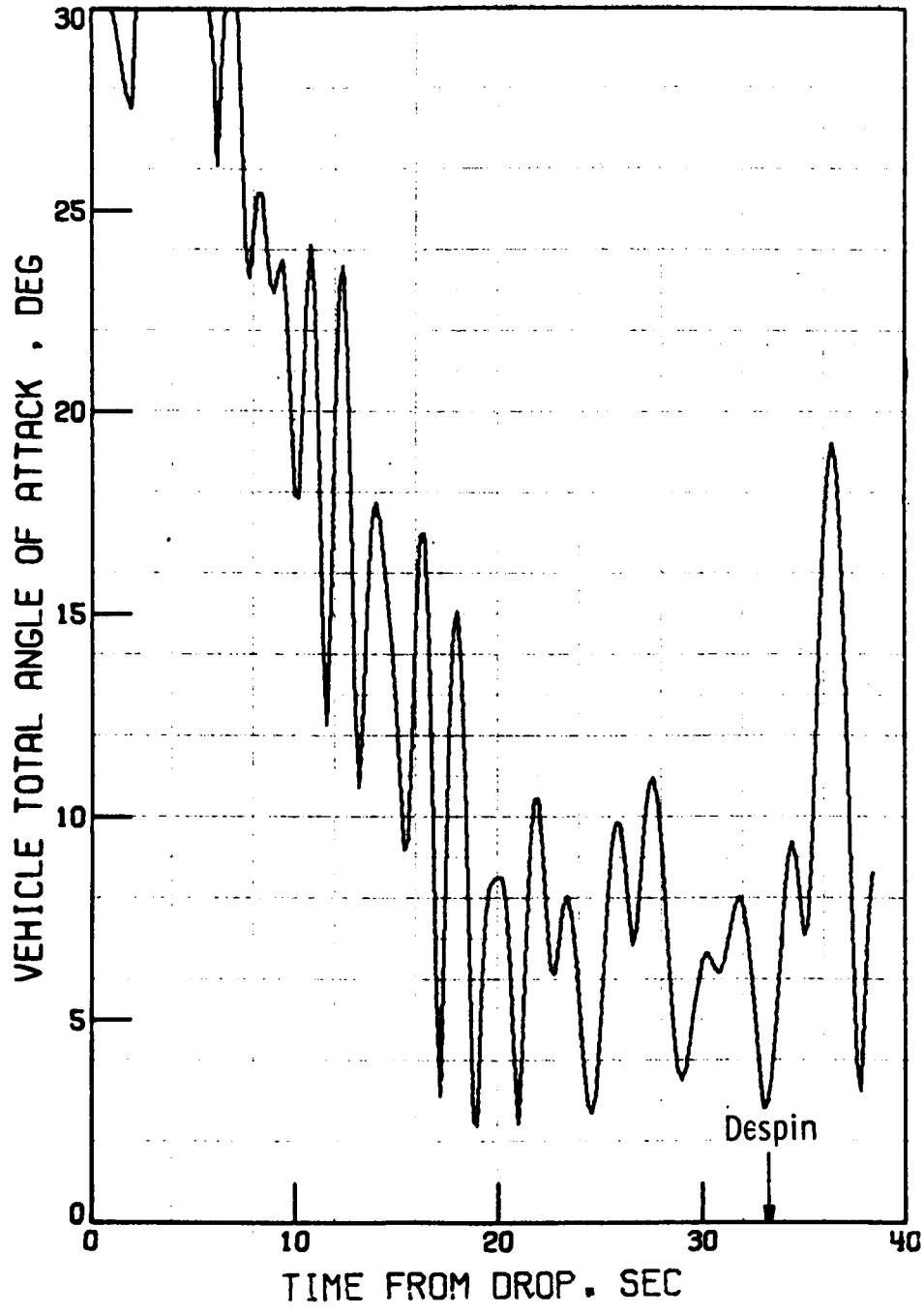


Figure 104.- Time history of total angle of attack. AV-2.

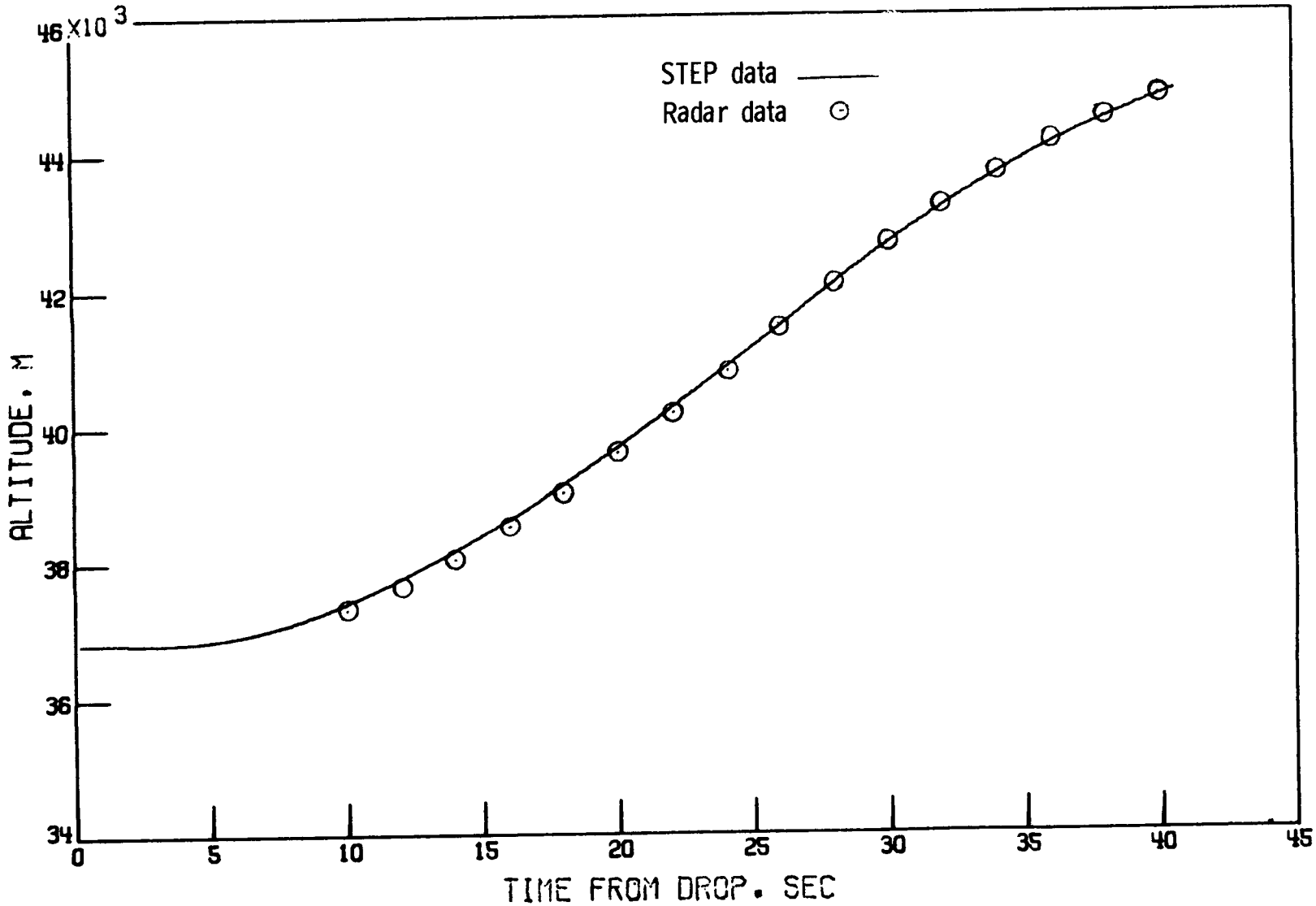


Figure 105.- History oi test vehicle altitude. AV-4.

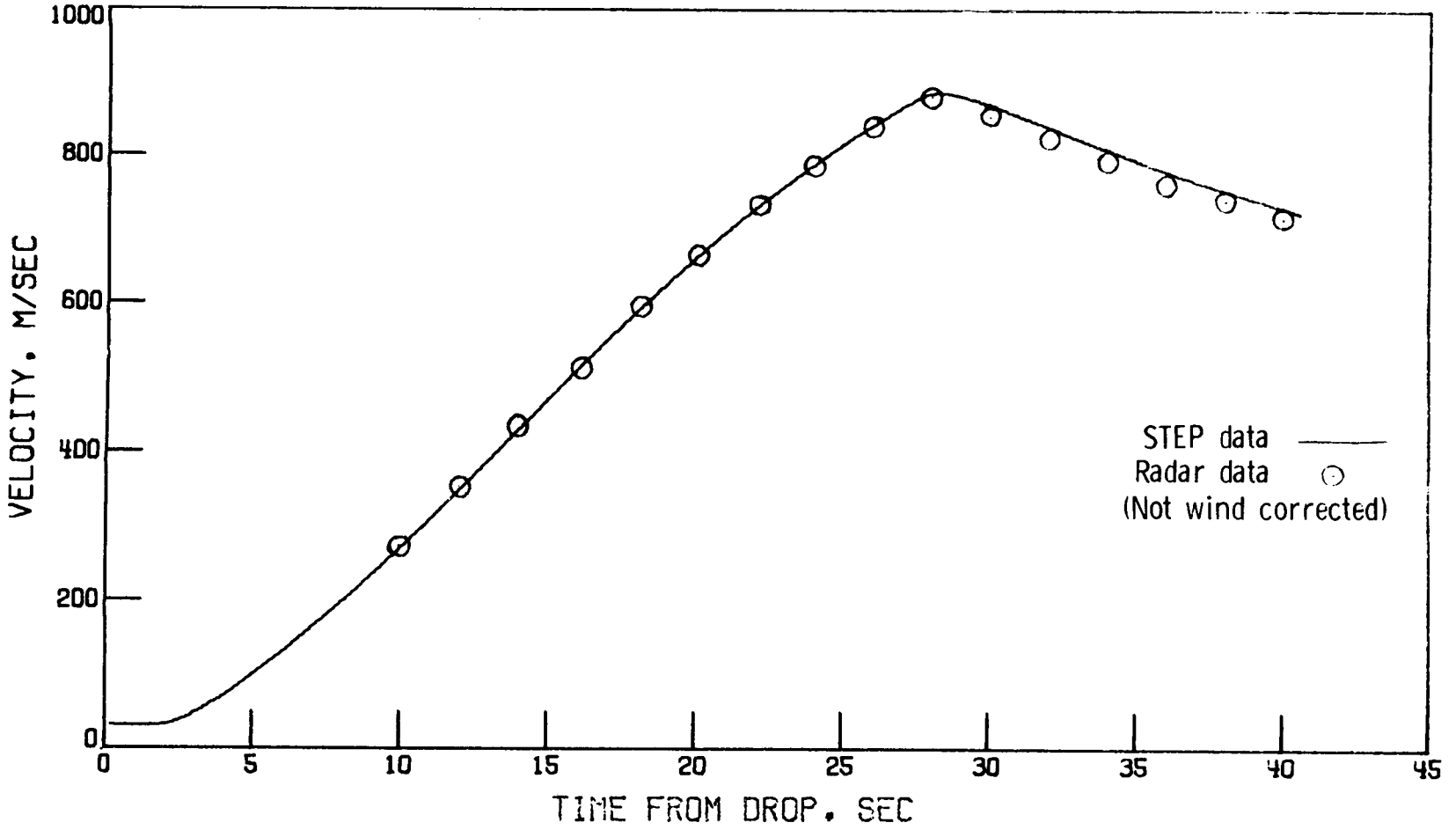


Figure 106.- History of test vehicle velocity. AV-4.

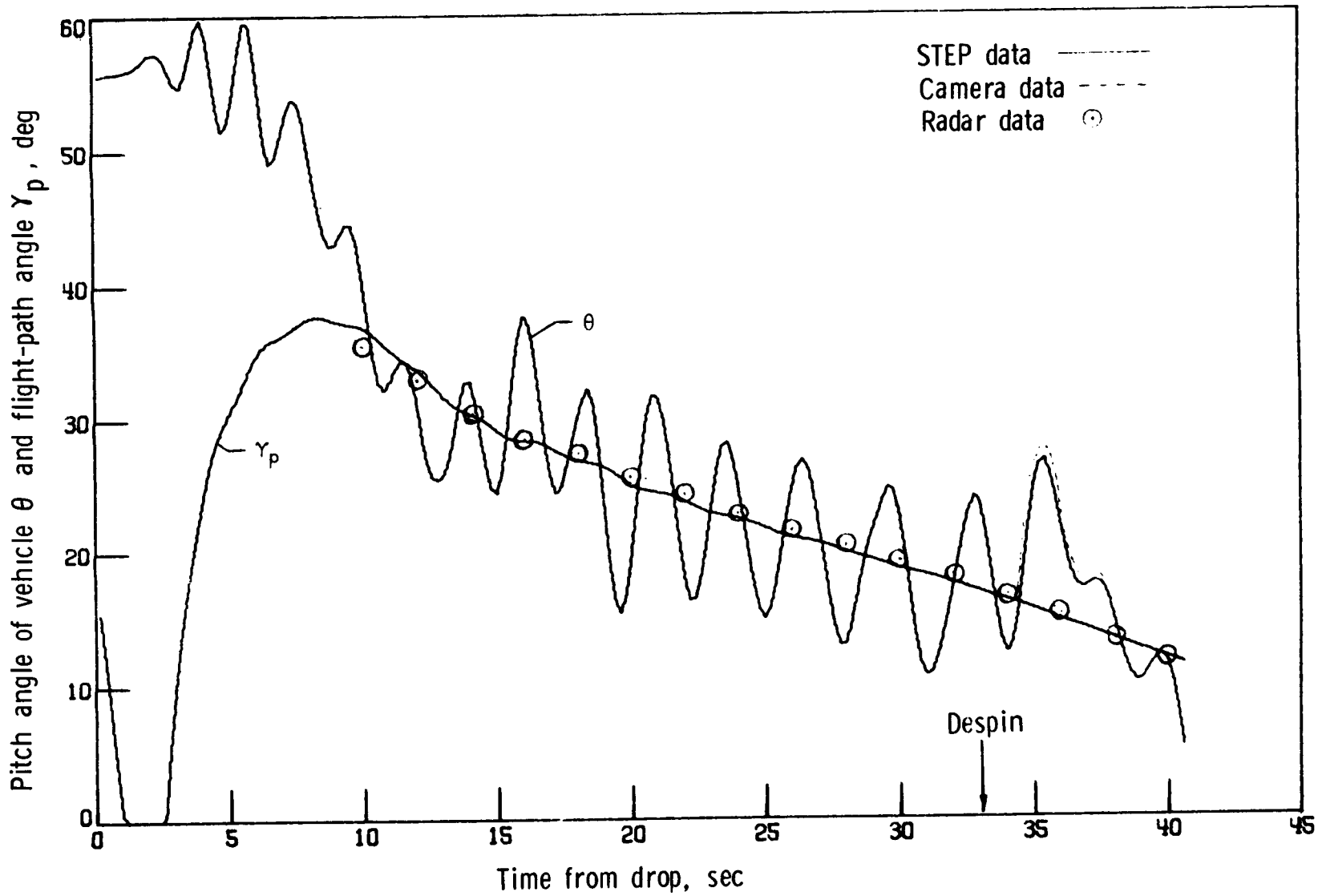


Figure 107.- History of test-vehicle pitch attitude θ and flight-path angle γ_p. AV-4.

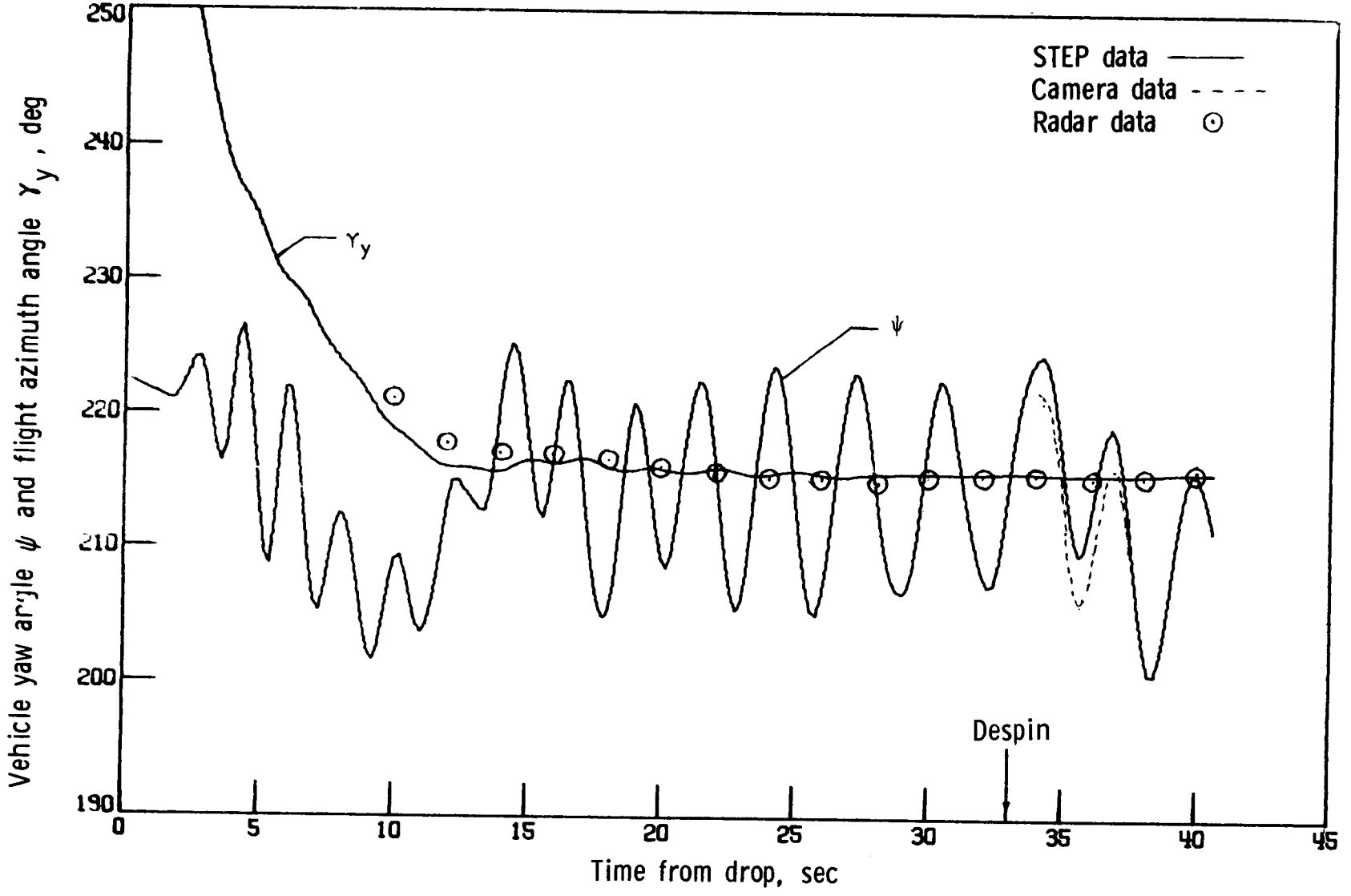


Figure 108.- History of test vehicle heading ψ and flight azimuth γ_y. AV-4.

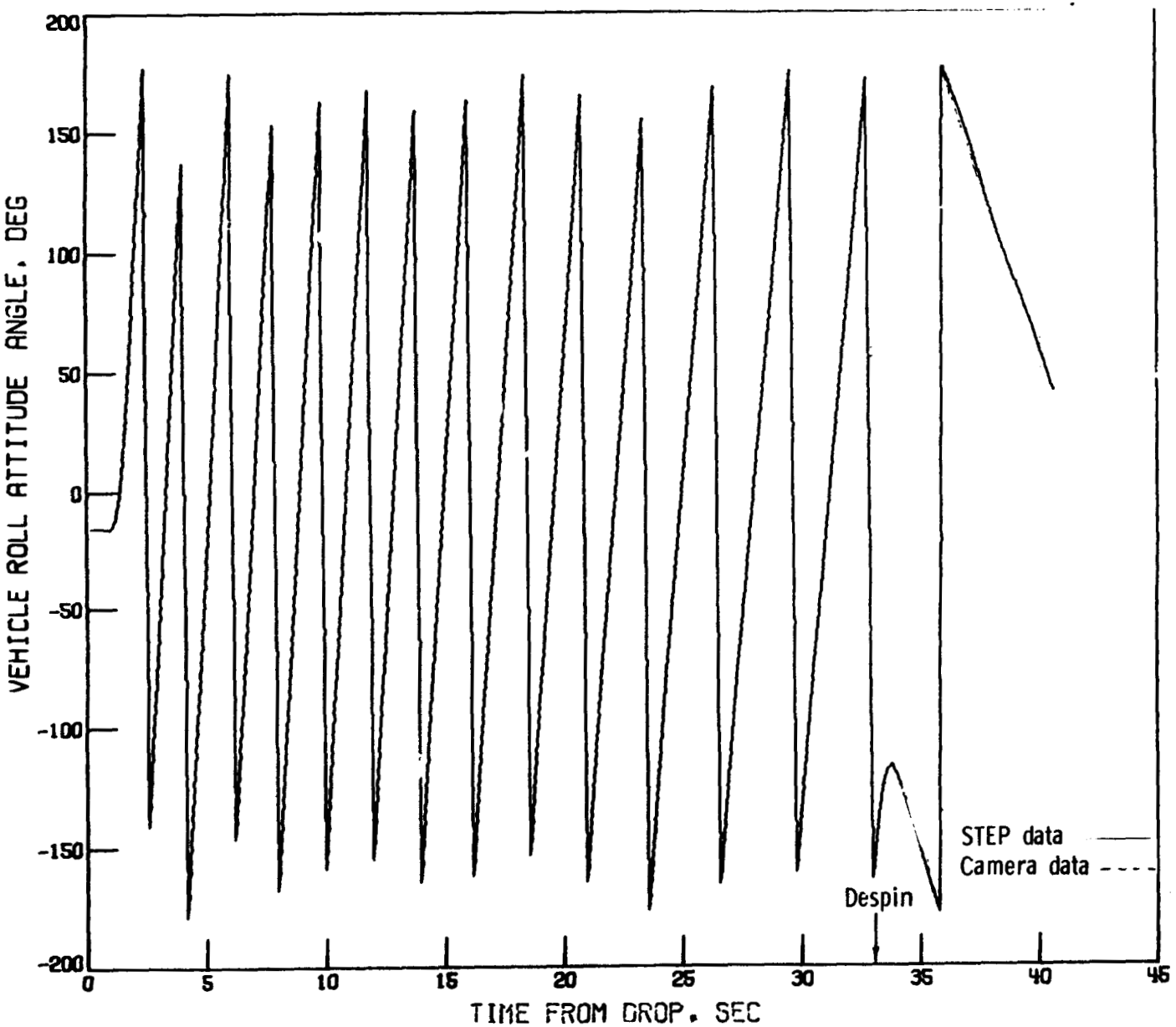


Figure 109.- Test-vehicle roll attitude history. AV-4.

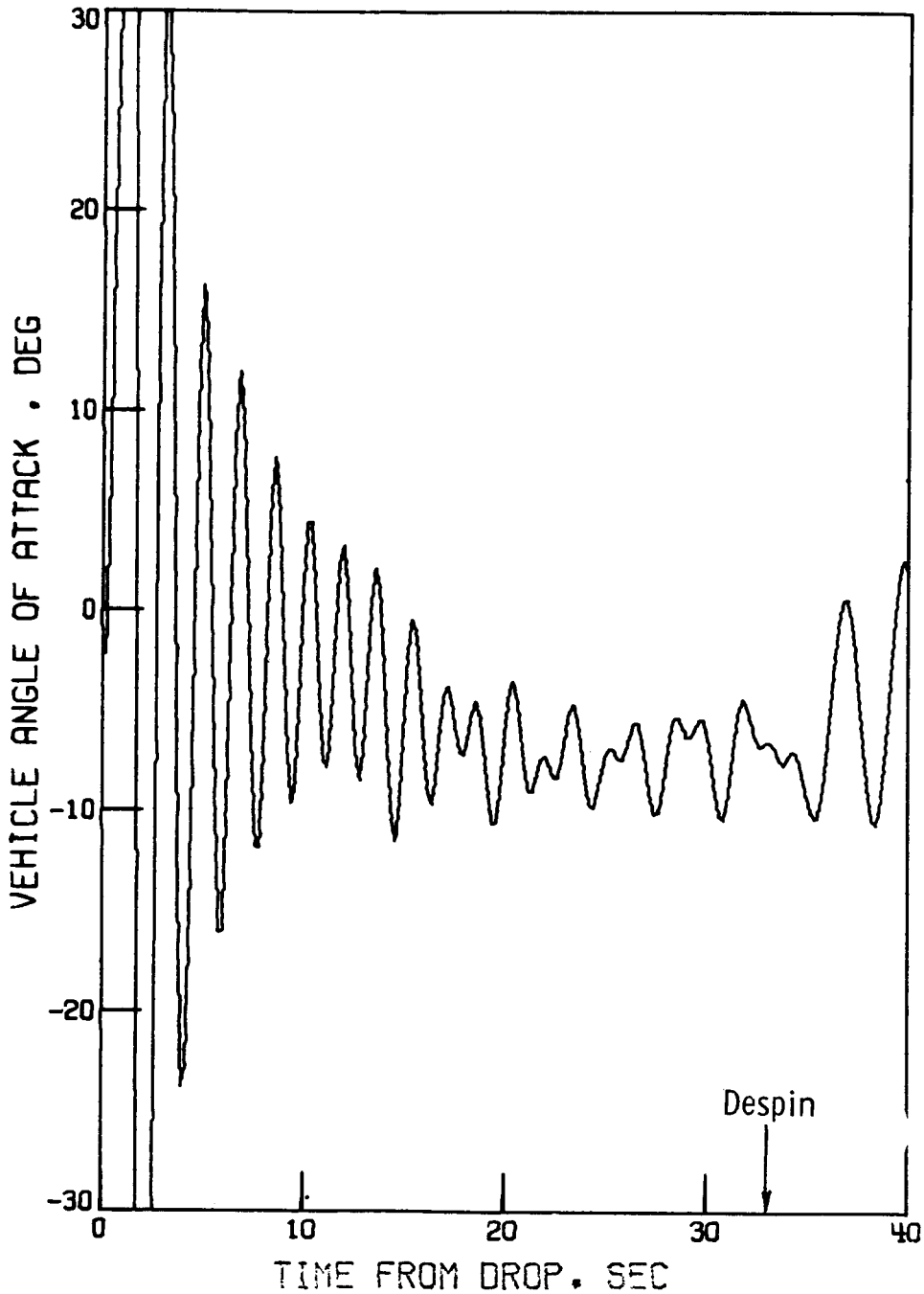


Figure 110.- Time history of angle of attack. AV-4.

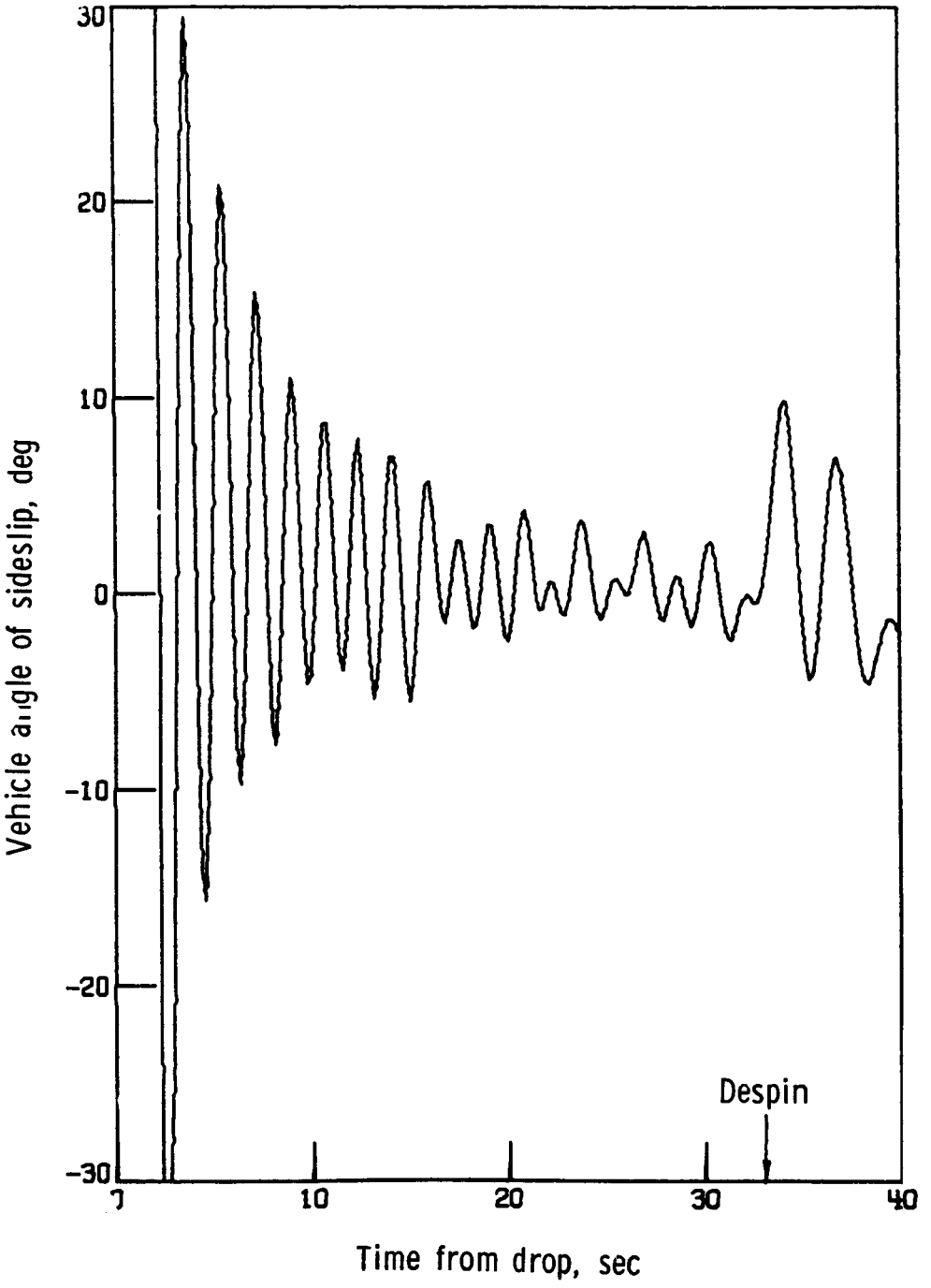


Figure 111.- Time history of angle of sideslip. AV-4.

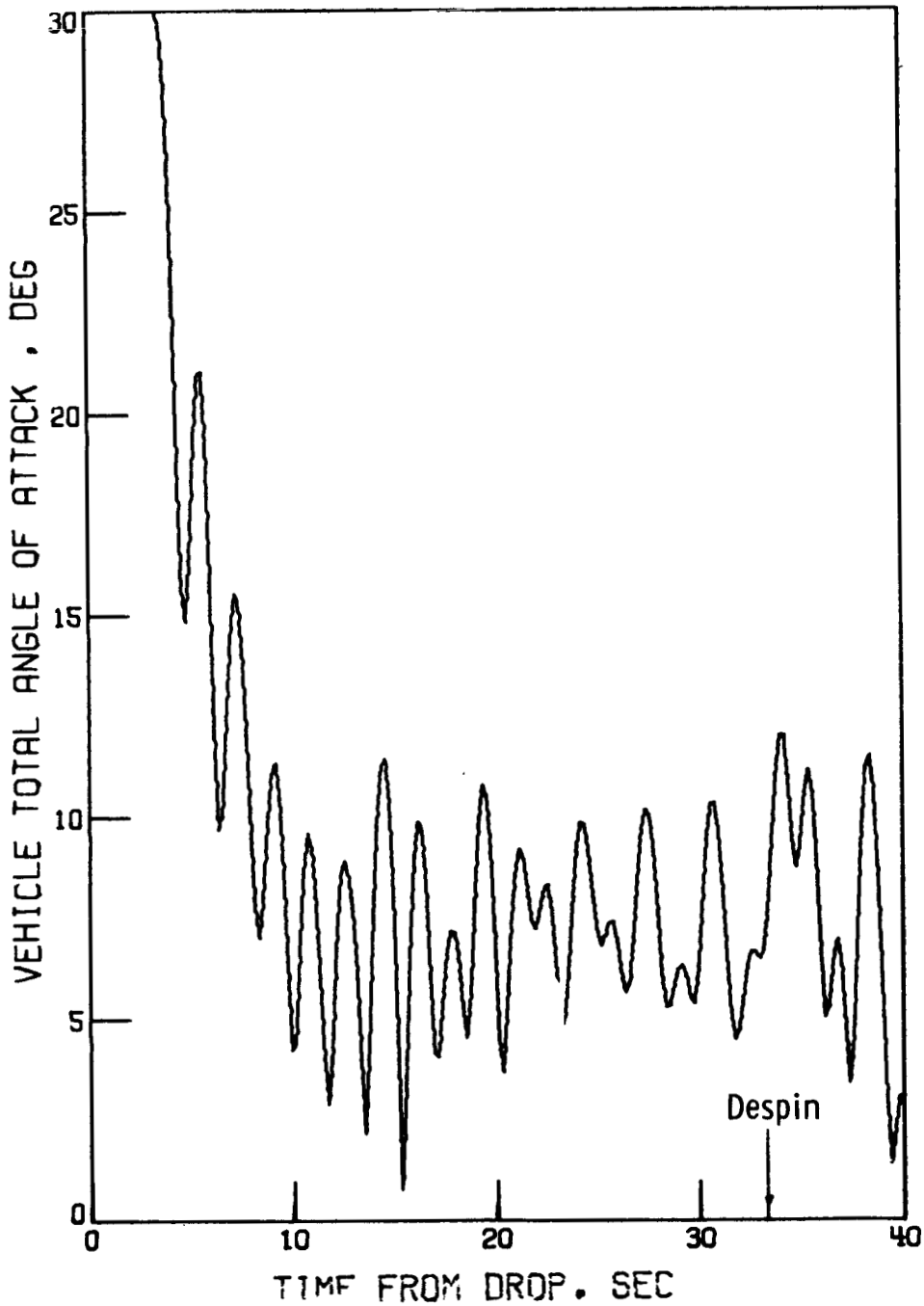


Figure 112.- Time history of vehicle total angle of attack. AV-4.

U.S. GOVERNMENT PRINTING OFFICE: 1974 635-044, 34

ERRATA

NASA Technical Note D-7692

FLIGHT TESTS OF VIKING PARACHUTE SYSTEM IN THREE MACH NUMBER REGIMES

I – VEHICLE DESCRIPTION, TEST OPERATIONS, AND PERFORMANCE

By Reginald R. Lundstrom, James L. Raper,
Richard J. Bendura, and E. William Shields

October 1974

Page 4: The definition for z' should read as follows:

distance measured from X-axis in the XZ-plane, cm (in.)

Page 51: Replace page with the attached page 51.

Page 74: Replace page with the attached page 74.

Issued March 1976

CASE FILE COPY